



UCL

University College London
Department of Chemistry
Centre for Doctoral Training in Molecular Modelling and Materials Science
EngD Molecular Modelling and Materials Science

The Fabrication and Characterisation of Economically Viable Functionalised Surfaces for Superhydrophobic and Antimicrobial Applications

Sam S. Cassidy

Supervisors:
Prof Claire J. Carmalt
Dr Elaine Allan
Prof Ivan P. Parkin

September 2022

Declaration

I, Sam Sebastian Cassidy confirm that the work presented in this thesis is my own. Where information has been derived from other sources, I confirm that this has been indicated in the thesis.

Acknowledgements

I would like to begin by thanking the EPSRC, M3S, and Altro Ltd. for funding my research, with a special mention for Susanna Halls and Tracy Perry, who have been staunch supporters of this project. Without you this project would not have been possible, but there are also a number of other people who without their support, this thesis would not have been possible.

First and foremost, I would like to thank my supervisors Claire, Elaine, and Ivan. Both the guidance you have offered me and the freedom you have given me to work has allowed me to prosper in my time at UCL. From the time I arrived at UCL you pointed me in a direction, told me where to go, and allowed me to get there how I pleased, and for this I will forever be grateful. I would also like to thank Sean Nair for collaborating with me on the work I carried out investigating carotenoids in *S. aureus* and the rest of the Eastman for their support.

Sunny Baines and Stephen Potts, you guided me through my time teaching at UCL, and as I leave UCL to go teach at Kings, I owe much of this opportunity to the both of you.

I would like to thank everyone who has passed through office 302 during my time at UCL, it was an excellent environment to be in for a discussion, a debate, or just to ponder for a while. A special mention to my Altro project partners Kris and Cesar, it has been a pleasure to work with you both and I hope to work together again in the future as you continue to prosper at UCL. Tim, Jameel, Joe, my M3S cohort, the Scanlon group, and most recently my mentee Eimear, you have been a constant presence on the steps outside chemistry, or sometime after 2pm on a Friday.

To all of my parents, brothers, grandmothers, aunts and uncles, cousins, the support you have given me over the years will never be forgotten. The same to my friends both at home and those who made moving to London so easy. Finally, Suzannah Chalmers, love you.

Abstract

This thesis investigates the fabrication and characterisation of economically viable functionalised surfaces for superhydrophobic and antimicrobial applications. This included the production of a ZnO incorporated PVC nanocomposite, a ZnO stearic acid latex paint, and a ZnO stearic acid polyurethane coating. All samples were produced while avoiding expensive raw materials and using manufacturing techniques viable for large scale production.

To begin with, PVC and ZnO nanoparticles were identified as viable materials for an antimicrobial nanocomposite. Samples produced with compression moulding were then tested and proved to be qualitatively antimicrobial against both *S. aureus* and *E. coli*. Quantitatively, the samples were shown to kill 99.67% of *E. coli*, while only having a 58.78% kill against *S. aureus*. This was followed by mechanism testing that identified singlet oxygen as the nanocomposite's primary mechanism. A further study of *S. aureus* was able to rule out carotenoids as its primary method of defence against singlet oxygen.

This work was followed by the development of a superhydrophobic paint. The paint was fabricated using predominantly ZnO or SiO₂, stearic or palmitic acid, and one of four latexes. Once optimised, the surfaces underwent testing and analysis to determine both the surfaces' physical and chemical properties. This culminated with a surface producing an \bar{x} WCA (water contact angle) of 170.3°, while also displaying qualitative antimicrobial properties against both *S. aureus* and *E. coli*, while lacking sufficient quantitative antimicrobial properties.

Finally, durable superhydrophobic polymer coatings were investigated. Both polyurethane and epoxy surfaces were combined with particles and fatty acids in an effort to produce the coatings. This work achieved a durable superhydrophobic polyurethane coating containing ZnO, with an \bar{x} WCA of

167.5°, qualitative antimicrobial properties against both *S. aureus* and *E. coli*, while again lacking sufficient quantitative antimicrobial properties.

Impact Statement

This thesis looks at the fabrication and characterisation of economically viable functionalised surfaces for superhydrophobic and antimicrobial applications. It does this while avoiding costly raw materials, materials of industrial concern, and using manufacturing techniques that are scalable for large scale production. It is hoped that this work will not only be relevant in academia, but also relevant outside of it. It is a common occurrence in academic projects to overlook the potential industrial application of the products being produced. This means that products are often produced with amazing properties, yet due to their cost or scalability, are commercial nonviable. Throughout this project, the industrial application of all products was always considered.

After seeing the impact of the COVID-19 pandemic, antimicrobial surfaces may be more important now than ever before. The use of expensive metals, specifically silver but also more recently gold, are at the forefront of industrial and academic research when considering antimicrobial surfaces. This project looked to avoid these materials and instead looked at ZnO as a viable antimicrobial reagent. While there have been academic studies of ZnO as an antimicrobial reagent, it has little to no prominence in commercial products. One of the main goals of this project was to change this, with the aim of proving ZnO to be a viable antimicrobial reagent for commercial products.

When considering superhydrophobic surfaces, it is very hard to avoid thinking about Teflon. However, Teflon, like many other superhydrophobic products, relies on fluorinated compounds, which industries are currently looking to move away from due to their impact on the environment and human health. Instead, this project looked at using relatively innocuous fatty acids as the superhydrophobic component. By producing viable superhydrophobic surfaces with fatty acids, this work will help progress the move away from fluorinated surfaces, both inside and outside of academia.

The impact of the application of these surfaces should also be considered. Superhydrophobic surfaces could have applications as water repellent

surfaces, self-cleaning surface, anti-icing surfaces, etc. As society looks to move away from fossil fuels, the efficiency of renewable energy production must be maximised. Superhydrophobic surfaces offer multiple ways to reduce drag, increasing the efficiency of wind turbines, while also offering means to keep the surfaces of solar cells free from disruptions.

When considering antimicrobial surfaces, any impact they can have on the death toll of 136,000 caused by healthcare acquired infections across the USA and Europe, can only be seen as a positive. With industrial applications in mind, their use on public transport systems may also be able to curb the spread of the next epidemic before it reaches pandemic levels. It may also be possible that antimicrobial surface may be capable of the reducing the spread of pathogens sufficiently, so that we are far more able to live with pathogens transmitting through touch surfaces, avoiding future lockdowns.

Therefore, it is hoped that this work will not only have academic and industrial relevance but will also help bridge that gap between the two.

Table of Content

Declaration	<i>i</i>
Acknowledgements	<i>ii</i>
Abstract	<i>iii</i>
Impact Statement	<i>v</i>
Table of Content	<i>vii</i>
List of Figures	<i>x</i>
List of Tables	<i>xix</i>
List of Equations	<i>xx</i>
List of Abbreviations	<i>xxi</i>
1 Introduction	<i>1</i>
1.1 Antimicrobial surfaces	<i>1</i>
1.1.1 Why are antimicrobial surfaces required?	<i>1</i>
1.1.2 Touch surfaces	<i>3</i>
1.1.3 Pathogens	<i>5</i>
1.1.4 Antimicrobial mechanisms	<i>10</i>
1.2 Superhydrophobic surfaces	<i>13</i>
1.2.1 Surface free energy	<i>14</i>
1.2.2 Surface roughness	<i>17</i>
1.2.3 Applications of superhydrophobic surfaces	<i>18</i>
1.3 Polymers	<i>20</i>
1.4 Aims	<i>23</i>
2 The Production and Initial Testing of an Economically Viable Antimicrobial Surface	<i>25</i>
2.1 Aims	<i>25</i>
2.2 Background	<i>25</i>
2.3 Experimental	<i>30</i>
2.3.1 Materials	<i>30</i>
2.3.2 The manufacture of ZnO incorporated PVC	<i>30</i>

2.3.3	Material characterisation and properties	32
2.3.4	Basic antimicrobial testing	33
2.3.5	The identification of a surfaces antimicrobial ROS	35
2.3.6	Determining the impact carotenoid levels have on a surface's antimicrobial properties.....	35
2.4	Results and discussion	35
2.4.1	Sample production	35
2.4.2	Analysis of optical properties	37
2.4.3	SEM imaging and elemental analysis	41
2.4.4	Antimicrobial testing.....	46
2.4.5	Investigation of the antimicrobial mechanism	49
2.4.6	Investigating the role of carotenoids in <i>S. aureus</i> 's defence against the antimicrobial activity of ZnO incorporated PVC	51
2.5	Summary and conclusion.....	53
3	<i>The Production, Application, and Testing of Superhydrophobic Paint</i>	56
3.1	Aims.....	56
3.2	Background.....	56
3.3	Experimental	59
3.3.1	Materials	60
3.3.2	The functionalisation of particles with a hydrophobic capping agent.....	60
3.3.3	The production of superhydrophobic paints.....	61
3.3.4	Material characterisation and functional testing.....	62
3.4	Results and discussion	63
3.4.1	The production of superhydrophobic particles functionalised with a hydrophobic capping agent.....	63
3.4.2	Characterisation and testing of functionalised particles.....	68
3.4.3	The production and optimisation of superhydrophobic paints.....	76
3.4.4	The characterisation and testing of superhydrophobic paints.....	86
3.4.5	The functional testing of superhydrophobic paints.....	93
3.5	Summary and conclusion.....	100
4	<i>The Production, Application, and Testing of Superhydrophobic, Durable Coatings</i>	102
4.1	Aims.....	102

4.2	Background.....	102
4.3	Experimental.....	106
4.3.1	Materials	106
4.3.2	The production of superhydrophobic durable coatings.....	106
4.3.3	Testing superhydrophobic surfaces wetting properties and functionality.....	107
4.3.4	The antimicrobial testing of submerged superhydrophobic surfaces.....	109
4.3.5	Determining the metal ion concentration of a liquid using XRF	110
4.3.6	Anti-icing testing.....	111
4.3.7	Material characterisation and functional testing.....	111
4.4	Results and discussion	112
4.4.1	The production of superhydrophobic durable coatings.....	112
4.4.2	The characterisation and testing of superhydrophobic durable coatings.....	115
4.4.3	Detailed testing of the wetting properties of superhydrophobic coatings.....	120
4.4.4	Antimicrobial testing of superhydrophobic surfaces.....	126
4.4.5	Determining the quantitative leaching of ions from samples surfaces using X-ray fluorimetry	129
4.4.6	Anti-icing testing.....	131
4.5	Summary and conclusion.....	133
5	<i>Incomplete and Future Work.....</i>	135
5.1	Determining a surface's surface free energy and the surface roughness	135
5.2	Modifying samples for increased antimicrobial properties	139
5.3	New methods for the production of bulk superhydrophobic polymers	143
5.4	New methods of antimicrobial testing.....	145
6	<i>Conclusion.....</i>	149
7	<i>Bibliography.....</i>	151

List of Figures

- Figure 1-1 The four main viral structures and examples. Reproduced from Lenard.²⁷ 6
- Figure 1-2 An example of a possible bacterial cell and some of its features. Reproduced from Jiménez-Jiménez et al.⁴¹ 7
- Figure 1-3 Comparison of a Gram positive and a Gram negative cell's envelope. Reproduced from Berezin et al.⁴² 7
- Figure 1-4 There are a number of mechanisms by which antimicrobial surfaces can operate. A) Anti-biofouling surfaces can stop adhesion by forming a protective layer of matter between it and the microbes or can use specific energies at the surface to stop adhesion by or to repel pathogens. B) Biocidal nanocomposites can release incorporated species that are biocidal to microbes or can produce biocidal species by acting as a catalyst. C) Nanostructured surfaces can physically rupture bacterial cells with an affinity to the surface; however, it is as of yet unclear as to the exact impact of nanostructured surfaces on virions. Reproduced from Cassidy et al.²² 10
- Figure 1-5 The physical rupture of *S. aureus* (left) and *E. coli* (right) cells due to the affinity between the cells' surface and the surface structures. Reproduced from Jenkins et al.⁶⁰ 11
- Figure 1-6 The excitation of a photosensitiser (PS) to generate reactive oxygen species through type 1 and type 2 photosensitised oxidation reactions. Reproduced from Dai et al.⁶⁷ 12
- Figure 1-7 A schematic diagram of the influence that the polar (σ^p) and dispersion (σ^d) surface free energy values can have on surfaces with the same total surface free energy value. Reproduced from Jin et al.⁸⁷ ... 15
- Figure 1-8 A force diagram representing Young's equation and how a contact measurement is taken. Reproduced from Simpson et al.⁸⁹ 16
- Figure 1-9 Two possible surface-droplet interactions. Wenzel state where the droplet is in full contact with the surface it is resting on (left). The Cassie-

Baxter state where the droplet sits on a layer of air trapped between the surface structures.....	18
Figure 1-10 Vinyl chloride polymerises to polyvinyl chloride polymer	22
Figure 1-11 Polyurethane synthesised through the reaction of di-isocyanate and polyol.....	22
Figure 1-12 Epoxy synthesised through the reaction of bisphenol-A and epichlorohydrin.....	23
Figure 1-13 Common latex monomers	23
Figure 2-1 Stainless steel mould	31
Figure 2-2 Compression moulding setup.....	32
Figure 2-3 Compression mould formed samples of pure PVC (right) and PVC containing 5% ZnO (left)	32
Figure 2-4 Humidity chambers containing 0% ZnO samples (left) and 5% ZnO samples (right)	34
Figure 2-5 FT-IR analysis of PVC (green), 100 nm ZnO nanoparticles (red), and a 5% ZnO PVC blend (grey).	38
Figure 2-6 UV analysis of nanocomposites, control samples, and the nanoparticles. All spectra were obtained using an integrating sphere unless otherwise stated. 0% spectrum represents a PVC control sample. 5% spectrum represents a ZnO incorporated PVC sample containing 5 wt% ZnO. 0vs5% spectrum represents a ZnO incorporated PVC sample containing 5 wt% ZnO using PVC control sample as a reference. Nps (nanoparticles) spectrum represents 100 nm ZnO nanoparticles, dispersed in BaSO ₄ . Nps In Eth spectrum represents 100 nm ZnO nanoparticles, dispersed in ethanol, and measured using transmission UV-Vis spectroscopy.....	39
Figure 2-7 SEM imaging of control samples containing 0% ZnO nanoparticles	42
Figure 2-8 SEM imaging of 5% ZnO incorporated PVC samples	42

Figure 2-9 (Top) EDX analysis of control samples containing 0% ZnO nanoparticles. (Bottom) EDX analysis of 5% ZnO incorporated PVC samples.....	43
Figure 2-10 Elemental maps of 5% ZnO incorporated PVC samples. Red dots represents Zn (top), Cl bottom.	44
Figure 2-11 Antimicrobial activity of 5% ZnO incorporated PVC samples against 0% ZnO PVC control samples. Samples inoculated with <i>E. coli</i> suspension (left) and <i>S. aureus</i> suspension (right) were left at room temperature, for 6 h, under dark conditions.	46
Figure 2-12 Antimicrobial activity of 5% ZnO incorporated PVC samples against 0% ZnO PVC control samples. Samples were inoculated with <i>S. aureus</i> and left at room temperature under; ~300 Lx for 6 h (top left) <1 xl for 24 h (top right) ~300 Lx for 24 h (bottom)	48
Figure 2-13 Antimicrobial activity of 5% ZnO incorporated PVC samples against 0% ZnO PVC control samples. Samples were inoculated with <i>E. coli</i> and left at room temperature under dark conditions for 6 h. a) Control b) Catalase ~35 unit/ml c) Mannitol 110 mM d) Super oxide dismutase 30 unit/ml e) L-histidine 6.5 mM	50
Figure 2-14 <i>S. aureus</i> plated on mannitol salt agar. WT (yellow), crtM (pale)	52
Figure 2-15 Antimicrobial testing of samples against different <i>S. aureus</i> strains. (top left) 8325-4, (top right) WT, (bottom) crtM.	52
Figure 3-1 C16 palmitic acid (top). C18 stearic acid (bottom).	57
Figure 3-2 Functionalised ZnO powder (left powder). Functionalised ZnO powder on double sided tape (left). Functionalised SiO ₂ powder (right powder). Functionalised SiO ₂ powder on double sided tape (right)....	61
Figure 3-3 ZnO, stearic acid, plus latex, ethanol paint applied to microscope slides using a gravity fed spray gun, after 5 min of sonication, using 3 bar of pressure.	62

Figure 3-4 DSA image of a 5 μ l water droplet on stearic acid coated ZnO particles (100 nm) made using acetone as the solvent, adhered to double sided tape on a microscope slide.....	68
Figure 3-5 DSA image of a 5 μ l water droplet on fatty acid coated ZnO particles (100 nm) adhered to double sided tape on a microscope slide. Top left: Palmitic acid coated ZnO made using ethanol as the solvent. Top right: Stearic acid coated ZnO made using ethanol as the solvent. Bottom: Palmitic acid coated ZnO made using acetone as the solvent.....	70
Figure 3-6 Zinc stearate	70
Figure 3-7 The comparison of the transmission FT-IR spectra of the raw materials with functionalised nanoparticles made in acetone. Blue: ZnO. Red: Stearic acid. Yellow: ZnO functionalised with stearic acid.....	72
Figure 3-8 The comparison of the transmission FT-IR spectra of the raw materials with functionalised nanoparticles made in acetone. Blue: SiO ₂ . Red: Stearic acid. Yellow: SiO ₂ functionalised with stearic acid.	72
Figure 3-9 Zn 2p XPS analysis of ZnO particles (top), and functionalised ZnO particles (bottom)	73
Figure 3-10 Si 2p XPS analysis of SiO ₂ particles (top), and functionalised SiO ₂ particles (bottom)	73
Figure 3-11 The comparison of the transmission FT-IR spectra of palmitic acid and stearic acid	75
Figure 3-12 The comparison of the transmission FT-IR spectra of ZnO functionalised with stearic acid in acetone and ZnO functionalised with palmitic acid in acetone.....	75
Figure 3-13 The comparison of the transmission FT-IR spectra of ZnO functionalised with stearic acid in acetone and ZnO functionalised with stearic acid in ethanol.	76
Figure 3-14 The comparison of the transmission FT-IR spectra of ZnO functionalised with palmitic acid in acetone and ZnO functionalised with palmitic acid in ethanol.....	76

Figure 3-15 Transmission FT-IR spectrum of Acronal Plus 2483 latex	78
Figure 3-16 Transmission FT-IR spectrum of Acronal Edge 6295 latex.....	79
Figure 3-17 Transmission FT-IR spectrum of Acronal A 750 latex.....	79
Figure 3-18 Transmission FT-IR spectrum of Acronal A 684 latex.....	80
Figure 3-19 Transmission FT-IR spectra of different latex paints made up using acetone (Act) containing ZnO and stearic acid (SA).....	86
Figure 3-20 Transmission FT-IR spectra of different latex paints made up using acetone (Act) containing SiO ₂ and stearic acid (SA).....	88
Figure 3-21 Transmission FT-IR spectra of a paint and the main components used to make it. The paint contained SiO ₂ , Plus latex (Plus), stearic acid (SA), made up in acetone (Act).....	89
Figure 3-22 Top: Zn 2p XPS analysis of a paint containing ZnO, Plus latex, stearic acid, made up in acetone. Bottom: Si 2p XPS analysis of a paint containing SiO ₂ , Plus latex, stearic acid, made up in acetone.	90
Figure 3-23 Top: Zn 2p XPS analysis of a paint containing ZnO, 750 latex, stearic acid, made up in acetone. Bottom: Si 2p XPS analysis of a paint containing ZnO, 684 latex, stearic acid, made up in acetone.	90
Figure 3-24 SEM imaging of: paint containing no particles, Plus latex, stearic acid, made up in acetone (left). Paint containing ZnO particles, Plus latex, stearic acid, made up in acetone (right).	92
Figure 3-25 SEM imaging of: paint containing ZnO particles, Edge latex, stearic acid, made up in acetone (left). Paint containing ZnO particles, 750 latex, stearic acid, made up in acetone (right).	92
Figure 3-26 SEM imaging of: paint containing ZnO particles, 684 latex, stearic acid, made up in acetone (left). Paint containing SiO ₂ particles, Plus latex, stearic acid, made up in acetone (right).	92
Figure 3-27 Paint stain testing. All paints contained stearic acid. The top row of paints were made up in acetone, while the bottom row were made up in ethanol. Each sample also contained ZnO or SiO ₂ particles, as well as	

a latex. Each sample was tested with 20 ppm crystal violet (left), instant coffee (middle), and wine (right).....	94
Figure 3-28 Paint stain testing. All paints contained palmitic acid. The top row of paints were made up in acetone, while the bottom row were made up in ethanol. Each sample also contained ZnO or SiO ₂ particles, as well as a latex. Each sample was tested with 20 ppm crystal violet (left), instant coffee (middle), and wine (right).....	94
Figure 3-29 The results of tape tests consisting of the firm application and removal of 10 strips of Scotch Magic Tape consecutively. Top: Paint consisting of ZnO, Plus latex, stearic acid, made up in an acetone base. Bottom: Paint consisting of ZnO, Plus latex, palmitic acid, made up in an acetone base.....	99
Figure 3-30 DSA image of a 5 µl water droplet on painted surface after a completed tape test. Left: Paint consisting of ZnO, Plus latex, stearic acid, made up in an acetone base. Right: Paint consisting of ZnO, Plus latex, stearic acid, made up in an acetone base.	100
Figure 4-1 Functionalised polyurethane coated glass slides sprayed with: ZnO, stearic acid, Altro Seal, made in an acetone base (left). SiO ₂ , stearic acid, Altro Seal, made in an acetone base (right).	107
Figure 4-2 Sample chambers attached to a rocking table containing paint coated samples (left, center) and a copper control (right).....	110
Figure 4-3 An observable colour change occurs as methylene blue solution freezes (left to right)	111
Figure 4-4 Transmission FT-IR spectra of an Altro Seal coating and the main components used to make it. The coating contained ZnO, Altro Seal (Seal), stearic acid (SA), made up in acetone (Act).....	116
Figure 4-5 Transmission FT-IR spectra of two Altro Seal coating. The coatings contained either ZnO or SiO ₂ , as well as Altro Seal (Seal), stearic acid (SA), and was made up in acetone (Act)	116

Figure 4-6 XPS survey of superhydrophobic durable coatings. The coatings contained either ZnO (top) or SiO₂ (bottom), as well as Altro Seal, stearic acid, and was made up in acetone..... 118

Figure 4-7 Top: Zn 2P XPS analysis of a superhydrophobic durable coating containing ZnO. Bottom: Si 2P XPS analysis of a superhydrophobic durable coating containing SiO₂. 119

Figure 4-8 SEM imaging of: Altro Seal containing ZnO particles and stearic acid (left). Altro Seal containing SiO₂ particles and stearic acid (right). 120

Figure 4-9 DSA image of a 5 µl water droplet on polymer coating surface. Left: Polymer coating consisting of ZnO, stearic acid, and Altro Seal made up in an acetone base. Right: Polymer coating consisting of SiO₂, stearic acid, and Altro Seal made up in an acetone base..... 120

Figure 4-10 A demonstration of how a rolling angle measurement is taken. The stage is set to a designated angle, at which point a 13 µl water droplet is applied to the surface, using a syringe dispenser, raised 10 mm above the surface. If the water droplet unable to stay on the surface, the current angle was deemed the surfaces rolling angle..... 121

Figure 4-11 A demonstration of the self-cleaning properties of the ZnO stearic acid Plus latex paint. To begin, the surface at ~10° (±1°) is covered in glitter. Water droplets are then applied to the surface using a Pasteur pipette. If the surface has self-cleaning properties, the water droplets will roll across the surface picking up the dirt (glitter) as can be seen in the images above. If not, the water will stick to, or slide across the surface, with the dirt (glitter) remaining in place. 122

Figure 4-12 Stain testing. ZnO stearic acid Altro Seal (left). SiO₂ stearic acid Altro Seal (right). Each sample was tested with 20 ppm crystal violet (left), instant coffee (middle), and wine (right). As both surfaces were able to repel the solutions, they were left unstained. 123

Figure 4-13 An outline of the procedure by Huhtamäki et al used to obtain contact angle hysteresis measurements. Reproduced from Huhtamäki et al.²¹⁹ 124

Figure 4-14 The advancing and the receding (after the red line) contact angle measurements of: ZnO palmitic acid Plus latex paint, ZnO stearic acid Plus latex paint, ZnO stearic acid Altro Seal, SiO₂ stearic acid Altro Seal. 124

Figure 4-15 The contact angle hysteresis and rolling angle of: ZnO palmitic acid Plus latex paint, ZnO stearic acid Plus latex paint, ZnO stearic acid Altro Seal, SiO₂ stearic acid Altro Seal. 125

Figure 4-16 The results of tape tests consisting of the firm application and removal of 10 strips of Scotch Magic Tape consecutively. Top: ZnO stearic acid Altro Seal. Bottom: SiO₂ stearic acid Altro Seal. 126

Figure 4-17 DSA image of a 5 µl water droplet on polymer coating surface after a completed tape test. Left: Polymer coating consisting of ZnO, stearic acid, and Altro Seal made up in an acetone base. Right: Polymer coating consisting of SiO₂, stearic acid, and Altro Seal made up in an acetone base. 126

Figure 4-18 Antimicrobial activity of copper coupons, ZnO stearic acid Plus latex paint that was made up in acetone, and the ZnO stearic acid Altro Seal that was also made up in acetone. Samples were tested against an E. coli suspension (left) and a S. aureus suspension (right). This was performed at room temperature, for 24 h, under normal lighting conditions. 128

Figure 4-19 XRF analysis of tested bacterial inocula to determine the ion concentration. These inocula included: a control that was not exposed to any surfaces (ctl), an inoculum exposed to copper surfaces (Cu), an inoculum exposed to a surface coated with the ZnO stearic acid Plus paint (Paint), an inoculum exposed surface coated with ZnO stearic acid Altro Seal (Seal). 130

Figure 4-20 Anti-icing results. Control: Pure Altro Seal coating. ZnO SA: Coating of Altro Seal mixed with ZnO and stearic acid. SiO₂ SA: Coating of Altro Seal mixed with SiO₂ stearic acid 132

Figure 5-1 SEM imaging of a ZnO Plus latex stearic acid paint made in acetone. Left: sample after spraying. Right: sample after polishing. 136

Figure 5-2 Dye-sensitised 5% ZnO incorporated PVC. Left: 10 ppm methylene blue. Right 100 ppm methylene blue.....	140
Figure 5-3 The production of reactive oxygen species via electron transfer, due to the self-corrosive properties of Zn/ZnO coreshell particles. Reproduced from Yi et al. ²²⁷	140
Figure 5-4 Initial SEM comparison between Zn particles (left) and Zn/ZnO coreshell particles (right).....	141
Figure 5-5 SEM comparison between Zn/ZnO coreshell particles produced using different reaction times (1 hour intervals). Top left: 1 h. Top middle 2 h. Top right 3 h. Bottom left 4 h. Bottom right 5 h.	142
Figure 5-6 Bulk polyurethane fabricated using a similar formulation to the superhydrophobic Altro Seal coatings (section 4.3.2).....	144
Figure 5-7 DSA image of a 5 µl water droplet on bulk polyurethane sample consisting of ZnO, stearic acid, and Altro Seal made up in an acetone base.	144
Figure 5-8 Nutrient agar plates sprayed with different concentrations of bacterial inocula. Top left: <i>S. aureus</i> 10 ⁵ CFU. Top right: <i>E. coli</i> 10 ⁵ CFU. Bottom left: <i>S. aureus</i> 10 ⁷ CFU. Bottom right: <i>E. coli</i> 10 ⁷ CFU.....	147

List of Tables

Table 1-1 Persistence of bacterial pathogens on common inanimate dry surfaces (e.g. plastics, stainless steel or flooring). * CFU (Colony forming units). ²²	4
Table 1-2 Persistence of viral pathogens on common inanimate dry surfaces (e.g. plastics, stainless steel or flooring). * TCID ₅₀ (50% tissue-culture infectious dose). ²²	4
Table 2-1 The composition of ZnO incorporated PVC samples	30
Table 2-2 (Left) XRF analysis of control samples containing 0% ZnO nanoparticles and (Right) 5% ZnO incorporated PVC samples	45
Table 3-1 Components and results of the initial functionalisation of particles with a fatty acid after 4 h of stirring at 50 °C.	65
Table 3-2 Components and water contact angles of the optimised particles functionalised with a fatty acid after 2 h of stirring at 50 °C.	69
Table 3-3 DSA images of latex paints and \bar{x} water contact angles. Formulations consist of a latex (Plus, Edge, 750, 684), ZnO or SiO ₂ , stearic acid (SA) or palmitic acid (PA), with Orotan and texanol, made up in acetone (Act) or ethanol (EtOH). Continues on next page.....	84
Table 3-4 DSA images of latex paints and \bar{x} water contact angles after stain testing and cleaning. Formulations consist of a latex (Plus, Edge, 750, 684), ZnO or SiO ₂ , stearic acid (SA) or palmitic acid (PA), with Orotan and texanol, made up in acetone (Act) or ethanol (EtOH). Continues on next page	97

List of Equations

Equation 1 Young's Equation	15
Equation 2 Owens, Wendt, Rabel, and Kaelble method	16
Equation 3 Wenzel model.....	17
Equation 4 Cassie-Baxter model	17
Equation 5 Intermediate model.....	17
Equation 6 Roughness factor	138

List of Abbreviations

684	Acronal A 684
750	Acronal A 750
Act	Acetone
AFM	Atomic force microscopy
ATCC	American Typed Culture Collection
BHI	Brain heart infusion
<i>C. albicans</i>	<i>Candida albicans</i>
CFU	Colony forming units
COVID-19	Coronavirus Disease 2019
crtM	<i>Staphylococcus aureus</i> crtM JE2
Ctl	Control
DNA	Deoxyribonucleic acid
DSA	Drop shape analyser
<i>E. coli</i>	<i>Escherichia coli</i>
Edge	Acronal Edge 6295
EDX	Energy-dispersive X-ray
EtOH	Ethanol
FT-IR	Fourier transform infrared
HAI	Healthcare acquired infection
IBAD	Ion beam assisted deposition
<i>L. monocytogenes</i>	<i>Listeria monocytogenes</i>
MALDI-TOF	Matrix-assisted laser desorption/ionisation – time of flight
MDR	Multiple drug resistant
MERS-CoV	Middle East Respiratory Syndrome Coronavirus
MSA	Mannitol salt agar
Nps	Nanoparticles
OWRK	Owens, Wendt, Rabel, and Kaelble
PA	Palmitic acid
PBS	Phosphate buffered saline solution
Plus	Acronal Plus 2483

PS	Photosensitiser
PVC	Polyvinyl chloride
RNA	Ribonucleic acid
ROS	Reactive oxygen species
<i>S. aureus</i>	<i>Staphylococcus aureus</i>
SA	Stearic acid
SARS-CoV-2	Severe Acute Respiratory Syndrome Coronavirus 2
Seal	Altro Seal
SEM	Scanning electron microscope
SFE	Surface free energy
SFT	Surface free tension
Tect	Altro Tect
UV-Vis	Ultraviolet-visible
WCA	Water contact angle
WHO	World Health Organization
WT	<i>Staphylococcus aureus</i> wild-type JE2
\bar{x}	Mean average
Zn:P	Zinc:Phosphorus

1 Introduction

The aim of this project was to investigate antimicrobial and superhydrophobic surfaces with the goal of manufacture surfaces that would be economically viable across multiple industries, using manufacturing techniques that would be scalable for large scale production. This required the avoidance of expensive materials and techniques known to produce good antimicrobial or superhydrophobic properties, such as gold or ion etching.^{1,2} The following work takes place under this remit.

1.1 Antimicrobial surfaces

1.1.1 Why are antimicrobial surfaces required?

Beginning with the discovery of “morbid matter” in 1846 by Ignaz Phillip Semmelweis, over the last 200 years our understanding of disease and our ability to combat them has increased inordinately.³ It was the link between post-mortem examinations and maternal deaths identified by Semmelweis, which led to the introduction of the first handwashing protocols in hospitals. Louis Pasteur would then go on to show that “morbid matter” was actually bacterial pathogens, before continuing on to the “germ theory of disease”.⁴ These discoveries, along with the work of Robert Koch whose discovery of anthrax bacillus helped launch the field of medical bacteriology, outlined the fundamentals of modern day hygiene and cleaning protocols.⁵

The 1920s saw the discovery and development of Alexander Fleming’s wonder drug, penicillin.⁶ The use of penicillin and the discovery of further antibiotics revolutionised the way in which patients were treated. However, through an initial lack of understanding of how antibiotics worked, proceeded by general carelessness and misuse, meant that by the 1950s multiple drug resistant (MDR) pathogens began to emerge.⁷ Since then, a continued arms race between pathogens and antibiotics has led the World Health Organization (WHO) to declare that drug resistant pathogens are one of the top global public health threats facing humanity.⁸

The healthcare industry is perhaps where these pathogens are of the biggest concern, and where the biggest impact is felt. The reason for concern could be clearly seen in 2016 when healthcare acquired infections (HAIs) led to a combined death total of 136,000 across the USA and Europe.⁹ The impact could also be seen monetarily, with the costs related to the HAIs exceeding €13 billion across the two regions. Due to the difficulty treating the associated infections and diseases, MDR bacterial pathogens account for a large proportion of these deaths and costs. On top of this, an alarming trend has developed where these nosocomial pathogens have begun to appear more commonly in public areas.¹⁰ It is these deaths, costs, and reach that had put bacterial pathogens at the vanguard of concern, however in 2020, viral pathogens swiftly returned to the forefront.

Over the past 20 years, the emergence of Zika virus, Zaire ebolavirus, Middle East Respiratory Syndrome Coronavirus (MERS-CoV), and other zoonotic diseases, led many experts to believe that a global pandemic was inevitable.¹¹ Not only did these experts believe a pandemic was inevitable, but they also warned we were ill-prepared to deal with it. Unfortunately, these premonitions rang true in 2020 with the emergence and spread of Severe Acute Respiratory Syndrome Coronavirus 2 (SARS-CoV-2), and the associated Coronavirus Disease 2019 (COVID-19). As of the 2nd of August 2022, the WHO had reported over 6.4 million COVID-19 related deaths.¹² Another aspect of the pandemic was the unprecedented blow to the global economy, with an estimated \$2.2 trillion wiped off the global gross domestic product in 2020.¹³

In 2022, as global economies attempt to recover from the pandemic, interruptions in supply chains due to COVID-19, are now contributing to record levels of inflation.¹⁴ This is just as outbreaks of monkeypox serve as a stark reminder that the next pandemic may just be around the corner.¹⁵ With more than 1,500 pathogens discovered since 1970, and humanity showing no signs of limiting its interference with, or encroachment into nature, it is only a matter of time until another pathogen capable of causing a global pandemic arises.¹¹ Whether the next pandemic is caused by a zoonotic viral pathogen as was the

case with the Spanish Flu and COVID-19, or whether it is due to a zoonotic bacterial pathogen as the Black Death was, we must take steps to develop and implement precautionary measures.^{16,17} It is only through these measures that we can hope to mitigate the impact the of the next pandemic on society.

1.1.2 Touch surfaces

There are many different methods by which pathogens can spread, with some requiring an exchange of bodily fluids, while others can spread more easily through drinking water, with others being airborne.¹⁸⁻²⁰ Even the oral expulsion of pathogens is considered a direct contact method of spread, as 99% of droplets remaining airborne for less than 90 s.²¹ People are generally aware of the risk of infection due to direct contact with a pathogen source, and more often than not, take precautions to mitigate these risks by taking simple actions, such as avoiding sick people, or drinking bottled water. However, it is far harder for people to mitigate the risk of infection when dealing with indirect methods of infection.

Table 1-1 and Table 1-2 show the period of detectability of some common pathogens on inanimate dry surfaces.²² While these figures do not relate to infective doses, it can be seen that viral pathogens can be detected for up to 7 days after contamination. When you consider that SARS-CoV-2 and the H1N1 influenza both had incubation periods of ≥ 4 days, during which a host could be contaminating touch surfaces, it is easy to see how viral pathogens can spread. On the other hand, bacterial pathogens could be detected on the surface for >90 days after exposure, and when you consider that *Yersinia pestis* bacterium responsible for plague has a 32 day incubation period, it is easy to see how 200 million people died during the Black Death.¹⁶

These timeframes give an indication of the impact touch surfaces can have on the spread of pathogens. Consider London, a city served by six international airports, which prior to the COVID-19 pandemic, averaged ~485,000 passengers daily.²³ All of these airports are served by many modes of public transport, which many of the air travellers will use to make their way to the city.

An infected traveller could unknowingly, easily contaminate many touch surfaces associated with the public transport services. It is these transport services, that are also used by London commuters to complete ~10.9 million journeys daily, that are an example of how the spread of a pathogen could easily be facilitated, before spiralling out of control.²⁴

Bacterial Pathogens	Initial Inoculation	Period of Detectability	Associated Sickness
<i>Clostridium difficile</i> (spores)	~ 1 x 10 ⁶ CFU*	5 months	Bowel infection, diarrhoea
<i>Escherichia coli</i>	~ 1 x 10 ⁵ CFU*	36 days	Kidney failure, bloody diarrhoea, vomiting
<i>Klebsiella spp.</i>	~ 1 x 10 ⁵ CFU*	32 days	Pneumonia, septicaemia, meningitis
<i>Staphylococcus aureus</i>	~ 4 x 10 ⁵ CFU*	> 90 days	Pneumonia, septicaemia

Table 1-1 Persistence of bacterial pathogens on common inanimate dry surfaces (e.g. plastics, stainless steel or flooring). * CFU (Colony forming units).²²

Viral Pathogens	Initial Inoculation	Period of Detectability	Associated Disease
Influenza	~ 1 x 10 ⁴ TCID ₅₀ *	2 days	Influenza
Norovirus	~ 2 x 10 ⁵ TCID ₅₀ *	7 days	Gastroenteritis
Rhinovirus	~ 1 x 10 ⁴ TCID ₅₀ *	4 days	Common cold
SARS-CoV-2	~ 10 ⁵ TCID ₅₀ *	3 days	COVID-19

Table 1-2 Persistence of viral pathogens on common inanimate dry surfaces (e.g. plastics, stainless steel or flooring). * TCID₅₀ (50% tissue-culture infectious dose).²²

An obvious solution to this would be regular cleaning, as this could remove pathogens from a surface or kill them.²⁵ The issue is how regular would cleaning need to be, and how immaculate would it need be for it to stem the spread of pathogens. A study across 27 intensive care units using fluorescent tracers found that after cleaning, on average, only 47.9% of a touch surface was actually clean.²⁶ Further analysis of the data showed that when looking at some high traffic touch surfaces, such as light switches and door handles, the proportion of the surfaces actually clean dropped to $\leq 25\%$. Results like this show that a reliance on cleaning protocols is not practical, and that many pathogens with low infective doses could spread effectively, regardless of these protocols.

1.1.3 Pathogens

To better understand exactly how to combat pathogens, we must first have some sort of an understanding of how pathogens function and differ. Firstly, the main pandemic causing pathogens are either viral or bacterial pathogens. Viruses are relatively simplistic but do have a number of structures (Figure 1-1). They consist of genetic material in the form of either DNA (deoxyribonucleic acid) or RNA (ribonucleic acid) surrounded by a protein capsid.²⁷ Viruses may then be further enveloped, meaning the capsid is surrounded by a lipid membrane, which may contain transmembrane proteins such as the infamous COVID-19 spike protein.²⁸ These transmembrane proteins can target host cells, which viruses require to replicate, as they cannot replicate on their own. It is also these specific transmembrane proteins that are often the target of vaccines.²⁹ However, when looking to pre-emptively target an unknown virus a more general targeting solution is required.

When targeting viruses, enveloped and non-enveloped viruses have different susceptibilities.³⁰⁻³³ Enveloped viruses are typically easier to inactivate than non-enveloped viruses as the lipids in their membranes can be targeted by lipophilic reagents, such as alcohols. For non-enveloped viruses, the only targets are the nucleic acid or the protein capsid. This means that amphiphilic reagents can target the largest range of viruses.³² Reactive oxygen species

(ROS) are capable of damaging lipids, proteins, and nucleic acids.³⁴ Metals, and metal nanomaterials, have been shown to interfere with viruses' ability to bind to host cells, correctly replicate, and destabilises viral envelopes.³⁵

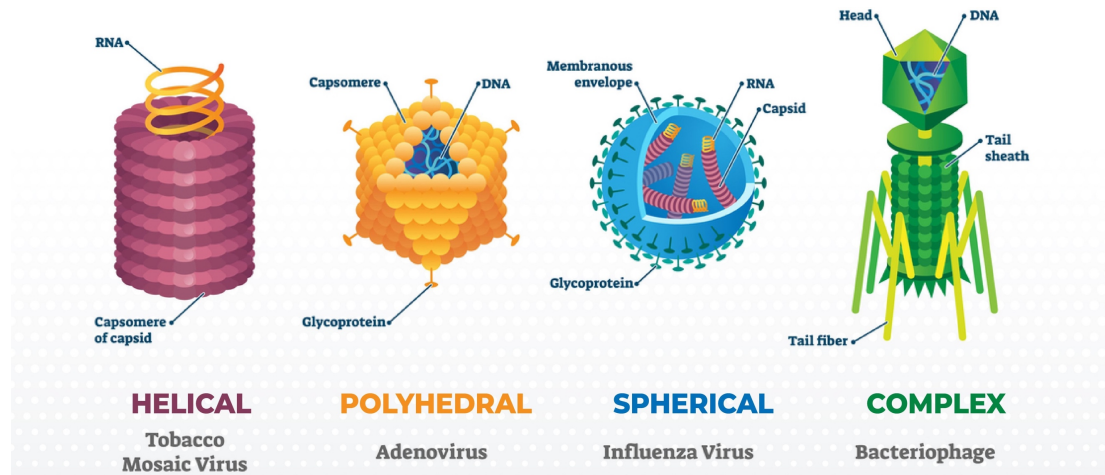


Figure 1-1 The four main viral structures and examples. Reproduced from Lenard.²⁷

Compared to viruses, bacteria are far more intricate. While both bacteria and viruses can cause harm, bacteria are essential for human life. In humans, they are required for normal gut function, with some acting as antitoxins, while others assist in the degradation of food.³⁶ They are also essential for the breakdown of plant matter in the environment, with the nitrogen cycle of particular importance.³⁷ That being said, the essential role of viruses in the global ecosystem is slowly becoming more apparent.³⁸

Figure 1-2 gives an example of a bacterial cell and some of its features, some of which can be targeted by antimicrobials as they are areas where cells can be susceptible to attack. This includes their cell wall, cell membrane, capsule, nucleic acids. As the cell envelope has an influence on the mentioned susceptibilities, typically to begin with, bacteria are generally broken down into two subsets based on their cell envelope.³⁹ Based on the results of a staining procedure devised by Cristian Gram, bacteria are classified as Gram-positive or Gram-negative (Figure 1-3).⁴⁰

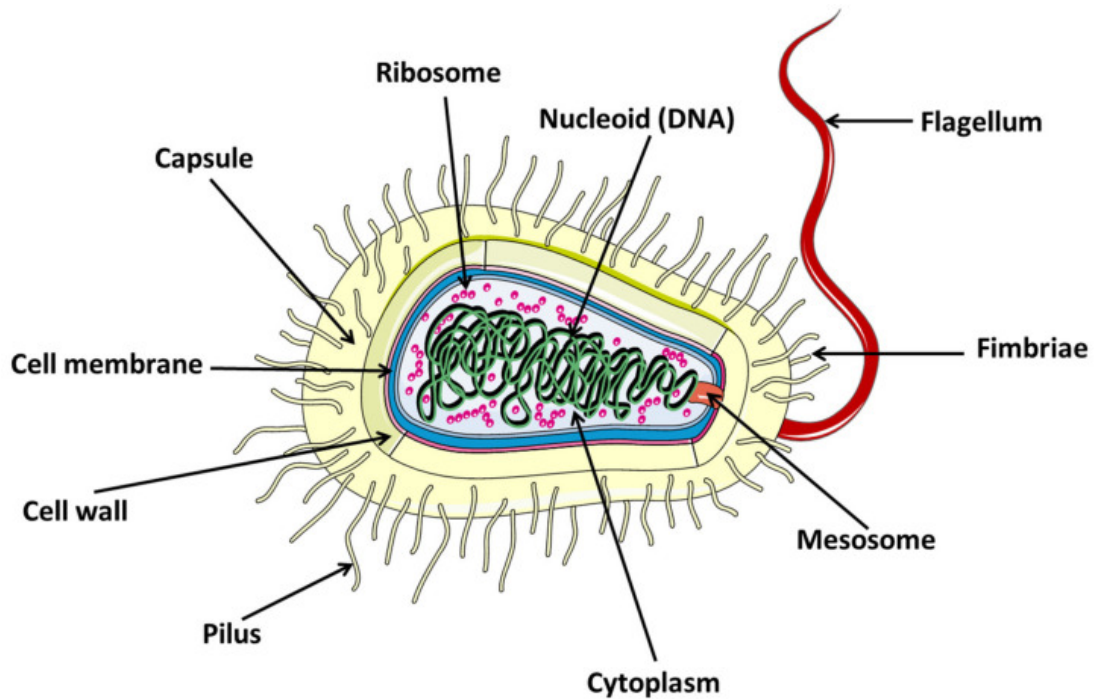


Figure 1-2 An example of a possible bacterial cell and some of its features. Reproduced from Jiménez-Jiménez et al.⁴¹

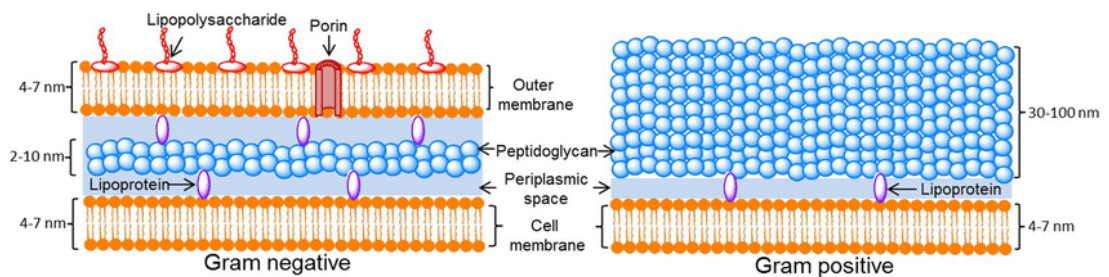


Figure 1-3 Comparison of a Gram positive and a Gram negative cell's envelope. Reproduced from Berezin et al.⁴²

Gram-negative bacteria have a cell envelope consisting of three main layers: the cell membrane, a thin peptidoglycan cell wall, and an outer membrane.^{41,43} The outer membrane is a layer that is innate to Gram-negative bacteria. It is a lipid bilayer consisting of an outer leaflet of just lipopolysaccharides and an inner leaflet that also contains phospholipids.⁴⁴ A number of different porins (transport proteins) are also present in this layer and are essential for the structure and transport functions of the membrane, while also giving the cells a selective permeability.⁴⁵ While these lipopolysaccharides and porins may offer the cells protection from some threats, they also leave them susceptible to other specific threats. Iron ions have been shown to disrupt porins, and

lipopolysaccharides are a common target for drugs specific to Gram-negative bacteria.^{46,47}

The next layer is a periplasm surrounded peptidoglycan cell wall. Despite being thin in Gram-negative cells, the cell wall is still the structural backbone of the cells, acting as a rigid exoskeleton.⁴³ There are also lipoproteins that cross the periplasm and are essential for securing the cell wall to the outer membrane.⁴¹ While the periplasm can protect the cell from potentially harmful enzymes, the cell's reliance on lipoproteins and peptidoglycan for structure mean they can be targeted to disrupt Gram-negative cells.⁴⁶ ROS have been shown to interfere with proteins present in the periplasm, while also interfering with peptidoglycan production.⁴⁸

The inner membrane is the final layer of Gram-negative cells. It is mainly a phospholipids layer but also incorporates a diverse group of proteins and other lipids important for the cell metabolism.^{41,48} Unlike eukaryotic cells that have intracellular organelles present, protein secretion, lipid biosynthesis, and energy production all take place in the inner membrane.⁴³ Being the inner most layer of the cell envelope, the inner membrane is the most protected layer. However, due to the importance of the processes that take place in the layer, minor damage to the inner membrane can have dire consequences for the cell. Possibly due to the requirement of specific metals for metabolism, many components of the inner membrane can be targeted by metals with similar properties to those required by the cell, that do not allow the components to carry out their required functions.^{49,50}

While Gram-negative and Gram-positive cells have many similarities, they also differ in several aspects, altering their susceptibilities and resistances. Unlike its Gram-negative counterpart, Gram-positive envelopes are only bilayered, and lack an outer membrane. This means they lack the susceptibilities that the lipopolysaccharides and porin introduce, but the cells also lack the protection this layer offers. The outer membrane offers Gram-negative cells a distinct resistance against some antibiotics, a resistance Gram-positive cells cannot replicate.⁵¹

The lack of an outer membrane also leaves the Gram-positive cell wall exposed to toxic molecules the outer membrane would normally filter out.⁴¹ However, while Gram-positive bacteria lack an outer membrane, they have a much thicker cell wall, which allows them, like Gram-negative bacteria, to live in harsh conditions, such as the gut.⁴³ Incorporated throughout the Gram-positive cell wall are teichoic acids, which are a type of long anionic polymer. One of the many functions of teichoic acids is to bind to cationic groups, leading to a stockpile of ions just below the cell surface.⁵² Having a stockpile of ions might prove useful when trying to combat certain ROS, however mistaking one metal ion for another can prove fatal to a cell.^{48,50}

Between the cell wall and the inner membrane, there is a single periplasm layer, similar to the two present in a Gram-negative envelope.⁵³ Past the periplasm, the inner membranes of both Gram-negative and Gram-positive cells are similar, however due to the difference in permeability of the outer layers, the inner membranes may be exposed to different contaminations. This means that even if both the inner membranes are susceptible to an antimicrobial reagent, the reagent may be blocked by an outer layer in one of the cells, allowing it to survive, while reaching the inner membrane in the other, causing death or deformation.

Inside the cell envelope of both Gram-negative and Gram-positive cells is the cytoplasm. While the cytoplasm does lack the cell organelles that eukaryotic cells have, it still contains important enzymes, as well as ribosomes and chromosomes.⁵⁴ Despite the layers of protection surrounding the cytoplasm, cells require passage through the cell envelope for processes such as waste removal, or to allow essential materials into the cell as required. These pathways give specific antimicrobial reagents the opportunity to enter the cell, with ROS and metals ions being particularly effective at targeting DNA.^{55,56}

1.1.4 Antimicrobial mechanisms

Antimicrobial surfaces look to take advantage of pathogen vulnerabilities, offering low maintenance effective ways to passively tackle the spread of pathogens. Antimicrobial surfaces can be broken into two basic subcategories: antibiofouling, and biocidal surfaces. Antibiofouling surfaces stop pathogens from propagating on them through means such as a reduced adherence, which may also assist cleaning protocols, but do not kill the pathogens.⁵⁷ Comparatively, biocidal surfaces stop pathogens from propagating on them, by killing them. Figure 1-4 shows some of the mechanisms by which antimicrobial surfaces can operate.

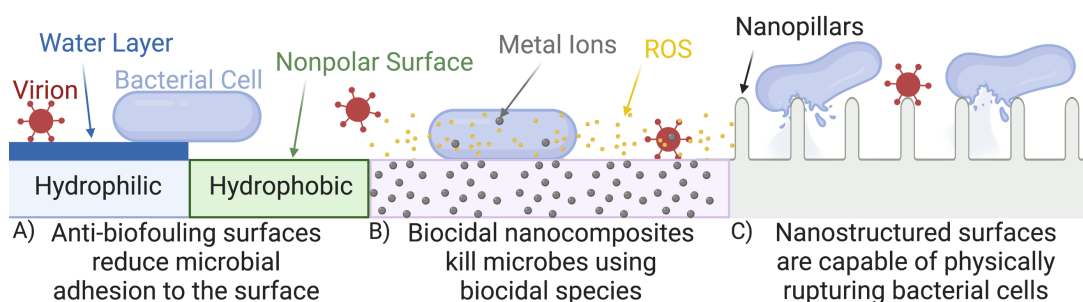


Figure 1-4 There are a number of mechanisms by which antimicrobial surfaces can operate. A) Anti-biofouling surfaces can stop adhesion by forming a protective layer of matter between it and the microbes or can use specific energies at the surface to stop adhesion by or to repel pathogens. B) Biocidal nanocomposites can release incorporated species that are biocidal to microbes or can produce biocidal species by acting as a catalyst. C) Nanostructured surfaces can physically rupture bacterial cells with an affinity to the surface; however, it is as of yet unclear as to the exact impact of nanostructured surfaces on virions. Reproduced from Cassidy et al.²²

Anti-biofouling surfaces take advantage of surface free energy (SFE), to either repel pathogens, or by forming a film at their surface. SFE is the excess energy present at a material's surface in comparison to the bulk material. Superhydrophilic surfaces have a high surface energy, meaning they are looking to bind with other molecules to spread their surface energy, and raise their entropy. If these surfaces have a high enough surface energy, they can tightly bind to available water molecules, forming a hydrated layer that can protect the surface from microbial adhesion.⁵⁸

SFE is also an important factor when considering interactions between a surface and a microbe's surface. Continuing with superhydrophilic surfaces,

if a microbe has a low SFE, it will be entropically unfavourable for it to bind to the surface, meaning the pathogen will repel the surface. Even if a low SFE pathogen does end up on a surface with an incompatible SFE, it can interfere with the pathogen's ability to propagate on the surface.⁵⁹ The same interaction can be reversed for low SFE superhydrophobic surfaces, where it is entropically unfavourable for the surface to bind to high SFE pathogens, leading to the surface repelling the pathogens.⁵⁹

The other interaction to consider when looking at surfaces with superwettabilities, is when the surface and the pathogens bind favourably. As pathogens regularly propagate surfaces, favourable binding conditions must be common.²² However, antimicrobial surfaces can use this affinity to their advantage. Figure 1-5 shows the physical rupture of bacterial cells attempting to bind to surfaces of a much greater surface area.⁶⁰ As the surface area of the surface is much greater than the cells, the cells begin to stretch as they bind to more and more of the surface.^{61,62} This continued stretching can compromise the cells' envelope to the point where it ruptures, or can easily be penetrated by the surface structures.

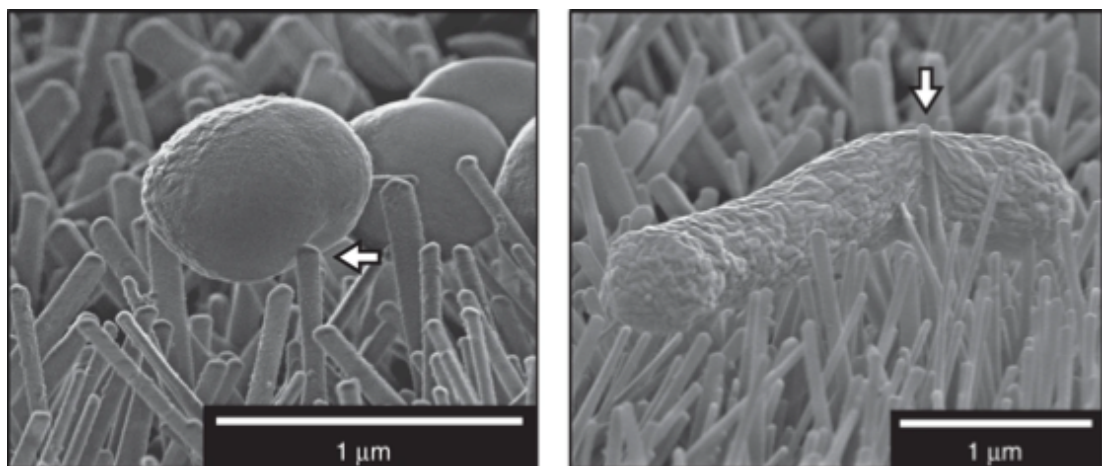


Figure 1-5 The physical rupture of *S. aureus* (left) and *E. coli* (right) cells due to the affinity between the cells' surface and the surface structures. Reproduced from Jenkins et al.⁶⁰

Another mechanism by which antimicrobial surfaces can operate, is through the production of chemical species. These species can be produced through catalytic processes or through ion leaching.^{63,64} Generally, surfaces that produce ions, do so through leaching. This means that metal ions incorporated

in the materials simply make their way to the surface, where they can then interact with pathogens. Silver is one of the most popular antimicrobial metals and is capable of attacking a cell through multiple pathways.⁶⁵ Silver has the capability to interfere with cell DNA to inhibit cell replication, denature proteins so they are no longer functional, detach the cell wall from the membranes, etc. Ionic mimicry is when a non-essential metal like lead, replaces an essential metal like zinc, without the ability to act as a Lewis catalyst, causing enzyme inhibition.⁶⁶ However, surfaces that rely on ion leaching, have a limited reservoir, which means their potency can be reduced over time.

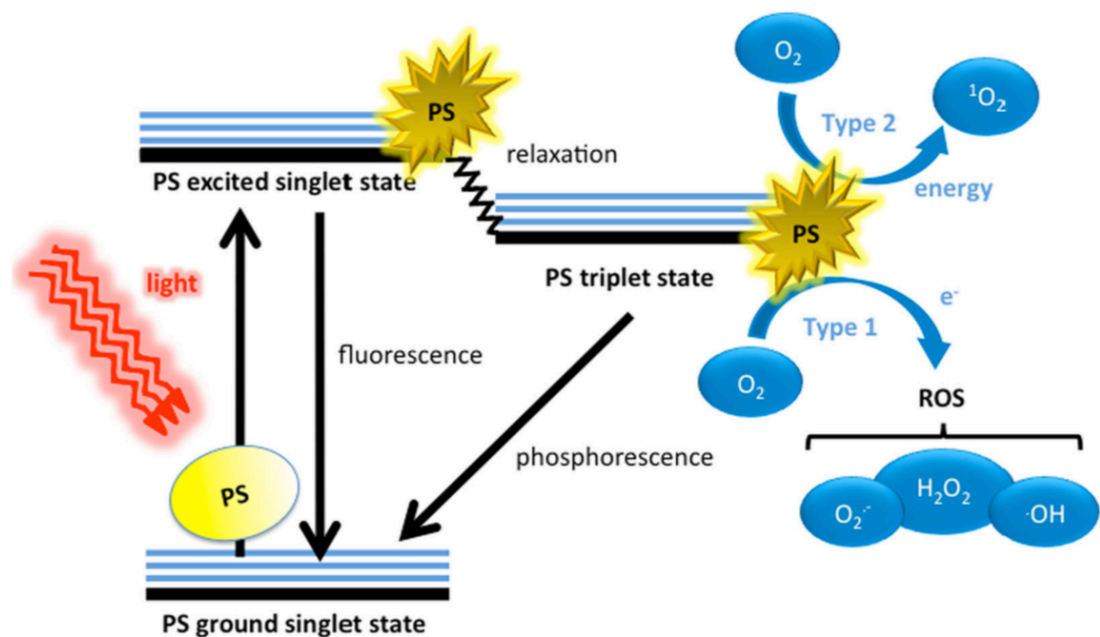


Figure 1-6 The excitation of a photosensitiser (PS) to generate reactive oxygen species through type 1 and type 2 photosensitised oxidation reactions. Reproduced from Dai et al.⁶⁷

On the other hand ROS are highly potent reduced forms of molecular oxygen, which are produced through catalytic means.⁶⁶ Figure 1-6 outlines how ROS can be produced through the photoexcitation of an electron.⁶⁷ In this process, the electron can relax directly back to a ground state, emitting a photon, or the electron can undergo relaxation into the photosensitiser's triplet state.⁶⁸ If the photosensitiser is in the triplet state, one of three things can occur:

1. The electron relaxes down to the ground state and phosphorescence occurs.

2. The photosensitiser can undergo a type 1 reaction where the electron is transferred to molecular oxygen to form a superoxide anion (O_2^-), or to a different molecule possibly forming other ROS.
3. The electron relaxes down to the ground state by transferring energy to molecular oxygen (triplet state), forming singlet oxygen (1O_2).

Similar to ions, ROS are capable of attacking cells through a number of pathways.⁶⁹ Superoxide is capable of releasing iron already in the cell, which goes onto damage DNA. Hydrogen peroxide is capable of damaging both DNA and enzymes essential to cell function. Singlet oxygen can kill cells by damaging the inner membrane.⁷⁰ Hydroxyl radicals are capable of destroying phospholipids by inducing lipid peroxidation.⁷¹

While drugs generally have quite specific targets, antimicrobial surface mechanisms generally attack multiple sites through multiple pathways.^{22,72} It is the specificity of drugs that means a single mutation can render them useless while also creating a drug resistant pathogen. Contrary to this, the ability to kill pathogens through multiple pathways at the same time, means that even if a mutation occurs giving the pathogen a resistance at a specific site, it can still be killed through another pathway before it can replicate.⁷³

While pathogen envelopes will be capable of blocking some ROS and metal ions, pathogens cannot simply evolve to block all ROS and metal ions, as they are essential for a cell functionality.^{74,75} Cells do have ROS scavengers and metal ion chelators present to regulate the concentration of both ROS and metal ions.⁷⁶ However, the concentration of both scavenger and chelates will vary from species to species, meaning different pathogens will have different susceptibilities to different antimicrobial surfaces.

1.2 Superhydrophobic surfaces

Superhydrophobic surfaces are surfaces that are water repellent and often biomimetically inspired. Like their naturally occurring counter parts, the properties of superhydrophobic surfaces are influenced by both their SFE and

their surface topography.⁷⁷ Since being reported on by Dettre and Johnson in 1964, the lotus leaf has been a staple inspiration for superhydrophobic surfaces.⁷⁸ The lotus plant combines a low energy waxy layer called the cuticle, with a rough surface caused by topological microstructures. This gives the plant leaves not only superhydrophobic properties but also self-cleaning properties.⁷⁹

Surfaces with superhydrophobic properties could have a number of applications across industries. Superhydrophobic surfaces could have applications as water repellent surfaces, self-cleaning surface, anti-icing surfaces, etc.⁸⁰⁻⁸² While these properties are desired by the textile industry for obvious reasons, these properties are also desired by the energy industry too. As we continue to move away from fossil fuels, the efficiency of renewable energy production must be maximised.

One of the issues with solar cells is that they are often in isolated areas making them tough to maintain. The build-up of water, dirt or ice can massively impact the cells energy production efficiency.⁸³ If a superhydrophobic clear coating could be developed, this would either greatly increase the cell's efficiency, or greatly reduce the cell's maintenance. Similar issues occur with wind turbines in relation to drag, where the build-up of water, dirt or ice can increase drag significantly impacting the turbines energy production efficiency.⁸⁴ Again superhydrophobic surfaces offer ideal properties to solve this issue.

1.2.1 Surface free energy

In order to fully grasp the superhydrophobic properties of a surface, an understanding of the impact SFE has on a surface's interactions with liquids is required. As touched on previously, SFE is the excess energy present at a materials surface in comparison to the bulk material for a solid. Surface free tension (SFT) is the equivalent term when describing liquids. Water has a total SFT of 72.8 mN/m at 20 °C.⁸⁵ Both the SFE and the SFT value can be further broken down into their dispersion force value (e.g. London forces) and their polar force value (e.g. Keesom forces). At 20 °C water has a SFT dispersion

value of 21.8 mN/m and a SFT polar value of 51 mN/m.⁸⁶ These values are important, as even if the total SFE and SFT values are suitable, surfaces may not interact as expected if the polar and dispersion forces are mismatched. Figure 1-7 attempts to explain how two surfaces with the same total SFE value, interact differently with the same liquid.

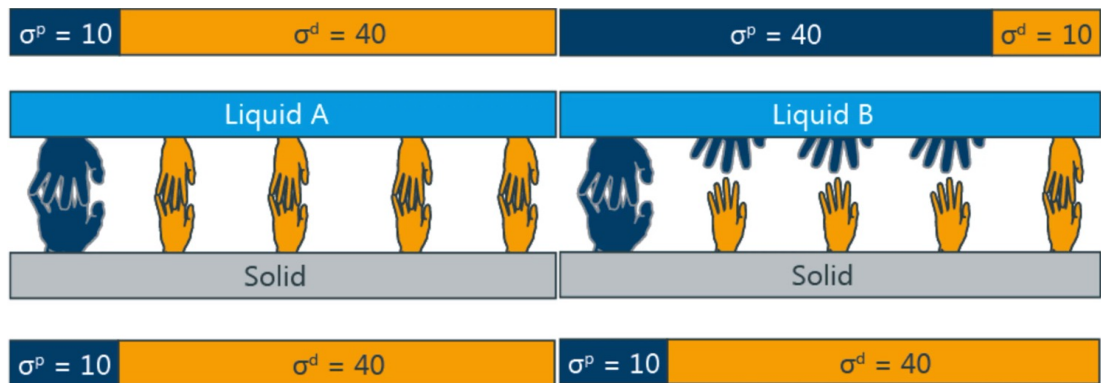


Figure 1-7 A schematic diagram of the influence that the polar (σ^p) and dispersion (σ^d) surface free energy values can have on surfaces with the same total surface free energy value. Reproduced from Jin *et al.*⁸⁷

In 1805 Thomas Young attempted to describe the relationship between the SFE of a surface and its wetting properties with his equation (Equation 1).⁸⁸ At its most basic, the water contact angle (WCA) of a surface can be used to define its wetting properties (Figure 1-8). The wetting properties of a surface can be described as superhydrophilic ($WCA \leq 5^\circ$), hydrophilic ($5^\circ < WCA < 90^\circ$), hydrophobic ($90^\circ < WCA \leq 150^\circ$) and superhydrophobic ($WCA \geq 150^\circ$). Young's equation shows that the contact angle (θ_Y) is inversely proportional to the SFE (σ_{SV}).

Equation 1 Young's Equation

$$\cos \theta_Y = (\sigma_{SV} - \sigma_{SL}) / \sigma_{LV}$$

θ_Y = Young's contact angle

σ_{SV} = SFE of the solid-vapour interface

σ_{SL} = interfacial tension of the solid-liquid interface

σ_{LV} = SFT of the liquid-vapour interface

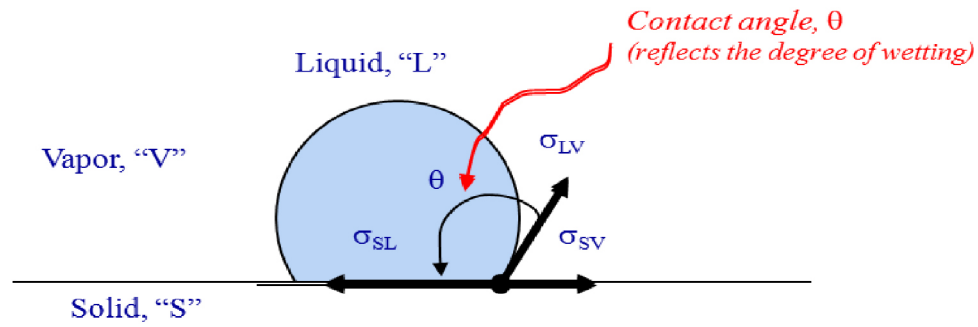


Figure 1-8 A force diagram representing Young's equation and how a contact measurement is taken. Reproduced from Simpson et al.⁸⁹

While Young's equation can be used to calculate the SFE of a sample, some information is required. The SFT values (σ_{LV}) can be gained by using liquids with known SFT values that have been reported in the literature.⁹⁰ Contact angle measurements can be taken using a drop shape analyser (DSA). This leaves two unknown variables: the SFE value and the interfacial tension value (σ_{SL}). However, the Owens, Wendt, Rabel, and Kaelble (OWRK) method can use the DSA measurement of a polar and a nonpolar liquid to determine the SFE of a surface.⁹¹

Equation 2 Owens, Wendt, Rabel, and Kaelble method

$$\sigma_{LV}(1 + \cos \theta^Y) = 2\sqrt{\sigma_{LV}^d \sigma_{SV}^d} + \sqrt{\sigma_{LV}^p \sigma_{SV}^p}$$

$$\sigma_{SV} = \sigma_{SV}^d + \sigma_{SV}^p$$

By using a nonpolar liquid with a polar σ_{LV} of 0, the dispersion σ_{SV} value of the surface can be calculated without knowing the polar σ_{SV} value. Once the dispersion σ_{SV} is known, the polar liquid can be used to determine the polar σ_{SV} by substituting in the surface's dispersion σ_{SV} value. Once the polar and dispersion σ_{SV} values are known, they can be added together to obtain the total SFE value. This value can then be substituted back into Young's equation to determine the interfacial tension of the solid-liquid interface. However, calculations are only valid for flat surfaces.

1.2.2 Surface roughness

Like SFE, surface roughness is a key factor when determining the wetting properties of a surface. This was realised by Robert Wenzel who in 1936 advanced Young's equation with his own model to account for a roughness factor (Equation 3).⁹² The roughness factor was simple the actual surface area, divided by the planar surface area. However, the Wenzel model does not account for air that may be trapped in between the liquid and the surface. It would be 8 years later when Drs A.B.D Cassie and S. Baxter would introduce a model that did account for this (Equation 4).⁹³

Equation 3 Wenzel model

$$\cos \theta_W = r \cos \theta_Y$$

θ_W = Wenzel's contact angle

r = the roughness factor

Equation 4 Cassie-Baxter model

$$\cos \theta_C = \Phi_S \cos \theta_Y + \Phi_S - 1$$

θ_C = Cassie-Baxter contact angle

Φ_S = the fraction of material in contact with the droplet

Figure 1-9 displays a water droplet on a surface using both the Wenzel and the Cassie-Baxter models. In reality, both of these states occur, as well as states somewhere in between. These states can be determined using the intermediate model (Equation 5).⁷⁷ When in a Cassie-Baxter state, droplets will roll across a surface. In a Wenzel state, droplets appear sticky and will slide across a surface. In the intermediate state, droplets will be similar and will also slide across a surface, just at a greater speed, due to reduced drag on the surface.

Equation 5 Intermediate model

$$\cos \theta_r^{CW} = \Phi_S r \cos \theta_Y + \Phi_S - 1$$

θ_r^{CW} = the apparent contact angle

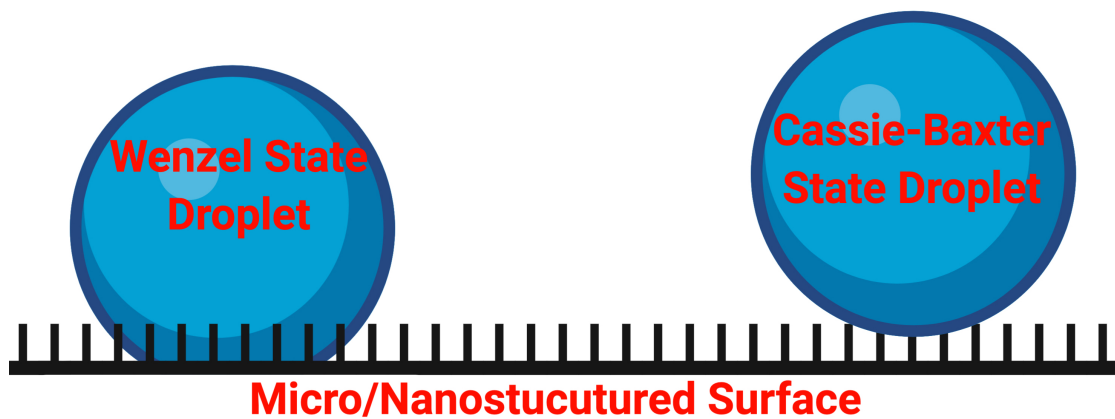


Figure 1-9 Two possible surface-droplet interactions. Wenzel state where the droplet is in full contact with the surface it is resting on (left). The Cassie-Baxter state where the droplet sits on a layer of air trapped between the surface structures.

1.2.3 Applications of superhydrophobic surfaces

Self-cleaning surfaces are surfaces that are capable of removing unadhered dirt from its surface when exposed to water. Surfaces with Cassie-Baxter modelled wetting are generally preferred for self-cleaning properties as the rolling water droplets are more capable of picking up dirt off a surface than sliding droplets.⁹⁴ Not only this, but surfaces with a Cassie-Baxter modelled wetting are more likely to have a lower SFE than surfaces with Wenzel modelled wetting.⁹⁵ This means there is less dispersion and polar forces adhering dirt to the surface.

Icephobic surfaces are surfaces that diminish the hazards associated with icing. For a surface to have icephobic properties it is required to perform at least one of the following tasks: repel incoming water, lower ice-solid adhesion strength, or delay the nucleation of ice.⁹⁶ The ability to repel incoming water is inherent to superhydrophobic surfaces. When the temperature drops below freezing, ice cannot form on a surface if there is no water. This means superhydrophobic surfaces can avoid icing over when the temperature drops below freezing, where the water on other surfaces will quickly begin to freeze.

As water transitions to ice, it undergoes a change to its SFE. At 0 °C water has a SFT of 75.6 mN/m, with 52.3 mN/m attributed to polar SFT and 23.3 mN/m attributed to dispersion SFT.⁹⁷ Comparatively, ice at 0 °C has a raised

total SFE of 106.0 mN/m, however the breakdown of the polar and dispersion SFE is far more conflicting to the water values. Unlike water, the dispersion SFE is dominant at the surface of ice with a value of 94.6 mN/m, compared to the much lower polar SFE, which has a value of 11.4 mN/m. This reversal in the dominant fraction of the SFE means that a superhydrophobic surface may not necessarily have a low adhesion to ice (Figure 1-7). This also means that superhydrophobic properties are not a required preface to low ice adhesion surfaces.

Surfaces with Cassie-Baxter modelled wetting are able to take advantage of their superhydrophobic properties to delay the nucleation of ice. It is the ability of Cassie-Baxter modelled surfaces to trap air between the surface and the water droplet that reduces the contact area between the droplet and the surface (Figure 1-9). It is due to the presence of these air pockets that there is a reduced heat transfer between the surface and the droplet, and also a reduced chance for heterogeneous nucleation to occur at the droplet-surface interface where the activation energy is lower.^{98,99} While homogeneous nucleation may still begin regardless of the surface, has a higher nucleation barrier, so occurs at lower temperatures.¹⁰⁰

Superhydrophobic surfaces can also operate as antimicrobial surfaces, or antimicrobial surfaces can be modified to be superhydrophobic.^{101,102} These dual-functional surfaces can occur naturally and are of massive importance to some fauna and flora. Winged insects are an excellent example of animals that have evolved dual-functional surfaces on their wings.¹⁰³⁻¹⁰⁵ Due to the small size of these animals, the ability for their wings to repel water, avoid microbial contamination, and to self-clean are essential for maintaining their functionality.^{62,106} Insect wings achieve these dual-function surfaces through nanostructured surfaces, with low SFE, that are physically able to repel or rupture microbes, similar to surfaces seen in Figure 1-5. Biomimetic surfaces inspired by these insect wings have been fabricated in labs using chemical vapour deposition and lithography techniques.^{107,108}

While these biomimetic surfaces are innately dual-functional surfaces, other dual-functional surfaces have been created by using additives to give either superhydrophobic surfaces antimicrobial properties, or antimicrobial surfaces superhydrophobic surfaces. Previous work has shown that a superhydrophobic surface could be made antimicrobial through the addition of lysozyme (an enzyme that breaks down cell walls) to fluorosilane surfaces.¹⁰⁹ In another work, a copper antimicrobial surface was made superhydrophobic by electroplating through a solution containing stearic acid.¹¹⁰ When using additives to impart additional properties to a surface, care must be taken not to interfere with inherent desirable properties. This may occur if the additive alters a surface's SFE, or if an additive acts as a chelate or ROS scavenger.

1.3 Polymers

Polymers are arguably the most versatile materials on the planet. While they can be inorganic, the majority of polymers are carbon based.¹¹¹ Polymers are long-chained molecules that are made up of shorter repeating units called monomers.¹¹² In industry, polymers can be broken into five subcategories: rubbers, plastics, coatings, adhesive, and fibres.¹¹³ Although many polymers are naturally occurring materials, many of these are now synthesised due to convenience or cost.¹¹⁴ There are other polymers which do not occur in nature, and have been synthesised by scientists due to their unique properties.¹¹⁵

Perfluorocarbons are one such group of polymers that do not occur in nature. Perfluoro chemicals can be produced by simply fluorinating carbon via various substitution patterns.¹¹⁶ Once synthesised, the carbon fluorine bond is one of the strongest molecular single bonds.¹¹⁷ This means perfluoro chemicals have some of the lowest SFE of any materials, providing it with chemically inert and superhydrophobic properties.¹¹⁸ The use of perfluoro chemical coatings and plastics for non-stick and waterproofing applications has led to Teflon (polytetrafluoroethylene) becoming one of the most recognisable materials globally. However, recent concerns about the impact of Teflon on the environment and human health means that industries are now looking to move away from perfluorocarbons.^{119–121}

Saturated fatty acids (long chain carboxylic acids) are chemicals of interest when considering possible replacements for perfluorocarbons. Compared to perfluorocarbons, fatty acids are relatively innocuous and found in many foods, meaning comparatively they are of minimal risk to human health.¹²² Unlike perfluoro chemicals, which are extremely hard to break down, have been nicknamed forever chemicals, and have a detrimental impact on the environment, fatty acids have minimal to no impact on the environments and can be readily degraded into nutrients.^{120,121,123} While fatty acids do not have SFE quite as low as perfluoro chemicals, their minimal negative impact means they show promise for low SFE applications.¹²⁴

While fatty acids have desirable SFE, they are not polymers, so lack many of their desirable properties required for coatings and plastics. Instead, fatty acids can be used to functionalise base polymers with more desirable inherent properties, so the base polymer will be able to express superhydrophobic properties. This is not only true of fatty acids, other additives can also be incorporated into polymers so that the polymer can express the desired properties.¹²⁵ This technique has been used to make plastics: conductive, antimicrobial, etc.^{126–128}

Polyvinyl chloride (PVC), along with polyethylene and polypropylene are the most produced polymers in the world.¹²⁹ PVC is a plastic produced through suspension polymerisation, where liquid vinyl chloride is reacted in an aqueous solution (Figure 1-10). Once synthesised, there are a number of manufacturing techniques that can be used to form PVC products, including extrusion, injection, and compression moulding.¹³⁰ Due to PVC's versatility and use across the wall cladding, flooring, and healthcare industries, it is an ideal touch surface to target for modification.^{131–133}

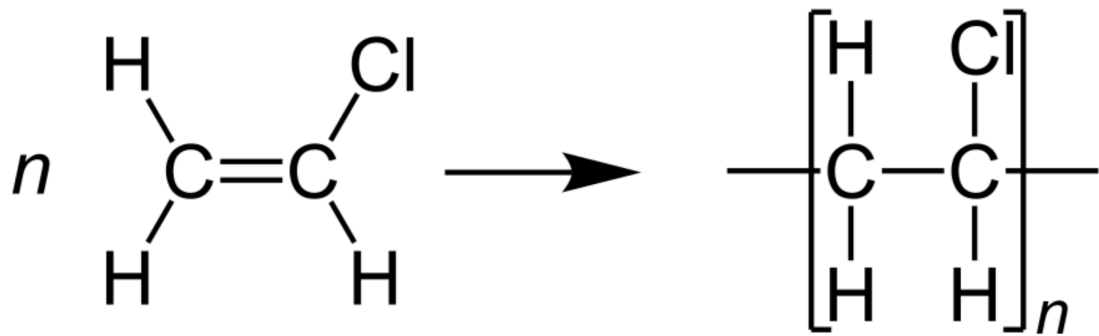


Figure 1-10 Vinyl chloride polymerises to polyvinyl chloride polymer

Although polymer plastic touch surfaces can be manufactured and put in places of high traffic, this would require the replacement of already in place touch surfaces. Polymer coatings on the other hand can be used to modify already in place touch surfaces. Polyurethane (Figure 1-11) and epoxy (Figure 1-12) are two polymers of interest when considering this concept. Unlike PVC, the synthesis of polyurethane and epoxy are far less defined and can be made up of a number of starting materials, using a number of techniques.^{134,135} Depending on how they are synthesised, and what starting materials are used, liquid polymers can be obtained. These coating can then be applied where required, before being cured. Curing is the process by which the crosslinks occur between polymer molecules, forming a solid.¹³⁶ There are a number of methods by which polymer curing can be triggered, with the addition of a curing agent or the removal of a solvent arguably the simplest.¹³⁷

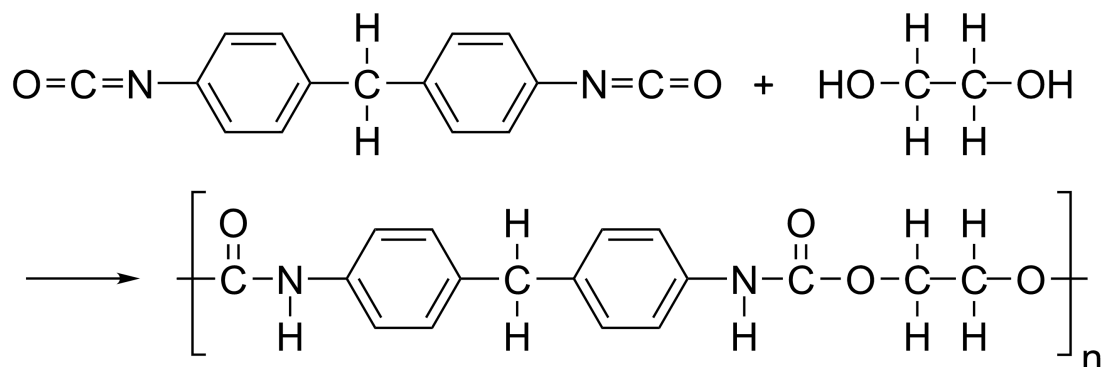


Figure 1-11 Polyurethane synthesised through the reaction of di-isocyanate and polyol

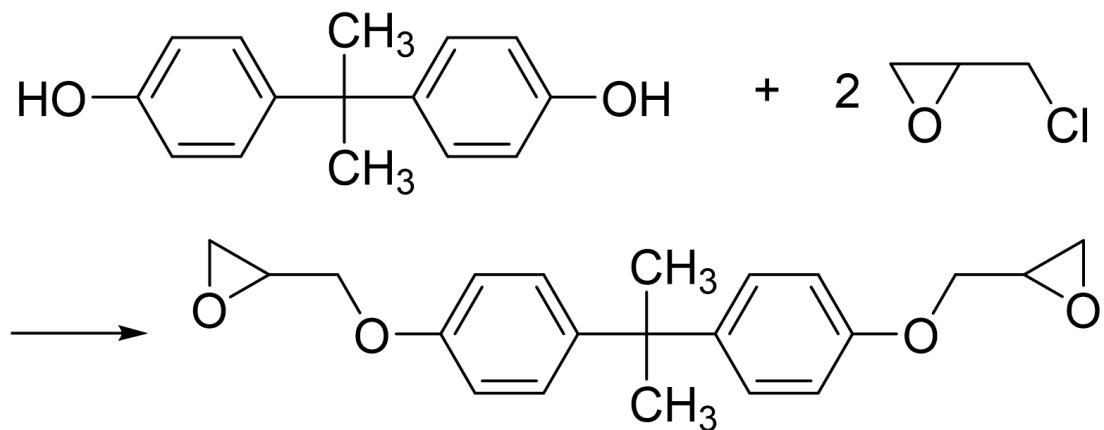


Figure 1-12 Epoxy synthesised through the reaction of bisphenol-A and epichlorohydrin

Paints are a subcategory of polymer coatings, with latex based paints being the most popular. Latex is a broad term used to describe a water-borne dispersion of polymer particles, which may be naturally occurring and obtained from trees, or can be made synthetically.¹³⁸ Latex monomers must be able to polymerise through emulsion polymerisation. Emulsion polymerisation requires the emulsification of one or more monomer in the presence of a surfactant, which stabilises the latex and reduces the size of monomer particles.¹³⁹ The polymerisation is then triggered by an initiator that generates free radicals, which drives the monomer reaction and allows for polymer particles to form in the suspension. Common monomers include acrylates, methacrylates, styrenes, and vinyl esters (Figure 1-13).¹⁴⁰

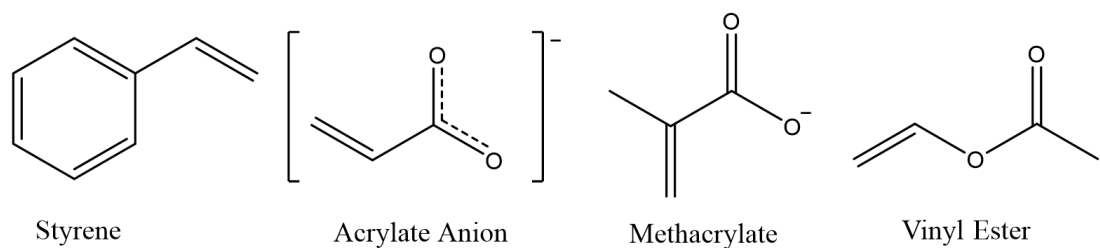


Figure 1-13 Common latex monomers

1.4 Aims

This thesis is broken into three distinctive experimental chapters, followed by a chapter outlining some of the concepts currently being worked on, as well as future work. Each experimental chapter will outline: the aim of the experiments, review the related literature, outline the experimental method, and discuss the results. The first chapter will take a look at antimicrobial touch surfaces and the methodologies required to test them. The second chapter will investigate superhydrophobic surfaces, their properties, and some of the characteristics associated with the surfaces. The last experimental chapter brings together the first two, with the antimicrobial properties of superhydrophobic surfaces investigated, while also proceeding with some advanced characterisation techniques.

2 The Production and Initial Testing of an Economically Viable Antimicrobial Surface

2.1 Aims

In the introduction it has been outlined how antimicrobial surfaces may help to stem the spread of pathogens. The aim of the experiments in this chapter was to develop a polymer using inexpensive raw materials, establish a manufacturing technique, and to test whether the polymer had antimicrobial properties. This work required the production of polymer surfaces, followed by functional testing to establish the surface's chemical, physical, and antimicrobial properties.

2.2 Background

The concept of these experiments was brought to us by our industrial partner, Altro Ltd. The goal was to produce an antimicrobial polymer that could be used for wall cladding and other touch surfaces. This also came with a supply of their PVC that is used to manufacture interior wall cladding, which could be used as the base polymer for these experiments. With PVC being so versatile, it has previously been functionalised by others with antimicrobial properties, for many different potential applications. This has been done through a number of techniques, and for applications across a number of industries, including PPE, medical device, food packaging, etc.^{63,141,142}

While there are a number of different methods to measuring antimicrobial surfaces, dilution and diffusion methods are the most popular.¹⁴³ Disk diffusion tests were first developed in the 1940s and are routinely used for antimicrobial susceptibility testing. This method required the inoculation of an agar plate with a microbe of interest at a given concentration. Next a sample of a certain size is placed on the agar plate so that its antimicrobial properties can be measured. The plate is then incubated for a given amount of time under specific conditions. Once completed, the inhibition zone around the sample is

measured. While disk diffusion testing is relatively simple and cheap, and inhibition zones are good for determining qualitative results of microbial susceptibility, quantitatively there are more accurate methods for determining antimicrobial activity.¹⁴⁴

Dilution methods, while more meticulous and expensive, can be used to carry out accurate quantitative measurements.^{143,144} To measure antimicrobial properties through a dilution method, a sample is exposed to a known amount of a microbial inoculum, of a known concentration, for a period of time. The inoculum is then recovered and is diluted to obtain a viable count of surviving bacteria. Once the incubation period has elapsed, the agar plates are inspected for colony forming units (CFU). By assuming that each CFU represents a single bacterium from the original culture, CFU can be counted to accurately determine microbial concentration.¹⁴⁵

Braga et al. developed antimicrobial films for use as food packaging, by incorporating silver nanoparticles into PVC.⁶³ Films were formed through a solvent cast method which simply adds all the components to a solvent and pours it into a cast. This led to the testing of PVC films with silver concentrations of 1-8%. Visually, a significant change occurred for films with a silver concentration $\geq 4\%$. These films transitioned from clear to opaque, while SEM imaging also showed the films appeared to be significantly different structurally. It was suggested that the higher concentration of silver may have caused the agglomeration of particles, which in turn may have compromised the physical properties of the films. However, the higher concentration's poor antimicrobial results made this irrelevant.

A disk diffusion method was used to assess the antimicrobial activity of the films against two fungi (*Aspergillus niger* and *Fusarium solani*) and Gram-positive bacterium (*Bacillus subtilis*). Interestingly, neither the samples with 4% nor 8% silver concentrations displayed any antimicrobial activity, while the samples with lower concentrations did against all the microbes to varying degrees. It was speculated that at the higher concentrations the agglomeration of particles may have reduced the diffusion of silver out of the

film, or to its surface. As no Gram-negative bacteria were included in the experiment, the films' antimicrobial properties against Gram-negative bacteria remain unknown. However, this experiment did show that silver incorporated PVC can produce antimicrobial properties against Gram-positive bacteria and fungi, while also showing that higher concentrations of the functionalising agent (silver) is not always better.

Widmer et al. investigated the impact of a commercially available silver incorporated PVC foil (PURZON060B produced by Hexis) in a hospital setting.¹⁴⁶ The film being investigated had a 2% silver concentration and was applied to high-touch surfaces in patient rooms. The films were sampled twice weekly, with matrix-assisted laser desorption/ionisation – time of flight (MALDI-TOF) used to identify suspected pathogens. The results showed that despite daily cleaning of all surfaces, there was a 1.8 log reduction in the number of pathogens present on the foil, when compared to the controls. Overall, 67% of the foil samples were free from pathogens. However, none of the pathogens investigated more comprehensively were Gram-negative, with the paper instead focusing on Gram-positive bacteria. The results did again show silver incorporated PVC to be a viable antimicrobial surface in some circumstances, with the foils proving to be still viable after 6 months.

While there was a large number of other papers conducting qualitative testing against metal incorporated PVCs, there were little to none to be found conducting quantitative testing. One paper of note was a paper by *Gaballah et al.* who incorporated silver or copper into PVC modified with ethyl 2-aminothiazole-4-carboxylate.¹⁴⁷ This was of particular interest as they showed qualitatively that their surface could not only kill fungi and Gram-positive bacteria, but it could also kill Gram-negative bacteria.

Shifting the emphasis towards the possible metal options for a composite, the antimicrobial properties of metals and metal-incorporated polymers were investigated. Continuing with silver, Ag/TiN films have been shown to have antimicrobial properties against Gram-negative bacteria. *Zhao et al.* used ion beam assisted deposition (IBAD) to form multilayer Ag/TiN films, which were

shown to kill 99% of a Gram-negative bacterium, *Escherichia coli* (*E. coli*).¹⁴⁸ *Maharubin et al.* showed an ~1 log reduction in a Gram-positive bacterium, *Staphylococcus aureus* (*S. aureus*) attachment to a PVC surface when it was coated in silver nanoparticles, and a further ~0.5 log reduction when ZnO nanowire was used in addition to the silver nanoparticles.¹⁴⁹

Copper's antimicrobial properties are well known, with copper piping being used for drinking water distribution for this reason.¹⁵⁰ Copper has been shown to be effective against Gram-positive and Gram-negative bacteria, as well as against fungi.¹⁵¹ *Bogdanović et al.* showed that at concentrations of 32 ppm, after 2 h copper nanoparticles were able to kill: 99.9% of *E. coli*, 98% of *S. aureus*, and 99.9% of *Candida albicans* (*C. albicans*).¹⁵² *Hassan et al.* found similar results when producing thin films by aerosol-assisted chemical vapour deposition, with their results showing >99% kill against *E. coli* and *S. aureus* after 60 min.¹⁵³

ZnO is another prominent antimicrobial reagent in the literature.¹⁵⁴ While ZnO does have innate antimicrobial activity, it also has the ability to produce ROS when irradiated with UV light. *Visnapuu et al.* coated surfaces with a film containing 5wt% ZnO nanoparticles via spin coating.¹⁵⁵ They then tested the antimicrobial properties of their surface against *E. coli*, *S. aureus*, and *C. albicans* both in the absence of light, and under UVA irradiation. Under dark conditions it was found that there was a <1 log reduction in most cases when compared to a glass substrate. The exception being a 1-2 log reduction in *S. aureus* when exposed to the ZnO coated surface. However, when the surface was irradiated by UVA, both the *E. coli* and *S. aureus* were reduced by at least 99.9%, while there was still a <1 log reduction in *C. albicans*.

Kanmani et al. prepared films by incorporating ZnO nanoparticles into biopolymers.¹⁵⁶ These films included a carboxymethyl cellulosic film, an agar film, and a carrageenan film, all loaded with ZnO nanoparticles and produced through a solvent cast method. The films were then tested against *E. coli* and Gram-positive bacterium, *Listeria monocytogenes* (*L. monocytogenes*). Their results showed that when compared to the initial inoculum, all three films had

similar antimicrobial properties, with a 2-3 log reduction in *E. coli* and a 4-5 log reduction in *L. monocytogenes* after 12 h.

Finally, *Noimark et al.* again investigated both the ZnO's innate antimicrobial activity, as well as its ability to produce ROS under irradiation.¹⁵⁷ A swell-encapsulation-shrink method was used to incorporate ZnO nanoparticles into silicone, along with a crystal violet dye. The crystal violet dye was incorporated into the surfaces in order to dye-sensitise the ZnO, reducing its apparent bandgap, giving it the ability to produce ROS under white light conditions. As samples were only tested against *S. aureus* for 1 h, it is hard to get a full indication of all the surfaces antimicrobial properties. However, during these tests, under both dark conditions and irradiation, minimal antimicrobial activity was produced by the ZnO incorporated silicone. Yet, when the crystal violet ZnO incorporated silicone was irradiated with white light, there was a 3.36 log reduction in *S. aureus*.

When analysing the samples against *E. coli* the maximum exposure time was increased to 6 h, giving a much better indication of the surface's antimicrobial properties. Under dark conditions the ZnO incorporated silicone produced a 1.41 log reduction of *E. coli*, with it also producing a 1.9 log reduction over the same period of time, while being irradiated by white light. However, while being irradiated by white light, the crystal violet ZnO incorporated silicone reduced *E. coli* 99.99%, to below the detection limit of 100 CFU.

While there was a minimal information available about the antimicrobial properties of ZnO incorporated PVC, there was no adverse reasoning in the literature as why this combination could not produce a successful antimicrobial surface. With this in mind, PVC was selected as the base polymer for this experiment, as it is already used for the surface's required applications.¹²⁹ ZnO was selected as the antimicrobial agent for the experiment, as it has been shown to have antimicrobial activity, is a considerably cheaper raw material than silver or copper and may be able to offer improved functionality through dye-sensitisation in the future.¹⁵⁷

2.3 Experimental

Prior to commencing the experiments, the key materials were selected, as was the manufacturing technique, and an emphasis was put on the economic viability of the product. Although ZnO and PVC had not been combined previously in the literature, they were selected as the raw materials due to their low cost, commercial viability, and potential. Compression moulding was selected as the manufacturing technique, as it is commonly used, and can be easily scaled for mass production. Once viable samples were produced, analysis was run to characterise the surfaces' properties. A dilution method of antimicrobial testing was adapted from *Sehmi et al.* so quantitative antimicrobial results could be obtained.¹⁵⁸

2.3.1 Materials

An industrial PVC powder was supplied by the project's industrial partner (Altro Ltd). 100 nm ZnO nanoparticles, catalase, L-histidine, mannitol, and superoxide dismutase were purchased from Sigma-Aldrich. Mannitol salt agar, MacConkey agar, brain heart infusion broth (BHI), and phosphate buffered saline solution (PBS) were purchased from Oxoid Ltd, as was.

2.3.2 The manufacture of ZnO incorporated PVC

The first stage of the experiment was the production of samples. The samples were prepared by measuring out PVC and ZnO in accordance with Table 2-1. Next a uniform mixture was obtained by transferring the solids to a mortar and pestle and mixing for 120 s until a uniform blend was produced.

Material	0%	1%	2%	5%	10%
PVC	4.00 g	3.96 g	3.92 g	3.80 g	3.60 g
ZnO	0.00 g	0.04 g	0.08 g	0.20 g	0.40 g

Table 2-1 The composition of ZnO incorporated PVC samples

A stainless-steel mould (Figure 2-1) was made to manufacture the samples. An inert and thermally stable Melinex[®] 726 polyester) was used in the process to try and avoid sample sticking to the system, as well as to help reduce contamination. Figure 2-2 outlines how samples were formed by placing the mould on top of a stainless-steel plate of the same size, before adding ~1 g of a blend to each cavity in the mould. Another top plate was then carefully placed on the heaped piles of ZnO/PVC blend. The entire system was then transferred into a compression moulding press, which was preheated to 160-220 °C.

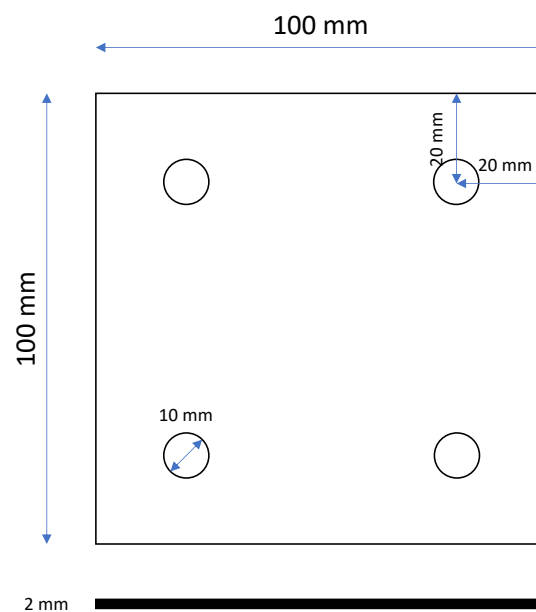


Figure 2-1 Stainless steel mould

Once the system was in place, a pressure of 100-300 psi was applied for 8-15 min. Once the time had expired, the pressure was released, the mould was removed, before being left to cool on the bench for 5 min. Finally, a rod with a diameter of just under 10 mm, was used to force the disks out of the cavities, resulting in samples \varnothing 10 mm x 2 mm (Figure 2-3).

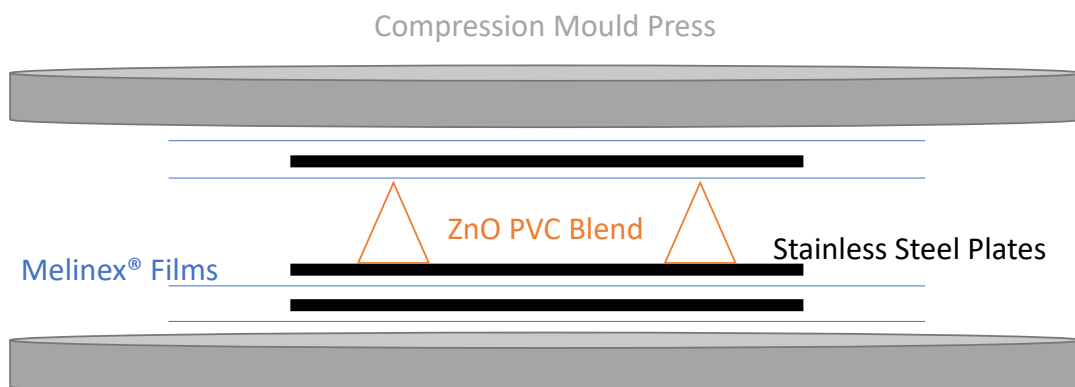


Figure 2-2 Compression moulding setup

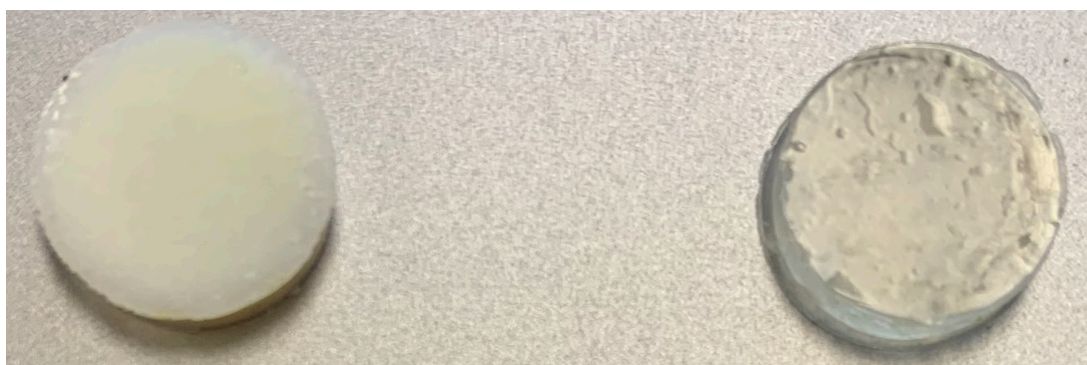


Figure 2-3 Compression mould formed samples of pure PVC (right) and PVC containing 5% ZnO (left)

2.3.3 Material characterisation and properties

UV-Vis (ultraviolet-visible) absorption and reflectance spectra were measured using a Shimadzu UV-2700 UV-Vis spectrophotometer. All spectra were measured within a wavelength range of 800-200 nm, with the 600-220 nm area of interest plotted.

Infrared transmission spectra were obtained using a Brüker Alpha Fourier transform infrared (FT-IR) spectrometer with a platinum ATR attachment. All spectra were obtained from the accumulation of 16 scans per sample, under an analysis range of 400-4000 cm^{-1} .

Topographic surface imaging was completed using a JEOL JSM-6700F field emission scanning electron microscope (SEM). Samples were coated with either gold or carbon prior to analysis and were analysed with an acceleration voltage of 10 kV.

Using 15 keV, an Oxford Instruments X-Act detector was used for Energy-dispersive X-ray (EDX) spectroscopy. EDX was used to both, perform elemental analysis, and to map the distribution of specific elements at both the surface and near surface of the polymer samples.

Elemental analysis was then run on the samples using a Panalytical Epsilon 4 X-ray Fluorimeter (XRF).

2.3.4 Basic antimicrobial testing

The antimicrobial properties of the samples were tested using a method adapted from *Sehmi et al.*¹⁵⁸ Basic testing used a Gram-negative bacterium, *E. coli* ATCC 25922 and a Gram-positive bacterium *S. aureus* 8325-4.¹⁵⁹ Selective agar plates were used to grow CFU, with mannitol salt agar (MSA) used to grow *S. aureus*, and MacConkey agar used for *E. coli*. Each experiment was performed in triplicate using two technical replicates in each experiment.

Bacteria were maintained as frozen stocks in glycerol broth at -80°C and cultured on either MSA (for *S. aureus*) or MacConkey agar (for *E. coli*). 10 ml BHI broths were then inoculated with a single colony of each bacterium and incubated in air at 37 °C for 18 h at 200 rpm until the culture reached approximately 10⁹ CFU/ml. UV-Vis spectrophotometry was then used to measure the broths absorbance at 600 nm, to confirm the 10⁹ CFU/ml approximation. This was later confirmed by plating dilutions and ensuring the results were consistent with an initial concentration of ~10 CFU/ml.

Next, to halt cell growth, the cells were removed from the BHI broth by forming a bacterial pellet through centrifugation (4000 rpm, 5 min, 20 °C) and decanting off the liquid. The cells were then washed by resuspending the cells in 10 ml of PBS by vortexing for 10 s, before reforming a pellet and decanting off the liquid. The wash step was repeated a total of three times before the cells were finally resuspended in 10 ml of PBS using a vortex. A final inoculum was

obtained through a x1000 dilution of the washed bacterial suspension, producing an inoculum of $\sim 10^6$ CFU/ml.

Humidity chambers were set up as shown in Figure 2-4. This was done by firstly adding two sheets of filter paper to a petri dish, followed by placing a flame sterilised microscope slide on top of two sterile toothpicks. Technical replicate samples were then placed in the humidity chamber, with the flame sterilised microscope slide acting as a sample stage. Each sample was then inoculated with 25 μ l of bacterial suspension ($\sim 10^6$ CFU/ml) and left for a specific period of time under specific lighting conditions.

Once the required exposure time had passed, the surviving bacteria were recovered by removing the sample from the humidity chamber and transferring it to a sample tube containing 450 μ l of PBS. The tubes were then vortexed for 20 s to ensure all of the viable bacteria were removed from the sample surface into the solution. Two measures of 200 μ l of this suspension were then added to two zero wells of a 96 well plate before undergoing multiple 10-fold dilutions. These dilutions were then plated on the corresponding selective agar plates, before being left to incubate at 37 °C for 24-48 h. Once viable colonies were visually identifiable, the plates were counted for colonies, and the number of viable bacteria was calculated.

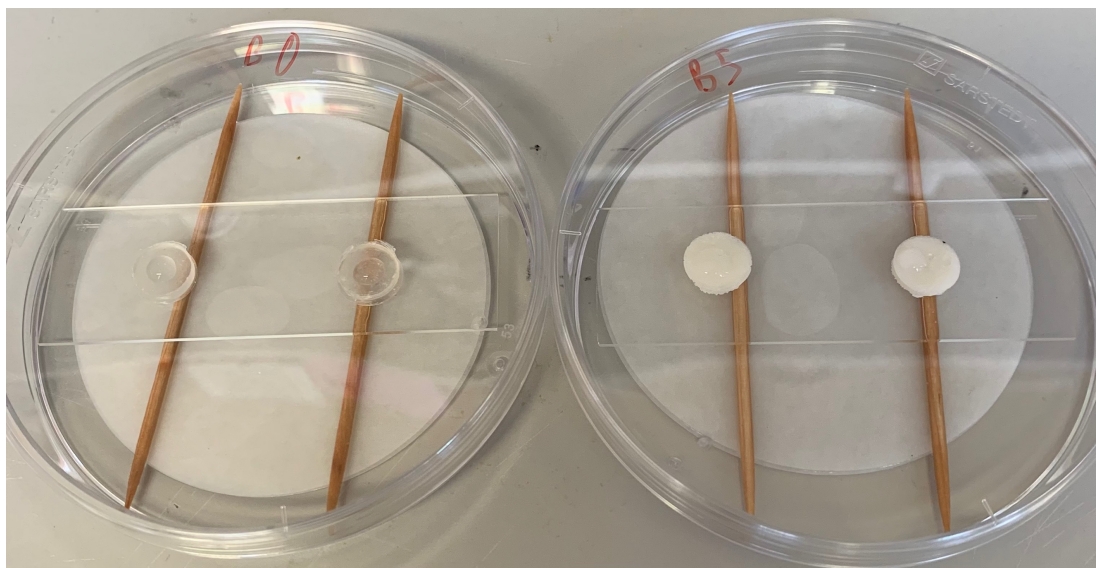


Figure 2-4 Humidity chambers containing 0% ZnO samples (left) and 5% ZnO samples (right)

2.3.5 The identification of a surfaces antimicrobial ROS

By adapting work from *Hwang et al.*¹⁶⁰ it is possible to determine if firstly, ROS (reactive oxygen species) were responsible for the observed bactericidal activity, and if so, which species. This was done by inoculating samples exactly as described in section 2.3.4 except that the inoculum was $\sim 10^5$ CFU/ml and was applied to the materials in the presence or absence of various ROS scavengers and quenchers. This method required a total of five inocula, including a control, to be made up in PBS solutions using *E. coli* ATCC 25922, at a concentration of $\sim 10^5$ CFU/ml. Apart from the control, the four other inocula were made up containing one of the following: 6.5 mM of L-histidine to quench singlet oxygen, ~ 35 unit/ml of catalase to remove hydrogen peroxide, 110 mM of mannitol to eliminate hydroxyl radicals, and ~ 30 unit/ml of superoxide dismutase to scavenge superoxide.

2.3.6 Determining the impact carotenoid levels have on a surface's antimicrobial properties

This experiment was designed to determine if bacterial carotenoids were impacting the surfaces antimicrobial properties. This experiment was done by inoculating samples exactly as described in section 2.3.4. The strains used in this experiment were *Staphylococcus aureus* 8325-4,¹⁵⁹ *Staphylococcus aureus* wild-type JE2 (WT),^{161,162} and *Staphylococcus aureus* crtM JE2 (crtM).^{161,162}

2.4 Results and discussion

2.4.1 Sample production

The first stage of this project was to identify the best method for the fabrication of the ZnO incorporated PVC samples. Although methods such as extrusion and injection were considered, it was ultimately decided that compression moulding would be the best method for fabricating the initial samples. As access to a heated compression moulding press was already available, only a

stainless-steel sample mould was required. A simple mould capable of making 4 samples at a time was designed then fabricated by the Mathematical and Physical Sciences workshop.

Once the stainless-steel sample mould had been delivered the next stage was to optimise the fabrication technique. The three main variables in the sample fabrication process were identified as the temperature, pressure, and duration. The first variable to be considered was temperature. Melinex 726 polyester has a melting point of 265 °C, while the compression moulding press has a maximum temperature of 250 °C.¹⁶³ Yet there was a risk the Melinex may melt under increased pressure, during the moulding process. As such, it was decided not to exceed 220 °C, so temperatures of 160, 180, 200, and 220 °C were tested.

Under a pressure of 100 psi, samples were heated for 15 min at the different temperatures. While samples produced at 200 and 220 °C appeared uniform in their texture throughout, the samples produced at lower temperatures did not. Samples produced at the lower temperatures tended to be more brittle, mainly due to defects caused by the PVC blend not melting and remaining as a powder. As the control samples (Figure 2-3) were partially transparent, it could also be visually observed when unmelted powder was present in the samples.

With samples successfully produced at temperatures of 200 °C and 220 °C, the optimisation process moved onto varying the duration of heating. Next samples were produced at both 200 °C and 220 °C under 100 psi of pressure for heating periods of 8, 10, 12, and 15 min. Samples heated for the 15 min were again uniform in texture throughout. Samples heated for 8 min however produced similar defects to earlier samples heated at lower temperatures, with pockets of the powder blend causing defects once more. The best samples were those produced with a heating duration of 10 and 12 min, yet even these samples lacked consistency, and occasionally contained defects due to unmelted powder.

After considering the effect varying the heating duration had on the sample consistency, the last variable was to increase the compression pressure the system was subjected to. This was done with the goal of achieving consistent and uniform samples in a shorter period of time than 15 min. Samples were therefore made under pressures of 200 and 300 psi, while being heated for a period of 10 min, at temperatures of 200 and 220 °C. The resultant samples produced under 300 psi were more consistent than those produced under 200 psi. While samples produced at both 200 and 220 °C were consistent and uniform, the Melinex film occasionally stuck to pieces of the apparatus. As samples could be produced consistently under 300 psi, without significantly impacting the Melinex, it was decided not to explore higher pressures.

Once all things were considered, the optimised production process was to produce samples under 300 psi, at a temperature of 200 °C, with a heating duration of 10 min, and a cooling duration of 5 min, before removing the samples from the mould.

2.4.2 Analysis of optical properties

Initial material characterisation was conducted by FT-IR analysis. FT-IR was chosen as it is quick and easy and can be used to identify some changes to materials or compounds. As the blending process uses a mortar and pestle, the powder is subjected to excess pressure and heat due to friction. Due to energy the pressure and heat may supply to the system, there was a chance that the powder may alter due to degradation, or the components may begin to react with each other, possibly altering the materials properties.¹⁶⁴

The results of this FT-IR analysis can be seen in Figure 2-5. The analysis shows that all peaks in the spectra of the PVC blend can also be identified in either the spectra of the ZnO or the PVC. It was suspected that peaks relating to organozincs, or zinc chlorides could indicate if any alterations were occurring, but as all peaks could be attributed to either of the component spectra, peaks corresponding to these products did not appear to be present. Overall, the FT-IR analysis spectra had the characteristics of mixed powders,

and with no identifiable peaks to the contrary of this. Due to this, it was assumed going forwards that the components did not alter during the blending process.

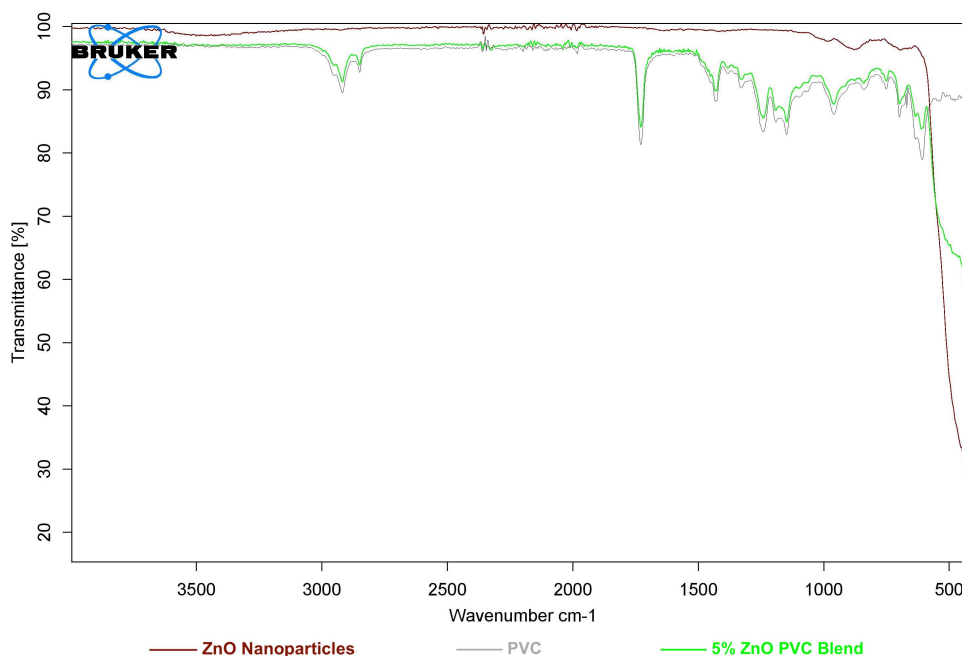


Figure 2-5 FT-IR analysis of PVC (green), 100 nm ZnO nanoparticles (red), and a 5% ZnO PVC blend (grey).

Next the optical properties of the samples and the raw materials were determined using UV-Vis spectroscopy. Analysis was performed with a wavelength range of 220-800 nm, while plotting a 220-600 nm area of interest (Figure 2-6). The spectra for Figure 2-6 were obtained using two methods of UV-Vis spectroscopy: transmission UV-Vis analysis, and reflectance UV-Vis analysis using an integrating sphere.

To perform this analysis, the ZnO nanoparticles were suspended in ethanol at a concentration of 1 mg/ml. Next the nanoparticle solution was transferred to a quartz cuvette, with quartz cuvettes used to ensure good measurements could be taken in the UV region. Using ethanol as the reference sample, transmission UV-Vis was then used to obtain the “Nps In Eth” spectrum in Figure 2-6. The resulting spectrum shows that the λ max was at 380 nm, firmly in the UV region.

Next the integrating sphere was fitted into the instrument to allow for the UV-Vis analysis of opaque samples. Prior to the polymer analysis, the ZnO nanoparticles were again analysed, but this time by dispersing a 2% concentration of the particles in BaSO₄. The ZnO/BaSO₄ blend was then compressed into a sample holder using a glass cylinder and loaded into the integrating sphere. Using pure BaSO₄ as the reference sample, UV-Vis absorption of the nanoparticles was measured with the resulting spectrum displayed in Figure 2-6 (“Nps”).

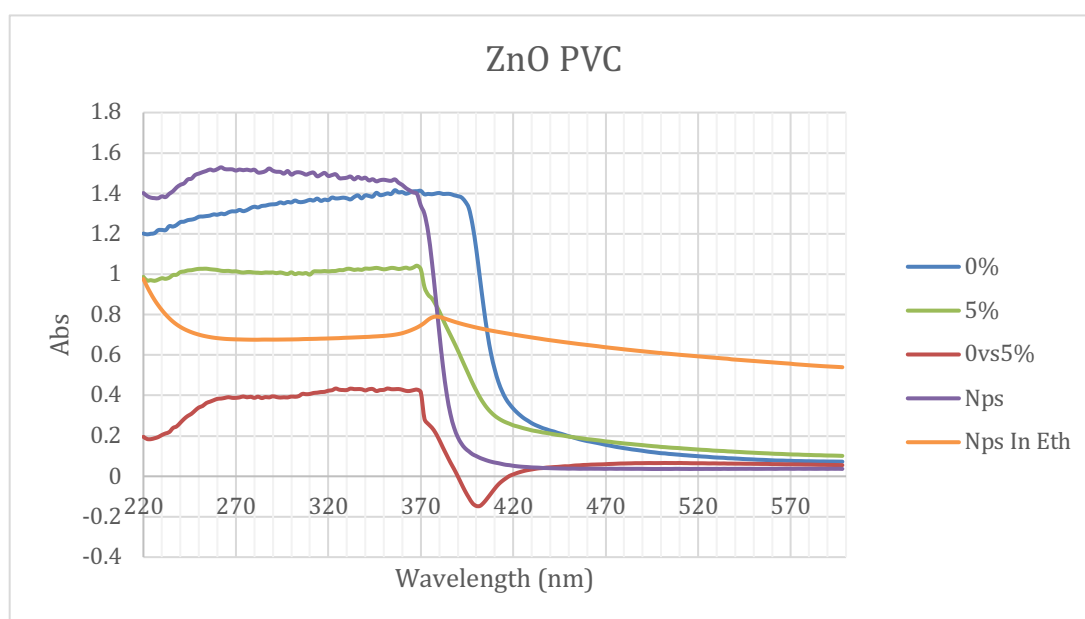


Figure 2-6 UV analysis of nanocomposites, control samples, and the nanoparticles. All spectra were obtained using an integrating sphere unless otherwise stated. 0% spectrum represents a PVC control sample. 5% spectrum represents a ZnO incorporated PVC sample containing 5 wt% ZnO. 0vs5% spectrum represents a ZnO incorporated PVC sample containing 5 wt% ZnO using PVC control sample as a reference. Nps (nanoparticles) spectrum represents 100 nm ZnO nanoparticles, dispersed in BaSO₄. Nps In Eth spectrum represents 100 nm ZnO nanoparticles, dispersed in ethanol, and measured using transmission UV-Vis spectroscopy.

Next, the spectra of the polymer samples were measured. This required the samples to be secured in the holder using the reference material BaSO₄. To do this, the holder needed to be partially packed with BaSO₄. A sample was then fitted in the centre of the sample holder and compressed with the glass rod, so it was held firmly in place, with the sample surface flush with the surface of the holder. A small brush was then used to ensure the sample surface was clean, before it was loaded into the integrating sphere for analysis. Once

loaded, and again using BaSO₄ as a reference sample, UV-Vis absorption measurements of the polymers were taken. This resulted in the “0%” and “5%” spectra in Figure 2-6.

Maintaining the 0% and 5% polymer samples in their sample holders, a final spectrum was measured. The final spectra directly measured the absorbance of the 5% sample against the absorbance of the 0% sample. This was done by fitting the 0% sample into the reference slot of the integrating sphere with the 5% sample loaded into the sample slot. The resulting spectra is labelled “0vs5%” in Figure 2-6.

Analysis of Figure 2-6 provides some insight into the optical properties of the materials and samples analysed. The collection of spectra includes the analysis of the ZnO nanoparticles dispersed in both ethanol and BaSO₄. Unsurprisingly, although the spectra differ due to the different analysis techniques, the ZnO particles showed similar properties in both media, with the “Nps In Eth” spectra having a λ max of ~380 nm. Although ZnO traditionally has an optical absorbance value of ~370 nm, the properties of nanomaterials can vary based upon, among other reasons, the size and shape of the particles, a λ max of ~380 nm, seemed reasonable when comparing to values for ZnO in the literature.^{165–168}

Analysis of the 0% and 5% spectra confirmed the visual observation that the optical properties of the ZnO incorporated PVC samples, and the control samples differed. The control samples absorbance was notably higher when compared to the ZnO. Comparatively, the ZnO incorporated PVC absorbance was significantly blue shifted when compared to the control sample. This was emphasised by the trough present when the ZnO incorporated PVC sample was directly measured against the control sample (“0vs5%”).

The main conclusion from this collection of spectra is that the ZnO incorporated PVC sample’s absorbance, appears to be slightly blue shifted when compared to the ZnO particles. With the λ max of the ZnO nanoparticles already on the border of the visible spectrum at ~380 nm, any blue shift in

optical absorbance will not help with the absorbance of visible light. This would suggest that electrons in the ZnO incorporated PVC samples, will not reached an excited state, when irradiated with visible light.

2.4.3 SEM imaging and elemental analysis

SEM and EDX were used to investigate a number of potential issues associated with the fabrication process of the samples. As the mixing process was relatively crude, there were concerns as to how uniform the PVC/ZnO blend was, and if the samples produced using the blend would have ZnO particles distributed throughout. Another concern was that compression moulding process might not be forming samples free from any major surface defects. SEM and EDX were used to investigate, firstly through visual means, then through elemental analysis.

Figure 2-7 and Figure 2-8 show the imaging of both control samples and ZnO incorporated PVC samples. Visual analysis of the SEM images was able to quickly determine that the samples were free from any major surface defects, although subcutaneous structural defects could not be ruled out. As can be observed in Figure 2-8 two materials, at or near the surface, were visually identifiable. Comparing Figure 2-8 to Figure 2-7, Figure 2-7 appeared far more uniform in colour. With this in mind, it is proposed that the lighter of the two compounds is the ZnO. This proposal would suggest that, while not uniformly distributed across the surface, the ZnO nanoparticles were well distributed across a large amount of the surface.

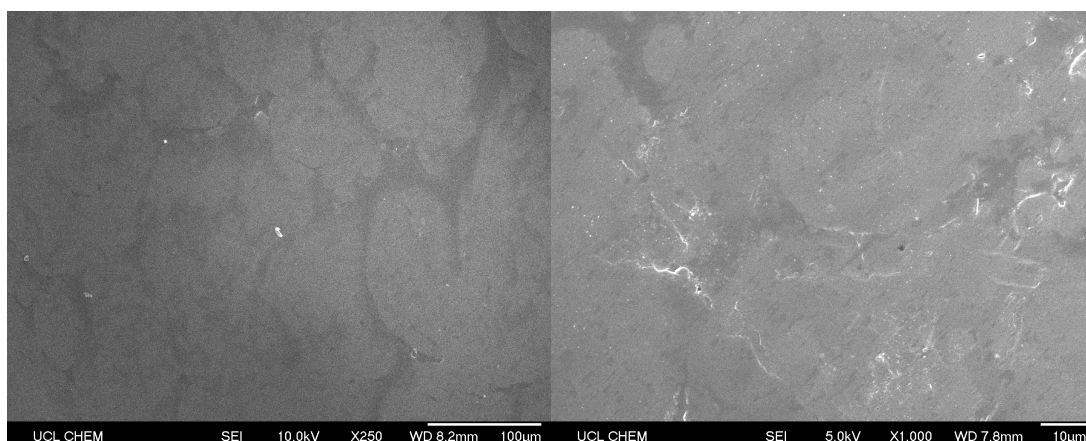


Figure 2-7 SEM imaging of control samples containing 0% ZnO nanoparticles

Following on from the visual analysis, elemental analysis using EDX was performed (Figure 2-9). With a detection limit of ~1000 ppm, qualitative analysis of the control samples was able to detect the main components of PVC, chlorine, and carbon (Figure 1-10). On top of this, oxygen could also be detected, this presence was attributed to oxidation at the surface. Comparatively, qualitative analysis of the ZnO incorporated PVC samples differed only by the presence of the Zn, which can be attributed to the ZnO nanoparticles that were incorporated into the polymer.

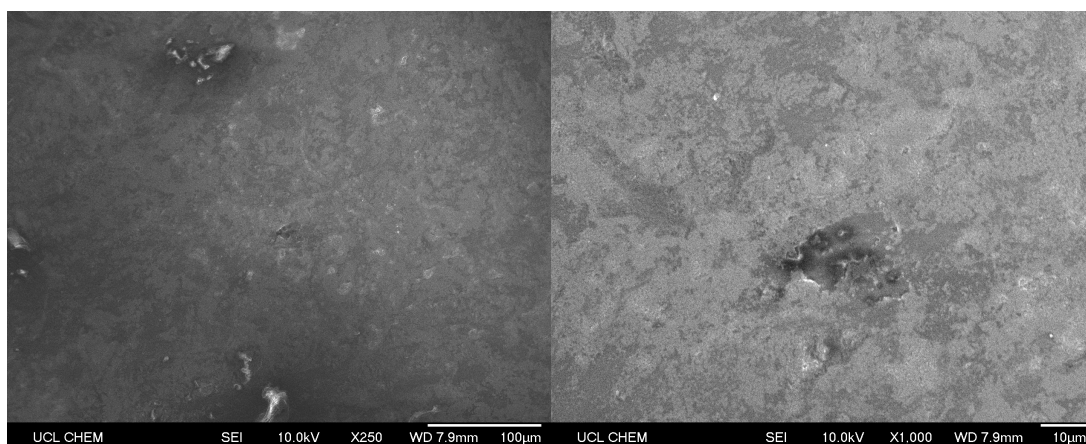


Figure 2-8 SEM imaging of 5% ZnO incorporated PVC samples

Next EDX was used to map the elemental distribution of Zn. This was done in order to corroborate the proposal that the ZnO nanoparticles were well distributed across a large amount of the surface. With a map of the much higher concentrated chlorine present for comparative purposes, Figure 2-10

shows the distribution of Zn across the surface. As hoped the elemental mapping of the Zn substantiates the proposal that the ZnO was well distributed across the surface.

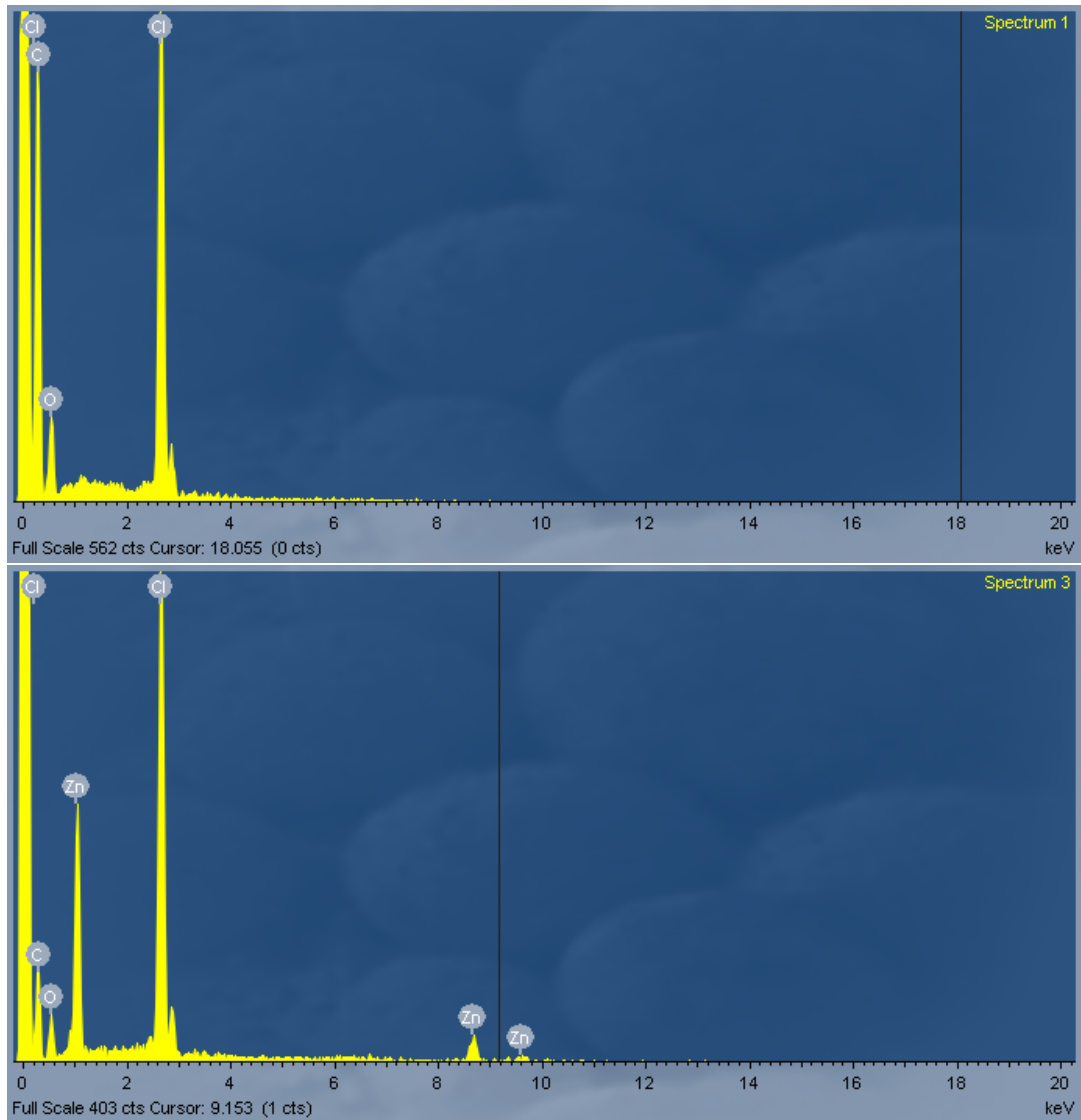


Figure 2-9 (Top) EDX analysis of control samples containing 0% ZnO nanoparticles. (Bottom) EDX analysis of 5% ZnO incorporated PVC samples

Lastly, XRF was used to validate the PVC. Although our industrial partner used and supplied the PVC, they had purchased it from a third party. This meant that the exact PVC composition was unknown. Although EDX has given us some indication, the detection limit of the XRF was ~1000 times greater than the previous EDX analysis. The main objective was to either identify, or rule out, the presence of elements that could interfere with any antimicrobial testing. To evaluate the results, it needed to be realised that % compositions

are proportionate to the detectable elements (atomic number ≥ 11) and cannot detect the considerable amounts of hydrogen, carbon, and oxygen present.

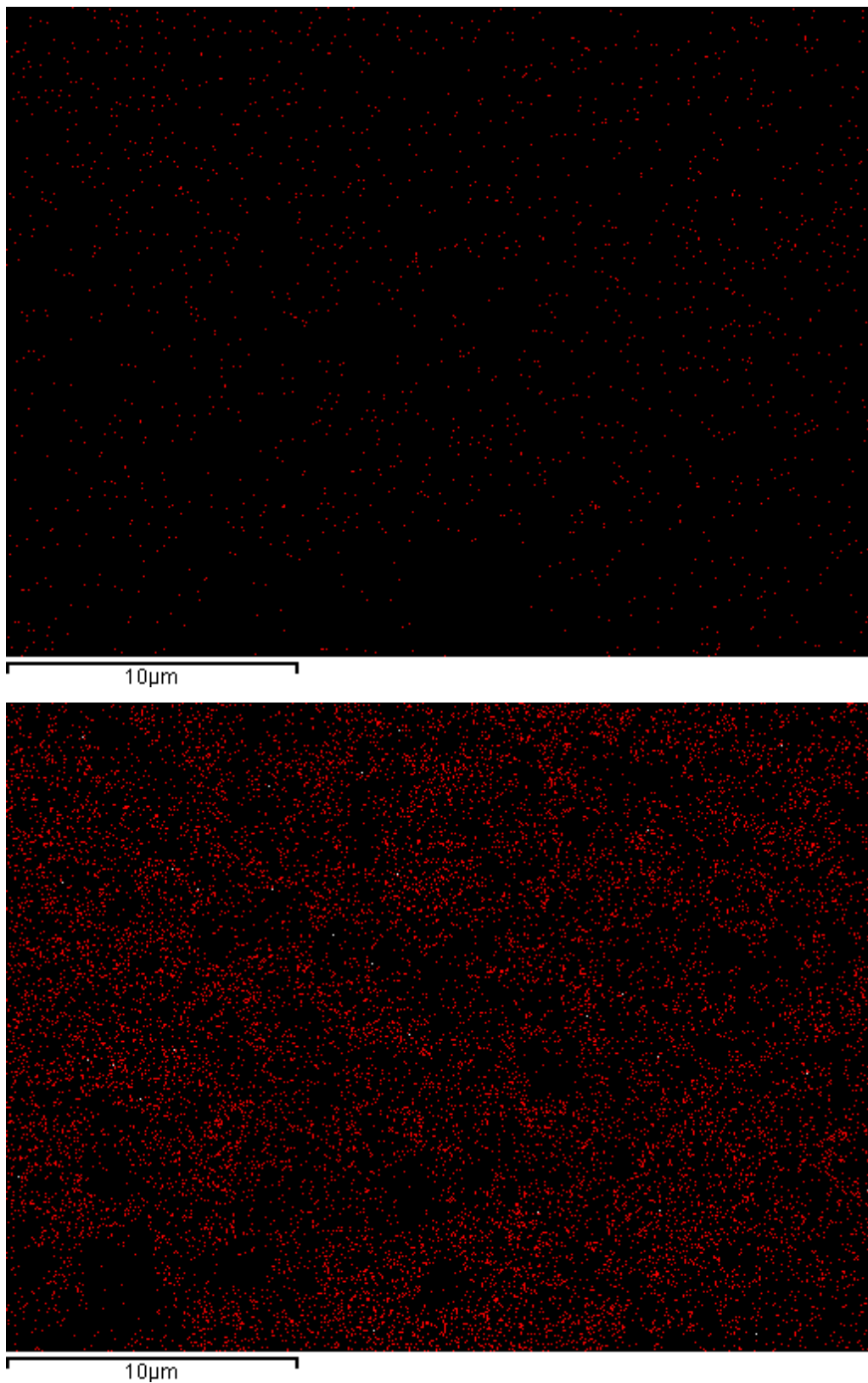


Figure 2-10 Elemental maps of 5% ZnO incorporated PVC samples. Red dots represents Zn (top), Cl bottom.

Table 2-2 show the results of the XRF analysis of both the control sample containing 0% ZnO, and 5% ZnO incorporated PVC sample. As expected, Cl was the most abundant of the detectable elements. While Zn was detectable in the control samples (7.35 ppm), unsurprisingly a far more significant amount of Zn was detectable in the ZnO incorporated PVC samples. It was also worth noting that EDX should have identified the other elements listed with concentrations $\geq 0.1\%$, however as these results are proportionate to the detectable elements, it can be assumed that the overall concentration of the elements in the samples fell below 0.1%.

Further scrutiny of the XRF analysis identified one area of concern. Many metals have antimicrobial properties, and there was concern that the presence of Sn may impact the results. Particularly, this may be an important factor if the control samples display any antimicrobial properties. However, further analysis of the literature on antimicrobial properties of Sn shows it has very poor antimicrobial properties, if any at all.^{169–171} This information effectively eliminated any final concerns about the formulation of the PVC, and the impact it may have on the sample's antimicrobial properties.

0% ZnO PVC			5% ZnO PVC		
Cl	98.22	wt%	Cl	90.33183	wt%
S	0.46	wt%	Zn	8.08513	wt%
Ca	0.44	wt%	S	0.45757	wt%
Sn	0.33	wt%	Sn	0.41	wt%
Na	0.27	wt%	Ca	0.38	wt%
P	0.22	wt%	P	0.23	wt%
Ti	355.66	ppm	La	377.58	ppm
Te	77.74	ppm	Yb	291.28	ppm
Fe	40.73	ppm	Te	111.71	ppm
Cr	32.66	ppm	Ti	80.55	ppm
V	31.74	ppm	Fe	62.29	ppm
Ni	14.78	ppm	Mn	58.37	ppm
Zn	7.35	ppm	Sb	40.76	ppm
Yb	2.77	ppm	Co	28.62	ppm
Re	1.34	ppm	Se	8.82	ppm

Table 2-2 (Left) XRF analysis of control samples containing 0% ZnO nanoparticles and (Right) 5% ZnO incorporated PVC samples

2.4.4 Antimicrobial testing

Initially antimicrobial testing was done to determine if the surface's had antimicrobial properties, and if so, to quantify those antimicrobial properties. Testing analysed the 5% ZnO incorporated PVC sample against the 0% ZnO PVC control. During the initial experimental optimisation, ZnO incorporated PVC samples of different ZnO concentrations were also partially investigated, but the samples with a 5% ZnO concentration provided the best results, while maintaining the physical properties of a PVC.

To begin, control samples (0% ZnO PVC) and nanocomposite samples (5% ZnO incorporated PVC) were inoculated with 25 μ l of a 10^6 CFU/ml suspension of either *S. aureus* or *E. coli*. The samples were then incubated at room temperature for 6 h under dark conditions (<1 Lx) before being processed as described in section 2.4.4, with the results displayed in Figure 2-11.

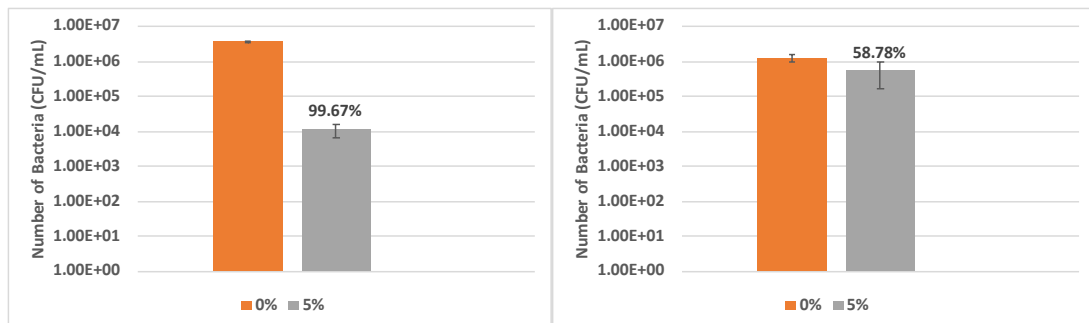


Figure 2-11 Antimicrobial activity of 5% ZnO incorporated PVC samples against 0% ZnO PVC control samples. Samples inoculated with *E. coli* suspension (left) and *S. aureus* suspension (right) were left at room temperature, for 6 h, under dark conditions.

Results showed that the nanocomposite exhibited good antimicrobial properties against *E. coli* when compared to the properties of the control sample. On average, a 99.67% difference in kill was observed when comparing the nanocomposite sample's results to the control samples. This was of particular note, as previous experiments using different polymer nanocomposites, had been unable to achieve this significant kill against Gram-negative bacteria under dark conditions.^{148,156,158,172}

The same optimism could not be maintained when considering the nanocomposite's potential as an antimicrobial surface against *S. aureus*. The results against *S. aureus* demonstrated the nanocomposite's poor antimicrobial properties despite recording on average a 58.78% kill when compared to the control samples. Comparing the *S. aureus* results to those of other publications, the results generally contrast those previously reported. Typically, nanocomposites exhibit better antimicrobial properties against Gram positive bacteria than against Gram negative ones.¹⁵⁵⁻¹⁵⁷ Some studies have reported >99.9% kills against Gram-positive bacteria, with most publications reporting at least a 1 log reduction.^{149,155,156}

In light of the initial results, it was decided to concentrate on the nanocomposites antimicrobial properties against *S. aureus*. The first step was to determine the impact of the experimental conditions on the nanocomposite's antimicrobial properties. The two main variables considered at this time were: exposure time, and sample illumination. So as not to stray too far from real world conditions, the Chartered Institution of Building Services Engineers' guidelines for hospital lighting (300 Lx) was chosen.¹⁷³ Increased exposure times were also tested.

Figure 2-12 outlines the results of the experiments carried out with the varied parameters. With the goal of achieving a better antimicrobial activity, while using the same 5% ZnO incorporated PVC nanocomposite, both the Lx levels and exposure times were altered. Although increasing the exposure time did have an impact on the nanocomposite's antimicrobial activity, it was a minor, 5.75% bump. Although a slightly better result, the outcome was much the same for the increase Lx levels as the antimicrobial activity increased by 8.45%, which may simply be down to the cells susceptibility to light. While the combination of both the increased light level and the increased exposure time did have impact on the antimicrobial activity, the improved figure of 71.90% was still far below that of the 90% kill reported by *Maharubin et al.*, *Kanmani et al.*, and *Visnapuu et al.*^{149,155,156}

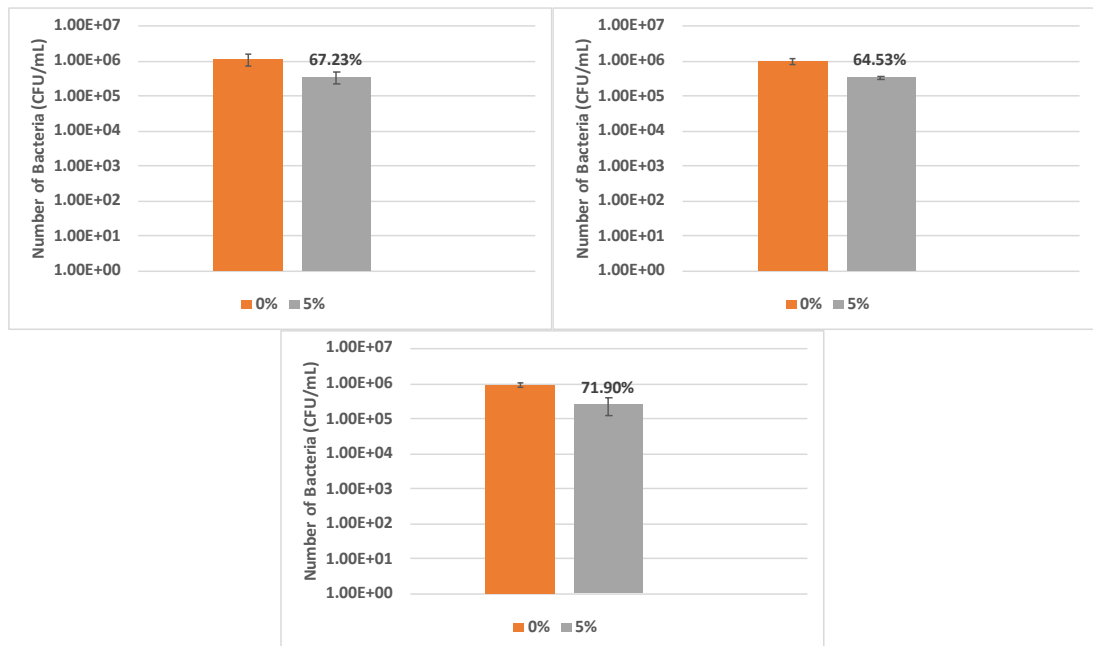


Figure 2-12 Antimicrobial activity of 5% ZnO incorporated PVC samples against 0% ZnO PVC control samples. Samples were inoculated with *S. aureus* and left at room temperature under; $\sim 300\ \text{Lx}$ for 6 h (top left) $<1\ \mu\text{l}$ for 24 h (top right) $\sim 300\ \text{Lx}$ for 24 h (bottom)

Unfortunately, even under more favourable experimental conditions, when dealing with *S. aureus*, the ZnO incorporated PVC nanocomposite failed to come close to the replicating the antimicrobial properties exhibited when testing against *E. coli*. This variation in the nanocomposite's antimicrobial properties may be due to an innate difference between Gram-positive and Gram-negative cells, as there are several differences between the two cells.¹⁷⁴

As outlined in section 1.1.3, the differences between Gram-positive and Gram-negative cells can be both structural and chemical.¹⁷⁴ It may be that the antimicrobial mechanism targets the Gram-negative bacteria's outer membrane, which Gram-positive cells lack. On the other hand, the Gram-positive bacteria's thick peptidoglycan cell wall (20-30 nm), may better protect the cell against this specific antimicrobial mechanism than the Gram-negative bacteria's thinner cell wall (8-12 nm). Chemically, Gram-negative cell's lipids and lipoproteins that may be targeted, as they are in a much higher concentration, when compared to the concentration present in a Gram-positive cell. Alternatively, Gram-positive cells have teichoic acids, which are short linear anionic polysaccharides, present on their surface, giving them a negative surface charge, and acting as a defensive mechanism. While there

are many more variables between the two cell types by which they may be defending themselves, the nanocomposite has a much smaller number of possible mechanisms by which it could be killing the cells.

2.4.5 Investigation of the antimicrobial mechanism

In an effort to better understand the interaction between the nanocomposite and the bacteria, mechanism testing was performed on the nanocomposite. ROS are a mechanism of kill that have been shown to be produced by nanocomposites. With this in mind, mechanism testing was performed to determine if the mechanism of kill was indeed due to ROS, and if so, which ones.

ROS scavengers, like metal chelates, are defensive mechanisms that are naturally present in bacterial cells.¹⁷⁵ However, cells contain a finite amount, and require time to produce more when reservoirs are depleted. This can leave cells vulnerable to high concentrations of ROS and metal ions. When investigating ROS mechanisms singlet oxygen, hydrogen peroxide, hydroxyl radicals, and superoxide are four common ROS that initially need to be accounted for, with a specific scavenger required for each.¹⁶⁰

The antimicrobial mechanism of the ZnO incorporated PVC samples was determined under dark conditions (<1 Lx), with an exposure time of 6 h, at room temperature, as per section 2.3.5. *E. coli* was selected due its greater susceptibility to the nanocomposite's antimicrobial properties. By using the more susceptible bacteria, a greater contrast between the results should be visible if a scavenger is hindering a specific mechanism.

Figure 2-13 reveals the results of the mechanism testing. Inoculum **a** was a control suspension, containing no scavengers at all, and was used as a baseline for the experiment. When tested against the control solution, the nanocomposite antimicrobial properties did have a lower than expected efficacy, but still exceeded a 99% kill (99.07% kill). Inoculum **b** containing catalase, ruled out hydrogen peroxide as the dominant mechanism, with the

nanocomposite proving to be extremely potent, and registering a 99.73% kill. Similar outcomes occurred when testing inocula **c** and **d** against the nanocomposite. The nanocomposite produced a >99.4% kill against both inocula, eliminating hydroxyl radicals (**c**) and superoxide (**d**) as possible primary mechanisms of kill. This was due to the presence of mannitol (**c**) and superoxide dismutase (**d**).

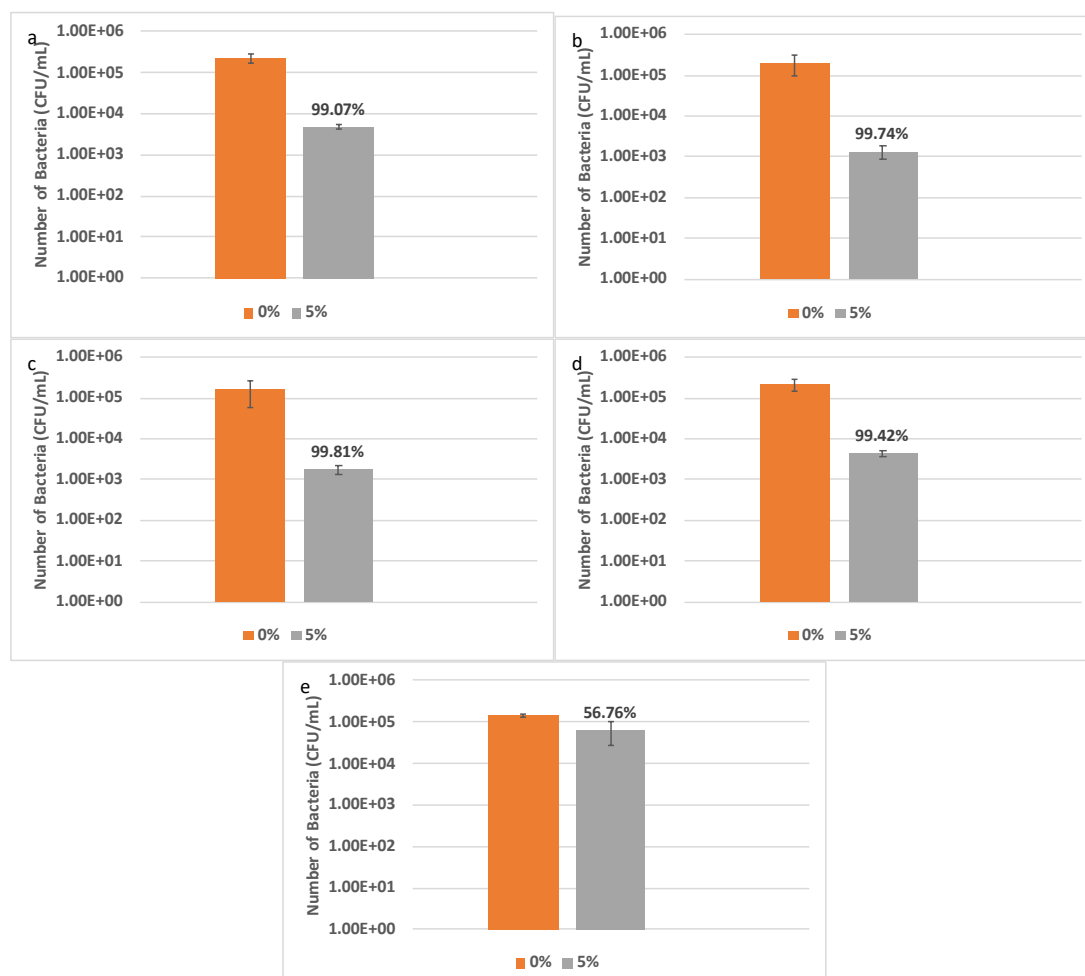


Figure 2-13 Antimicrobial activity of 5% ZnO incorporated PVC samples against 0% ZnO PVC control samples. Samples were inoculated with *E. coli* and left at room temperature under dark conditions for 6 h. a) Control b) Catalase ~35 unit/ml c) Mannitol 110 mM d) Super oxide dismutase 30 unit/ml e) L-histidine 6.5 mM

Comparably, inoculum **e** produced a far more distinctive result when exposed to the nanocomposite. Inoculum **e** contained L-histidine which is capable of scavenging any singlet oxygen produced by the surface. As the nanocomposite was only able to average a 56.76% kill against inoculum **e**, it can be deduced that singlet oxygen or type 2 ROS mechanisms (Figure 1-6) play a significant role in the surface's antimicrobial properties. Comparably,

Sehmi et al. found their dye-sensitised ZnO incorporated polyurethane to be both type 1 & 2 ROS active, while *Hwang et al.* found their dye-sensitised gold silicone's main mechanism to be hydrogen peroxide, with singlet oxygen also contributing.^{158,160} However, both these mechanism tests were done under irradiation.

This result would suggest that *S. aureus*, may have a specific mechanism that is protecting it from singlet oxygen. More specifically it is possible that it has a scavenger similar to L-histidine present within the cell. While there are other singlet oxygen scavengers that may be present within a bacterial cell, such as glutathione, carotenoids stand out as a scavenger, known to be present within *S. aureus*, and absent from *E. coli*.^{161,176,177} The reason carotenoids stand out specifically, as they are a pigment responsible for *S. aureus*'s golden colour. Therefore, if carotenoids are responsible for *S. aureus*'s defensive mechanism against the nanocomposite's antimicrobial properties, the potency of the nanocomposite should increase when tested against a strain lacking carotenoids.

2.4.6 Investigating the role of carotenoids in *S. aureus*'s defence against the antimicrobial activity of ZnO incorporated PVC

Carotenoids have been shown to be an effective antioxidant capable of scavenging singlet oxygen.^{161,178} As singlet oxygen is the nanocomposite's main antimicrobial mechanism against *E. coli*, this experiment was designed to test if carotenoids were responsible for *S. aureus*'s resistance to the nanocomposite's antimicrobial properties, or whether there were other contributing factors. This was done by using a WT and a *crtM* strain which is an isogenic mutant identical to the WT, with the exception being the *crtM* cannot synthesise carotenoids.^{161,162} 8325-4 was used for consistency and to make the results comparable.

Three *S. aureus* suspensions were prepared (WT, *crtM*, 8325-4). Each bacterial suspension was then exposed to a ZnO incorporated PVC sample's surface for a period of 24 h, under dark conditions, at room temperature.

Following this, the suspension was recovered using PBS and plated. Once plated, a difference in colour could be observed unaided when comparing the WT cells to the *crtM* cells. This was due to the variation in carotenoid levels, as carotenoids give the cells their colour (Figure 2-14).

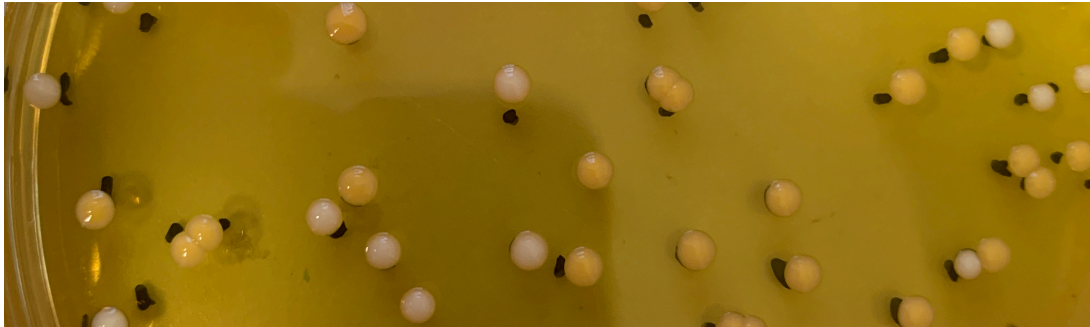


Figure 2-14 *S. aureus* plated on mannitol salt agar. WT (yellow), *crtM* (pale)

Figure 2-15 shows the results of the antimicrobial testing do not support the hypothesis. Despite the WT cells having the greatest concentration of carotenoids, the 8325-4 had the greatest resistance to the surface's antimicrobial properties. In fact, the difference in the surface's % kill vs the WT and the *crtM* was <3%.

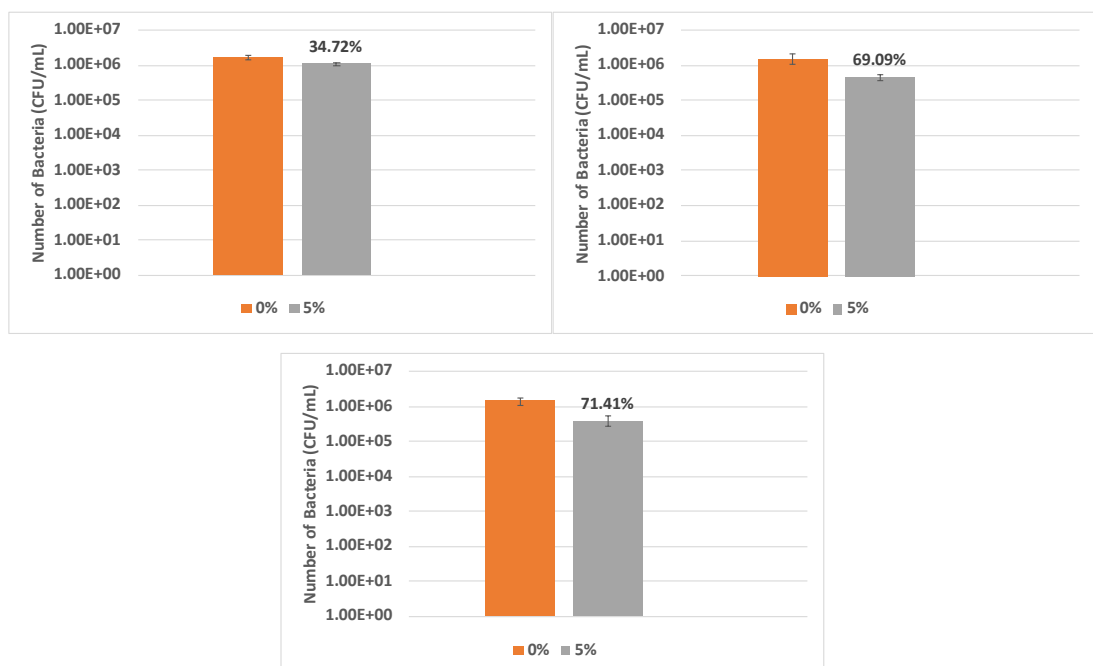


Figure 2-15 Antimicrobial testing of samples against different *S. aureus* strains. (top left) 8325-4, (top right) WT, (bottom) *crtM*.

While these results did not support the hypothesis, they did show that the cell's carotenoid concentration had minimal impact on its resistance to the nanocomposite's antimicrobial properties. Although it may be possible that another singlet oxygen scavenger is present within the cells, there are also many other factors that could account for the cell's resistance (section 1.1.3). With this experiment doing little to assist the objective of improving the surfaces antimicrobial activity, eliminating individual defence mechanisms one by one, would not appear to be viable. However, we do know that *S. aureus* is susceptible to other antimicrobial mechanisms such as hydrogen peroxide.¹⁶⁰ With this in mind, going forwards the best course of action may be to alter the nanocomposite using additives, so as to increase the nanocomposite's potency.

2.5 Summary and conclusion

The production and initial testing of an economically viable antimicrobial surface achieved mixed results. Importantly, it was possible to produce a polymer with what appear to be desirable physical properties, using relatively cheap materials. This was achieved using PVC as the bulk material, while also incorporating ZnO nanoparticles, in the hope that the nanoparticles may express some of their antimicrobial properties onto the bulk polymer. By doing this, while using compression moulding as a manufacturing technique, the initial goal of producing an economically viable surface, which in the long run, could be upscaled for larger production volumes, was achieved.

Initial antimicrobial testing produced varied results. Although the nanocomposite displayed poor antimicrobial properties against *S. aureus*, the nanocomposite's antimicrobial properties were shown to be much better against *E. coli*. Prior to any optimisation attempts, in an effort to better understand the nanocomposite's antimicrobial properties, mechanism testing was performed. Using a test designed with the express purpose of testing if ROS contributed to the nanocomposite's antimicrobial properties it was revealed that ROS, or more specifically, singlet oxygen contributed significantly to the nanocomposite's antimicrobial properties. This was done

by adding scavengers specific to different ROS to different inocula, prior to exposing the inocula to the nanocomposite's surface.

Once singlet oxygen had been identified as a major contributor to the nanocomposite's antimicrobial properties, carotenoids emerged as obvious defence mechanism, which the *S. aureus* could be employing against the nanocomposite's antimicrobial properties. Carotenoids were a plausible contributing factor given what we know.¹⁶¹ This led to the comparative testing of a mutant strain, devoid of carotenoids, to other *S. aureus* strains, to determine the impact of carotenoids, on the *S. aureus*'s ability to resist the nanocomposite's antimicrobial properties. Unfortunately, the results did not support the hypothesis that they played a significant role in the defence of the *S. aureus* against the nanocomposites antimicrobial properties.

Next, we had begun to investigate the irradiation of the nanocomposite's surface with UV light. This was done with the hope of causing excitation at the surface, so additional ROS might be produced. Unfortunately, as this experiment was ongoing the pandemic occurred, effectively removing our ability to perform any antimicrobial testing for nearly two years. To compound the issue, once our ability to perform antimicrobial testing was restored, our supply of the specific PVC we had been using ceased. This was due to the fact that our industrial partner was in the process of changing their raw materials supplier, so this posed another significant delay before we could begin experimenting with the nanocomposite again.

As we had been granted access to the chemistry department comparatively quickly, work began exploring the synthesis and characterisation of superhydrophobic surfaces, as this could be done without access to the microbial diseases department. As such, the proceeding chapters will go onto investigate these surfaces, and detail the results of characterisation and testing on their surfaces. However, significant time was spent investigating ways to improve the nanocomposite's antimicrobial properties, and synthesising additives for the nanocomposite. This work will be included in the

final chapter along with other concepts currently being worked on and some future work.

3 The Production, Application, and Testing of Superhydrophobic Paint

3.1 Aims

In the introduction it was explained that coatings with superhydrophobic properties could have applications across a number of industries. The aim of the experiments in this chapter were to develop and understand superhydrophobic surfaces, free from fluorinated compounds. The first stage of this work required the identification of a hydrophobic component, capable of enhancing a surface's hydrophobic properties. A particle was also required to act as a scaffold for the hydrophobic component. The next requirement was an organic solvent capable of dissolving a sufficient amount of a hydrophobic additive, while also allowing for aqueous suspensions to be mixed in, without causing the hydrophobic component to crash out. A suitable latex also needed to be identified, capable of forming a durable surface, while also not interfering with the hydrophobic components of the mixture. Finally, an application method needed to be decided on.

3.2 Background

Based on their unique wetting properties, superhydrophobic surfaces have a number of potential applications.^{80–82} However, many superhydrophobic surfaces are reliant on the presence of fluorine to achieve a low surface energy. Considering the potential harm to human health and the environment, industries are looking to move away from composites containing fluorine.^{119–121} When looking through the literature for fluorine free superhydrophobic surfaces, a number of reviews have identified long-chain fatty acids as potential fluorine replacements.^{179–181}

Of the different types of fatty acids, two in particular were commonly used: stearic acid and palmitic acid (Figure 3-1).^{182–185} *Agrawal et al.* were able to produce superhydrophobic nanoparticles through the functionalisation of ZnO

with palmitic acid.¹⁸⁶ The particles were functionalised by mixing ZnO and palmitic acid at a 1:10 weight ratio in ethanol and stirring continuously at 40 °C for 15 h. Once dried, it was determined that the particles had a WCA of ~161°.

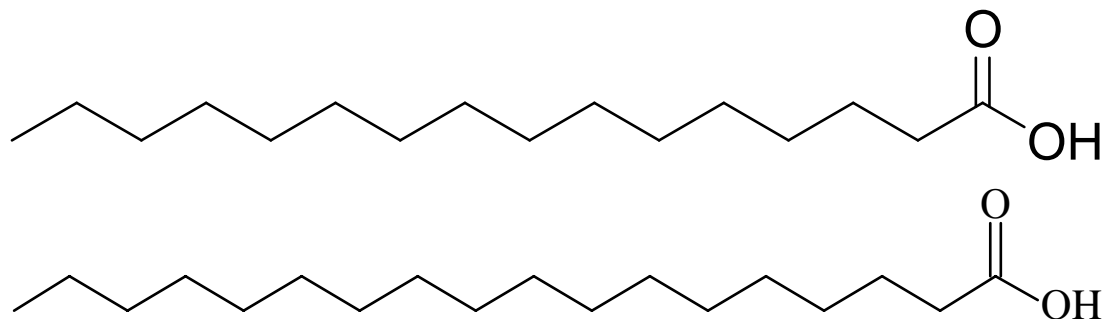


Figure 3-1 C16 palmitic acid (top). C18 stearic acid (bottom).

Zhu et al. produced superhydrophobic nanoparticles through a similar means, this time functionalising ZnO with stearic acid.¹⁸⁷ While a number of different functionalisation procedures were investigated, the optimal functionalisation process involved mixing ZnO with stearic acid at a 9:1 molar ratio. This was done at 70 °C in ethanol with constant stirring for 12 h. When the particles were washed and dried, they were determined to have a WCA of 158.3°.

Heale fabricated similar superhydrophobic particles, this time using SiO₂.¹⁸⁸ This was done in both an aqueous and an organic medium (ethanol), although the aqueous medium needed to be altered to a pH of 8 to assist in the dissolution of the stearic acid. Both methods used a 5:2 weight ratio of SiO₂ to stearic acid, mixing them for 20 min at 30 °C with continuous stirring. While the washed and dried particles did not prove to be superhydrophobic (WCA of 97°), when they were used in a slurry with the stearic acid, the slurry could be drop cast and dried to form a thin film with a WCA of ~164°.

Advancing on from the functionalisation of the SiO₂ particles and the slurry, *Heale* proceeded to use the particles in paint formulations.¹⁸⁸ This was done by first adding the particles to an aqueous mixture at pH 8, heated to 75 °C. Using Orotan CA2500 to aid with the dispersion of the particles, after 30 minutes latex was added to the formulation and stirred for another 30 min. Finally, texanol was mixed into the formulation for 10 minutes to aid with film

formation. A film applicator was then used to apply the paints to glass substrates. After drying overnight, the best paint was able to obtain a WCA of $\sim 140^\circ$. The formulation consisted of a weight ratio of 3.86% stearic acid, 5.79% functionalised SiO_2 , 86.71% water, 0.12% Orotan, 3.35% latex, and 0.18% texanol. However, these results are not repeatable as the latexes used are not commercially available.

Jafari et al. produced similar superhydrophobic paints using CaCO_3 functionalised with stearic acid and a commercial latex.¹⁸⁹ For this experiment, a mix of organic and aqueous solvents were required for the formulation, with acetone used as the organic solvent over ethanol. The organic phase simply consisted of acetone and the stearic acid, which was mixed with an aqueous phase containing the CaCO_3 particles and the Acronal[®] NX4787X latex. This was done at 30°C for 10 minutes with constant stirring, at a 1:10 weight ratio of stearic acid to CaCO_3 /latex, although it is not clear what the particle to latex ratio was. A spray technique was then used to apply the paints to a polished aluminium alloy to achieve a WCA of $\sim 158^\circ$.

Ma et al. produced a superhydrophobic coating using ZnO functionalised with silicone instead of a fatty acid.¹⁹⁰ They also opted not to use a latex, instead using just polyacrylate, which is a polymer commonly used in latexes used for paints. To begin, a silicone was prepared with terminal alkenes at either end, and a hydrosilane bond. This hydrosilane bond allowed for the functionalisation of the ZnO with the silicone. Next using the prepared silicone, a silicone/polyacrylate emulsion was made. Finally, 1 g of the functionalised particle were added to 15 ml of anhydrous ethanol, along with 0.5 g of the silicone/polyacrylate emulsion. This was then stirred for 30 mins at 60°C . Coatings were then made by spraying the formulation onto a substrate and drying the coating for 30 mins at 60°C . When measured, an average WCA of 157.8° was acquired.

One of the takeaways from these results is that results described by *Heale* had the lowest reported WCA.¹⁸⁸ This was despite having a similar formulation to *Jafari et al.*¹⁸⁹ One key difference between the two, was the application of their

paint to the substrate. While *Heale* used a film applicator, *Jafari et al* used a spray application, as did *Ma et al.*¹⁹⁰ This difference in application technique may account for the significant difference in WCA, as a spray technique generates hierarchical structures in a way that a film applicator does not allow for.

Simovich et al. investigated the extreme of this, by considering spray coating as a bottom-up technique.¹⁹¹ They found that through rapid evaporation of the coating's solvent, they were able to form an ultra-rough, durable, superhydrophobic surface. While their method to obtain an ultra-rough surface required the heating of the substrate to high temperatures, due to the nature of volatile solvents, altering the spray distance of a formulation can impact its evaporation time.¹⁹² This is due to the fact that volatile solvents are liable to evaporate as they move through the air. Therefore, by altering the spray distance of a formulation onto the substrate, the amount of solvent present in the coating on application can be altered. This allows for a more rapid drying and a build-up of hierarchal structures.

Palmitic acid and stearic acid appear to offer a solution to fluorine free superhydrophobic surfaces.^{179–181} They can be combined with ZnO to make functionalised superhydrophobic particles, similar to those used in differing formulations of superhydrophobic paints.^{186–190} While these particles may be able to provide a low surface energy, the formation of hierarchical structures through spray techniques, may achieve the surface roughness required for high WCA's.^{191,192}

3.3 Experimental

Prior to commencing the experiments, a number of components to the mixture were investigated and identified as promising. Stearic acid and palmitic acid were identified as possible hydrophobic agents as they have previously been used in this capacity.¹⁹³ Work by *Jafari et al.* had previously achieved a WCA of $\sim 158^\circ$ using BASF products, due to this, we tested four BASF latexes that BASF thought promising.¹⁸⁹ Ethanol and acetone were selected as the organic

solvents as they had good dissolution properties when interacting with the fatty acids. Another important property required for the organic solvents was that they could be mixed with the latex and water at certain ratios, where the latex stayed in suspension and the fatty acid stayed dissolved. Finally, SiO₂ and ZnO were selected to act as the scaffold used to assist in film formation. SiO₂ was selected, as it had previously been used successfully in the group, while ZnO was selected in an effort to produce antimicrobial properties.¹⁹⁴

3.3.1 Materials

The latexes Acronal Plus 2483 (Plus), Acronal Edge 6295 (Edge), Acronal A 750 (750), and Acronal A 684 (684), were all supplied by BASF. Palmitic acid, stearic acid, 100 nm ZnO nanoparticles, >5 µm ZnO particles, acetone, ethanol, and texanol were all purchased from Sigma Aldrich. Orotan CA-2500 was purchased from the Dow chemical company. Evonik acematt HK 400 SiO₂ particles (6.3 µm) were supplied by Alto Ltd. Kit 300B gravity fed spray gun and air hose kits were purchased from Clarke International.

3.3.2 The functionalisation of particles with a hydrophobic capping agent

The first experiment performed looked at the functionalisation of both the SiO₂ and ZnO particles, with both the palmitic and stearic acids. This experiment was performed in both ethanol and acetone. 1-3 g of fatty acid was added to a beaker containing 47 ml of solvent, at 50 °C, while being stirred at 500 rpm. Once the fatty acid was added, a watch glass was used to cover the beaker to slow down the rate of evaporation. The solution was then left for 20 min, until the fatty acid was fully dissolved. After 20 min, 1-10 g of particles were added to the solution, and stirred for 1-6 h under the same condition.

When the time had elapsed, the beaker was removed from the hotplate and the contents were transferred to a centrifuge tube. The suspension was then centrifuged at 4000 rpm for 5 min. Once centrifuged, the liquid was decanted, and the particles were washed by re-suspending the particles in the organic

solvent. Shaking and vortexing was used to ensure the particles were sufficiently washed, before being centrifuged again. The wash step was completed at least three more times, until no more stearic acid was present in the decanted liquid. The tube containing the particles was transferred to a vacuum oven to dry at 50 °C for at least 36 h.

Once dry, the particles were forced through a metal mesh to form a powder, before being analysed by either adding them directly to an instrument, or by adding them to double sided tape, adhered to a microscope slide (Figure 3-2).



Figure 3-2 Functionalised ZnO powder (left powder). Functionalised ZnO powder on double sided tape (left). Functionalised SiO₂ powder (right powder). Functionalised SiO₂ powder on double sided tape (right)

3.3.3 The production of superhydrophobic paints

The next experiment was aimed at producing a superhydrophobic paint. Different formulations were made up using: SiO₂ and ZnO particles, palmitic and stearic acids, ethanol and acetone solvents, as well as Plus, Edge, 750, and 684 latexes. Again, 0.5-2 g of fatty acid was added to a beaker containing 35-50 ml of solvent, at 50 °C, while being stirred at 500 rpm for 20 min while being covered with a watch glass.

Separately, in a centrifuge tube, 100 µl of orotan was added to 5-15 ml of H₂O and vortexed for 10 seconds at full power. This was followed by adding 0.1-3 g of particles before being vortexed again. Finally, 0.5-3 ml of latex was added to the aqueous solution before being vortexed a final time and added to the organic solution once the initial 20 min had elapsed. This suspension was

then left to continue stirring under the same conditions for 20 min before 150 μ l of texanol was added to the suspension, and left for another 10 min. Once complete, the paint was transferred to a reagent bottle, and organic solvent was added to ensure paint's total volume was 60 ml (if required). The paint was then left to rest for at least 12 h.

Next, immediately before spraying, the paint was shaken and sonicated for 5 min. This was done to ensure the components in the paint were dispersed and homogenous, as clumps caused the spray gun to clog. Once mixed, ~ 30 ml of paint was added to a spray gun, with the spray gun's jet opened 1.5 rotations. Using a 24 L air compressor set to 3 bar, 30 ml of paint was applied across five microscope slides which were held onto black card by masking tape (Figure 3-3). Samples were then left for at least 24 h to dry at room temperature before any tests were performed.

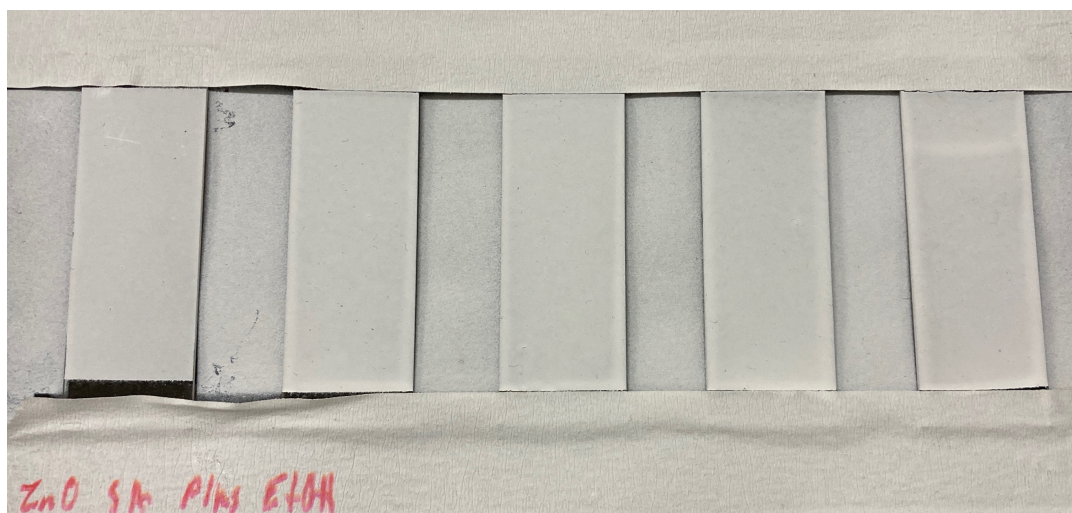


Figure 3-3 ZnO, stearic acid, plus latex, ethanol paint applied to microscope slides using a gravity fed spray gun, after 5 min of sonication, using 3 bar of pressure.

3.3.4 Material characterisation and functional testing

Infrared transmission spectra were obtained using a Brüker Alpha Fourier transform infrared spectrometer with a platinum ATR attachment. All spectra were obtained from the accumulation of 16 scans per sample, under an analysis range of 400-4000 cm^{-1} .

Topographic surface imaging was completed using a JEOL JSM-6701F field emission scanning electron microscope. Samples were coated with either gold or carbon prior to analysis and were analysed with an acceleration voltage of 10 kV.

Stain testing was performed by securing the sample at an 80° angle. Separate drops of 20 ppm crystal violet, instant coffee, and wine were then applied to the surface using a plastic pipette. The result was then recorded by imaging the samples.

A tape test was performed by firmly adhering Scotch Magic Tape to a surface, before pulling it off in a single motion. This process was repeated nine times, using a fresh strip of tape each time, before any measurements were taken.

X-ray photoelectron spectroscopy was performed using a Thermo Scientific X-ray photoelectron spectrometer with a monochromated Al-K α X-ray source (8.3381 Å). Data was interpreted using CasaXPS software, with binding energies adjusted for adventitious carbon (284.6 eV)

WCA measurements were performed using a Krüss DSA25E Droplet Shape Analyser. A DS3252 dosing unit was used to apply a 5 μ l droplet to each coating at room temperature. A Young-Laplace fit was then used to calculate the contact angle of each droplet. Each measurement was performed in triplicate, with all reported measurements having a standard deviation of <1.5°.

3.4 Results and discussion

3.4.1 The production of superhydrophobic particles functionalised with a hydrophobic capping agent.

Due to many variations of the functionalisation procedure in the literature, developing and optimising a functionalisation procedure was the first task.^{186–188} Initially ethanol and water were selected as the two solvents to be tested during this experiment. Despite the fact that the fatty acids are hydrophobic in

nature, by applying heat, and altering the pH of the water, it was possible to dissolve them in water. However, this was a difficult process, that did not produce particularly stable solutions. On top of this, operating at an altered pH risked interfering with, or damaging additional components, such as latex, that were due to be added in the future. With this in mind, acetone was chosen to replace water as it is already a common paint solvent and can dissolve fatty acids comparatively better.

For this experiment, the amount of starting solvent used was kept constant at 47 ml. To start with, 3 g of stearic acid was added to ethanol and heated (50 °C) with stirring (500 rpm) for the 20 min. Once the 20 min had elapsed the solution was checked to ensure the solution was not saturated and that all the stearic acid was dissolved. To ensure that there would be an excess of stearic acid, only 1 g of ZnO was added to the solution and left for 4 h. Once completed, the particles were centrifuged, and the liquid was decanted off.

Rather than throwing away the liquid when decanting, the liquid was added to water to quickly determine whether there was an excess of stearic acid. When this was done a large amount of stearic acid crashed out of the solution, showing that there was a clear excess of stearic acid. This was repeated for each wash step, with excess stearic acid still being rinsed off the particles after three wash steps. An aqueous wash step was then attempted, but this caused the stearic acid to congeal with the particles, effectively causing the experiment to fail.

The next experiment drastically reduced the amount of stearic acid used. A 1:1 weight ratio of stearic acid to ZnO was used this time around, using 1 g of each. All the steps were repeated as before, up until the wash stage. Again, during the washing, stearic acid was still clearly being rinsed off the particles after three wash steps. A total of 5 washes of the particles were complete at which point, minimal stearic acid was observed in the decanted liquid. The particles were then dried and adhered to double-sided tape on a microscope slide. A Pasteur pipette was then used to add a drop of water to the particles,

which immediately rolled off. The differing variations of the experiment were then completed with the results shown in Table 3-1.

Solvent (47 ml)	Fatty Acid (1 g)	Particle (1 g)	Wetting Property
Acetone	Stearic Acid	ZnO	Superhydrophobic
Acetone	Palmitic Acid	ZnO	Superhydrophobic
Acetone	Stearic Acid	SiO ₂	Superhydrophilic
Acetone	Palmitic Acid	SiO ₂	Superhydrophilic
Ethanol	Stearic Acid	ZnO	Superhydrophobic
Ethanol	Palmitic Acid	ZnO	Superhydrophobic
Ethanol	Stearic Acid	SiO ₂	Superhydrophilic
Ethanol	Palmitic Acid	SiO ₂	Superhydrophilic

Table 3-1 Components and results of the initial functionalisation of particles with a fatty acid after 4 h of stirring at 50 °C.

Firstly, it is worth noting that it was generally easier to work with acetone as a solvent overall and particularly during the washing and drying steps. Looking at the results listed in Table 3-1, it can be seen that swapping out most of the components had little impact on the particles wetting properties, with the exception being the impact of varying the metal oxide particles. In all cases, when ZnO was used, the resultant functionalised particles were superhydrophobic, whereas when SiO₂ was used, the resultant functionalised particles were superhydrophilic.

This difference in results may be attributed to a number of obvious differences between the two particles. Firstly, the particles differ in their chemical properties, but also in physical properties. The physical properties of the ZnO and the SiO₂ particles varied significantly in two aspects: size and permeability. While the SiO₂ (6.3 µm) was significantly larger than the ZnO (100 nm), the SiO₂ is also porous in nature, differing from the solid nature of the ZnO.

The biggest impact of the porous nature of the SiO₂ is the significant increase to the overall surface area of the particles. This should only impact the experiment if the increased surface area was significant enough that the fatty

acid was no longer in excess. However, this was not the case as the fatty acid was always observed in the decanted liquid during the wash step. If anything, the increased size of the SiO₂ particles may add to the surface roughness, which should theoretically increase the hydrophobicity of the particles, if they had been functionalised correctly.

Regardless, to determine the impact that the difference in size of the two particles had, an experiment was done simply using larger ZnO particles (~5 µm). All the variations of the experiment using the different solvents and fatty acids resulted in the same superhydrophobic wetting properties that the smaller particles had produced. These results would indicate that the size of the particles had little impact on the wetting properties of the functionalised particles.

These results would suggest that the issue with the functionalisation of the SiO₂ was due to the innate chemical properties of the particles. In a final effort to produce superhydrophobic SiO₂ particles, an experiment with more favourable conditions was performed. Ethanol was heated to 70 °C and once the stearic acid (1 g) was dissolved (20 min) the particles (1 g) were added to the solution and left for 6 h. Once the time had elapsed, the normal washing protocol was followed, with an excess of stearic acid observed in the washes (3). Once the drying was completed, the particles were analysed and found to still be hydrophilic.

These results were similar to those found by *Heale*.¹⁸⁸ They also found that after trying to functionalise the SiO₂, the dry particles did not have superhydrophobic properties. However, they were still able to produce superhydrophobic films and paints by incorporating the particles into slurries and paints. This meant that it was possible that the SiO₂ particles would work better in a one pot method once the latex was introduced, while also being confident that if it did fail, the functionalised ZnO particles were more promising.

To reduce the time spent on optimisation, acetone, ZnO (100 nm) and stearic acid were used as the components. Acetone was used as washing and separation steps were easier than when using ethanol. Stearic acid was used as similar properties had been observed across the two fatty acids and using both during the optimisation process seemed wasteful and time consuming. ZnO was used as it was the particle that produced the superhydrophobic functionalised particles previously.

The first thing to be optimised was the particle to fatty acid ratio. To ensure there was enough fatty acid present, the goal was to have an excess of fatty acid present in both the first and second wash, but little to none in the third wash. Still using the 47 ml of acetone, the amount of stearic acid was fixed at 0.5g, while varying amounts of ZnO were used, starting at 1 g. Once it was clear that there was a clear excess of fatty acid, the amount of ZnO was increased in 0.5 g intervals, until at 2 g, where the desired stearic acid to ZnO ratio appeared to be. With this ratio in mind, the experiment was quickly scaled up to use 2.5 g of stearic acid and 10 g of ZnO, and it was again found that an excess of fatty acid was present in both the first and second wash, but little to none in the third wash. Once washed, the particles were again dried and tested, with the water droplet immediately rolling off the surface of adhered particles.

Finally different time intervals for the functionalisation of the particles in solution was tested. Different experiments were set up to functionalise the particles for different time periods ranging from 0.5-4 h at 30 min intervals. When analysing the results, anything that had been functionalised for less than 1.5 h or less had too high an excess of stearic acid in the washing (considerable amount in the third wash). This was not the case for the particles that had been functionalised for 2 h, which had a similar excess of stearic acid to the particles functionalised for 4 h.

3.4.2 Characterisation and testing of functionalised particles

To ensure the particles were optimised, the particles were again adhered to double sided tape on a microscope slide for testing and characterisation. Using a Pasteur pipette, it was shown that a water droplet rolled off the particles, showing they had superhydrophobic properties. The wetting properties were then further analysed through drop shape analysis. The resultant testing found \bar{x} WCA to be 174.2°. Figure 3-4 shows an image of a water droplet sitting on top of the functionalised particles.

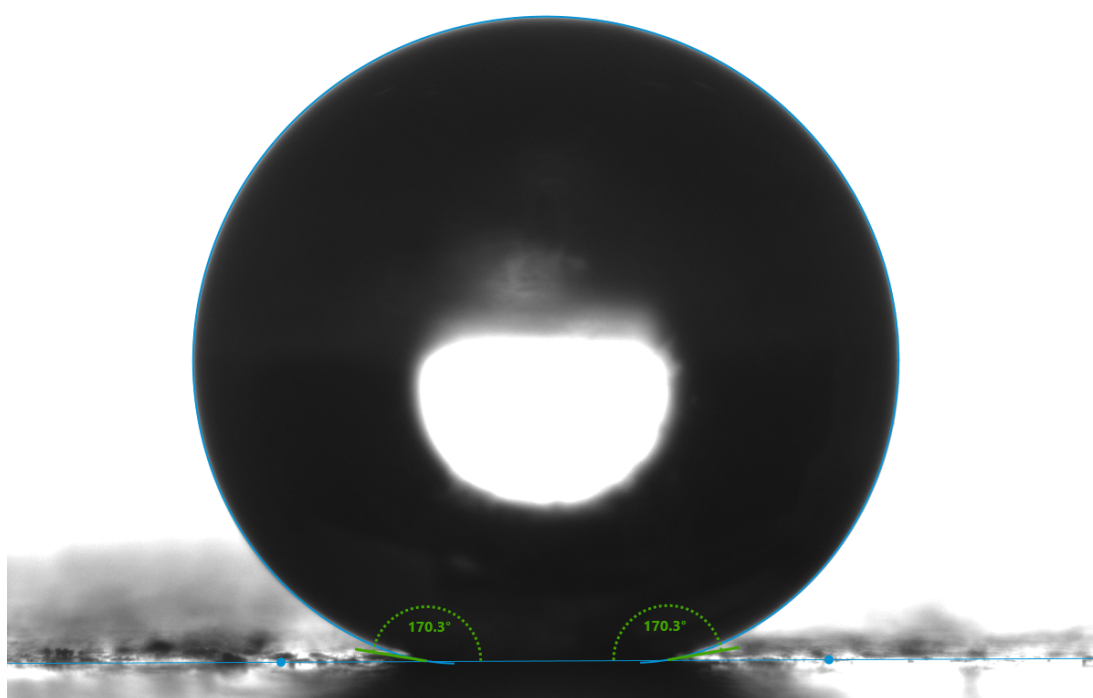


Figure 3-4 DSA image of a 5 μ l water droplet on stearic acid coated ZnO particles (100 nm) made using acetone as the solvent, adhered to double sided tape on a microscope slide.

This result exceeded the best WCA recorded by both *Zhu et al.* and *Agrawal et al.*^{186,187} The 1:4 fatty acid to ZnO ratio was of stark contrast to the formulation reported by *Agrawal et al.*, who used a 10:1 fatty acid to ZnO ratio. While the formulation did still contrast the 1:9 fatty acid to ZnO ratio reported by *Zhu et al.*, their formulation was a closer match. There was also a stark contrast in the time spent functionalising the particles, compared to the times reported in the literature. While *Zhu et al.* and *Agrawal et al.* spent 12 and 15 h functionalising their particles, the particles produced in this work were only

functionalised for 2 h. One final difference of note was that both had used ethanol as the solvent as opposed to acetone favoured in this work. The main difference between the solvents is that acetone is more nonpolar, which may have allowed it to interact more favourably with the nonpolar components of the formulations.

The optimised process was then used to make particles using the different variations of solvents, particles, and fatty acids. The experimental results are displayed in Table 3-2 and Figure 3-5. As can be seen in the results, even using the optimised process, the SiO₂ remained superhydrophilic. This meant no WCA could be obtained using the DSA. On the other hand, all of the other variations that used ZnO as the particles had superhydrophobic properties. Further analysis showed that acetone performed better than ethanol as a solvent, and that stearic acid performed slightly better as the hydrophobic component than palmitic acid. However, it was very difficult to take WCA measurements above 165° due to environmental factors (vibrations and airflow) causing the droplet to shake. This means that the difference in the WCAs of the particles functionalised with the different fatty acids, may just be down to instrumental error, as might the difference attributed to the different solvents, although this was more significant.

Solvent (47 ml)	Fatty Acid (2.5g)	Particle (10g)	Wetting Property	\bar{x} WCA
Acetone	Stearic Acid	ZnO	Superhydrophobic	174.2°
Acetone	Palmitic Acid	ZnO	Superhydrophobic	172.4°
Acetone	Stearic Acid	SiO ₂	Superhydrophilic	NA
Acetone	Palmitic Acid	SiO ₂	Superhydrophilic	NA
Ethanol	Stearic Acid	ZnO	Superhydrophobic	169.6°
Ethanol	Palmitic Acid	ZnO	Superhydrophobic	167.8°
Ethanol	Stearic Acid	SiO ₂	Superhydrophilic	NA
Ethanol	Palmitic Acid	SiO ₂	Superhydrophilic	NA

Table 3-2 Components and water contact angles of the optimised particles functionalised with a fatty acid after 2 h of stirring at 50 °C.

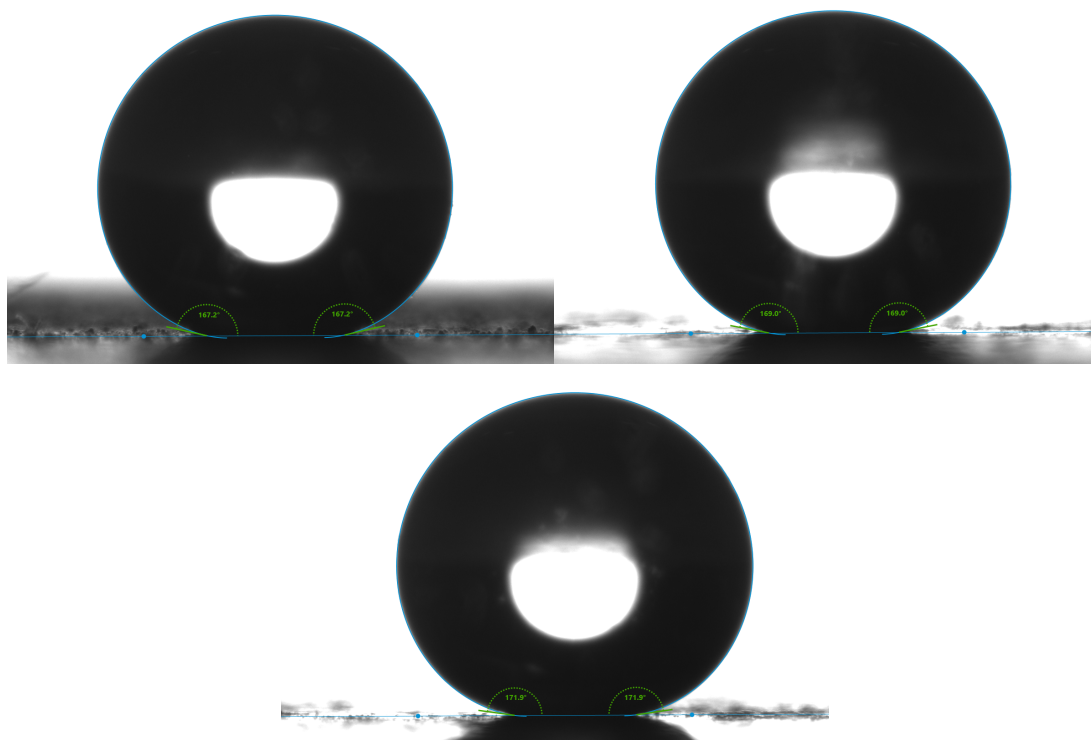


Figure 3-5 DSA image of a 5 µl water droplet on fatty acid coated ZnO particles (100 nm) adhered to double sided tape on a microscope slide. Top left: Palmitic acid coated ZnO made using ethanol as the solvent. Top right: Stearic acid coated ZnO made using ethanol as the solvent. Bottom: Palmitic acid coated ZnO made using acetone as the solvent.

To better understand the functionalised materials, FT-IR analysis was carried out on both the functionalised compounds and the raw materials. Figure 3-7 gives a comparison of the ZnO particles functionalised with stearic acid in acetone, and the raw materials. The ZnO spectrum has no discernible peaks until a significant drop in transmission occurs at $\sim 600\text{ cm}^{-1}$. This is as expected as this is the region where absorption associated with the Zn-O bonding occurs, with this peak is also being present in the functionalised ZnO spectrum.^{195,196} Comparatively, the other spectra are far more dynamic with the stearic acid spectrum including notable peaks such as: an OH peak associated with carboxylic acids at 3017 cm^{-1} , a C=O peak at 1699 cm^{-1} , and a large C-O peak at 1297 cm^{-1} .^{197,198} These peaks are of particular note due to their prominence in the stearic acid spectrum, but also due to their absence in the functionalised ZnO spectrum.

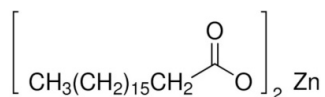


Figure 3-6 Zinc stearate

The disappearance of these peaks can be explained when considering how the stearic acid is binding to the ZnO. Binding most likely occurs when the hydrogen is removed from the terminal oxygen on two stearic acid molecules (eliminating the OH peak at 3017 cm^{-1}), which then undergo ionic bonding with the ZnO particles surface, effectively forming zinc stearate (Figure 3-6). Once bound to the surface, the oxygen atoms go into resonance, eliminating the C=O and C-O peaks. These peaks are instead replaced with a symmetric COO^- stretch at 1399 cm^{-1} and an asymmetric COO^- stretch at 1540 cm^{-1} that occur due to the resonance.¹⁹⁹

When analysing the equivalent spectra involving SiO_2 , the results are contrasting to the ZnO results. Figure 3-8 show minimal difference between the unfunctionalised and the supposedly functionalised SiO_2 particles. None of peaks related to either the stearic acid or the carboxylate anion were present in the spectrum for the SiO_2 functionalised with stearic acid. This suggest that fatty acid never adhered to the particles, which is not all that surprising with the particles never displaying superhydrophobic properties.

These FT-IR results are also backed up by XPS analysis. When comparing the Zn 2p spectra of the raw material ZnO to the functionalised ZnO (Figure 3-9), a significant broadening of the Zn peaks FWHM ($1.805\text{-}1.960\text{ eV}$) was observed. This broadening would suggest a change in the bonds contributing to the Zn peak shape.²⁰⁰ In contrast, this broadening does not occur when looking at the Si 2p spectra (Figure 3-10). This again would suggest that the ZnO was well functionalised, where the SiO_2 was not.

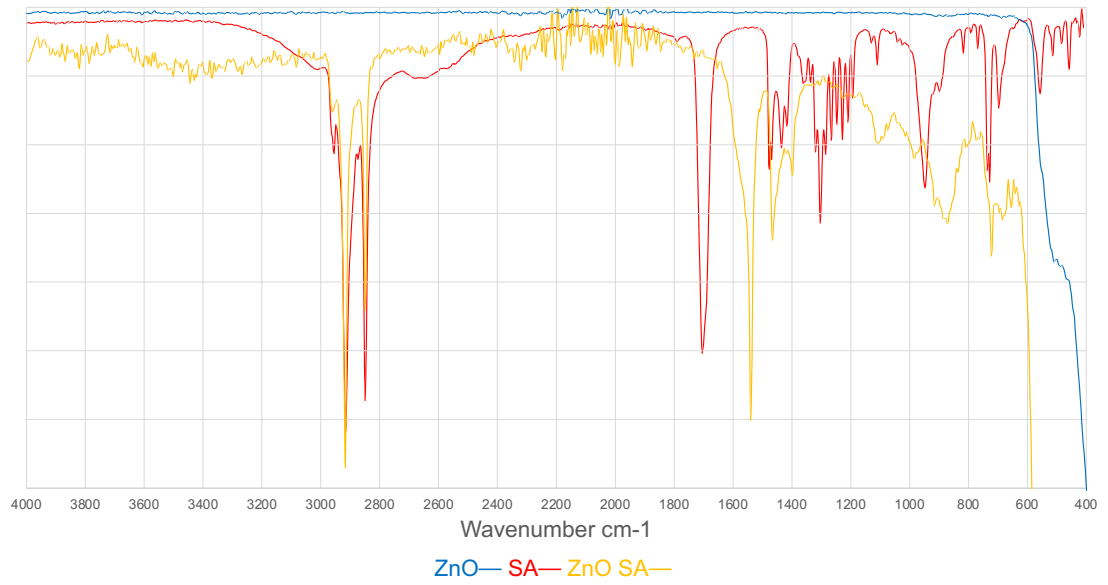


Figure 3-7 The comparison of the transmission FT-IR spectra of the raw materials with functionalised nanoparticles made in acetone. Blue: ZnO. Red: Stearic acid. Yellow: ZnO functionalised with stearic acid.

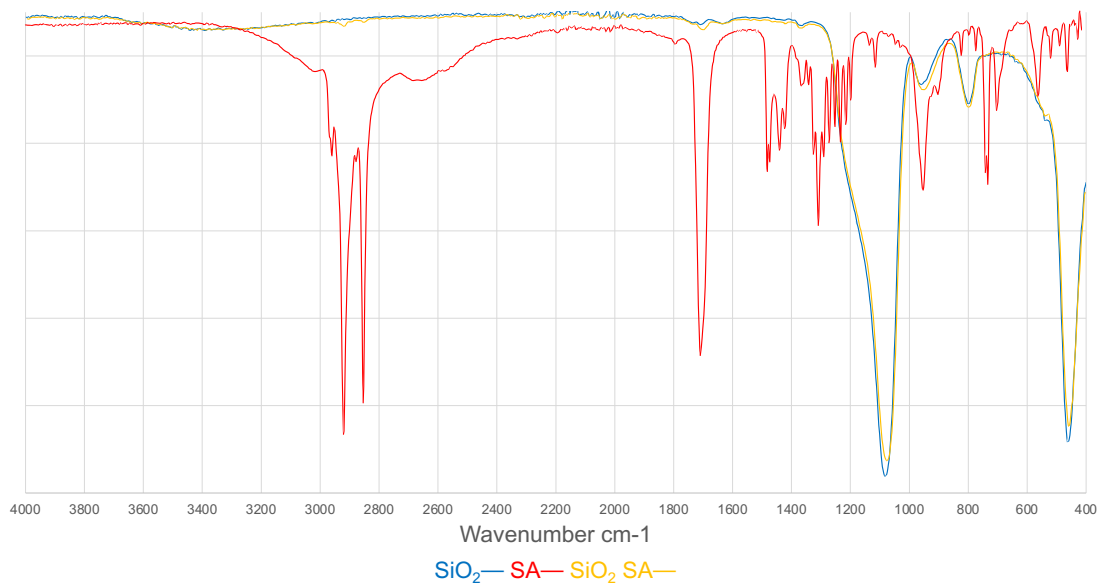


Figure 3-8 The comparison of the transmission FT-IR spectra of the raw materials with functionalised nanoparticles made in acetone. Blue: SiO₂. Red: Stearic acid. Yellow: SiO₂ functionalised with stearic acid.

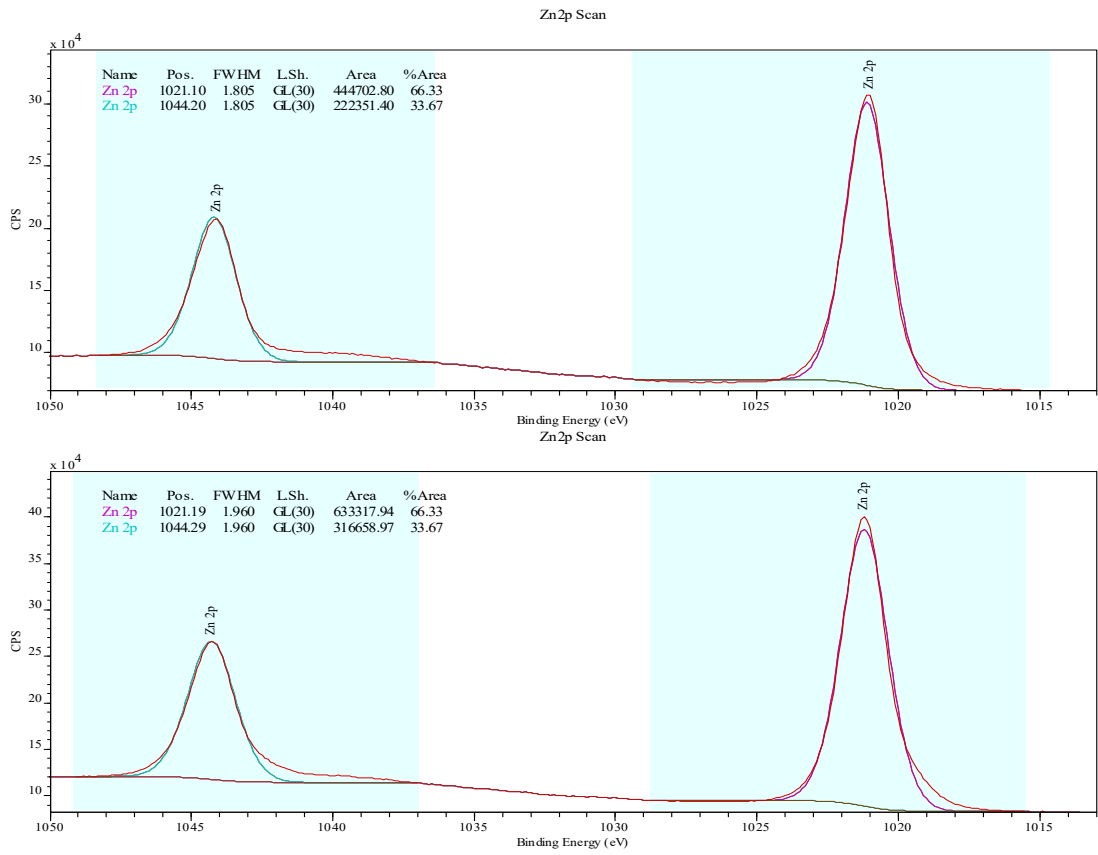


Figure 3-9 Zn 2p XPS analysis of ZnO particles (top), and functionalised ZnO particles (bottom)

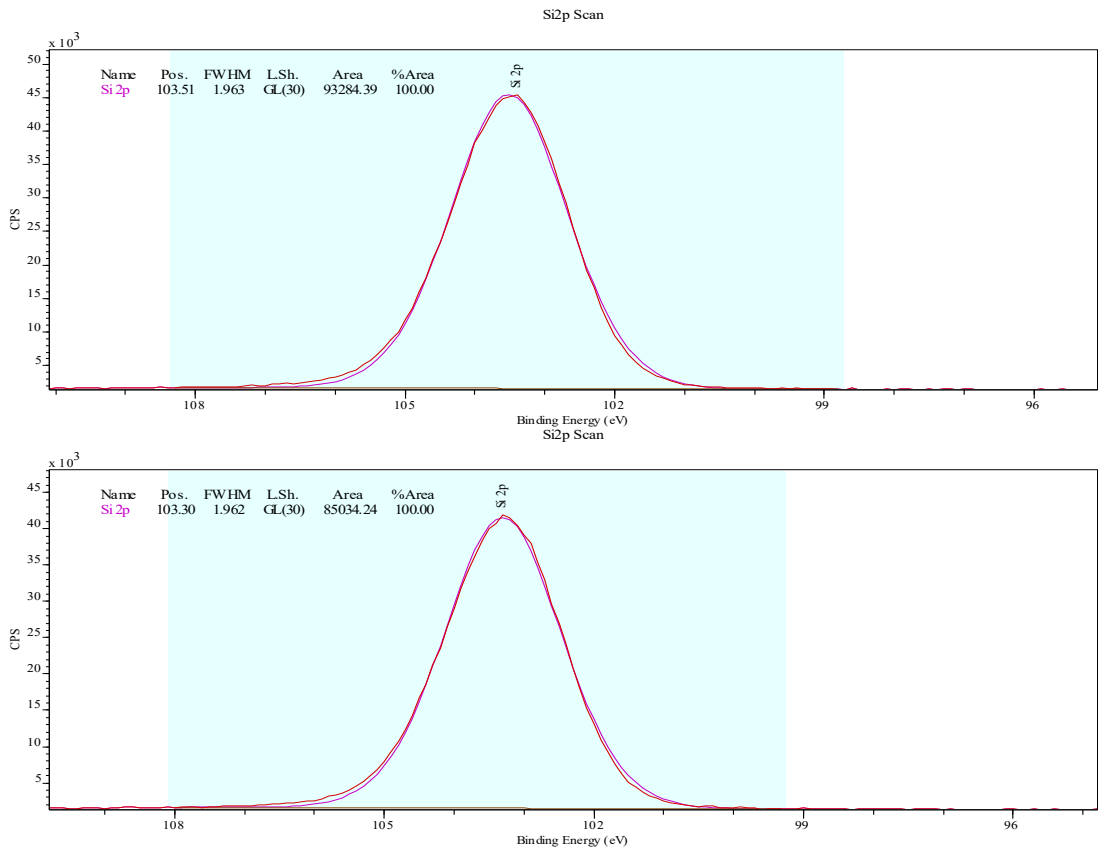


Figure 3-10 Si 2p XPS analysis of SiO₂ particles (top), and functionalised SiO₂ particles (bottom)

Other FT-IR spectra were also run to investigate if significant differences could be observed when varying the components. Figure 3-11 shows that both the stearic acid and the palmitic acid have near identical IR spectra, which is expected when you consider their chemical formula to be $C_{18}H_{36}O_2$ (stearic acid) and $C_{16}H_{32}O_2$ (palmitic acid). Figure 3-12 further emphasises the similarities with near matching spectra produced by both the stearic and the palmitic acid functionalised ZnO.

When looking at the impact of the solvent on the chemical properties of the functionalised particles (Figure 3-13), the spectra appear similar, but there are also some significant differences. When examining the resonance peaks at 1399 cm^{-1} and 1540 cm^{-1} , these peaks had a higher resolution and less broadness when ethanol was the solvent, as opposed to when acetone was used. Another difference was the fact that when looking at the spectra where ethanol was used, the peak at 1540 cm^{-1} was more prominent than the peak at 2917 cm^{-1} . This is opposite to what had previously been observed when analysing the spectrum where acetone had been used. These observations were also true when comparing the impact of the solvent on the ZnO functionalised with palmitic acid (Figure 3-14). While these are noteworthy changes, it is hard to tell the overall impact these differences have on the functionalised particles properties.

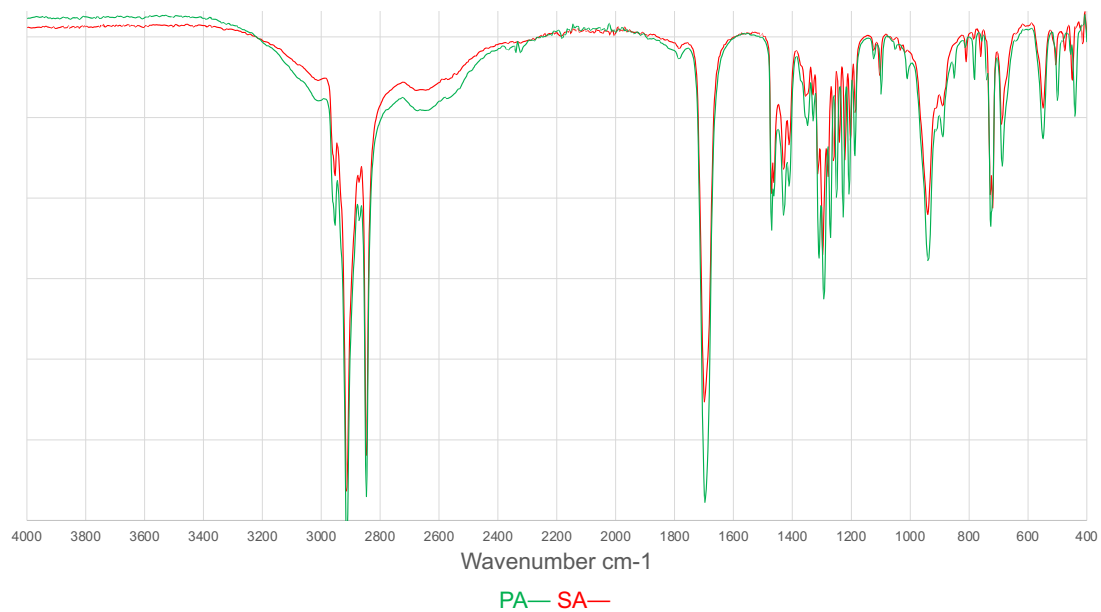


Figure 3-11 The comparison of the transmission FT-IR spectra of palmitic acid and stearic acid



Figure 3-12 The comparison of the transmission FT-IR spectra of ZnO functionalised with stearic acid in acetone and ZnO functionalised with palmitic acid in acetone.

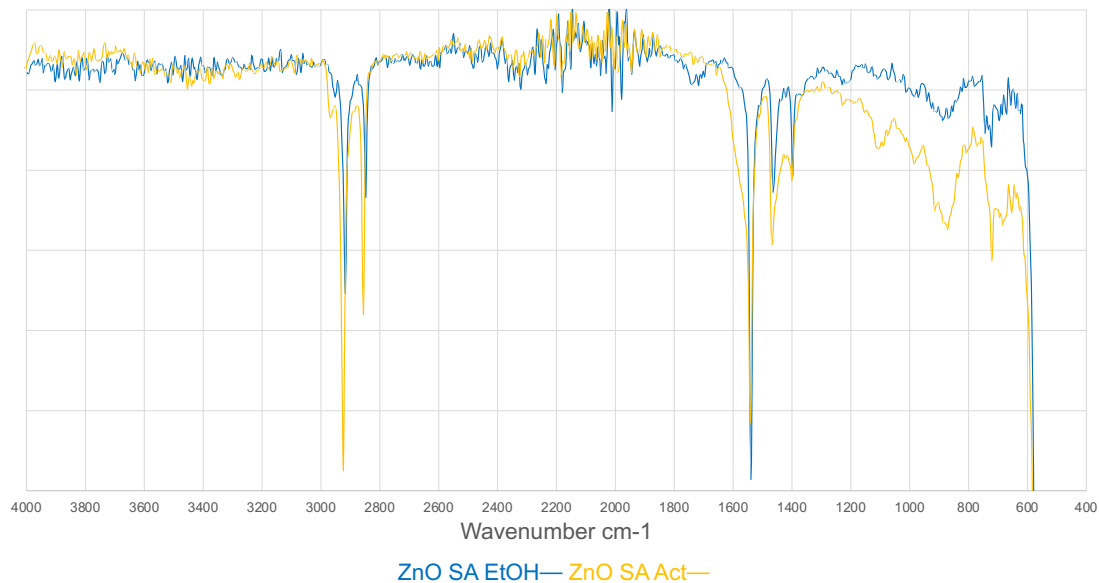


Figure 3-13 The comparison of the transmission FT-IR spectra of ZnO functionalised with stearic acid in acetone and ZnO functionalised with stearic acid in ethanol.

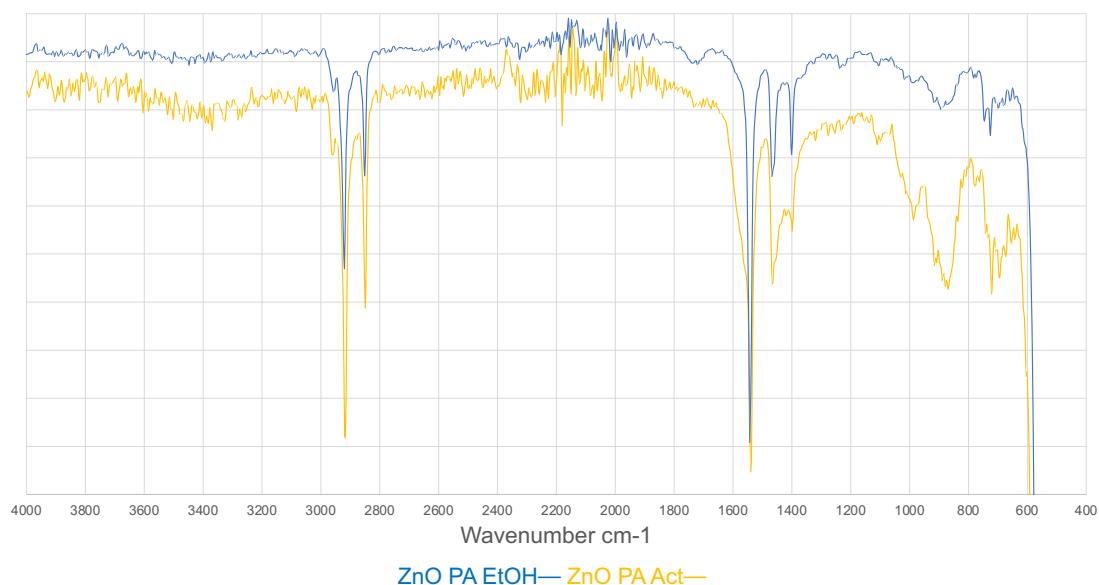


Figure 3-14 The comparison of the transmission FT-IR spectra of ZnO functionalised with palmitic acid in acetone and ZnO functionalised with palmitic acid in ethanol.

3.4.3 The production and optimisation of superhydrophobic paints

Continuing on from the previous work that aimed to produce superhydrophobic particles, the same components were again used to attempt the production of a superhydrophobic paint. Unlike the previous experiment, this experiment was designed to be a “one pot” experiment where all the components would

be combined in stages to form a paint, without the need for a wash step prior to spraying. Following the work of *Heale*, the formulation required the additional components of orotan CA-2500, texanol, and a latex.¹⁸⁸ Orotan is hydrophobic copolymer pigment dispersant used to help with the dispersal of the nanoparticles.²⁰¹ Texanol is a coalescing aid that helps with the film forming (drying) phase, even under varied temperatures and humidity levels.²⁰² Latex is the base polymer used in the paint and as such it has the biggest impact on the paint's properties. For this reason, four different latexes: Plus, Edge, 750, and 684 were investigated.

As these latexes were supplied by BASF, there was only limited information about each. The Plus is an aqueous dispersion of a polymer based on acrylic ester and styrene. The Edge is based on acrylic ester, methacrylic ester and styrene. The 750 is based on acrylic ester. The 684 is based on acrylic ester and methacrylic ester. On top of this, the solid content of each is known to be roughly the same at ~50%. In order to better understand the latexes, FT-IR analysis was performed on each one.

Figure 3-15 shows the Plus spectrum that contains acrylic ester and styrene. This spectrum includes very distinctive peaks associated with styrene including mono substituted aromatic ring bend peaks at 698 cm^{-1} and 759 cm^{-1} , aromatic ring modes at 1493 cm^{-1} and 1603 cm^{-1} , decreasing aromatic CH peaks at 3027 cm^{-1} , 3061 cm^{-1} and 3084 cm^{-1} .^{198,203} There is also two large peaks associated with acrylic esters with a C=O at 1728 cm^{-1} and a C-O at 1156 cm^{-1} . The spectrum also matches up well with spectra found in the literature for poly(acrylic ester-co-styrene).²⁰⁴

Figure 3-16 shows the Edge spectrum that contains acrylic ester, methacrylic ester and styrene. The peaks associated with styrene that were previously observed in the Plus spectrum can be observed again, although far less prominent than in the Plus spectrum. The reduced prominence of the peaks associated with styrene would suggest that the styrene component is present in a lower concentration in this latex when compared to the Plus. While the C=O at 1728 cm^{-1} was present as it was in the Plus spectra, there was a split

peak around the C-O absorption area (1144 cm^{-1} and 1163 cm^{-1}) that would suggest the C-O bonds associated in the acrylic ester and methacrylic ester absorb at different wavenumbers. Finally, there was absorption present between $3200\text{-}3600\text{ cm}^{-1}$ that can be attributed to O-H bonding.²⁰³

Looking at the final two spectra (Figure 3-17, Figure 3-18) they are reasonably consistent with what has been previously observed in the first two spectra. Neither the 750 nor the 684 latexes contain styrene, so neither have any peaks associated with styrene. When compared to the Edge latex, both spectra appear to have greater O-H absorbance between $3200\text{-}3600\text{ cm}^{-1}$. They also display the C=O peak at 1728 cm^{-1} seen in all the spectra. Looking at the C-O peaks at $\sim 1150\text{ cm}^{-1}$, the 750 which only has an acrylic ester, has a single peak, while the 684 that contains both the acrylic ester and the methacrylic ester, has a doublet peak.

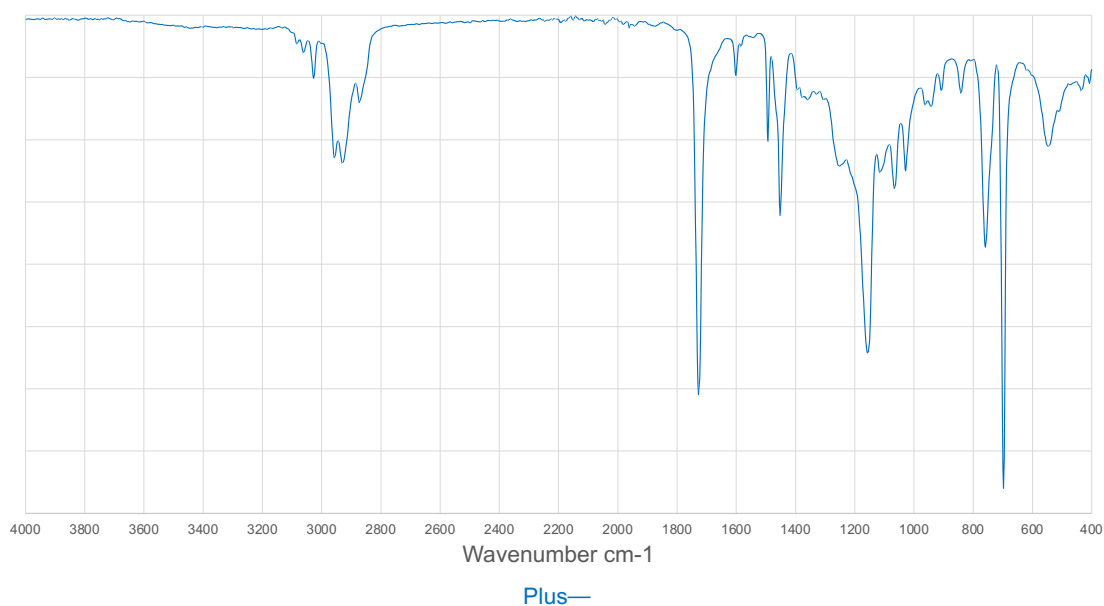


Figure 3-15 Transmission FT-IR spectrum of Acronal Plus 2483 latex

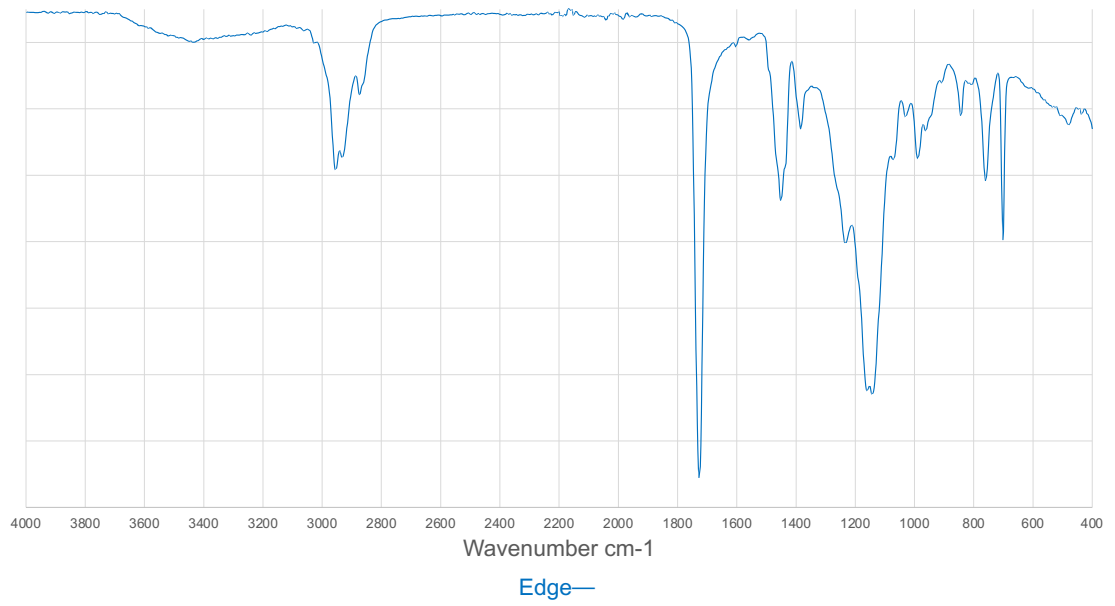


Figure 3-16 Transmission FT-IR spectrum of Acronal Edge 6295 latex

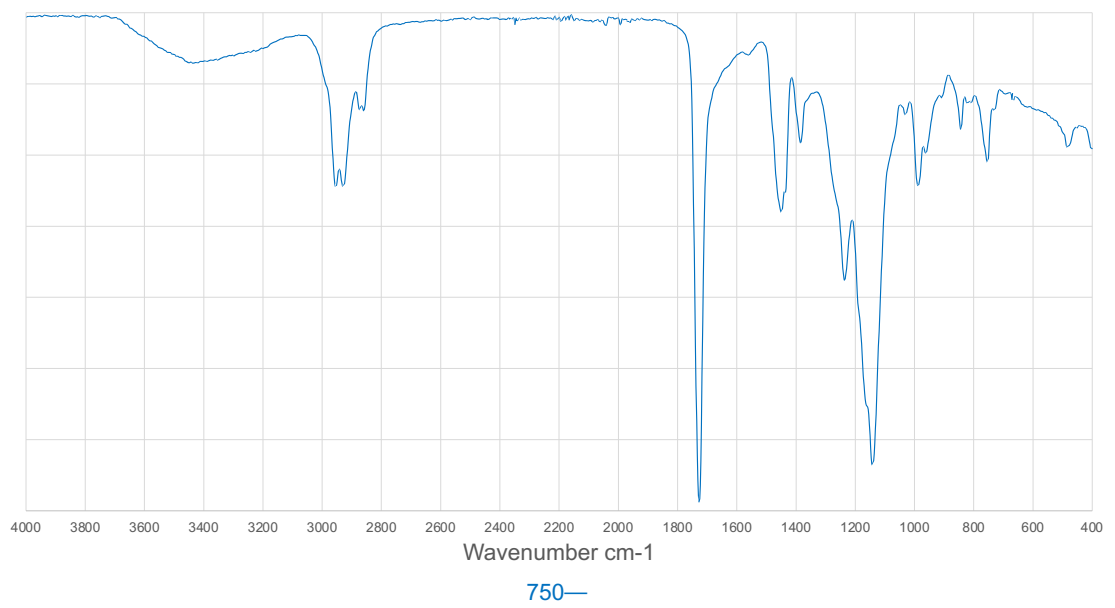


Figure 3-17 Transmission FT-IR spectrum of Acronal A 750 latex

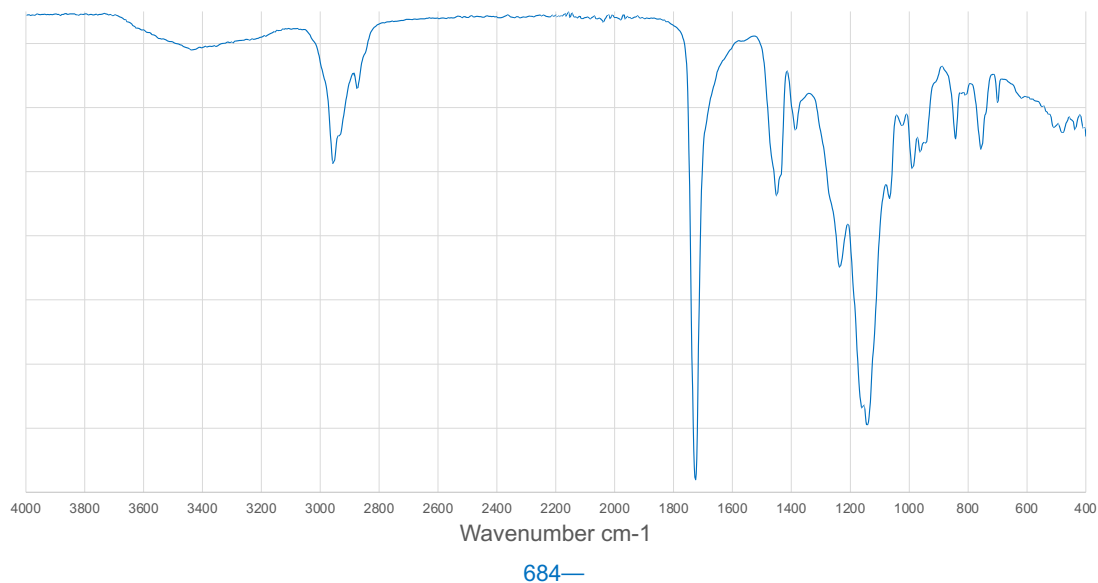


Figure 3-18 Transmission FT-IR spectrum of Acronal A 684 latex

Once some of the differences between the latexes had been established, work began on the paint formulation. Due to the polar nature of the latex and the nonpolar nature of the fatty acids, the first thing that needed to be worked out was the ratio of water to organic solvent. This was difficult as if the H₂O concentration was too high the fatty acid would crash out, whereas if the H₂O concentration too low, the latex would crash out.

Initially 1 g of particles and 1 g of fatty acid were used. As always, the first 20 min was spent dissolving the fatty acid in the organic solvent. This was followed by the addition of the aqueous phase which included H₂O, 100 µl of Orotan, and 1 g of particles. Through a trial and error, it was eventually found that if 1 ml of latex was added to 9 ml of H₂O, the 10 ml solution could be added to 50 ml of organic solvent without either the fatty acid or the latex crashing out. Once the aqueous and organic components had been stirring for 20 min, 150 µl of texanol was added to the suspension and stirred for an additional 10 min. The suspension was then transferred to a reagent bottle and sealed before being left for at least 12 h prior to spraying.

The spray application proved to be rather precarious and inconsistent initially. The spray guns could operate at a maximum pressure of 3.5 Bar. So as not

to push them to their limit, the guns were operated at 3 Bar with the jet flow on the gun opened 1.5 rotations. Once spraying had commenced, the first issue occurred when the spray gun would occasionally clog up while spraying. While this did not always happen, it was decided to sonicate the paints just prior to spraying, which completely eliminated the issue.

The next issue concerned how the paint was deposited on the surface. If the paint was sprayed onto the surface from too close a distance, the paint would run, however if the paint was sprayed onto the surface from too far away, the paint would dry in the air and deposit on to the surface as a dry powder that was easily removed. The first attempted solution was to spray from a set distance, but this did not produce consistent results. It was then realised that during the fabrication of the paints, different amounts of solvents were evaporating off, despite the use of a watch glass to reduce evaporation. To increase the paints' consistency, the organic solvent was used to make up all paints to 60 ml at the end of the fabrication process.

While making all the paints up to 60 ml did increase the consistency of the paints, it did not fully solve consistency issues when spraying. The remaining issue was thought to be due to the volatility of the organic solvents and the inconsistent environmental conditions. It was observed that at higher temperatures, the ideal spray distance was a shorter length than at lower temperatures. Due to the fact that the temperature of the lab could not be controlled, and that the lab could vary in temperature by up 20 °C (<10 °C in the winter, to >30 °C in the summer), a set spray distance was not practical. Unfortunately, this meant that the only way to achieve consistent spray deposition, was through practice. After enough practice an operator was able to get a feel for the correct spray distance, regardless of the environmental conditions. The spray distance also varied based upon which organic solvent was being used, and which latex.

The next stage of the experiment was to explore formulations that had different concentrations of particles and fatty acids. Varying the concentration of fatty acid was explored first. Suspensions containing 0.5-2.5 g of fatty acid at 0.5

g intervals were made up. Throughout the experiment the stearic acid and the palmitic acid produced results that did not appear to be significantly different. Suspensions containing 2 g or more of fatty acid had a different consistency to those previously produced. They appeared to partially split into two phases with a foam layer sitting on top of the liquid. These paints regularly clogged the spray guns and did not produce a very uniform surface when sprayed.

When looking at the suspensions with 0.5-1.5 g of fatty acids, they produced a much more uniform paint. Once sprayed, all three surfaces looked similar and uniform. However, the surfaces could be distinguished by using a Pasteur pipette to apply a drop of water to the surface. The 0.5 g surfaces tended to have Wenzel style hydrophobic properties. The other surfaces had Cassie-Baxter style properties, but the 1.5 g surfaces had a lower rolling angle than the 1 g surfaces. Some brushes and sticky tapes were used to roughly grade the durability of the surfaces, which appeared to be similar. As such, moving forwards, 1.5 g of fatty acid was used in each suspension.

Next, formulations were made using different amounts of particles. Again, suspensions containing 0.5-2.5 g of ZnO or SiO₂ particles at 0.5 g intervals were made up. When considering the optimised formulations of the paints containing the different particles, the different paints have contrasting objectives. As SiO₂ was only required to act as a scaffold that structures could form around, the goal was to use minimal amounts without compromising the surfaces durability or wetting properties. On the other hand, ZnO was being used for its antimicrobial properties, and as such, the goal was to use the highest concentration of particles, again without compromising the surfaces durability or wetting properties.

All formulations produced similar and consistent suspensions. These paints also caused no issues during the spraying process and produced uniform and consistent surfaces. The issues began when looking at the surfaces' durability and wetting properties. While the surfaces that contained ≤ 1 g of particles had no issues, both the surfaces durability and wetting properties began to deteriorate once the particle content was increased to 1.5 g. With a particle

content of 1.5 g the wetting properties began to shift toward Wenzel style properties, while the polymer also seemed compromised by the increased particle concentration. On the other hand, reducing the amount of particles present had little to no impact on the surface's properties. As such, the SiO₂ particle content was further reduced down to 0.25 g while still maintaining similar properties. Further reducing the particle content did tend to reduce the wetting properties, so 0.25 g was seen as the minimum particle content.

All this work led to the conclusion that the optimised paint formulation contained 50 ml of organic solvent, 1.5 g of fatty acid, 9 ml of deionised H₂O, 1 ml of latex, 100 µl of orotan, 150 µl of texanol, and either 0.25 g of SiO₂ or 1 g of ZnO particles. This formulation was then used to make up paints using the different combinations of components and latexes. Table 3-3 outlines the different combinations of components and latexes, with each combination of components tested with each latex.

Looking at the results, the paints containing the Plus latex clearly had the best wetting properties. Overall, the paints containing the Plus had the highest average WCA of 163.8°, which increased to 167.0° when isolating the paints that used the ZnO particles and decreased to 160.5° when SiO₂ particles were used. The 163.8° value exceeded the next average value by >25°, which was the 750, that averaged a WCA of 138.2°. The paints containing the Edge averaged a WCA of 134.5° while those containing the 684 had an average of 135.6°.

These results were interesting as it meant that no single component in the latex stood out as having a strong influence on the surfaces wetting properties. While the Plus contained acrylic ester, so did all the other latexes. The Plus also contained styrene, but so did the Edge, which had the worst hydrophobicity overall. It was noted that when comparing the IR spectra of the Plus and Edge (Figure 3-15, Figure 3-16) that the Plus seemed to have a higher concentration of styrene, which may have had an impact.

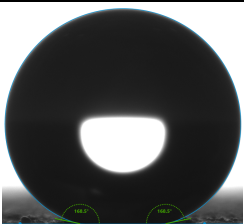
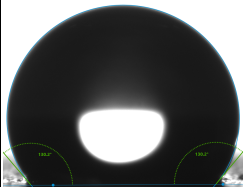
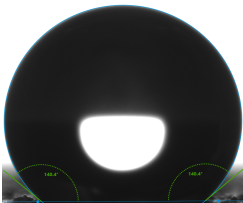
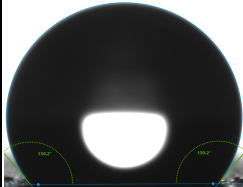
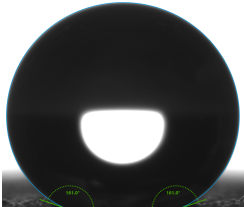
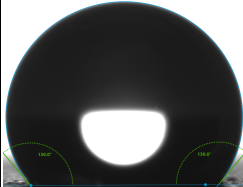
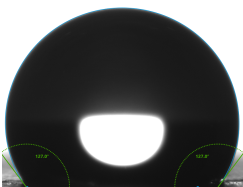
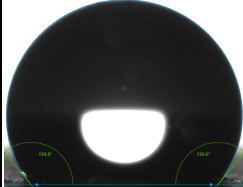
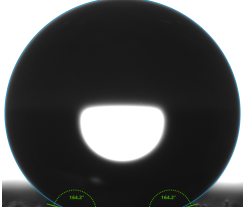
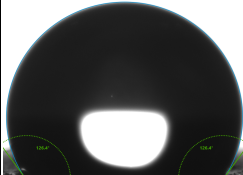
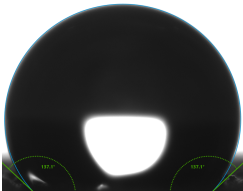
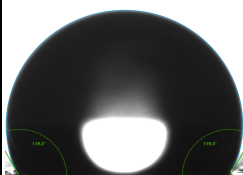
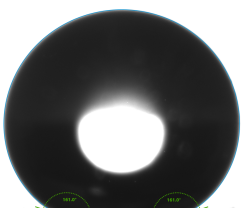
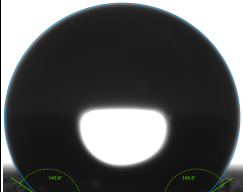
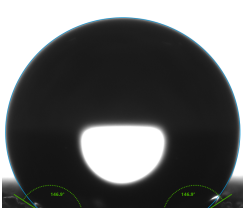
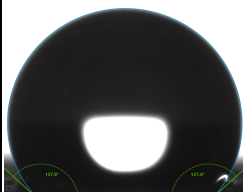
Formulation	Plus	Edge	750	684
ZnO SA Act	 \bar{x} 170.3°	 \bar{x} 130.3°	 \bar{x} 141.6°	 \bar{x} 133.4°
SiO ₂ SA Act	 \bar{x} 160.0°	 \bar{x} 131.2°	 \bar{x} 127.4°	 \bar{x} 131.4°
ZnO PA Act	 \bar{x} 168.0°	 \bar{x} 127.2°	 \bar{x} 136.8°	 \bar{x} 119.2°
SiO ₂ PA Act	 \bar{x} 160.8°	 \bar{x} 146.4°	 \bar{x} 150.1°	 \bar{x} 136.9°

Table 3-3 DSA images of latex paints and \bar{x} water contact angles. Formulations consist of a latex (Plus, Edge, 750, 684), ZnO or SiO₂, stearic acid (SA) or palmitic acid (PA), with Orotan and texanol, made up in acetone (Act) or ethanol (EtOH). Continues on next page

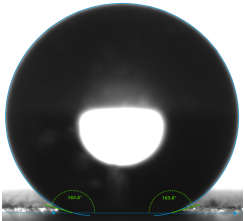
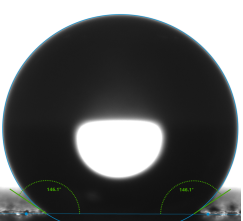
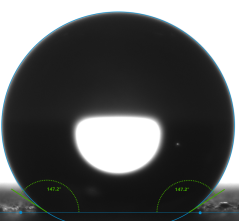
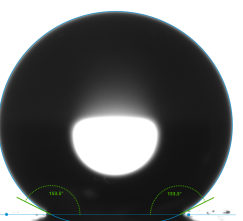
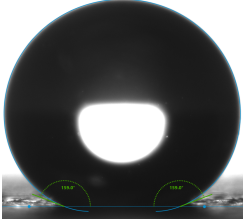
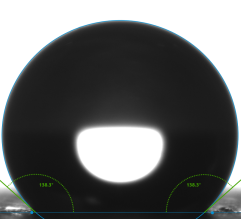
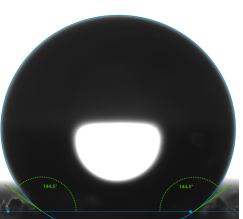
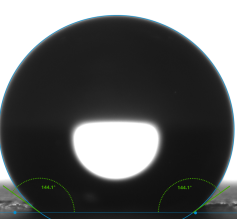
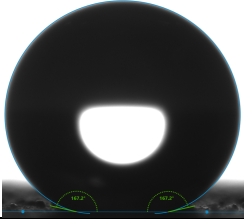
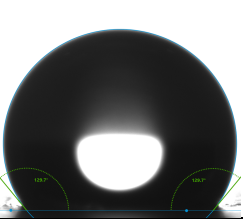
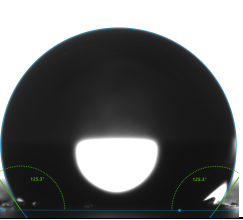
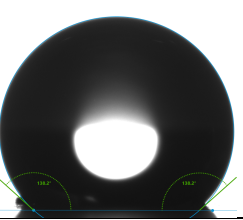
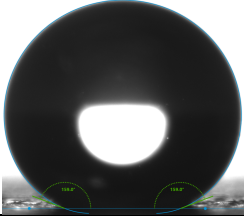
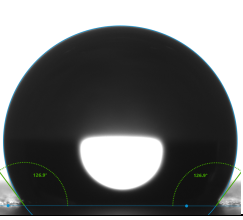
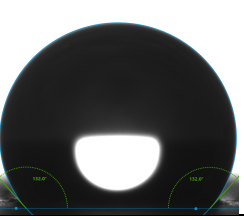
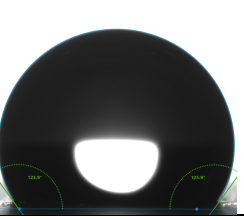
ZnO SA EtOH	 \bar{x} 166.0°	 \bar{x} 146.3°	 \bar{x} 149.2°	 \bar{x} 154.0°
SiO ₂ SA EtOH	 \bar{x} 160.6°	 \bar{x} 137.5°	 \bar{x} 143.1°	 \bar{x} 145.5°
ZnO PA EtOH	 \bar{x} 166.8°	 \bar{x} 130.4°	 \bar{x} 126.8°	 \bar{x} 138.7°
SiO ₂ PA EtOH	 \bar{x} 160.5°	 \bar{x} 127.0°	 \bar{x} 130.3°	 \bar{x} 125.6°

Table 3-3 continued

Comparing these results to the literature, many of the WCA of the paints exceed those reported.^{188–190} While the formulations mainly differed to those in the literature, in one way or another, the paint using the Plus latex, SiO₂ particles, stearic acid, and ethanol as the base, is a similar formulation to the one used by *Heale*.¹⁸⁸ Due to the similarities in formulation, it is possible that the surface roughness attributed hierarchical structures formed on the surface by the spray application, as opposed to a film applicator application, which could account for the ~20° difference in WCA. However, this may also simply be down to the different properties of the latexes.

3.4.4 The characterisation and testing of superhydrophobic paints

To begin with, FT-IR analysis was performed on the paints to see how they compared after the addition of the supplementary components. Figure 3-19 shows that the Edge, 750, and 684 paints all produced similar spectra, however, the Plus paint had a far more distinct spectrum. As the Plus paint was the paint with the most desirable wetting properties, this was of particular interest.

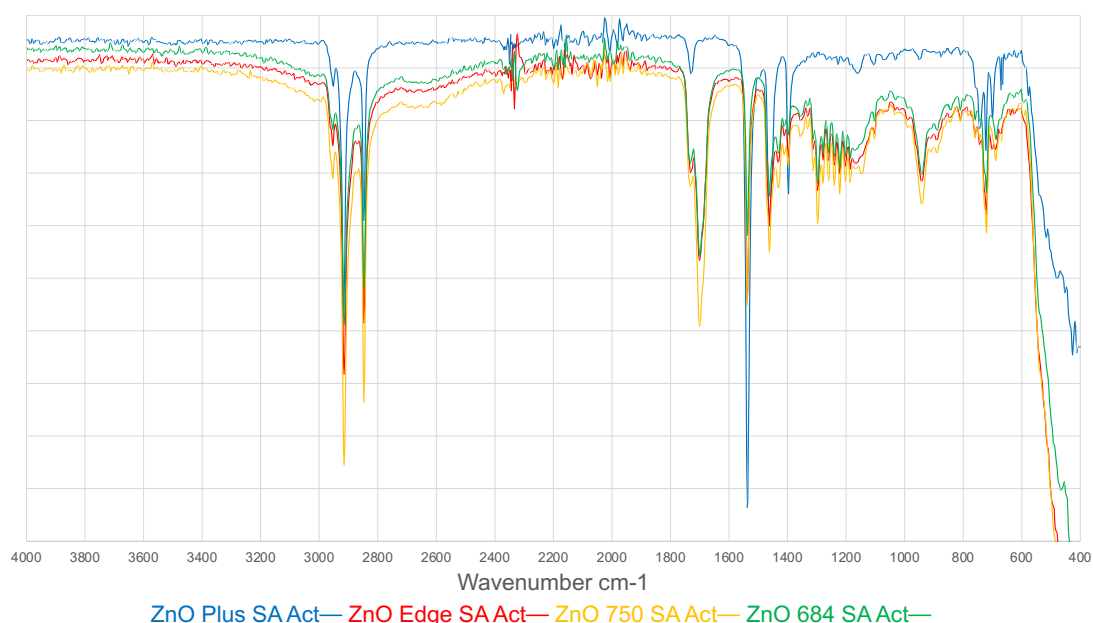


Figure 3-19 Transmission FT-IR spectra of different latex paints made up using acetone (Act) containing ZnO and stearic acid (SA).

All four spectra had reasonably similar C-H regions (2800-3000 cm^{-1}) and no other particularly discernible differences above 1800 cm^{-1} . At $\sim 1730 \text{ cm}^{-1}$ the first major difference can be observed. While the Plus spectrum has a small solitary peak in this region, the other latexes had a larger peak at $\sim 1730 \text{ cm}^{-1}$, as well as another peak 1700 cm^{-1} . The peak at $\sim 1730 \text{ cm}^{-1}$ is the C=O peak associated with the acrylic ester that has been present in all the latexes. Although the peak appears relatively small on the Plus spectrum, it is difficult to quantify this peak as it can only really be looked at relative to other peaks, which are not consistent across the spectra.

Interestingly, as observed previously when looking at the functionalised ZnO particles (Figure 3-7), the 1700 cm^{-1} peak has been completely eliminated in the Plus spectrum. This peak is associated with the C=O of the stearic acid and has again been replaced by three distinct peaks at three peaks at ~ 1540 , 1465, and 1400 cm^{-1} . These are the same peaks that have previously been observed when resonance is occurring. However, looking at the other 3 spectra, the peak at 1700 cm^{-1} is still present, although it appears to be reduced. These spectra also have the resonance peaks present, although the less distinct and in a more cluttered region.

Between 1400 and 800 cm^{-1} when analysing the Plus spectra, it was hard to discern any significant peaks due to the low intensity of the region. On the other hand, when looking at the Edge, 750, and 684 spectra, there were discernible peaks at $\sim 1300 \text{ cm}^{-1}$, $\sim 940 \text{ cm}^{-1}$, and 720 cm^{-1} . These peaks all appear in the stearic acid spectrum (Figure 3-11). It is evident by these peaks, in particular the C-O peak at 1300 cm^{-1} , that there is stearic acid present in the paint, which is not in resonance.¹⁹⁸

Finally, below 600 cm^{-1} , where the absorption due to Zn-O interactions is observed, the absorption was less dominant than previously seen (Figure 3-12). This could be due to one of two reasons: either components in the paint were altering the Zn-O bond, or the other peaks had increased so significantly, that the peaks associated with Zn-O were relatively less dominant than they

had previously been. This reduction in peak dominance could simply be down to the reduction in ZnO concentration due to the addition of the latex.

Comparatively, the SiO₂ Plus paint produced a much more equivalent spectrum, when compared to the other SiO₂ paint spectra (Figure 3-20). As such, the interesting comparison is between the paints and the components used to make them, with Figure 3-21 outlining this comparison. The C-H regions (2800-3000 cm⁻¹) were very similar to those seen in the majority of the ZnO paint spectra, with the visible peaks in the paint all associated with stearic acid. This may be due to reactions between the SiO₂ and the latex, or it may be due to the intensity of the stearic acid peaks masking the other peaks.

Between 1730-1700 a large peak with a shoulder peak can be seen. These are C=O peaks of the latex (~1730 cm⁻¹) and the stearic acid (1700 cm⁻¹) that have been previously observed. While there is a small bump at 1540 cm⁻¹, the intense resonance peaks previously seen are not present. This would suggest even in this one pot mixture, there is still no functionalisation of the SiO₂ by the stearic acid. However, the change of shape to the Si-O stretching peak at ~1080 cm⁻¹, and the splitting of the Si-O rocking peak at ~460 cm⁻¹ may suggest some sort of interaction between the SiO₂ and the latex.²⁰⁵

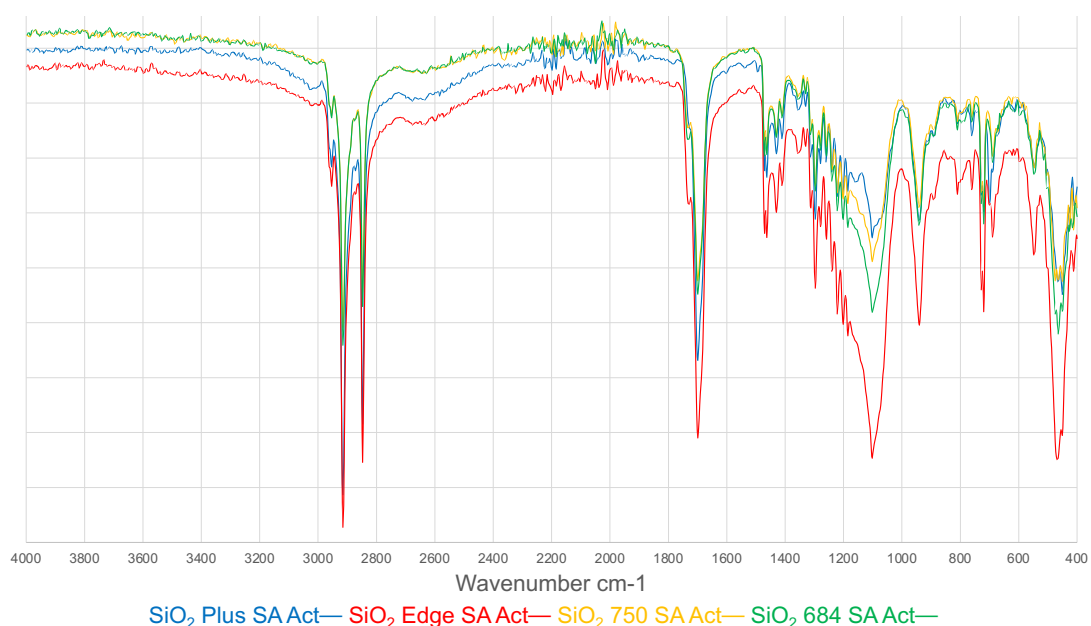


Figure 3-20 Transmission FT-IR spectra of different latex paints made up using acetone (Act) containing SiO₂ and stearic acid (SA).

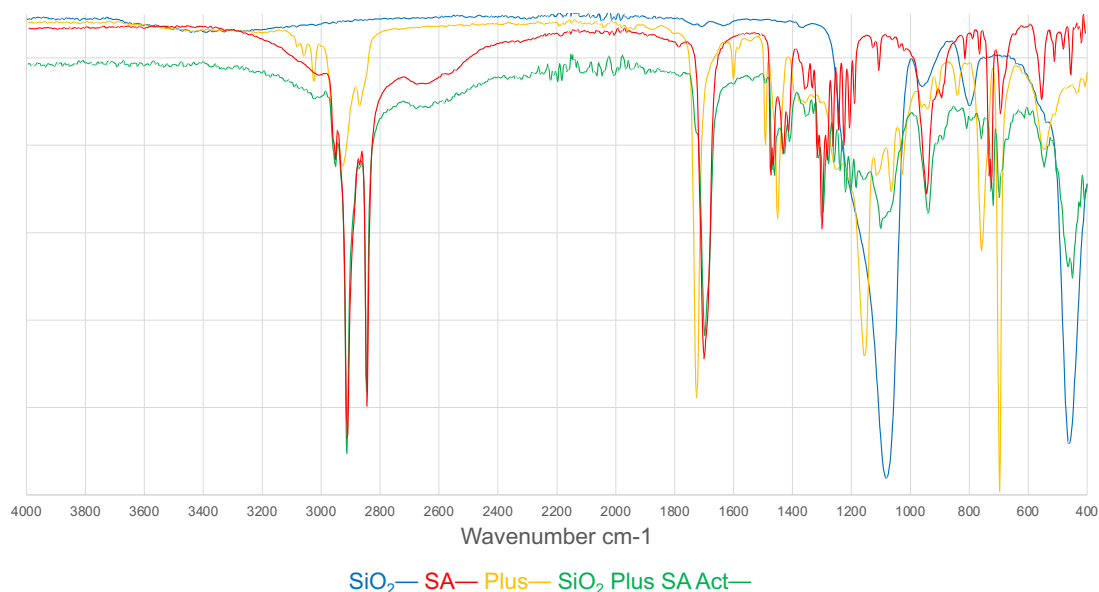


Figure 3-21 Transmission FT-IR spectra of a paint and the main components used to make it. The paint contained SiO₂, Plus latex (Plus), stearic acid (SA), made up in acetone (Act).

Again, XPS analysis was used to give further insight. When analysing the Zn and Si 2p spectra of the Plus paints (Figure 3-22), it can be seen that the value of the peaks FWHM for both the Zn (1.960-2.404 eV) and the Si (1.962-2.232 eV) have increased. This is also the case when analysing peaks in the Zn 2p spectra of both the 750 paint and 684 paint (Figure 3-23). This time, the FWHM of the Zn peaks increase from 1.960 eV to 2.241 eV for the 750 paint, and 2.238 for the 684 paint. These broadenings would suggest some sort of chemical interaction between the ZnO/SiO₂ and the latex.

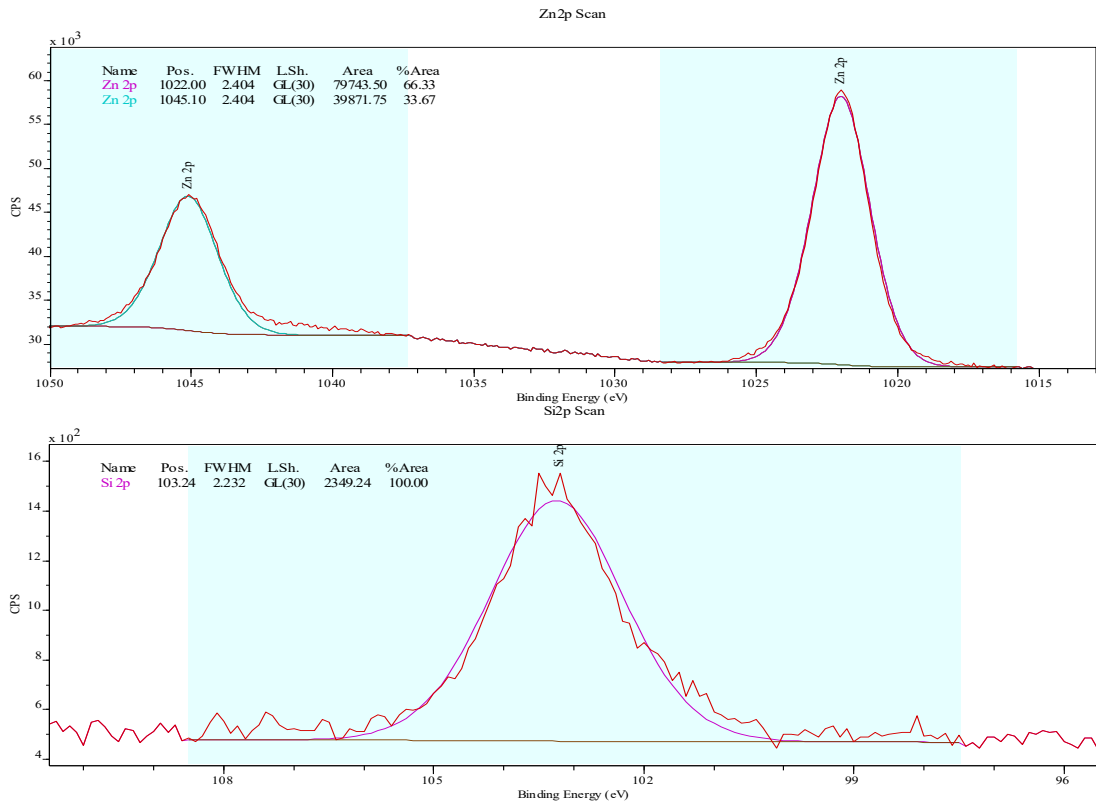


Figure 3-22 Top: Zn 2p XPS analysis of a paint containing ZnO, Plus latex, stearic acid, made up in acetone. Bottom: Si 2p XPS analysis of a paint containing SiO₂, Plus latex, stearic acid, made up in acetone.

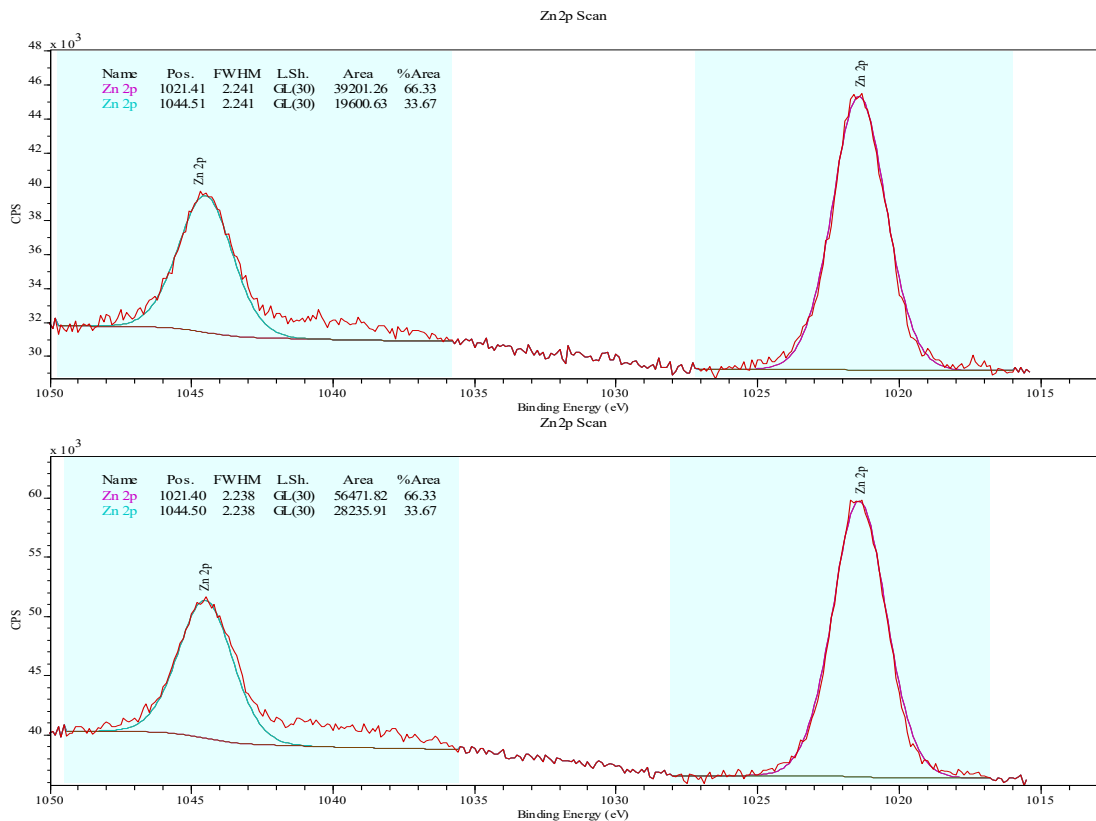


Figure 3-23 Top: Zn 2p XPS analysis of a paint containing ZnO, 750 latex, stearic acid, made up in acetone. Bottom: Si 2p XPS analysis of a paint containing ZnO, 684 latex, stearic acid, made up in acetone.

While the chemical properties of the surface are important, so are the physical properties, specifically, the surface roughness. Considering this, SEM analysis was performed on the surfaces with Figure 3-24–Figure 3-26 displaying a number of images. Figure 3-24 shows the impact the addition of the ZnO particles has on the surface structure by comparing the same paint formulations with or without particles present. It can be seen that the surface containing the ZnO was much more structured at the micro scale than the surface without. While we can see here that the topographic structures have been produced on the micro scale by the spray application, similar images taken by *Heale* showed similar, yet sub-micro scale topographic structures.¹⁸⁸ This supports the hypothesis that spray application allows for the formation of a rougher surface than a film applicator application.

Another interesting observation is that the surface without particles was relatively similar in structure to the surface that contained the larger SiO₂ particles (Figure 3-26). However, during functional testing, the surfaces containing the SiO₂ performed much better. During testing, when comparing the surface with no particles to the surface containing SiO₂, the drop test left a trail of water across the surface containing no particles, while also appearing to have reduced polymeric binding and reducing the durability, compared to the surface containing SiO₂.

Looking at the surfaces using the different latexes (Figure 3-24–Figure 3-26), it could be argued that the surface containing the Plus latex has the roughest surface. The Edge, 750, and 684 all have similar surface features, minimising the impact of surface roughness as a factor, when comparing their wetting properties. It should also be noted that ZnO containing Edge, 750, and 684 surfaces are far rougher on the microscale than the SiO₂ containing Plus paint (Figure 3-26), yet despite this, the SiO₂ paint has far more desirable wetting properties. This demonstrates the impact the chemical properties have on the surface, as well as the surface roughness.

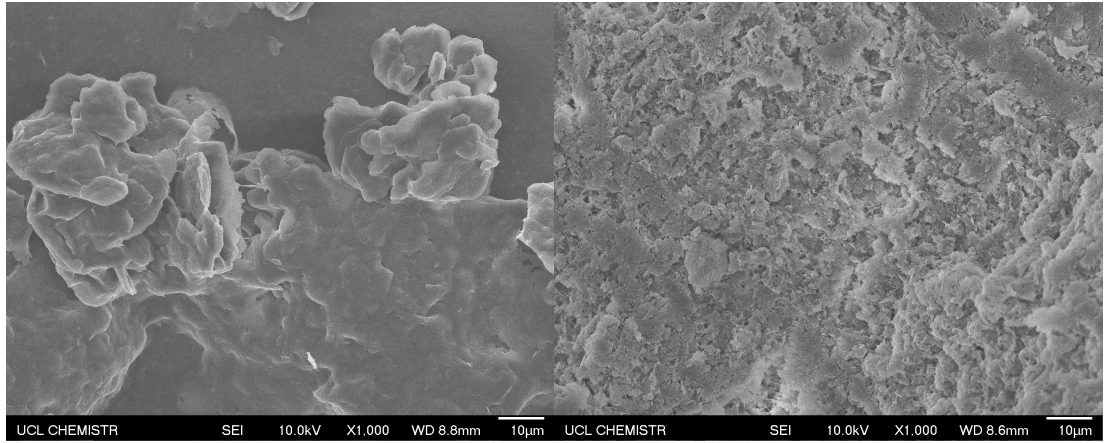


Figure 3-24 SEM imaging of: paint containing no particles, Plus latex, stearic acid, made up in acetone (left). Paint containing ZnO particles, Plus latex, stearic acid, made up in acetone (right).

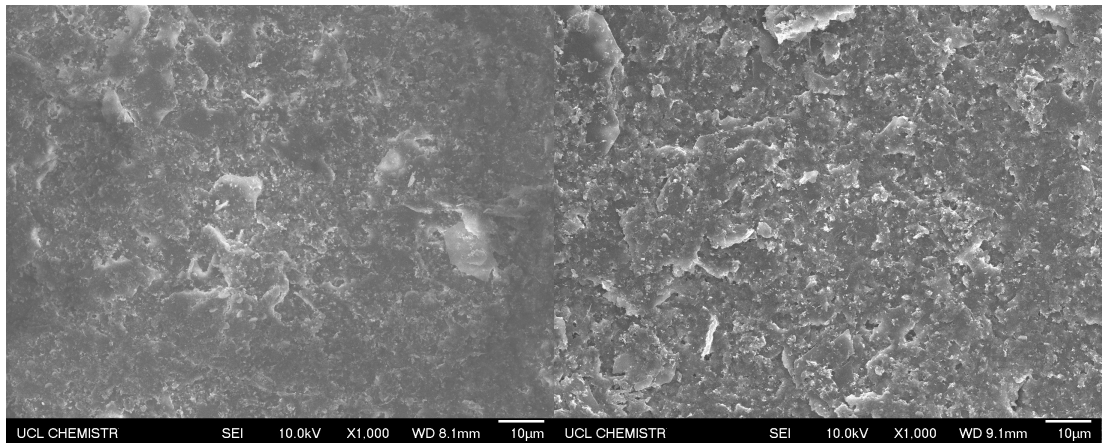


Figure 3-25 SEM imaging of: paint containing ZnO particles, Edge latex, stearic acid, made up in acetone (left). Paint containing ZnO particles, 750 latex, stearic acid, made up in acetone (right).

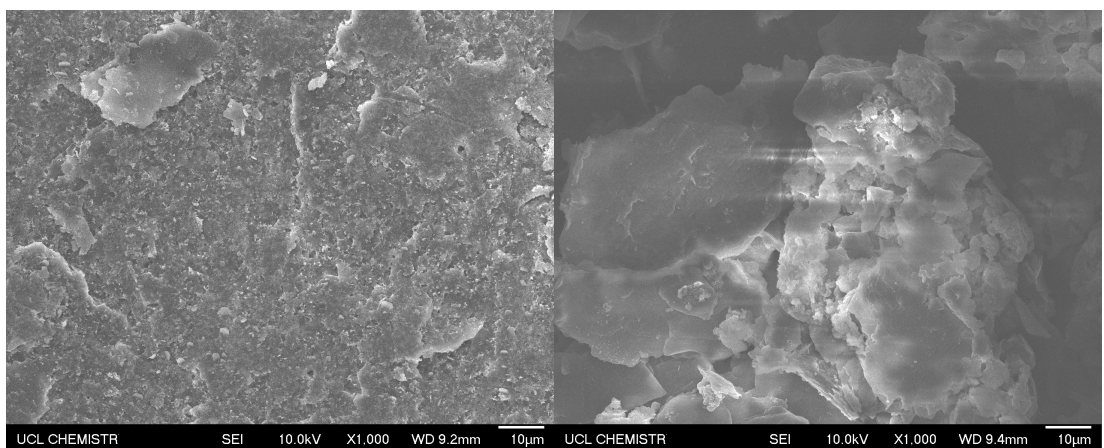


Figure 3-26 SEM imaging of: paint containing ZnO particles, 684 latex, stearic acid, made up in acetone (left). Paint containing SiO₂ particles, Plus latex, stearic acid, made up in acetone (right).

3.4.5 The functional testing of superhydrophobic paints

Once the characterisation of the paints had been completed, some functional testing was undertaken. The first test performed was a stain test. One of each sample was placed at an 80° angle, then a Pasteur pipette was used to apply a drop of a staining liquid to each surface. The stains used were crystal violet (20 ppm), red wine, and instant coffee. The results of these tests can be seen in Figure 3-27 and Figure 3-28.

Looking at the results, samples struggled the most with the wine, where the coffee and crystal violet produced similar results to each other. This is unsurprising as the ethanol present in the wine will interact well with the fatty acids, which operate as the hydrophobic agent. This interaction of the ethanol with the fatty acids was observed when ethanol was used as a solvent. On the other hand, the crystal violet and coffee are aqueous solutions, allowing the surface to repel them more easily.

When comparing the samples to each other, some interesting observations can be made. Looking at the different latexes, the Plus was the most successful at resisting staining, followed by the 750, with the Edge and 684 achieving similar results. These results follow the same pattern as the DSA results, where the Plus achieved the highest \bar{x} WCA (163.8°), followed by the 750 (138.2°), then 684 and Edge (135.6° and 134.5°).

Comparing the surfaces, the impact of the particles on the surfaces staining was also clear. The surfaces containing the ZnO had far superior stain resistance properties, when compared to those to that contained SiO₂. This can be most clearly observed when comparing the paints that used the Plus latex, and the different particles. In fact, only the two samples that used ZnO, Plus, and an acetone base, were able to completely resist staining. Interestingly, the corresponding paints that used ethanol as the solvent were unable to repel the wine. This is of particular interest, as there was little indication when comparing the FT-IR spectra (Figure 3-13) that this would be the case.

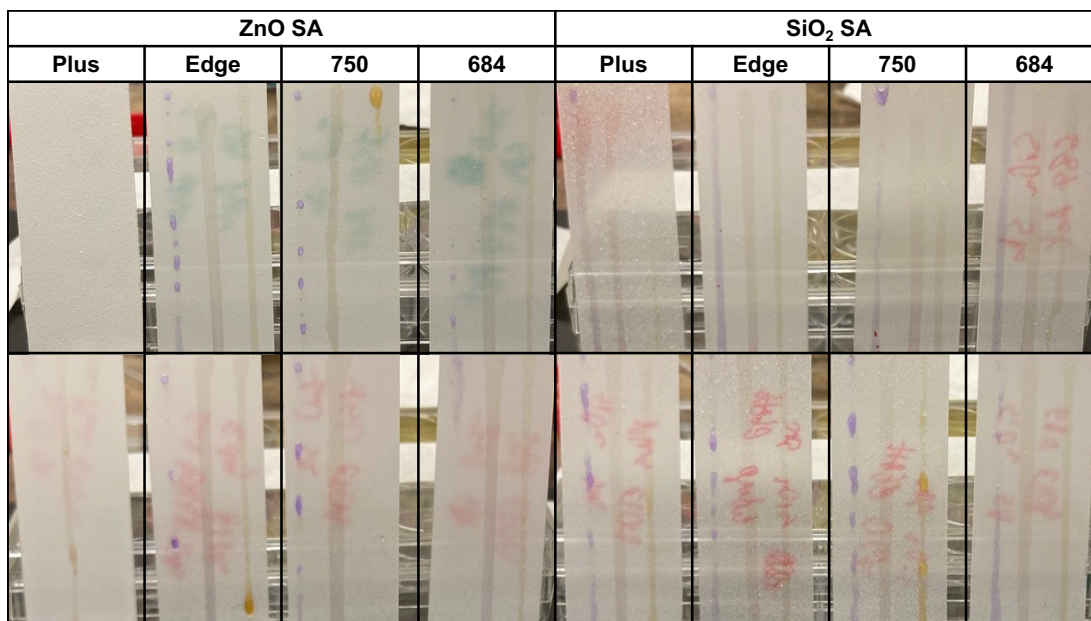


Figure 3-27 Paint stain testing. All paints contained stearic acid. The top row of paints were made up in acetone, while the bottom row were made up in ethanol. Each sample also contained ZnO or SiO₂ particles, as well as a latex. Each sample was tested with 20 ppm crystal violet (left), instant coffee (middle), and wine (right).

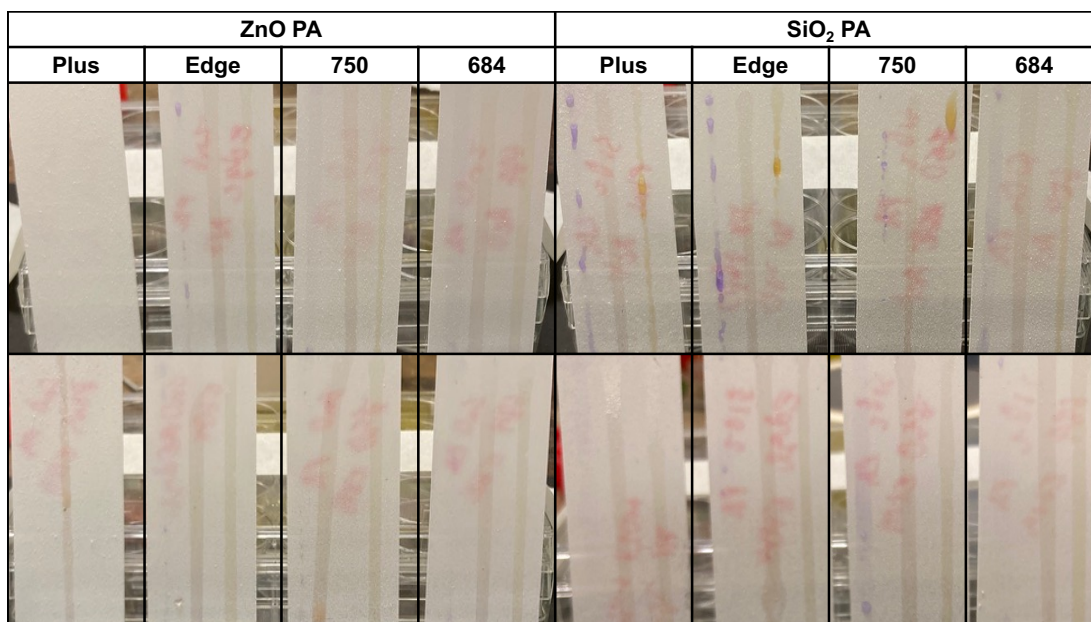


Figure 3-28 Paint stain testing. All paints contained palmitic acid. The top row of paints were made up in acetone, while the bottom row were made up in ethanol. Each sample also contained ZnO or SiO₂ particles, as well as a latex. Each sample was tested with 20 ppm crystal violet (left), instant coffee (middle), and wine (right).

Once the stain testing was complete, all samples were rinsed with deionised water and dabbed dry blue roll. A Pasteur pipette was then used to apply a few drops of water to the surfaces, to see if there were any obvious changes

in the surfaces wetting properties. While all the surfaces seemed to have some drop off in their hydrophobicity, the area where the wine had interacted with the surfaces, were particularly compromised. The exception for this was the ZnO Plus samples that used the acetone as a base, and completely repelled the wine.

Next, a ¾" paint brush was then used to brush the surfaces to access their durability. Comparatively, the paints using Edge, 750, and 684 as the latex, were more durable than those using the Plus. This was particularly evident when combined with an ethanol base. Overall, the acetone based paints appeared to be more durable than the ethanol based paints, as after brushing the acetone based paints remained intact and adhered to the surface, where the ethanol based paints did not. When analysing the impact the different particles had on the paint's durability, there did not appear to be a significant one. It is also worth noting that despite the apparent reduced durability of the paints containing the Plus latex, this was not the case for the paints that also contained the ZnO, the stearic or palmitic acid, that were made up in an acetone base. These surfaces were as durable as any of the other paints.

To assess the impact of the functional testing, the samples were subject to further DSA. The results of this testing can be seen in Table 3-3 and Table 3-4. Comparing the impact of the different latexes on the paints, the Plus had the biggest drop off in \bar{x} WCA (24.2°), while the other paints \bar{x} WCA drop of 14.3° - 15.3° . However, further analysis of these results is far more positive. When the Plus results are split based on the particle used in the samples, there is only a 9.2° drop in \bar{x} WCA for the paints that contained ZnO, compared to a massive 39.1° drop when they contained the SiO₂.

There are two factors to consider when evaluating these drops in hydrophobicity: changes to the surface energy, changes to the surface structure. When the wine comes into contact with the surface, it does not appear to change the surface structure. This means that the reduction in the surface's hydrophobicity due to the wine, is most likely down to a reaction between the wine and molecules at the surface, altering the surface energy.

As the surfaces readily repel water, a reduction in the hydrophobicity of the surface during the cleaning step, is more likely due to the destruction of surface structures when dabbing the surface dry. In fact, with enough pressure and force, all of the surfaces wetting properties could be reduced significantly. The hydrophobic properties of all of the paints could also be destroyed by submerging the surface in ethanol. Cleaning products that target organic molecules, such as washing up liquids, also destroyed the surfaces superhydrophobic properties.

Figure 3-29 shows the result of the tape test, which clearly shows that the tape is removing paint from the surface. The degradation of the surface due to the removal of the paint from the surface can also be observed. However, this had minimal impact on the surface's wetting properties. The paint containing ZnO, stearic acid, Plus latex, made up in acetone, saw a 4.2° reduction in its \bar{x} WCA, while the equivalent paint containing palmitic acid, actually saw its \bar{x} WCA increase by 3.6° . This must mean that a rougher surface was left behind when the tape was removed, as the chemical properties of the surface should not have changed.

What was also interesting was that surfaces that had previously had their superhydrophobic properties disabled, were able to be regenerated. This was effectively done by removing the top layer of the surface. To restore the surfaces superhydrophobic properties after chemical damage, a fine sandpaper was used to remove the chemically damaged compounds at the surface, exposing new undamaged compounds with their superhydrophobic properties still intact. This could also be used to restore surface roughness that had been removed due to physical damage.

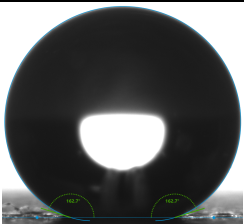
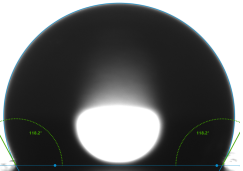
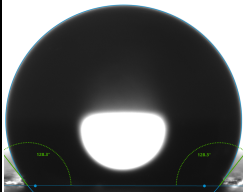
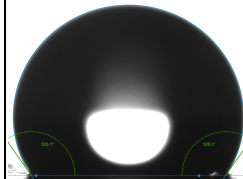
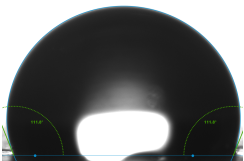
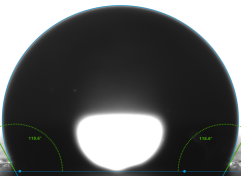
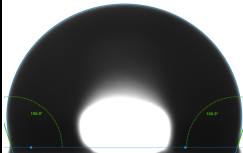
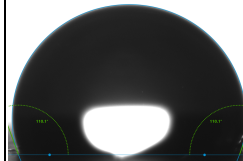
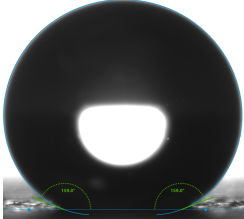
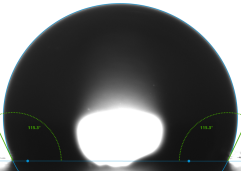
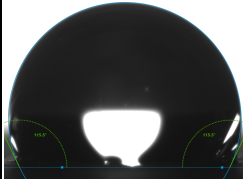
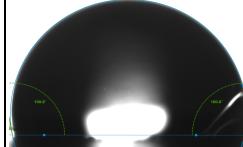
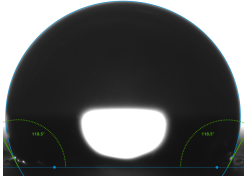
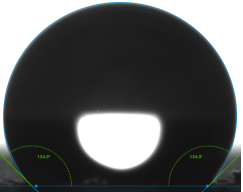
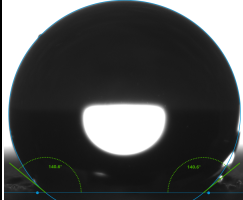
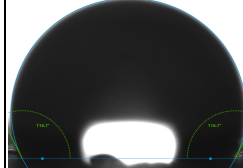
Formulation	Plus	Edge	750	684
ZnO SA Act	 \bar{x} 162.6°	 \bar{x} 119.7°	 \bar{x} 131.2°	 \bar{x} 122.8°
SiO ₂ SA Act	 \bar{x} 112.6°	 \bar{x} 120.9°	 \bar{x} 104.2°	 \bar{x} 113.9°
ZnO PA Act	 \bar{x} 158.1°	 \bar{x} 113.7°	 \bar{x} 116.4°	 \bar{x} 100.7°
SiO ₂ PA Act	 \bar{x} 118.8°	 \bar{x} 135.5°	 \bar{x} 139.6°	 \bar{x} 120.6°

Table 3-4 DSA images of latex paints and \bar{x} water contact angles after stain testing and cleaning. Formulations consist of a latex (Plus, Edge, 750, 684), ZnO or SiO₂, stearic acid (SA) or palmitic acid (PA), with Orotan and texanol, made up in acetone (Act) or ethanol (EtOH). Continues on next page

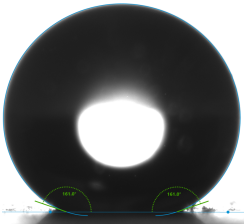
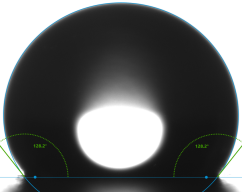
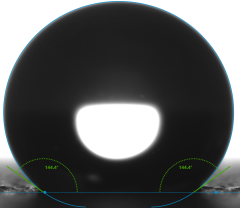
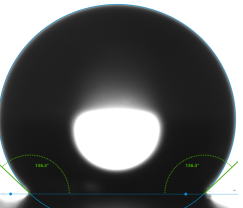
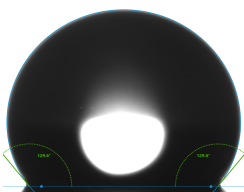
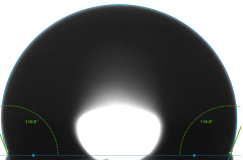
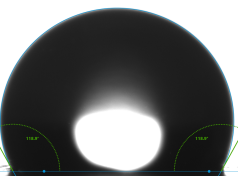
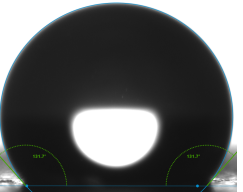
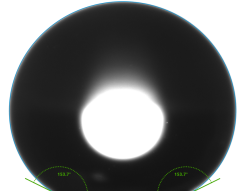
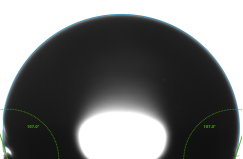
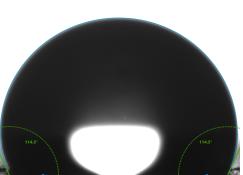
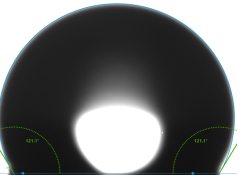
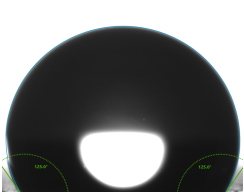
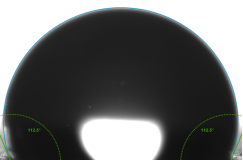
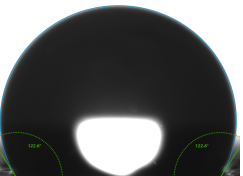
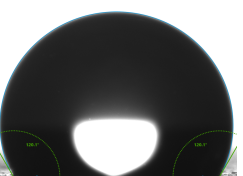
ZnO SA EtOH	 \bar{x} 158.8°	 \bar{x} 126.6°	 \bar{x} 143.3°	 \bar{x} 135.2°
SiO ₂ SA EtOH	 \bar{x} 129.1°	 \bar{x} 109.8°	 \bar{x} 116.7°	 \bar{x} 134.6°
ZnO PA EtOH	 \bar{x} 151.7°	 \bar{x} 110.8°	 \bar{x} 113.9°	 \bar{x} 122.2°
SiO ₂ PA EtOH	 \bar{x} 125.0°	 \bar{x} 117.0°	 \bar{x} 126.0°	 \bar{x} 119.9°

Table 3-4 continued.

The final test performed on these samples was a tape test. This test simply required the consecutive firm application and removal of 10 strips of Scotch Magic Tape to the painted surface. As both of the paints containing stearic or palmitic acid in combination with ZnO, Plus latex, and an acetone base, had displayed superior functional properties up until now, only those two surfaces were tested.

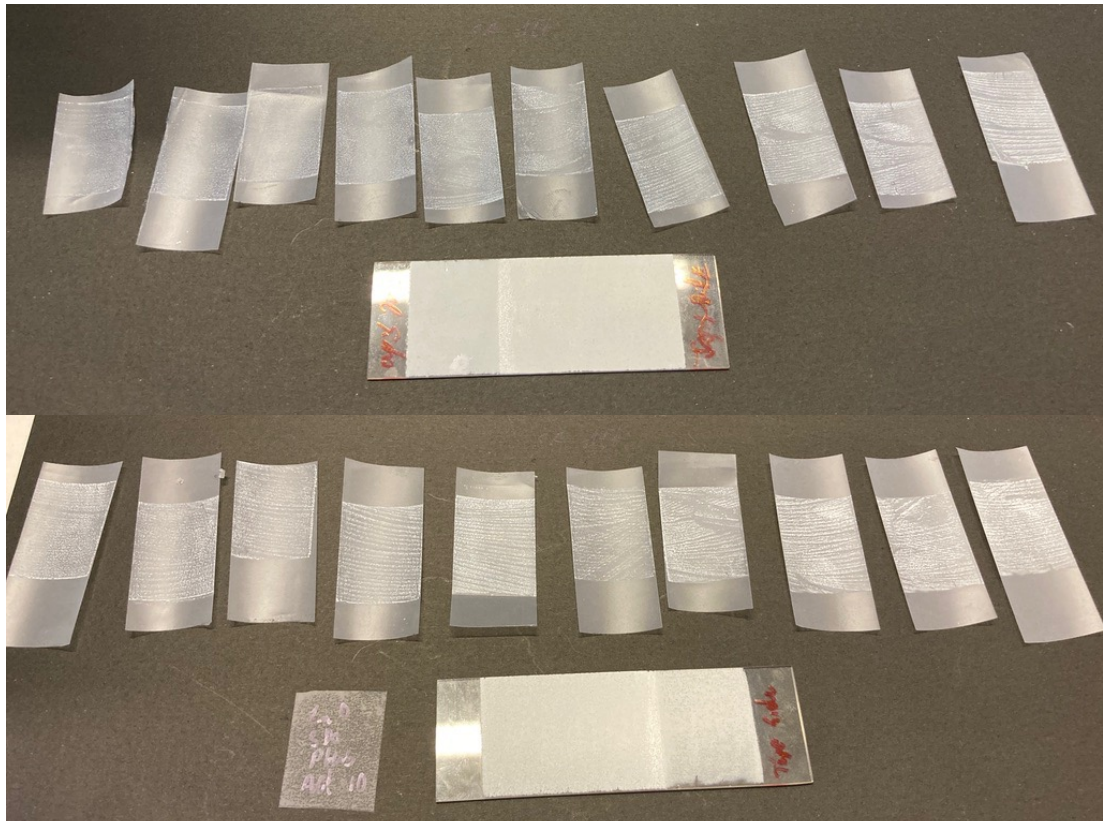


Figure 3-29 The results of tape tests consisting of the firm application and removal of 10 strips of Scotch Magic Tape consecutively. Top: Paint consisting of ZnO, Plus latex, stearic acid, made up in an acetone base. Bottom: Paint consisting of ZnO, Plus latex, palmitic acid, made up in an acetone base

Figure 3-29 shows that the tape removed thin layers of paint from the surface. Looking at the slides, significant cumulative damage caused by the tape test can be seen on the surface. However, when investigating the surfaces wetting properties, this damage had minimal impact on the surfaces superhydrophobic properties (Figure 3-30). Despite the fact that pressure was applied to the surface to adhere the tape, possibly compromising the surface structures, a new surface was formed when the tape removed the top layer. For the paint containing stearic acid, the newly exposed surface only had a minor drop in \bar{x} WCA (170.3° - 166.1°). For the paint containing palmitic acid, there was

actually a slight increase in \bar{x} WCA (168.0° - 168.6°) when comparing the newly exposed surface to the old one.

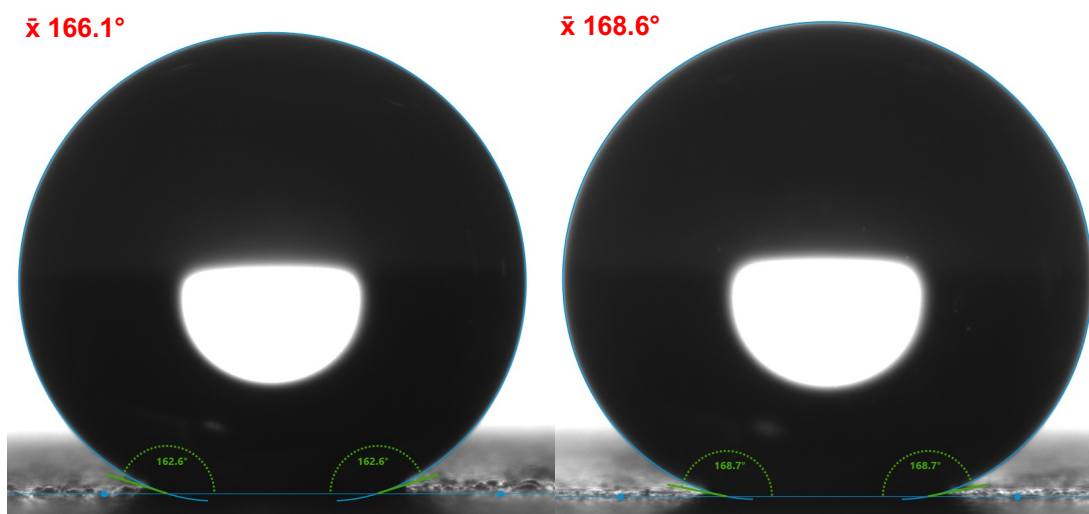


Figure 3-30 DSA image of a 5 μ l water droplet on painted surface after a completed tape test. Left: Paint consisting of ZnO, Plus latex, stearic acid, made up in an acetone base. Right: Paint consisting of ZnO, Plus latex, stearic acid, made up in an acetone base.

3.5 Summary and conclusion

Superhydrophobic particles capable of achieving WCAs in excess of 170° were fabricated, exceeding the WCAs of similar in the literature.^{186,187} To achieve this, a formulation consisting of a hydrophobic agent, a solvent, and a particle was required. Fatty acids were used as the hydrophobic agent, with both palmitic and stearic acid operating effectively as this aspect. Both ethanol and acetone operated efficiently as the solvent, although acetone was easier to work with, and achieved slightly better results. However, of the two particles selected for testing, only the ZnO particles were functionalised by the fatty acid, where the SiO₂ particles were not, and remained superhydrophilic. FT-IR analysis backed up this statement by clearly showing that the ZnO was reacting with the fatty acids, where the SiO₂ was not.

Next, superhydrophobic paints were formulated. This required the addition of a latex to the previous components. Four different latexes were tested, with paints produced using the Plus latex being functionally superior to those using the other latexes. Optimised paints containing Plus latex, using an acetone

base were capable of achieving \bar{x} WCAs above 170° , with these surfaces also demonstrated stain resistant properties. These WCA values again exceeded those of similar surfaces found in the literature.^{188–190} Unfortunately, these surfaces were susceptible to wear and tear by both physical and chemical means, reducing their hydrophobic properties. It is difficult to compare to durability of the surfaces to those in the literature, as there is no real standardised testing. However, the surfaces superhydrophobic properties could be restored by using sandpaper to carefully remove the top layer of the surface.

Overall, these were a highly successful set of experiments. The optimised paint was far more consistent than any previous coatings made in the group. It also operated functionally better than other paints that have been previously produced. Despite this, durability against everyday wear and tear may still be an issue. As latex would not be considered the most durable polymer, it was decided to investigate other polymers that are more durable and may be capable of producing similar functionalised surfaces. The next chapter will also investigate the paint's antimicrobial properties and others, comparatively to the durable polymer coating.

4 The Production, Application, and Testing of Superhydrophobic, Durable Coatings

4.1 Aims

The introduction covered how durable polymers could be functionalised for use as touch surfaces in high traffic areas. Continuing on from the work completed in the last chapter, the first aim of the experiments in this chapter was to produce superhydrophobic coatings using a more durable polymer than latex. Once coatings could be fabricated, the next step would be to perform characterisation and functional testing on the surfaces, so they could be assessed and compared to the latexes. This would require finding a durable polymer to replace the latex in the current mixture, with minimal disruption to the current process.

4.2 Background

In chapter 3 it was shown that superhydrophobic properties could be achieved using fatty acids as a functionalising agent. This was shown to be true for both the functionalisation of particles and paints. However, the durability of the surfaces undermined their practicality were they to be applied as a touch surface in a high traffic area. For this reason, polymers with a better durability than latex need to be investigated. With this in mind, Altro Ltd. were able to provide two durable polymer coatings: Altro Tect which is an epoxy resin and Altro Seal is a polyurethane coating. As it was planned to again use ZnO in these superhydrophobic coatings, the concept of dual-function surfaces was also explored.

Currently epoxy resins are base polymers of high interest with many research groups working towards superhydrophobic surfaces with an epoxy base.²⁰⁶ Qi *et al.* produced a superhydrophobic epoxy using SiO₂ nanoparticles and n-octyltriethoxysilane.²⁰⁷ This process began by dispersing 5 g of SiO₂ nanoparticles in 100 ml of toluene, before adding 10 ml of n-

octyltriethoxysilane to the suspension and stirring at 120 °C for 12 h. Rather than combining the functionalised particles with the epoxy in a single coating, the surface was first sprayed with an epoxy layer, before being sprayed with a coating of the functionalised particles dispersed in ethanol. Once dry, it was found that the highest recorded WCA of 173.1° could be achieved by using a 5% weight particle spray as the top coating.

Liu et al. chose to use an amine over a fatty acid or silane to produce a superhydrophobic epoxy surface.²⁰⁸ Unlike previous reported methods, epoxy rather than the particles was first modified with octadecylamine. This was done by dissolving 20 g of epoxy into 250 ml of toluene over a 30 min period. At the same time, 10 g of octadecylamine was mixed with 100 ml of ethanol. The two solutions were then combined and refluxed for 2 hrs at 45 °C, before the octadecylamine functionalised epoxy was purified via distillation. The next stage was to mix the functionalised epoxy with a curing agent and SiO₂ nanoparticles in acetone. The formulation was then sprayed onto a number of substrates, before being cured for 2 h at 120 °C. After curing, a 158.3° WCA was obtained for coatings with a 50:50 SiO₂ to epoxy weight ratio.

Penna et al used alumina nanoparticles functionalised with stearic acid to make superhydrophobic epoxy coatings.²⁰⁹ They began by refluxing 2 g of alumina particles with 5 g of stearic acid in 2-propanol for 23 h. The particles were then washed and dried overnight at 80 °C before proceeding. The next stage used a brush to apply the epoxy to a steel substrate, which was then cured for 3.5 h at 40 °C. 2 wt% of functionalised particles were then dispersed in 2-propanol before being sprayed onto the epoxy layer. The samples were then cautiously left 4 days to ensure total solvent evaporation and that the surface was fully cured. However, no WCA was registered on their optimised surface, as it appears their DSA was ill-equipped to handle high WCAs.

The other base polymer supplied was a polyurethane, which is another polymer of interest that many research groups working towards superhydrophobic surfaces use as the base.²¹⁰ *Hejazi et al.* incorporated superhydrophobic SiO₂ into a thermoplastic polyurethane using compression

moulding.²¹¹ Their work began by first forming substrate thermoplastic polyurethane sheets using granules and compression moulding. Once the substrate had been formed, superhydrophobic SiO₂ particles purchased from Evonic Industries that had been pre-functionalised with hexamethyldisilazane, were spread across the surface and pressed into the surface for up to 60 min using 4 MPa, with the temperature set to 180 °C. Finally, the samples were cleaned using ethanol and ultrasonication to ensure that the remaining particles were firmly embedded in the surface. Once dry, WCAs of ~160° were reported.

Jiang et al. used spin-coating to make a superhydrophobic polyurethane coating.²¹² First, under N₂ for inert atmospheric protection, SiO₂ was functionalised by mixing it with hexamethyldisilazane in methyl-isobutyl-ketone at 50 °C, for 24 h. The functional particles were then prepared for spin coating by suspending 3 wt% in toluene. Next a spin-coating process was used to coat 1:10 polyurethane to dimethylformamide solution onto a glass slide. As soon as the slide had been coated with polyurethane solution, another spin-coating process was carried out to coat the particle suspension onto the still wet polyurethane coating. Once dried, the optimised samples had a WCA of 166.2°.

Using a simple spray application, *Wu et al.* prepared superhydrophobic polyurethane based surfaces.²¹³ Firstly, a commercial superhydrophobic SiO₂ functionalised with trimethylsiloxy was acquired. Next, tourmaline particles were functionalised with hydroxyl silicone oil by autoclaving a 1:1 mixture under nitrogen, at 140 °C, for 12 h. Petroleum ether was then used to wash the particles, before they were dried for 12 h at 90 °C. A final suspension was then made up in dimethylformamide, consisting of 4.75 wt% polyurethane, 2 wt% functionalised SiO₂ particles, and 0.25 wt% functionalised tourmaline particles. The final suspension was then sprayed onto a polyurethane substrate and left to dry at room temperature, with the suggestion being that the dimethylformamide in the final solution would dissolve the substrate, allowing the functionalised particle to better incorporate into the surface. Once dry, this method produced samples with a WCA of ~165°.

The final surfaces of interest are dual-functional surfaces, which are both superhydrophobic and antimicrobial. While surfaces that rely on their topological features can be highly effective dual-functional surfaces, they require these features to have very specific spatial and geometric parameters. The issue is that these features are produced through techniques currently only viable on a small scale.^{104,107,108,214} A possible solution to dual-functional surfaces could be one of the many superhydrophobic surfaces being designed for large scale production, which already incorporate nanomaterials with associated antimicrobial properties into their formulations.^{215,216} However, the antimicrobial properties of many of these surfaces are currently not being untested.

There are some coatings that have been tested for both their antimicrobial and superhydrophobic properties. *Lai et al.* produced an antimicrobial and superhydrophobic coating by mixing 0.05 g of ZnO with 3.5 g of polydimethylsiloxane in 100 ml of ethanol.²¹⁷ Polyester fabric was then dipped in the coating formulation before being heated at 70 °C for 10 mins in an oven and plasma treated. Once fully processed, the resultant coating produced a WCA of 162.7°. It was also determined that after 18 h, the fabric had killed ≥99.85% of both the Gram-positive and the Gram-negative bacteria exposed to the fabric. In a similar study, although their methodology was not very clear, *Shaban et al.* found their ZnO coatings produced WCAs of up to ~154°. ²¹⁸ They also carried out qualitative testing showing that the surface was antimicrobial against both Gram-positive and Gram-negative bacteria, amongst other things.

While there is much literature on superhydrophobic epoxy and polyurethane surfaces, many of these surfaces are simply coated in a top layer of superhydrophobic material, rather than being a true superhydrophobic composite.^{207,209,211} However, there are some instances where the superhydrophobic reagent has been fully incorporated into the bulk polymer.²⁰⁸ There have also been instances where stearic acid has been used, ZnO has been used, and spray applications have been used.^{208,209,218} This should allow for the experiment to begin with parameters similar to those carried out in

chapter 3, with changes to the base polymers being the exception. Finally, while it has not been well reported, there are instances where ZnO incorporated coatings have produced dual-function properties, meaning this should be tested when possible.^{217,218}

4.3 Experimental

For these experiments, most of the components were those used previously (chapter 3). SiO₂ and ZnO were used as the particles, stearic and palmitic acid as the hydrophobic agent, and acetone and ethanol as the solvent. The new components used in this experiment were Altro Seal and Altro Tect, which replaced the latexes. Both components were supplied by our industrial partner Altro Ltd, with Altro Seal being a polyurethane resin, and Altro Tect being an epoxy resin.

4.3.1 Materials

Altro Seal™, Altro Tect™ and Evonik acematt HK 400 SiO₂ particles (6.3 μm) were supplied by Alto Ltd. Palmitic acid, stearic acid, 100 nm ZnO nanoparticles, acetone, and ethanol were all purchased from Sigma Aldrich. Kit 300B gravity fed spray gun and air hose kits were purchased from Clarke International.

4.3.2 The production of superhydrophobic durable coatings

For this experiment, different formulations were made up using: SiO₂ and ZnO particles, palmitic and stearic acids, ethanol and acetone solvents, as well as Altro Seal (Seal) and Altro Tect (Tect). To begin, 1.5 g of fatty acid was added to a beaker containing 50 ml of solvent, at 50 °C, while being stirred at 500 rpm for 20 min and covered with a watch glass. After 20 min the particles were added to the solution (0.25 g of SiO₂ or 1 g of ZnO) and left under the same conditions for another 20 min. While the particle and fatty acid solutions were stirring, the polymers were mixed using 7 parts base and 3 parts hardener. After the 20 min had elapsed, 1-15 g of the mixed polymer was added to the

solution and left for 20-240 min. Once the solution was ready, it was transferred into a reagent bottle, with solvent added to make 60 ml of final suspension, then left for at least 36 h before spraying.

Immediately prior to spraying, the suspensions were sonicated and shaken for ~5 min to ensure the suspension was uniform. ~30 ml of solution was then added to a spray gun set at 3 bar, using a 24 L air compressor. With the spray gun's jet flow set at 0.5 rotations, ~30 ml of solution was sprayed across five microscopes slides, attached to black card using masking tape (Figure 4-1). These samples were then left for 48 h to dry before the spray step was repeated to add a second coat. The coatings were then left to dry on a bench at room temperature for at least 48 h.

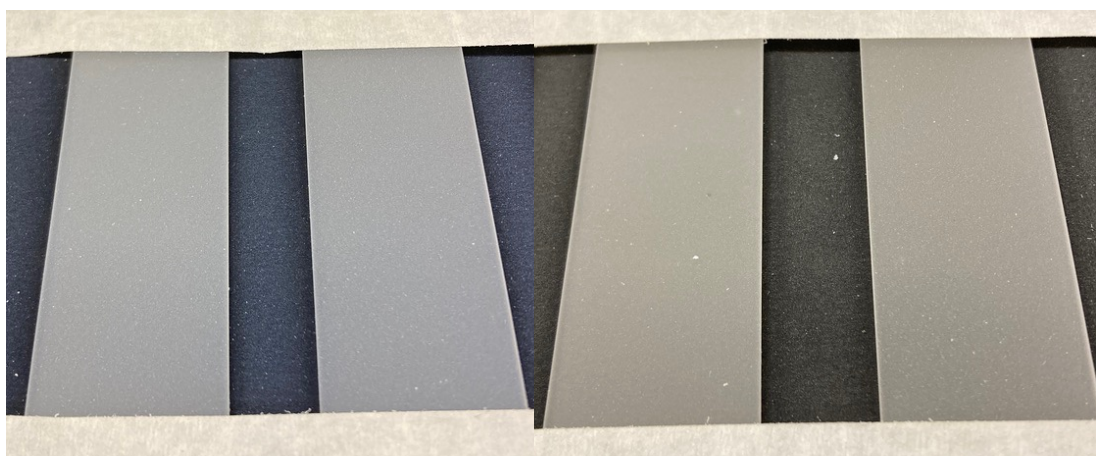


Figure 4-1 Functionalised polyurethane coated glass slides sprayed with: ZnO, stearic acid, Altro Seal, made in an acetone base (left). SiO₂, stearic acid, Altro Seal, made in an acetone base (right).

4.3.3 Testing superhydrophobic surfaces wetting properties and functionality

WCA measurements, contact angle hysteresis measurements, and rolling angle measurements were taken using a Krüss DSA25E Droplet Shape Analyser. For the WCA measurements, a DS3252 dosing unit was used to apply a 5 µl droplet to each coating at room temperature. A Young-Laplace fit was then used to calculate the contact angle of each droplet. Each measurement was performed in triplicate, with all reported measurements having a standard deviation of <1.5°.

For the contact angle hysteresis measurements, a protocol was adapted from *Huhtamäki et al.*²¹⁹ A syringe dosing unit was used to dispense and aspirate a water droplet on the surface of each coating. Over a minimum of 549 steps, the advancing and receding contact angles were measured. The contact angle hysteresis was then calculated by measuring the difference between the average advancing contact angle and the average receding contact angle.

For the rolling angle measurements, the tip of a syringe dosing unit was fixed 10 mm above the sample surface. The sample stage was then set at 1° intervals, with a 13 µl water droplet dispensed onto the surface below, between intervals. The rolling angle was defined as the angle the sample stage was set at which point a water droplet dispensed would not stay on the surface. The experiment was repeated three times in a row to confirm a result.

The self-cleaning of surfaces were tested by using glitter as a substitute for dirt. To begin, the surface was placed at ~10° (±1°) and soiled by covering it in glitter. Next, water droplets were applied to the surface using a Pasteur pipette. A surface was deemed to have self-cleaning properties, if the water droplets rolled across the surface, picked up the dirt (glitter), and removed it from the surface. A surface was deemed not to have self-cleaning properties if the droplets stuck to, or slid across the surface, leaving the dirt (glitter) in place.

Stain testing was performed by securing the sample at an 80° angle. Separate drops of 20 ppm crystal violet, instant coffee, and wine were then applied to the surface using a plastic pipette. The result was then recorded by imaging the samples.

A tape test was performed by firmly adhering Scotch Magic Tape to a surface, before pulling it off in a single motion. This process was repeated nine times, using a fresh strip of tape each time, before any measurements were taken.

4.3.4 The antimicrobial testing of submerged superhydrophobic surfaces

The antimicrobial properties of the samples were tested using a method designed to overcome the surfaces' superhydrophobic properties. Much of this method was completed as described in section 2.3.4. Testing was done with a Gram-negative bacterium, *Escherichia coli* ATCC 25922, and a Gram-positive bacterium, *Staphylococcus aureus* 8325-4.¹⁵⁹ Selective agar plates were again used to grow bacteria, with MSA used to grow *S. aureus*, and MacConkey agar used for *E. coli*. Each experiment was performed in triplicate using two technical replicates for each experiment.

Again, both bacteria were taken from freezer stocks, with single colonies of each bacterium used to inoculate 10 ml of BHI broth. This was then incubated in air at 37 °C for 18 h at 200 rpm, until the culture reached approximately 10⁹ CFU/ml. To halt cell growth, the bacteria were removed from the BHI broth by centrifugation, resuspended into PBS and washed three times with PBS, before a final 10⁹ CFU/ml suspension was made up in 10 ml PBS. 50 ml falcon tubes were used as sample chambers, with 15 µl of the 10⁹ CFU/ml suspension transferred into each. The suspensions were then diluted using 15 ml of PBS to give the final inocula.

For the experiment, copper coupons were used as controls. The controls along with the sample slides were each lowered into a sample chamber and the sample chambers sealed. The sample chambers were then securely taped to a VWR rocking platform shaker, which was set to 120 rpm for 24 h. At this point a visual observation was made to ensure that the inoculum was being washed across the sample surface.

After 24 h, 200 µl of each suspension was added to a zero well of a 96 well plate, before undergoing multiple 10-fold dilutions. As it was described in section 2.4.4, these dilutions were then plated on the corresponding selective agar plates and incubated for 24-48 h at 37 °C. Once viable colonies were

visually identifiable, these were counted, and the number of viable bacteria was calculated.

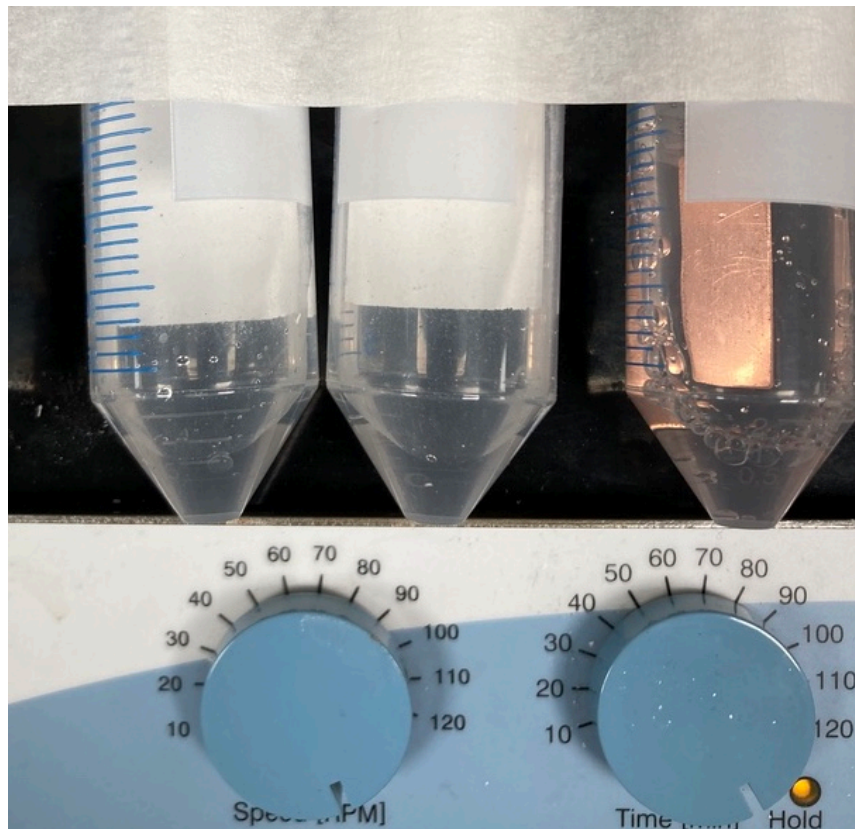


Figure 4-2 Sample chambers attached to a rocking table containing paint coated samples (left, center) and a copper control (right)

4.3.5 Determining the metal ion concentration of a liquid using XRF

A method to determine the amount of metal ions present in an inoculum post sample/control exposure was developed. Firstly, a standard curve was formed using ZnO solutions made up using the PBS from the experiment. Next the Zn:P (Zinc:Phosphorus) ratio corresponding to 1 ppm of Zn was calculated. This Zn:P ratio was then used to estimate the metal ion concentration of the inocula.

Prior to XRF analysis each inoculum was killed with bleach over a 24 h period. Once the 24 h period had elapsed, the solutions were neutralised with citric acid. Once neutralised, 5 ml of each inoculum was added to an XRF sample holder.

4.3.6 Anti-icing testing

Anti-icing functional testing was performed using a cooling chamber cooled with ethylene glycol, and set to $-10\text{ }^{\circ}\text{C}$. Samples and controls were each placed in the sample chamber, with $100\text{ }\mu\text{l}$ of 10 ppm methylene blue solution immediately dispensed on to the surface. Samples were then monitored for an observable colour change that occurred as the methylene blue froze (Figure 4-3). Triplicate measurements were taken of each sample.

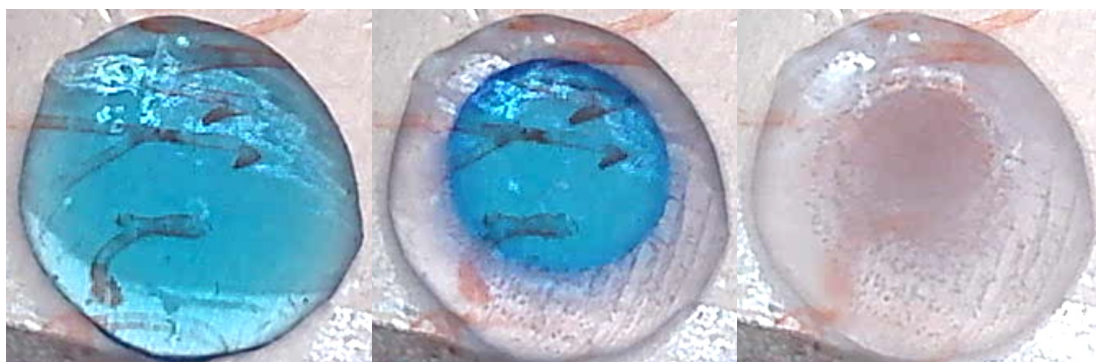


Figure 4-3 An observable colour change occurs as methylene blue solution freezes (left to right)

4.3.7 Material characterisation and functional testing

Infrared transmission spectra were obtained using a Brüker Alpha Fourier transform infrared spectrometer with a platinum ATR attachment. All spectra were obtained from the accumulation of 16 scans per sample, under an analysis range of $400\text{-}4000\text{ cm}^{-1}$.

Topographic surface imaging was completed using a JEOL JSM-6701F field emission scanning electron microscope. Samples were coated with either gold or carbon prior to analysis and were analysed with an acceleration voltage of 10 kV.

X-ray photoelectron spectroscopy was performed using a Thermo Scientific X-ray photoelectron spectrometer with a monochromated Al-K_{α} X-ray source ($8.3381\text{ }\text{\AA}$). Data was interpreted using CasaXPS software, with binding energies adjusted for adventitious carbon (284.6 eV)

Elemental analysis was then run on the samples using a Panalytical Epsilon 4 X-ray Fluorimeter.

4.4 Results and discussion

4.4.1 The production of superhydrophobic durable coatings

As this experiment was a continuation of the work previously described in section 3.4.3, many of the same components were used, as well as some of the optimisation work being retained. This was true of the optimised solvent to fatty acid ratio, which had previously been determined to be 1.5 g of fatty acid to 50 ml of solvent. As antimicrobial testing on both the latex paint surfaces and durable coatings was planned, the initial particle content was kept at 0.25 g of SiO₂ or 1 g of ZnO. This was for comparative purposes, as these were the amounts of particles added to the paints in section 3.4.3.

Unlike the latexes, the polymers both came in two parts, consisting of a base and a hardener. This meant they needed to be mixed, but as they begin to harden once mixed, this was done immediately prior to adding them to the mixture. Based on the accompanying instructions, 7 parts base and 3 parts hardener were mixed to formulate both the Tect and the Seal. Due to the nature of these polymers, this initial mixing stage was done using disposable equipment. This was due to the amount of solvent required to clean reusable equipment being so considerable, such as that both monetary and environmental cost was reduced by using single use paper cups and tongue depressors for mixing the formulations.

The first experiment replaced the latex for the new polymers. This meant that once the fatty acid had been dissolved, and the particles had been functionalised in the fatty acid solution for 20 minutes, 1 g of the mixed polymer was added to each suspension and left for 20 minutes. In a reagent bottle, the suspensions were then made up to 50 ml and left for a minimum of 12 h prior to spraying. No Orotan or texanol were used in these experiments since:

Orotan is normally added to an aqueous phase, and texanol is used for latex suspension. Regardless, there appeared to be no issues associated with particle dispersion or coalescing.

Once the suspensions had been sufficiently shaken and sonicated, so as to give a uniform suspension (~5 min), they were loaded into the spray gun. The spray gun was again set at 3 bar, but the spray gun's jet flow was set at only 0.5 rotations this time around. This was due to the suspension being less viscous than the paints. Again, due to the environmental factors and the volatility of the solvents, there was no set spray distance, with practice again required to spray adequate coatings. It is worth noting that the average spray distance was ~double that of the paints.

Once sprayed, the coatings were checked after 24 h, but deemed to still be "wet". They were then allowed to sit for another 24 h to ensure they were sufficiently dry. Despite using the same volume of polymer suspension as was used for the paints, it could be observed visually that the coatings were much thinner than the previous latex coatings. For this reason, a second coat of polymer suspension was added to the coatings. These were again left for at least 48 h to dry before any testing was performed.

Once dry, some basic functional testing revealed that the surfaces were not very good. While the wetting properties were favourable, the surfaces had no durability. The same was found for the next batches that contained 2 g of polymer. Batches were then made up containing 5 g, 10 g, and 15 g of polymer, with final volumes of 55 ml, 60 ml, and 65 ml. These batches showed, with some of the coatings to have good properties overall, but some surfaces simply did not work.

To begin with, the Tect suspensions that were made up in acetone turned a yellow colour. The solute in the Tect SiO₂ suspensions that were made up in ethanol, solidified and could not be dispersed back into the solvent despite a lengthy period of sonification and shaking. Coatings made from the Altro Seal solutions that used an ethanol base appeared to separate. With these

coatings, a migration seemed to occur, so that there was a thin layer of dust on top of a sticky layer.

Despite these issues, basic functional analysis of the coatings was able to provide some good early insight. Using a Pasteur pipette, drops were applied to all the surfaces to check their wetting properties. It was at this stage that the Tect was effectively eliminated as a viable option, as none of the Tect coating displayed superhydrophobic properties. While the ethanol based Altro Seal samples produced extremely good superhydrophobic properties to start, once the loose dust layer had been brushed off, the sticky layer, while still hydrophobic, did not possess the same wetting properties.

This was somewhat disappointing as epoxy had shown so much potential in the literature.²⁰⁷⁻²⁰⁹ One issue might be the solvents selected for the experiment. While they worked well with the latexes, and somewhat with the polyurethane, they may be having a negative impact on the epoxy formulations. Toluene may be a more suitable solvent when attempting experiments involving epoxy in the future, as it was used by both *Qi et al.* and *Liu et al.*^{207,208} However, toluene is a more dangerous solvent than either ethanol or acetone, and as such, a toluene based coating would require extra precautions and facilities that were not currently available.

Another point of concern arose when using the combination of the polyurethane and the ethanol. When examining formulations with these components, a large amount of the functionalised particles appeared to migrate to the surface. This then formed a superhydrophobic layer similar to some of the two step systems seen in the literature.^{207-209,211,212} While some surfaces from the literature did sufficiently test and prove their durability, others did not. This means some of these surfaces could deteriorate relatively quickly, if their superhydrophobic layer was easily removed. An example of this would be how a brush easily removed the majority of the superhydrophobic layer at the surface of the functionalised polyurethane coatings made up in ethanol.

With all this taken into account, and after eliminating surfaces with glaring deficiencies, the functionalised Altro Seal coatings made up in acetone were effectively the only viable surfaces. When looking at these coatings based on their Altro Seal content, the 5 g and 10 g coatings had similar wetting properties, while the 10 g and 15 g had similar durability properties. Overall, of the three different coatings, the coating containing 10 g Altro Seal appeared to have the best combination of properties. The 10 g Altro Seal coating appeared to have superhydrophobic wetting properties similar to those of the Plus latex paints, yet it displayed far better physical durability properties.

Throughout this process it was also realised that leaving the suspensions to sit for 12 h after their initial formulation was not long enough. It appeared that when the suspensions were left for a minimum of 36 h, the suspensions and surfaces produced were far more consistent and uniform. This meant that going forwards, all the suspensions were left to sit for 36 h prior to being sprayed, with a second coat applied to the surfaces after a 48 h drying period. While some other small modifications were attempted to the formulations, the optimised formulation going forward was: 50 ml of acetone, 1.5 g a fatty acid, 0.25 g of SiO₂ or 1 g of ZnO, and 10 ml of Altro Seal.

4.4.2 The characterisation and testing of superhydrophobic durable coatings

Characterisation of the surfaces began with transmittance FT-IR on the samples containing 10 g of polymer. This was done in order to better understand the surfaces, while also comparing the spectra to previous ones. Unfortunately, and rather surprisingly, due to the properties of the material, the FT-IR obtained of the polymer coatings (Figure 4-4) were not of the same quality of those obtained of the particles and paints. Due to the poor quality of the IR spectra, it was difficult to discern results and to compare them to the previous spectra.

Looking at the Seal Act spectrum in Figure 4-4, it can be seen that the spectrum is effectively noise the entire way down to ~1300 cm⁻¹. This is highly

unusual as you would expect to find peaks correlating to N-H, C-H, and C=O stretching in this region of a polyurethane spectra.^{197,198,204} Below 1300 cm⁻¹ some distinguishable peaks may be associated with expected peaks. These include a peak at ~1250 cm⁻¹ which could be associated with either C-N or C-O stretching, while another peak at ~1100 cm⁻¹ could also be associated with either.^{197,198,220}

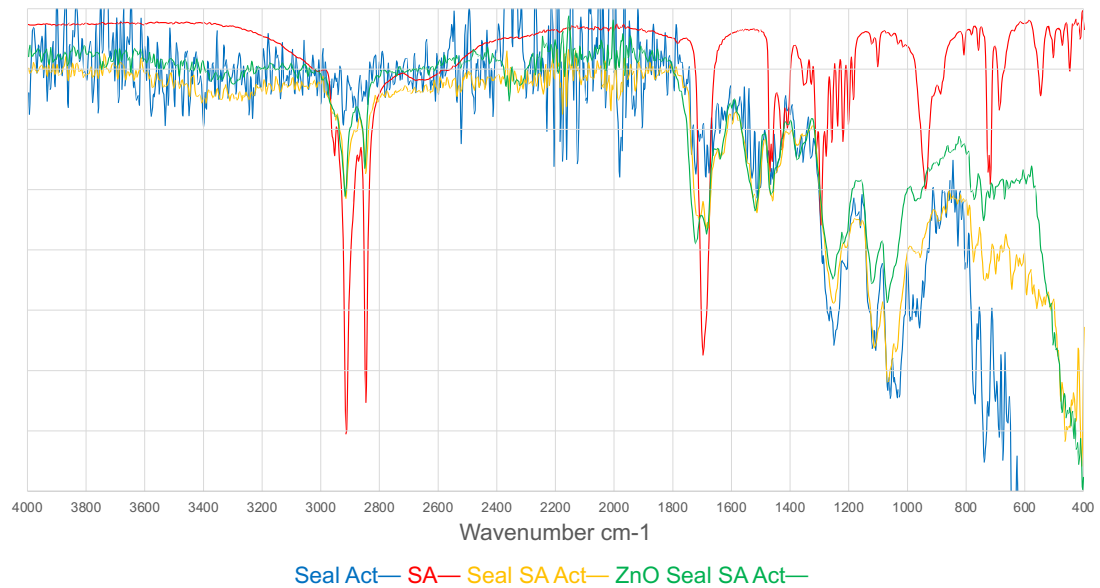


Figure 4-4 Transmission FT-IR spectra of an Altro Seal coating and the main components to make it. The coating contained ZnO, Altro Seal (Seal), stearic acid (SA), made up in acetone (Act)



Figure 4-5 Transmission FT-IR spectra of two Altro Seal coating. The coatings contained either ZnO or SiO₂, as well as Altro Seal (Seal), stearic acid (SA), and was made up in acetone (Act)

Figure 4-5 shows the spectra of the superhydrophobic durable coatings, which are comparably a lot clearer than the spectrum of Altro Seal on its own. Whereas previously the spectra that contained the different particles could be easily separated, these spectra looked more similar. Above 3000 cm^{-1} , there is again no clear N-H stretching which should be present in a polyurethane.^{195,197} Between $2800\text{--}3000\text{ cm}^{-1}$ the C-H region mirrors that of any stearic acid containing compound analysed so far.

Below 1800 cm^{-1} , C=O peaks can be observed at $\sim 1710\text{ cm}^{-1}$ and 1690 cm^{-1} . The peak at 1690 cm^{-1} has previously been observed and associated with stearic acid, meaning the peak at $\sim 1710\text{ cm}^{-1}$ is most likely due to the presence of the polyurethane. There is also a small peak at $\sim 1640\text{ cm}^{-1}$ that would indicate the presence of C=C bonds. Looking at the Altro Seal spectrum containing ZnO specifically, there are no apparent peaks at 1540 cm^{-1} and 1399 cm^{-1} which have previously been present due to symmetric and asymmetric COO^- stretching. This is the first time this has not been observed in a spectrum containing both the ZnO and stearic acid and would suggest the carboxylic acid was not in resonance.

Below 1600 cm^{-1} , there are peaks at $\sim 1515\text{ cm}^{-1}$ and $\sim 1380\text{ cm}^{-1}$ that could be due to N-O stretching. This would suggest that there may be a reaction between the stearic acid and the nitrogen on the polyurethane. This might also help to explain the lack of peaks related to N-H bonding. There is also a peak at $\sim 1465\text{ cm}^{-1}$ that is most likely a C-H bend. Further down, there are peaks at $\sim 1250, 1210, 1120, 1070\text{ cm}^{-1}$. These peaks most likely are most likely due to a combination of C-N and C-O stretching, although without an exact formulation for the polyurethane, it is very difficult to the specific peaks.

XPS analysis followed the IR analysis. Figure 4-6 is an important survey scan that showed that nitrogen was present in the both the coatings as expected. This was despite there being no clear evidence this was the case during the IR analysis. Figure 4-7 shows the relative 2p spectra of the coatings containing ZnO or SiO_2 . Comparing these results to the previous spectra, the

Zn FWHM in the Zn 2p spectrum (2.039 eV) falls in between the values of the functionalised ZnO (1.960 eV) and the ZnO paint (2.404 eV). The equivalent is also true for the Si FWHM in the Si 2p spectrum. The FWHM was 2.185 eV, compared to the 1.963 eV of the “supposedly” functionalised SiO₂ and the 2.232 eV of the SiO₂ paint.

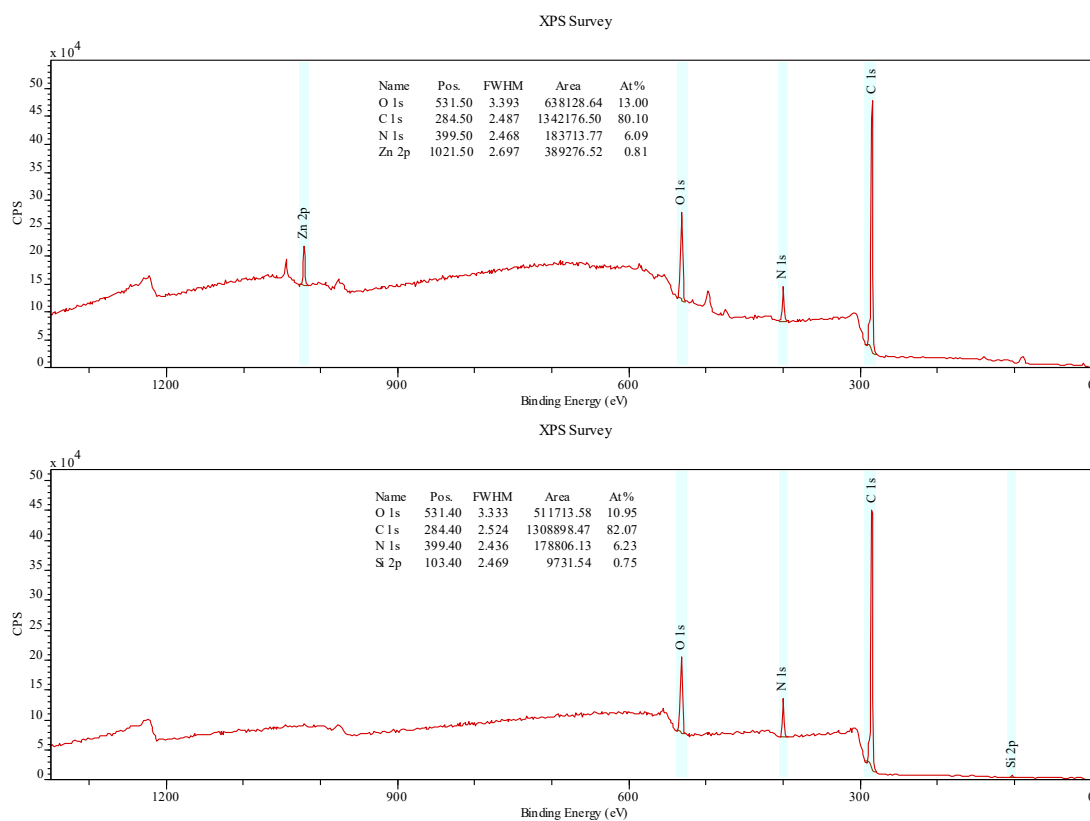


Figure 4-6 XPS survey of superhydrophobic durable coatings. The coatings contained either ZnO (top) or SiO₂ (bottom), as well as Altro Seal, stearic acid, and was made up in acetone.

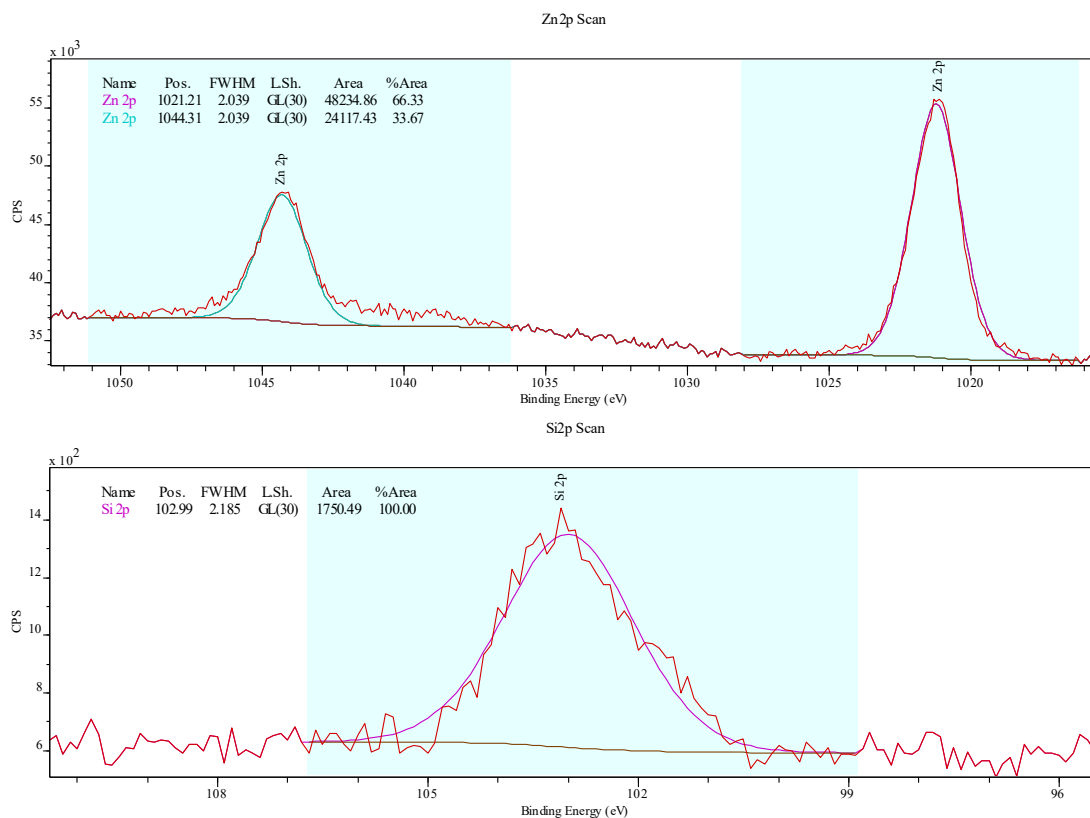


Figure 4-7 Top: Zn 2P XPS analysis of a superhydrophobic durable coating containing ZnO. Bottom: Si 2P XPS analysis of a superhydrophobic durable coating containing SiO₂.

SEM analysis was performed on the coatings, so that their surface structures could be observed. Figure 4-8 shows the imaging of the two modified Altro Seal coatings. The ZnO coating bears a similar resemblance to the paint coating that also contained ZnO (Figure 3-24–Figure 3-26). The SiO₂ surface on the other hand, does not bear resemblance to the corresponding paint surface (Figure 3-26), and is arguably the most structured and roughest surface on the micro scale. While this is the case for the SiO₂ surface, the ZnO surface appears rougher on the nanoscale. Considering what has previously been observed, the topological features of these surfaces should not be of any detriment to the surfaces superhydrophobic properties.

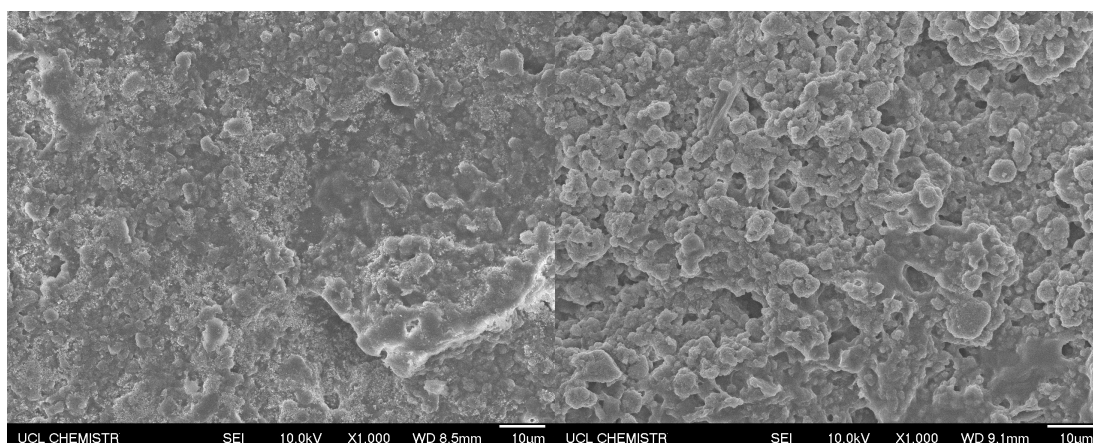


Figure 4-8 SEM imaging of: Altro Seal containing ZnO particles and stearic acid (left). Altro Seal containing SiO₂ particles and stearic acid (right).

4.4.3 Detailed testing of the wetting properties of superhydrophobic coatings

Once the characterisation had been completed, functional testing began with standard DSA to determine the WCA. The WCA of both the coatings containing ZnO or SiO₂, exceeded 167° (Figure 4-9). This was comparative to the ZnO containing paints produced in chapter 3, that also used acetone as a base, which were analysed using the same method (170.3° for the paint containing stearic acid and 168.0° for the surface containing palmitic acid). In an effort to further differentiate the four surfaces from each other, further analysis was carried out using the DSA.

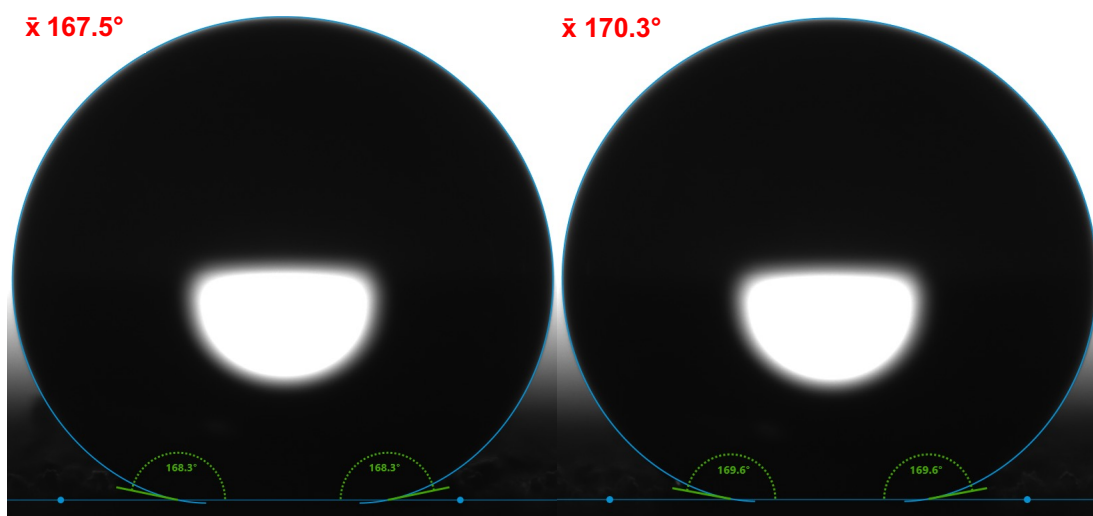


Figure 4-9 DSA image of a 5 µl water droplet on polymer coating surface. Left: Polymer coating consisting of ZnO, stearic acid, and Altro Seal made up in an acetone base. Right: Polymer coating consisting of SiO₂, stearic acid, and Altro Seal made up in an acetone base.

The next measurement to be taken was the surfaces rolling angle. This is another important functional property that relates to a surface's self-cleaning properties. It has been suggested in the literature that a superhydrophobic surface should have a rolling angle of $<10^\circ$, although the smaller the rolling angle, the better the self-cleaning properties.^{210,221} However, there is very little consensus on how this measurement should be carried out, or what qualifies a measurement. For instance, neither *Qi et al.* nor *Penna et al.* reported the height at which their water droplet was dropped from, or the volume of their droplet, both of which we found significantly impacted rolling angle measurements.^{207,209} Another issue is at what point should a measurement be taken or be valid. Is it when a droplet moves at all, or when the droplet clears the surface?

Due to these discrepancies, the rolling angle was clearly defined as the angle of tilt a surface needed to be at, to which a 13 μl water droplet dropped from 10 mm above the surface, would be unable to stay on the surface it was applied to, with the implementation of this method being shown in Figure 4-10. Testing was performed on the two paints containing ZnO, Plus latex, and stearic acid or palmitic acid. It was also performed on two Altro Seal coatings functionalised with stearic acid and SiO_2 or ZnO. All of the samples were made up in an acetone base and produced using spray coating, with the results of the testing displayed Figure 4-15.

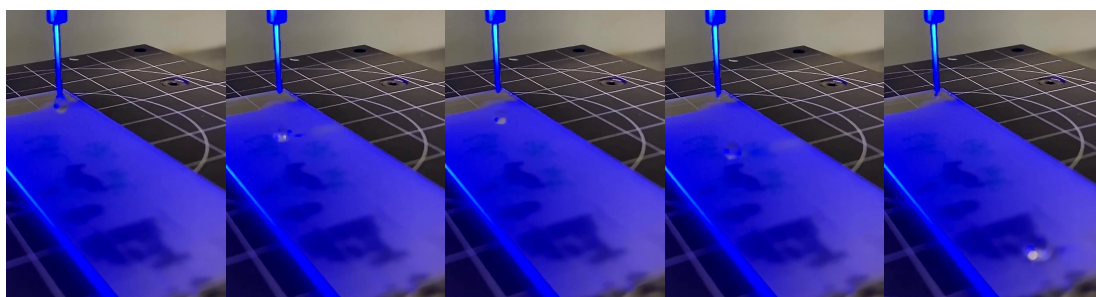


Figure 4-10 A demonstration of how a rolling angle measurement is taken. The stage is set to a designated angle, at which point a 13 μl water droplet is applied to the surface, using a syringe dispenser, raised 10 mm above the surface. If the water droplet unable to stay on the surface, the current angle was deemed the surfaces rolling angle.

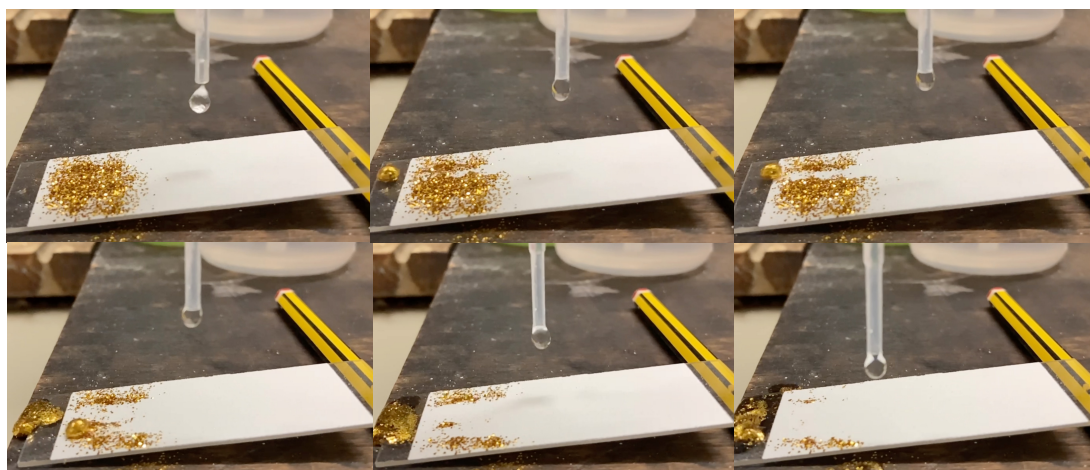


Figure 4-11 A demonstration of the self-cleaning properties of the ZnO stearic acid Plus latex paint. To begin, the surface at $\sim 10^\circ (\pm 1^\circ)$ is covered in glitter. Water droplets are then applied to the surface using a Pasteur pipette. If the surface has self-cleaning properties, the water droplets will roll across the surface picking up the dirt (glitter) as can be seen in the images above. If not, the water will stick to, or slide across the surface, with the dirt (glitter) remaining in place.

All the surfaces were determined to have rolling angles well below the 10° limit expected of a superhydrophobic surface (Figure 4-15).^{210,221} The SiO₂ stearic acid Altro Seal had the minimum rolling angle of 1° , while the ZnO stearic acid Plus latex paint had the highest value of 3° . While many of the literature did not determine their surfaces rolling angles, the SiO₂ stearic acid Altro Seal performed as well as *Qi et al.* and *Penna et al.* surfaces, which also had minimum rolling angles.^{207,209}

Once the rolling angle testing had been completed, the self-cleaning properties of all the surfaces were tested using the method demonstrated in Figure 4-11. The results of self-cleaning tests showed that all the surfaces had excellent self-cleaning properties. This was unsurprising due to the rolling angle's association with the self-cleaning properties, and the low rolling angles the surfaces had displayed.

The next stage was to test the surfaces' resistance to staining. As can be seen in Figure 4-12, both surfaces were stain resistant. This suggested that there may be a link between a surface's self-cleaning properties, and their ability to resist staining. With this in mind, the self-cleaning properties of both the paints consisting of ZnO, Plus latex, with stearic acid or palmitic acid, made up in an ethanol base were tested. Both samples were shown to have self-cleaning

properties, despite being stained by the wine. This result ended the notion that a surface with self-cleaning properties would be stain resistant. This would also suggest a difference in the surface's chemical properties, due to the base solvent, is hindering the surfaces stain resistant properties.

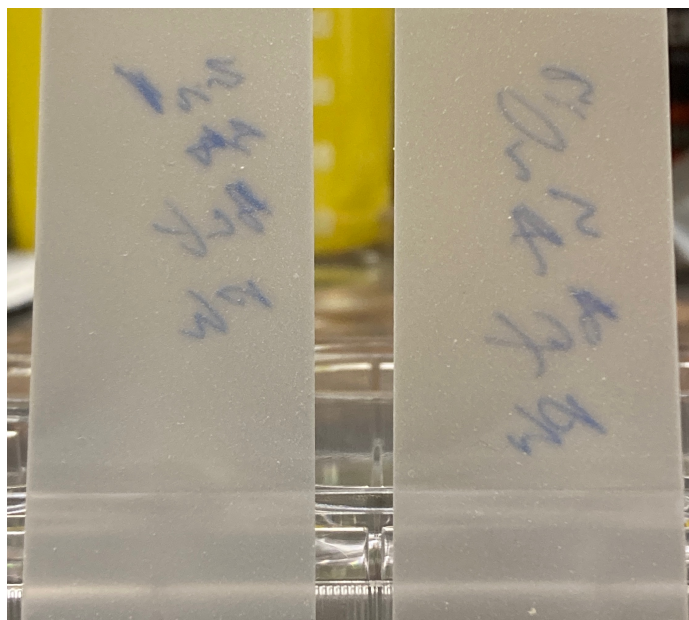


Figure 4-12 Stain testing. ZnO stearic acid Altro Seal (left). SiO₂ stearic acid Altro Seal (right). Each sample was tested with 20 ppm crystal violet (left), instant coffee (middle), and wine (right). As both surfaces were able to repel the solutions, they were left unstained.

The final analysis of the surfaces' wetting properties was an inspection of the surfaces' CAH. CAH is a measure of a surface's ability to keep a droplet in place, and as such does not specifically determine if a surface is superhydrophobic.²²² Surfaces with a low CAH value are better described as either, superhydrophobic, or have the potential to be superhydrophobic. This because surfaces with a low surface energy adhere poorly to water molecules, regardless of its surface roughness. This means if a surface has a low CAH value and a low WCA value, it must be relatively flat.²²³

In theory, as the CAH is a surface's ability to keep a droplet in place, the results should follow that same trend as the rolling angle analysis.²²² The CAH is determined by measuring the ACA and the RCA, with the difference between the two deemed the hysteresis.²²⁴ To do this, the ACA was measured as a water droplet was dispensed and expanded onto the surface being tested, with

the RCA then measured as the droplet was being retracted off the surface (Figure 4-13). Figure 4-14 displays the ACA and RCA measurements of the different surfaces.

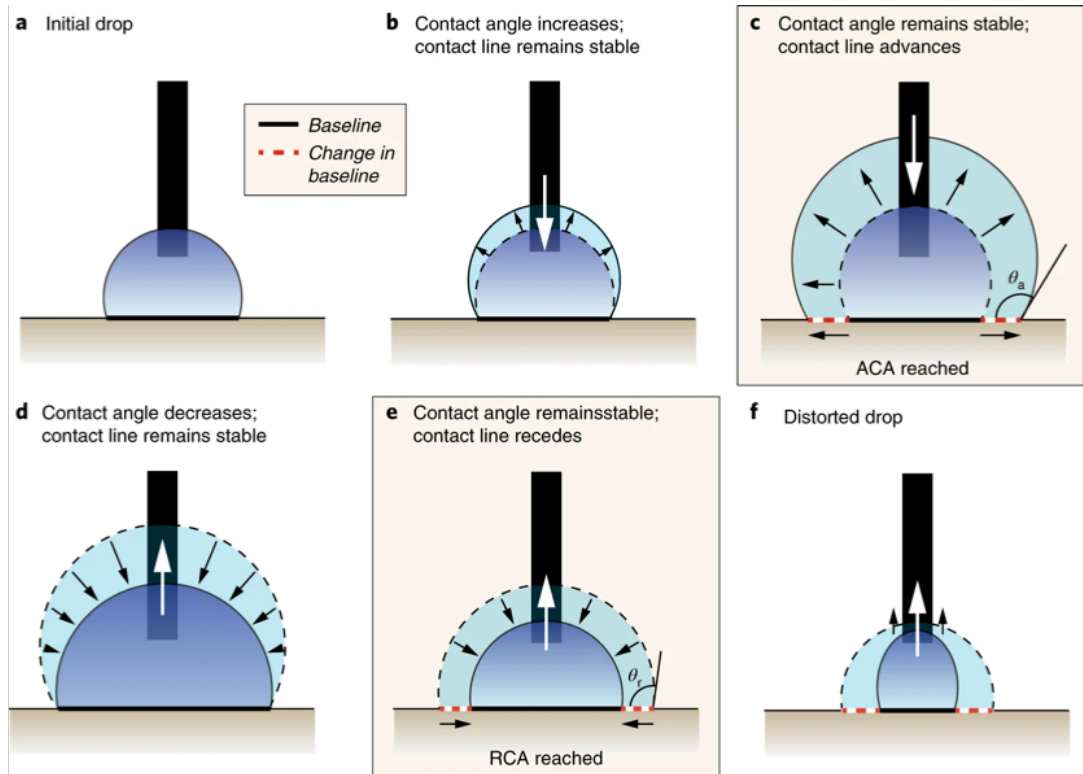


Figure 4-13 An outline of the procedure by Huhtamäki et al used to obtain contact angle hysteresis measurements. Reproduced from Huhtamäki et al.²¹⁹

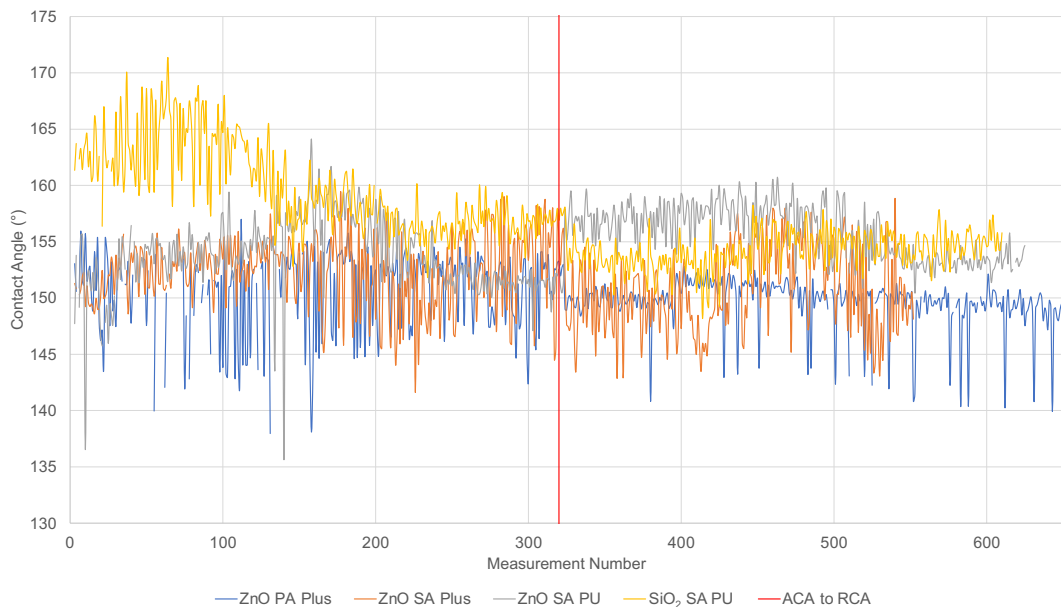


Figure 4-14 The advancing and the receding (after the red line) contact angle measurements of: ZnO palmitic acid Plus latex paint, ZnO stearic acid Plus latex paint, ZnO stearic acid Altro Seal, SiO₂ stearic acid Altro Seal.

Figure 4-15 shows that the ZnO palmitic acid Plus latex paint had the lowest hysteresis value, meaning water droplets should easily slide across the surface. The SiO₂ stearic acid Altro Seal had the highest value, meaning water droplets should be less mobile across the surface, however this result contradicts the rolling angle measurements (Figure 4-15). This contradiction is most likely due to the CAH not being a measure of a surface's superhydrophobicity, and more so a measure of a surface's potential to be superhydrophobic. In fact, as previously discussed, flat surfaces with a relatively low WCAs (~104°) can have a CAH value of 1°. ²²⁵ With this in mind, and by comparing the images in Figure 4-8, it is possible to consider that the ZnO stearic acid Altro Seal has better potential to be a superhydrophobic surface, yet the SiO₂ stearic acid Altro Seal may be displaying better superhydrophobic due to its greater surface roughness.

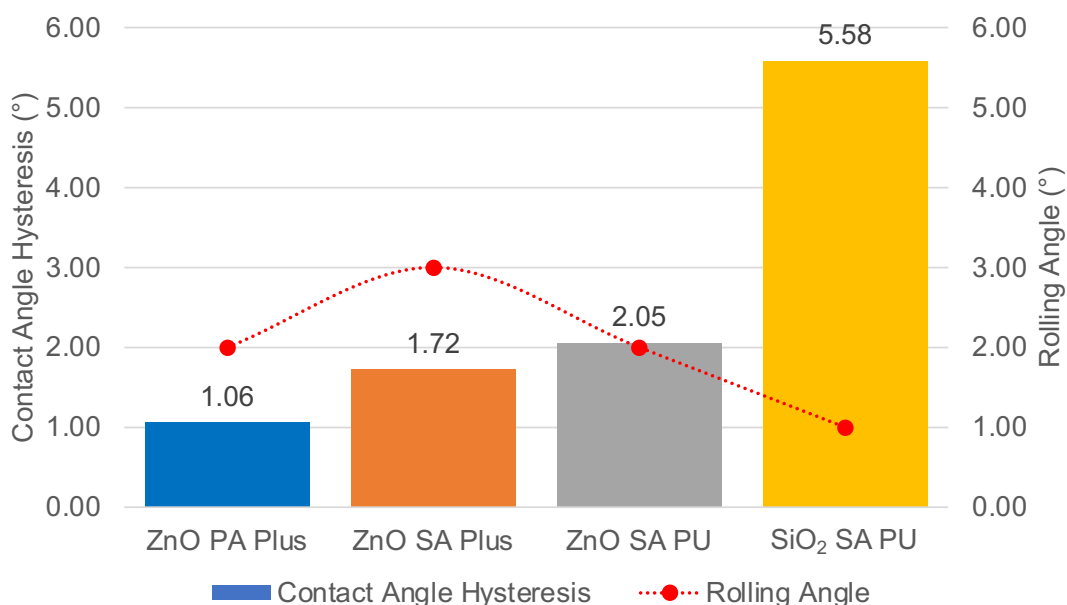


Figure 4-15 The contact angle hysteresis and rolling angle of: ZnO palmitic acid Plus latex paint, ZnO stearic acid Plus latex paint, ZnO stearic acid Altro Seal, SiO₂ stearic acid Altro Seal.

Finally, the durability of the surfaces was tested using a tape test. While previously the paints maintained their wetting properties admirably after a tape test, their durability proved to be lacking (Figure 3-29, Figure 3-30). The Altro Seal coatings on the other hand again maintained their wetting properties admirably, while also proving to be far more durable when tested. The durability of the surfaces is displayed Figure 4-16, where it can be seen that

little to none of the coating was removed by the Scotch Magic Tape. Figure 4-17 shows that there was $<1^\circ$ change in the WCA of either the coating containing ZnO ($167.5\text{--}167.3^\circ$) or SiO_2 ($170.3\text{--}169.7^\circ$).

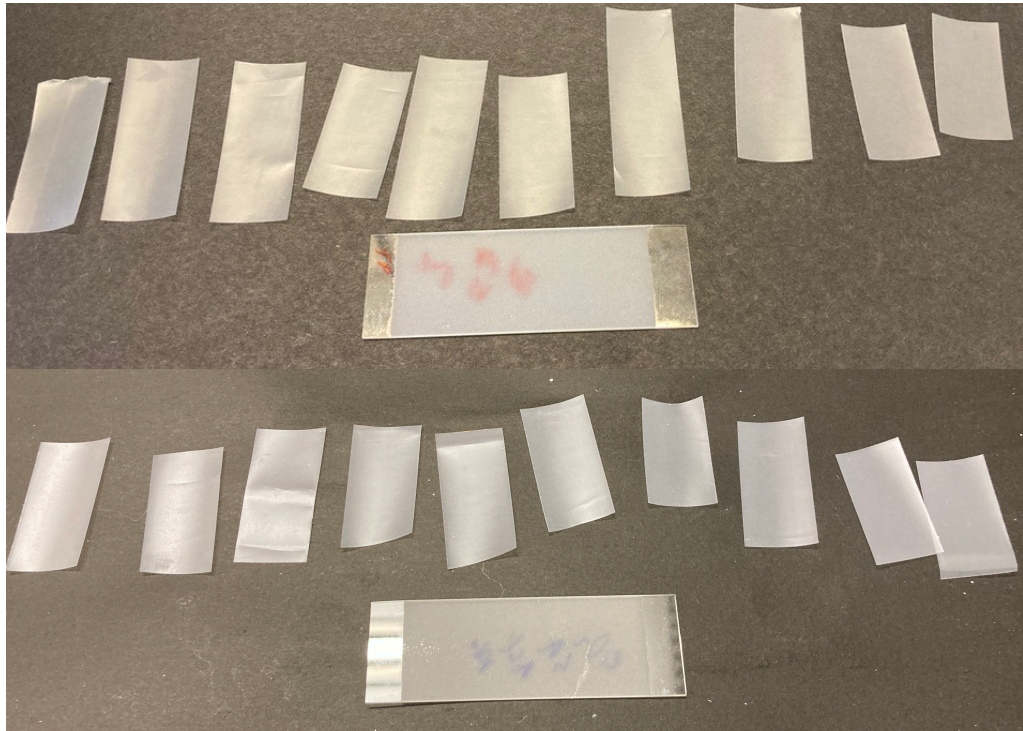


Figure 4-16 The results of tape tests consisting of the firm application and removal of 10 strips of Scotch Magic Tape consecutively. Top: ZnO stearic acid Altro Seal. Bottom: SiO_2 stearic acid Altro Seal.

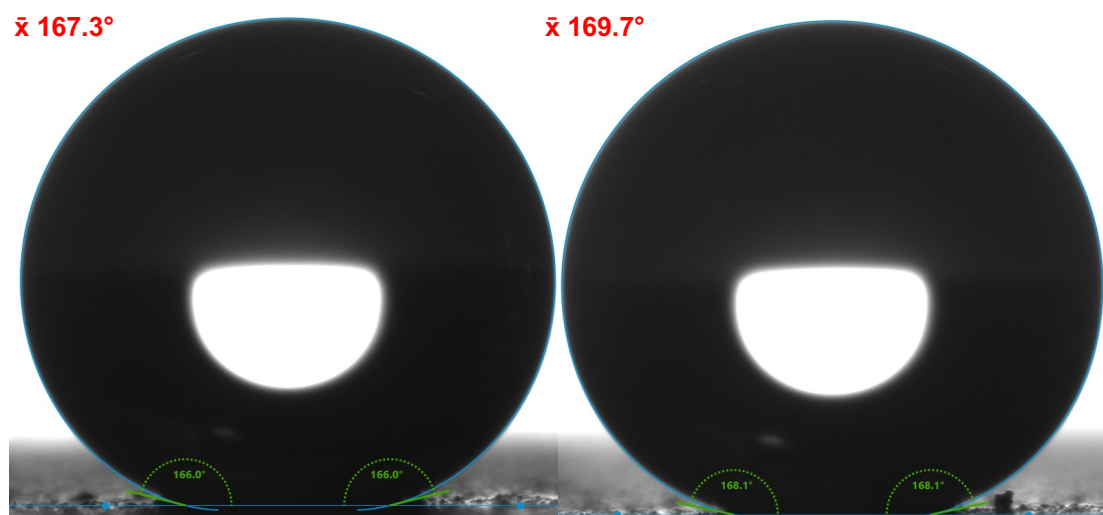


Figure 4-17 DSA image of a $5\ \mu\text{l}$ water droplet on polymer coating surface after a completed tape test. Left: Polymer coating consisting of ZnO, stearic acid, and Altro Seal made up in an acetone base. Right: Polymer coating consisting of SiO_2 , stearic acid, and Altro Seal made up in an acetone base.

4.4.4 Antimicrobial testing of superhydrophobic surfaces

Once the superhydrophobic properties of the coatings had been established, it was time to circle back around to the other remit of this project, the antimicrobial properties of the surfaces. With this in mind, it was decided to test the antimicrobial properties of both the superhydrophobic durable coatings and the superhydrophobic paints. Testing was performed on the ZnO stearic acid Plus latex paint that was made up in acetone, and the ZnO stearic acid Altro Seal that was also made up in acetone. These surfaces were selected as previous testing had shown them to be the best polymer surface and paint surface (sections 3.4.5 and 4.4.2)

For this experiment, the method laid out in section 2.3.4 was initially considered as the best option, but after further consideration of the innate properties of a superhydrophobic, it was realised that this was not the case. As the surfaces had Cassie-Baxter type wetting properties, when the inoculum was applied to the surface it remained as a round droplet. This led to the first issue which meant that minimal movement would cause the droplet to roll off the surface. Although it may have been possible to overcome this issue and have it so that the drop remained stationary, this led to the next issue. By using a stationary droplet, the contact between the droplet and the surface was minimised. As antimicrobial properties are generally reliant on pathogens coming near or into contact with the surface, stationary droplets were not practical for this experiment.

It was then decided the best way to overcome both these issues would be the inclusion of intentional movement in the experiment. This would mean that the first issue could be overcome by simply not being reliant on the droplet remaining still. The second issue could be overcome as more of the droplet would come into contact with the surface as it rolled across it. This would increase opportunity for the surface to interact with microbes present in the droplets, while the agitation would also better circulate any antimicrobial reagents throughout the liquid.

With these considerations, a new method of testing was designed around the concept that introducing movement to the testing would help to counteract the

issues caused by the surfaces' superhydrophobic properties. This was done by using sealed sample chambers that allowed the inoculum to move freely across the surfaces being tested. A rocking table shaker was decided on for the movement mechanism, as it was gentle enough so as not to damage the surfaces, yet it sufficiently moved the inoculum across the surface.

As this was a new method, on top of our normal controls, we required some sort of control to validate the method. This control was needed so that if there was no kill, it could be determined if it was due to the sample's properties, or if it was due to the method not being compatible with the proposed testing. Copper was selected to be used as this control as it had very good and well established antimicrobial properties.^{150,226} These coupons were simply copper coupons that were cut from a larger sheet, disinfected with ethanol, rinsed with deionised water, before being left to dry.

Once all of the apparent variables had been considered, testing commenced. Testing was relatively straight forwards and followed much of the methodology used to obtain results in section 2.4.4. A 24 h exposure period was decided on to ensure the samples had enough time to act on the inoculum efficiently. The results of the experiments can be seen in Figure 4-18.

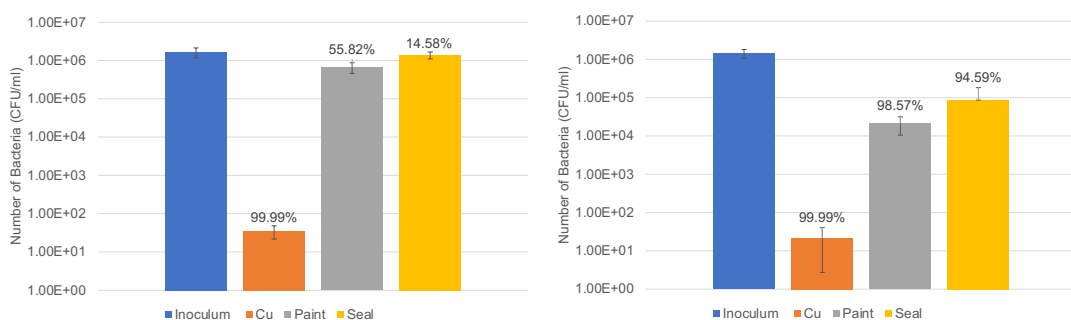


Figure 4-18 Antimicrobial activity of copper coupons, ZnO stearic acid Plus latex paint that was made up in acetone, and the ZnO stearic acid Altro Seal that was also made up in acetone. Samples were tested against an *E. coli* suspension (left) and a *S. aureus* suspension (right). This was performed at room temperature, for 24 h, under normal lighting conditions.

The first thing that was noted, is that the method was validated as the copper killed 99.99% of the bacteria, regardless of whether it was being tested against *E. coli* or *S. aureus*. Unfortunately, the other results were less positive.

Although the paint eclipsed the Altro Seal in terms of kill, they both fell significantly short of achieving a 99% kill across either of the pathogens. Yet, by showing kill against both Gram-positive and Gram-negative bacteria, the surfaces did match the qualitative results produced by the *Shaban et al.* made surfaces.²¹⁸ However, the results did fall far short of the quantitative results produced by *Lai et al.* where their surfaces were found to kill $\geq 99.85\%$ of both Gram-positive and Gram-negative bacteria.

These results meant that the superhydrophobic surfaces required further optimisation if they were to also act as antimicrobial surfaces. It was worth nothing that these surfaces' antimicrobial properties were more efficient when faced with *S. aureus* rather than *E. coli*, which is the opposite to what has previously been seen in our experiments. The swap in effectiveness when trying to tackle the different pathogens was curious as it suggested a different mechanism of kill was acting on the pathogens. On visual inspection, it could be seen that the inocula after testing had coloured slightly, leading to the hypothesis that ions might be leaching from the surfaces, which could in turn be contributing towards the kill.

4.4.5 Determining the quantitative leaching of ions from samples surfaces using X-ray fluorimetry

To check whether ion leaching had occurred, elemental analysis was performed on the inocula post testing, using XRF analysis. However, this was not as straight forwards as simply loading the samples into the instrument. The first issue was that the samples contained live bacteria that could not be experimented with outside of a category 2 laboratory. This meant that the inocula needed to be killed prior to analysis. This was done by making the solution up to be 0.05% bleach, which is known to kill both Gram-positive and Gram-negative bacteria effectively and quickly. To be cautious, the bleached inocula were left to rest a minimum of 12 h to ensure there was sufficient time to achieve a total kill. This was verified by plating the inoculum on a nutrient agar plate.

Next the inocula were loaded into sample holders that had a thin polymer film at the bottom. This is when the next issue arose, as the bleach dissolved the polymer film, spilling the contents out through the bottom. In order to stop this from occurring, citric acid was used to neutralise the bleach. To do this, citric acid was added to the inocula until they were measured to have a pH of 7 (± 1). Once this was completed, the samples were ready to run. However, as the XRF cannot detect elements below sodium, a method by which the ion concentration of the total solution (not just against the detectable particles) needed to be devised.

As all the inocula had been made up using the same PBS solution, the phosphorus concentration across the inocula was constant. Using this knowledge, a standard curve was formed analysing different PBS solutions with known concentrations of ZnO against the constant concentration of phosphorus. Using this standard curve, it was then possible to determine the ion concentration in the inocula by measuring the ion:phosphorus ratio. The results of this analysis can be seen in Figure 4-19.

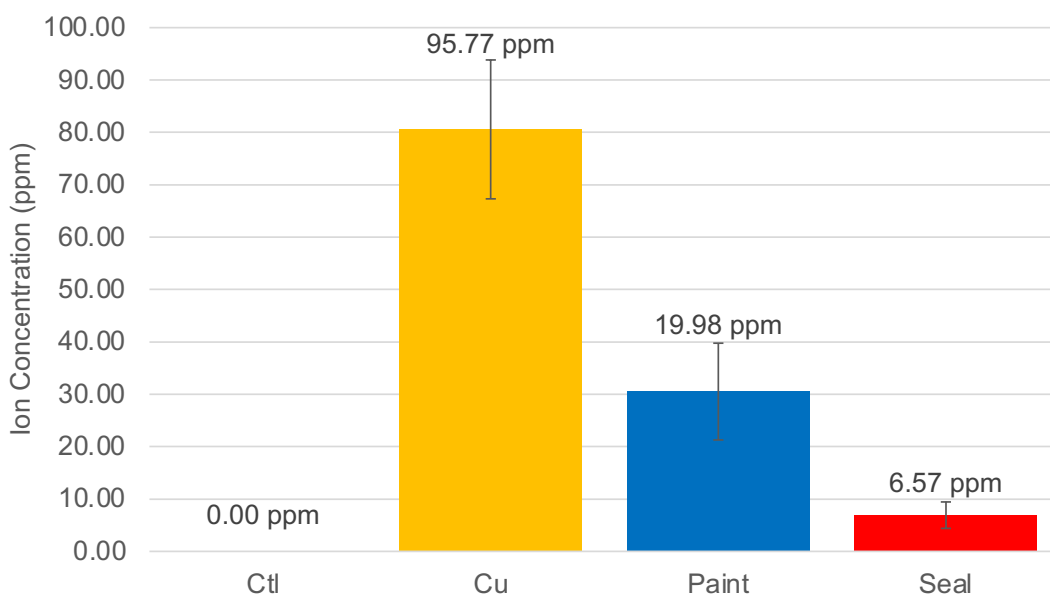


Figure 4-19 XRF analysis of tested bacterial inocula to determine the ion concentration. These inocula included: a control that was not exposed to any surfaces (ctl), an inoculum exposed to copper surfaces (Cu), an inoculum exposed to a surface coated with the ZnO stearic acid Plus paint (Paint), an inoculum exposed surface coated with ZnO stearic acid Altro Seal (Seal).

Looking at the results, the inoculum that had contained the copper coupons had the highest metal ion concentration. This was followed by the inoculum that contained the paint sample, then the one that contained the Altro Seal sample. These results were generally as expected and correlated with the antimicrobial results (Figure 4-18), in that the lower the number of surviving bacteria, the higher the metal ion concentration.

4.4.6 Anti-icing testing

Anti-icing testing was performed on the different Altro Seal samples, as they were the most applicable coating when considering real world applications. Tested samples included a control that was pure Altro Seal, ZnO SA which was ZnO stearic acid Altro Seal, and SiO₂ SA which was SiO₂ stearic acid Altro Seal. To begin with, the cooling chamber was primed by lowering the temperature of the chamber to -10 °C. Next the samples were carefully placed in the chamber using tweezers, with 100 µl of distilled water immediately dispensed onto the surface in the form of a water droplet. While being left to rest, the freezing of the droplet on the surface was recorded.

Due to the colourless nature of both ice and water, it was difficult to observe either with the eye, or through the recording, to determine when the water drop had frozen. To address this issue, a methylene blue solution was used to see if the freezing process could become more apparent. As can be seen in Figure 4-3, the use of the methylene blue solution worked perfectly with a clear and obvious colour change observed as the methylene blue froze. This allowed for clear and distinct freezing measurements to be made.

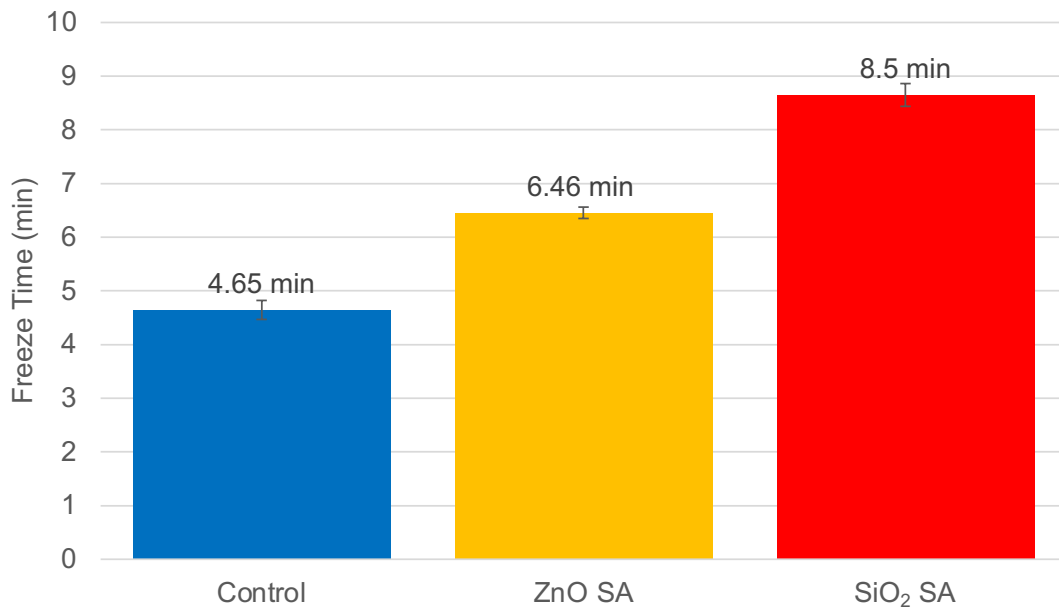


Figure 4-20 Anti-icing results. Control: Pure Altro Seal coating. ZnO SA: Coating of Altro Seal mixed with ZnO and stearic acid. SiO₂ SA: Coating of Altro Seal mixed with SiO₂ stearic acid

The results of the anti-icing tests can be seen in Figure 4-20. On average, the droplet on the control sample took 4.65 min to freeze. When looking at the ZnO SA samples, it 39% longer at 6.46 min, but the best samples were the SiO₂ SA samples, which took on average, 83% longer to freeze (8.5 min). Using the same method, *Heale* found that when exposed to their best AACVD samples, it took ~30 min for a water droplet to freeze, or 500% longer than their control (5 min), with most samples taking ~130% longer.¹⁸⁸ However, these surfaces differed significantly from those tested here, including a fluorinated Krytox coating on the surface.

The only other surfaces to have their anti-icing properties tested were those produced by *Qi et al.*²⁰⁷ Their testing was performed at the lower temperature of -40 °C, with their optimised surface (6:20 min) performing 153% better than their surface that recorded the shortest freezing time (2:30 min). While the surfaces are a long way off the 500% increase in freezing time achieved by *Heale*, achieving the 153% by *Qi et al* though optimisation seems reasonable. This would then suggest that the coatings may have promise as an anti-icing coating, with the possible anti-icing properties improved through specific anti-icing optimisation.

4.5 Summary and conclusion

While the work in the previous chapter had achieved excellent superhydrophobic properties, they lacked durability. To address this, the latex component of the previous formulation was replaced with a more durable polymer. Polyurethane was determined to be a viable replacement polymer and was incorporated into the previous formulation. The resulting coatings again appeared to have desirable superhydrophobic properties.

The surfaces were then characterised using a number of techniques. Unfortunately, the FT-IR spectra were not of the same quality of those obtained for the paints. This meant there was little discernible information to take away from the FT-IR, with little to suggest that nitrogen was present in the coatings at all, which is a component of polyurethane. However, the presence of nitrogen was confirmed with XPS survey spectra. Other spectra also saw the trend continue where the FWHM of the 2p spectra increased compared to the raw material particles. SEM analysis showed the surfaces had a roughness desirable for superhydrophobic properties.

Next, the superhydrophobic properties of the coatings were confirmed before a more in depth look at the coatings and the paints properties was taken. All of the surfaces demonstrated excellent rolling angles and self-cleaning properties. The coatings also demonstrated the same level of stain resistance that the paints had previously shown. When looking at the CAH, the surface with the lowest rolling angle had the highest CAH value, which was surprising, and also demonstrated the value of performing both tests. The tape tests displayed the superiority of the coatings' durability, when compared to the paints.

Circling back to the other remit of the project, the antimicrobial properties of the coatings and paints were analysed next. Due to the superhydrophobic nature of the coatings, this required developing and validating a new methodology. Once this was done, it was shown that none of the surfaces produced very good antimicrobial properties. In an effort to understand why,

a protocol was designed to perform elemental analysis on the surfaces, which found that the surfaces were leaching ions, which may be accounting for their antimicrobial properties.

Finally anti-icing tests showed that the coatings may have potential as an anti-icing surface with the right optimisation. Not only this, with the increase of the surfaces' durability achieved, other modifications of the formulation may also be able to give the surfaces other improved properties. The next chapter will look at current concepts being investigated, as well as future work.

5 Incomplete and Future Work

As with any project, there are a number of concepts or future works that have yet to be fully realised during this project. This issue was exacerbated during this project due to both the pandemic and the move of our antimicrobial lab to a new facility. Just prior to the pandemic, the process of moving our antimicrobial labs to the Royal Free Hospital began. This effectively mean that that antimicrobial labs were decommissioned, with the plan to be up and running in the new labs within a week or two. However, once the labs had been decommissioned, the pandemic struck, meaning we were unable to perform any antimicrobial testing for over 12 months.

This inability to do antimicrobial testing meant that ongoing antimicrobial research was interrupted, and a number of chemistry concepts were explored. As the amount of time we were without antimicrobial testing facilities was far longer than anyone initially predicted, not all of these concepts could be fully realised before the project ended. This chapter will outline some of these concepts and future works, including ways to improve sample properties, test their functionalities and properties, and different manufacturing techniques. This section will outline some of these concepts and future works, as well as providing some preliminary results.

5.1 Determining a surface's surface free energy and the surface roughness

As first discussed in section 1.2, superhydrophobic surfaces are influenced by both their SFE and their surface topography.⁷⁷ However, obtaining values for either the SFE or the surface topography is not always straight forward. One of the better methods of determining the SFE is the OWRK method which uses the DSA measurements of a polar and a nonpolar liquid (Equation 2).⁹¹ However, to obtain a SFE value using this method, there is a requirement that the surface sample is flat. One of the concepts currently under development is the fabrication of flat superhydrophobic surfaces.

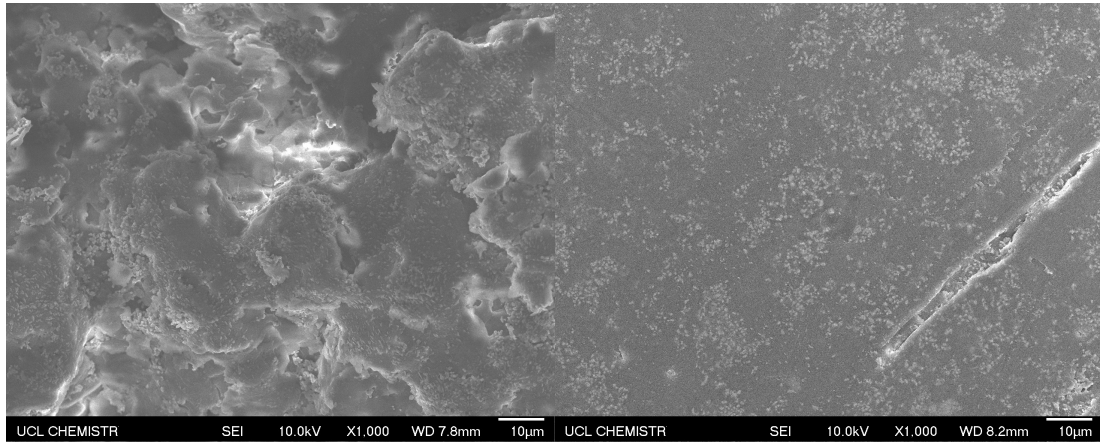


Figure 5-1 SEM imaging of a ZnO Plus latex stearic acid paint made in acetone. Left: sample after spraying. Right: sample after polishing.

Figure 5-1 displays an image of sprayed surface consisting of ZnO, Plus latex, stearic acid paint made in acetone, as well as the same surface after it had been polished using some blue roll. As can be seen in the image, the surface can be made practically flat by polishing the surface. In fact, polishing the surface caused the \bar{x} WCA to drop from 162.8° to 102.1°. However, the flat surface could then be used with the OWRK method to determine the SFE of the paint surface.

To do this an \bar{x} CA measurement of 61.0° was obtained for a nonpolar liquid diiodomethane. This value and the \bar{x} WCA value of 102.1° were used alongside the σ_{LV} values found in the literature, to determine the σ_{SV} values. For diiodomethane, we know that it has σ_{LV}^d value of 50.8 mN/m, with a σ_{LV}^p value of 0 mN/m due to it being nonpolar, giving it a total σ_{LV} value of 50.8 mN/m.⁸⁷ These values can then be used to determine the σ_{SV}^d value as follows

$$\begin{aligned}\sigma_{LV}(1 + \cos \theta^Y) &= 2\sqrt{\sigma_{LV}^d \sigma_{SV}^d} + \sqrt{\sigma_{LV}^p \sigma_{SV}^p} = \\ 50.8(1 + \cos 61.0^\circ) &= 2\sqrt{50.8 \times \sigma_{SV}^d} + \sqrt{0 \times \sigma_{SV}^p} = \\ \sigma_{SV}^d &= 28.0 \text{ mN/m}\end{aligned}$$

Once the σ_{SV}^d has been determined, we can use this value with the known water σ_{LV}^d value of 21.8 mN/m, with the σ_{LV}^p value of 51.0 mN/m, and the total σ_{LV} value of 72.8 mN/m to determine σ_{SV}^p value.

$$72.8(1 + \cos 102.1^\circ) = 2\sqrt{21.8 \times 28.0} + \sqrt{51 \times \sigma_{SV}^p} =$$

$$\sigma_{SV}^p = 0.3 \text{ mN/m}$$

so

$$\sigma_{SV} = \sigma_{SV}^d + \sigma_{SV}^p$$

$$\sigma_{SV} = 28.0 + 0.3$$

$$\sigma_{SV} = 28.3 \text{ mN/m}$$

While this seems like a promising method of determining the SFE of a surface that can be polished, there are some factors that need to be investigated further before this method can be validated. Firstly, applying heat and pressure during the polishing process could cause a reaction at the surface, altering the surface's chemical state. This can be resolved through chemical analysis pre- and post-polishing (IR, XPS, etc.), to determine if any changes have occurred.

Another variable to consider is if the surface is truly flat. While SEM imaging has shown the surface to be apparently flat at a x1000 magnification, higher magnifications should be used to confirm surface roughness. Other analytical instruments capable of determining surface roughness should also be utilised, including atomic force microscopy (AFM) or profilometry.

Once surface roughness can be confirmed, other values can also be extrapolated from this data. If we deem this surface to be flat, then we can take the 102.1° value to be Young's contact angle (θ_Y), with the 162.8° representing the other variable. Using the Wenzel model (Equation 3), we can calculate the roughness factor, r .

$$\cos \theta_W = r \cos \theta_Y$$

$$\frac{\cos 162.8^\circ}{\cos 102.1^\circ} = r$$

$$r = 4.56$$

Using the same information and Cassie-Baxter model (Equation 4), it is possible to calculate the fraction of material in contact with the droplet, Φ_S .

$$\cos \theta_C = \Phi_S \cos \theta_Y + \Phi_S - 1$$

$$\frac{\cos 162.8^\circ + 1}{\cos 102.1^\circ + 1} = \Phi_S$$

$$\Phi_S = 0.06$$

However, as the Wenzel model requires the droplet to be in full contact with the surface underneath, and the Cassie-Baxter model requires there to be the minimum amount of contact possible between the droplet and the surface, it is likely that neither the value calculated for r or Φ_S are fully correct. In reality, the surfaces are probably going to fall somewhere in between and follow the intermediate model (Equation 5). As both r and Φ_S are variables in this model, one needs to be measured. One method by which this might be possible is if a topological analytical technique can determine the actual surface area, which can then be paired with the planar area to calculate the roughness factor (Equation 6).

Equation 6 Roughness factor

$$r = \frac{\text{actual surface area}}{\text{planar area}}$$

Going forwards, there are a number of ways to better understand sample properties. If flat samples can be produced, then we can begin to extrapolate important information with regard to SFE. Also, if we can determine the actual surface area of a rough surface through topological analysis, we can then gain further insight into how the surfaces interact with water droplets through some of these calculations.

5.2 Modifying samples for increased antimicrobial properties

The concept of modifying samples to improve their antimicrobial properties was something that was touched on at the end of Chapter 2. However, plans to modify the ZnO nanocomposite were postponed due to COVID, with the extended delay eventually moving the majority of this work beyond the end of this project. At its most basic, this concept requires the use of an additive to increase the surfaces' antimicrobial properties. There are a number of ways this can work, with two ideas in particular considered for these samples going forwards.

The first idea is to dye-sensitise the samples with a photocatalytic dye. This would follow on from previous work carried out by *Sehmi et al.* and *Noimark et al.*, who also dye-sensitised ZnO nanocomposite polymers.^{157,158} By dye-sensitising their samples, *Noimark et al.* saw a >3 log increase to their kill when both samples were exposed to *S. aureus* for 1 h under white light. There was also an ~2 log increase to the sample's bactericidal activity when exposed to *E. coli* for 3 h under the same conditions. Similarly, *Sehmi et al.* saw a >3 log increase to their kill against both *S. aureus* and *E. coli* when their dye-sensitised samples were compared to the ZnO samples for 2 h under white light.

While both *Sehmi et al.* and *Noimark et al.* required the use of swell encapsulation to functionalise their materials, due to the nature of how the ZnO incorporated PVC is produced, an easier method could be used for their functionalisation. The first option would be to prefunctionalise the ZnO with the dye prior to the fabrication process. The other simpler method would just be to incorporate the dye during the fabrication process, as can be seen in Figure 5-2. However, if this method does not functionalise the ZnO sufficiently, the first method may be required. The hope is by doing this, we can see an increase of ROS production through both type 1 and 2 mechanisms, as *Sehmi et al.* did, and in turn, see an increase in the surface's antimicrobial properties.

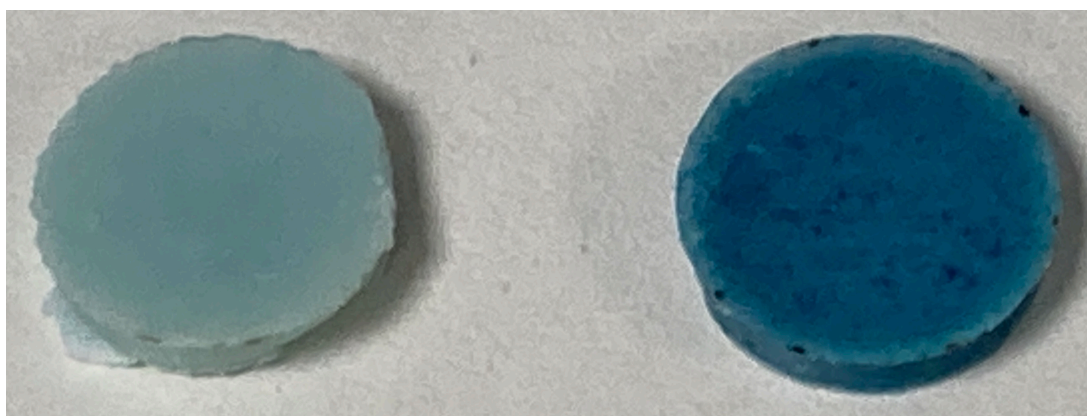


Figure 5-2 Dye-sensitised 5% ZnO incorporated PVC. Left: 10 ppm methylene blue. Right 100 ppm methylene blue.

Another more novel approach to improving the nanocomposite's antimicrobial properties could be the incorporation of Zn/ZnO coreshell particles. Originally investigated by Yi *et al.*, they found that when Zn/ZnO composites were formed, they would self-corrode, adding an electron into the ZnO conduction band (Figure 5-3).²²⁷ They were able to show a >8 log reduction in *E. coli*, *S. aureus*, and *C. albicans* after 24 h of exposure under dark conditions. They were also able to show that the mechanism of kill was predominantly down to O_2^- and H_2O_2 .

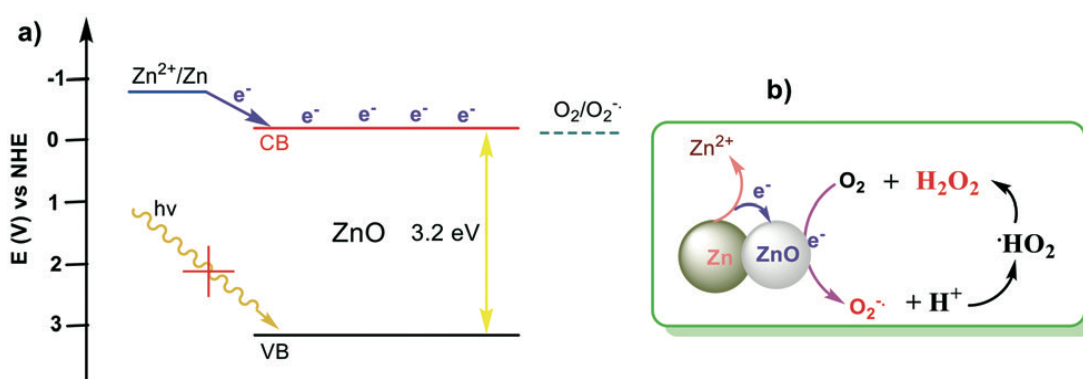


Figure 5-3 The production of reactive oxygen species via electron transfer, due to the self-corrosive properties of Zn/ZnO coreshell particles. Reproduced from Yi *et al.*²²⁷

While the Zn/ZnO coreshell nanocomposite is yet to be fabricated efforts have been made to replicate the coreshell particles. The initial method taken from Yi *et al.*, added 1 g of Zn particles to a 50:50 10 ml mixture of 0.5 M $Zn(NO_3)_2$

aqueous solution and 4 M KOH.²²⁷ The results of this initial testing (Figure 5-4) shows the clear functionalisation of the Zn particles with ZnO.

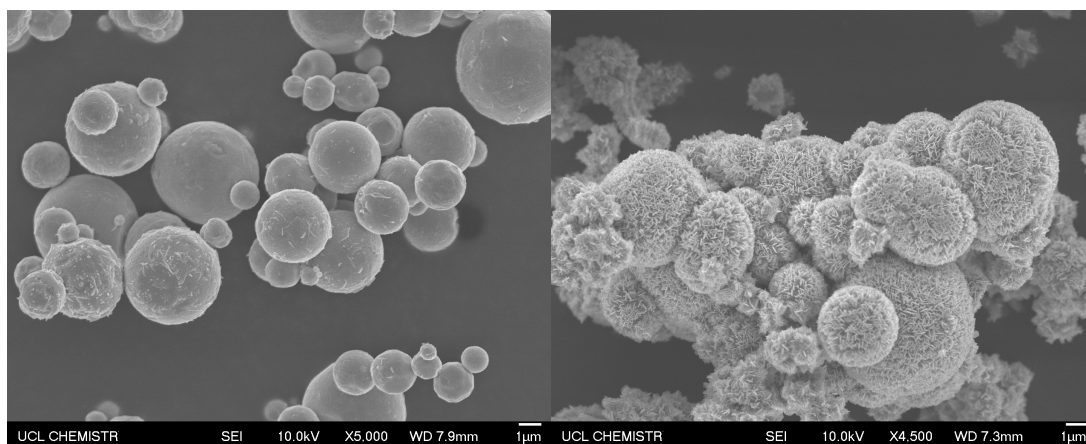


Figure 5-4 Initial SEM comparison between Zn particles (left) and Zn/ZnO coreshell particles (right)

While the initial method successfully produced the coreshell particles, it only produced slightly more than a gram of product, as such the next goal was to begin the optimisation process. Firstly, a more viable amount of product needed to be produced, by scaling up the experiment. As the available falcon tubes required for centrifuge had a maximum volume of 50 cm³, the mix of Zn(NO₃)₂ and KOH was increased to 40 ml, with the Zn particles also increased x4 to 4 g. However, when the scaled reaction was run for 2 h, product lacked consistency. This led to the scaled experiment being rerun, with different reaction times also investigated.

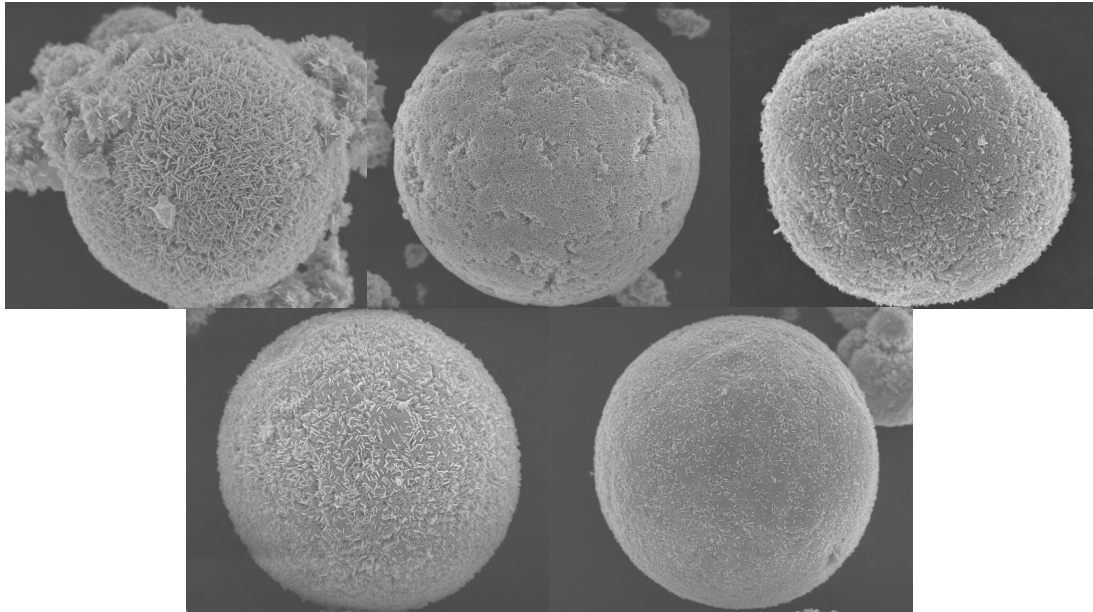


Figure 5-5 SEM comparison between Zn/ZnO coreshell particles produced using different reaction times (1 hour intervals). Top left: 1 h. Top middle 2 h. Top right 3 h. Bottom left 4 h. Bottom right 5 h.

Figure 5-5 gives examples of some of the particles made using different reaction times. While it is not readily observable in the SEM images provided, SEM analysis showed that 4 hours appeared to be the best reaction time. After 4 hours, the particles were relatively uniform, with no visible improvement at 5 hours. These results would suggest that different reaction times may need to be considered when changing the aspects of the reaction.

While both these strategies showed promise, comparatively there are positive and negative aspects to both. When considering the dye-sensitised nanocomposite, it is important to remember it is photocatalytic, and as such will not produce antimicrobial properties in the dark. Comparatively, the corrosion process of the coreshell particles requires no such input of energy, and therefore can operate under both light and dark conditions. However, once separated the Zn and the ZnO will be stable, resulting in diminishing antimicrobial properties over time. As a catalyst, the dye-sensitised nanocomposite will not degrade in the same way, meaning it will not have the same diminishing antimicrobial properties. All things considered, it is worth investigating both concepts.

5.3 New methods for the production of bulk superhydrophobic polymers

During this project, it has mainly been coatings that have been investigated for their superhydrophobic properties. However, there may also be applications for bulk polymers with superhydrophobic properties. As such we have begun to investigate whether a similar formula could be used to fabricate a bulk superhydrophobic polyurethane, while also considering if the PVC could be functionalised to be superhydrophobic.

As with the coating previously, the fabrication process began by dissolving 1.5 g of stearic acid into 40 ml of acetone at 50 °C. Once fully dissolved, 1 g of ZnO was added to the solution and functionalised for 20 min. Once the 20 min had elapsed, 20 g of the polyurethane (Altro Seal) was added and stirred for another 20 minutes. Next the beaker was transferred to a sonicator and left for approximately 3 h so the majority of the solvent had evaporated off. This was done as the agitation from the sonicator kept the components in the suspension relatively well dispersed. After 3 h the suspension was left to dry and cure for a minimum of 3 days.

Figure 5-6 shows the resultant polymer once fully cured. For an initial attempt, the resulting product had plenty of promise. One issue was that unlike the spray application process which garners a rough surface, the production process used to fabricate the bulk sample, did not produce a rough surface. To get around this, an artificial rough surface was produced by gently scuffing the surface with sandpaper. This worked very well, with the resulting surface producing an WCA of 168.52 (Figure 5-7).



Figure 5-6 Bulk polyurethane fabricated using a similar formulation to the superhydrophobic Altro Seal coatings (section 4.3.2)

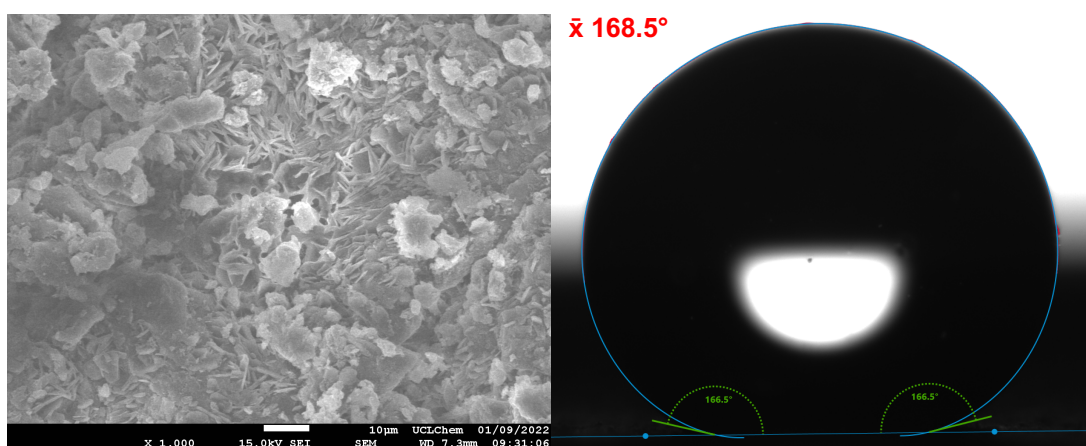


Figure 5-7 DSA image of a 5 μ l water droplet on bulk polyurethane sample consisting of ZnO, stearic acid, and Altro Seal made up in an acetone base.

Another aspect of this project that could be investigated is the functionalisation of the PVC nanocomposite for superhydrophobic properties. This could be done in a similar manner to how the bulk polyurethane was fabricated by incorporating stearic acid, or prefunctionalised superhydrophobic ZnO nanoparticles into the production process. This would again most likely require some form of artificial roughening as the compression moulding process produces a very smooth surface.

The other way the PVC nanocomposite could be functionalised for superhydrophobic properties, would be to use a method similar to that used by

*Hejazi et al.*²¹¹ Their method was to first produce a thermoplastic substrate by compression moulding before spreading superhydrophobic particles across the top. The next stage was to use the compression mould to imbed the particles into the surface, resulting in a surface capable of WCAs of ~160°. Imbedding superhydrophobic particles into the PVC, along with other methodologies discussed, offer the prospective ways to produce superhydrophobic bulk polymers.

5.4 New methods of antimicrobial testing

In Chapter 4 new methods of testing a surface's antimicrobial properties needed to be developed in order to test the basic antimicrobial properties of the superhydrophobic coatings. However, there are still other antimicrobial properties of the surfaces fabricated in this project that could be tested. By utilising and developing more antimicrobial testing methods, the surfaces' potentials could be further exploited.

While there was much testing against bacteria, none of the surfaces were tested against viruses. Although it is not as straight forward as swapping in a viral strain for a bacterial strain and using the same methods as previously done, the recent attention viral pathogens have garnered, means that viral testing is more important now than ever. ISO 21702:2019 is for the "measurement of antiviral activity on plastics and other non-porous surfaces" and gives an inclination into some of the differences between bacterial and viral testing.²²⁸

A very brief outline of the antiviral testing process sees the major difference between viral testing and bacterial testing being that the viral strains require host cells to function. This means that prior to surface exposure, the virus must first infect host cells. Once the viral infectivity titre of inoculum has been confirmed, it can then be exposed to the test surface as previously done in the bacterial testing.¹⁵⁸ Once the exposure period has elapsed, the inoculum is recovered and undergoes serial dilution. Next, rather than being grown on an agar, the dilutions are exposed and fixed to a monolayer of host cells. When

this happens, the viable virus will spread to the host cells forming viral plaque. This can then be made visible through staining, allowing for the infectivity titre of the virus to be determined.

Another aspect of the surfaces that was not fully explored, was the surfaces' ability to resist bacterial adhesion or biofilm formation. As previously discussed in section 1.1.4, superhydrophobic surfaces may have antibiofouling properties due to reduced microbial adhesion, or reduced biofilm formation. In order to test this, a spray application method was designed, that was capable of contaminating the surfaces with bacteria, which then could be observed by SEM, while also being a closer mimic to real world exposure.

This experiment began as outline in section 2.3.4, with bacteria taken from freezer stocks, single colonies were used to inoculate 10 ml of BHI broths, with the broths incubated until the culture reached approximately 10^9 CFU/ml. The BHI was then removed, with the bacteria washed with and resuspended in PBS, so as to avoid continued cell growth in the stock suspensions. Finally, a number of inocula of different concentrations were made up using PBS and either an *S. aureus* or *E. coli* stock suspension.

To spray the bacterial inocula, a Timbertech ABPST01 Airbrush Kit was purchased from Amazon. On receipt, the airbrush was first rinsed with 10 ml of ethanol, before being further rinsed with 10 ml of sterilised PBS. This was done to ensure the airbrush was free from bacterial contamination. Once cleaned, to validate the method, an inoculum was loaded into the airbrush and sprayed across a nutrient agar plate. This was initially done using inocula of 10^5 CFU. The agar plates were then incubated at 37 °C for ~36 h, with the results of the spraying visible in Figure 5-8.

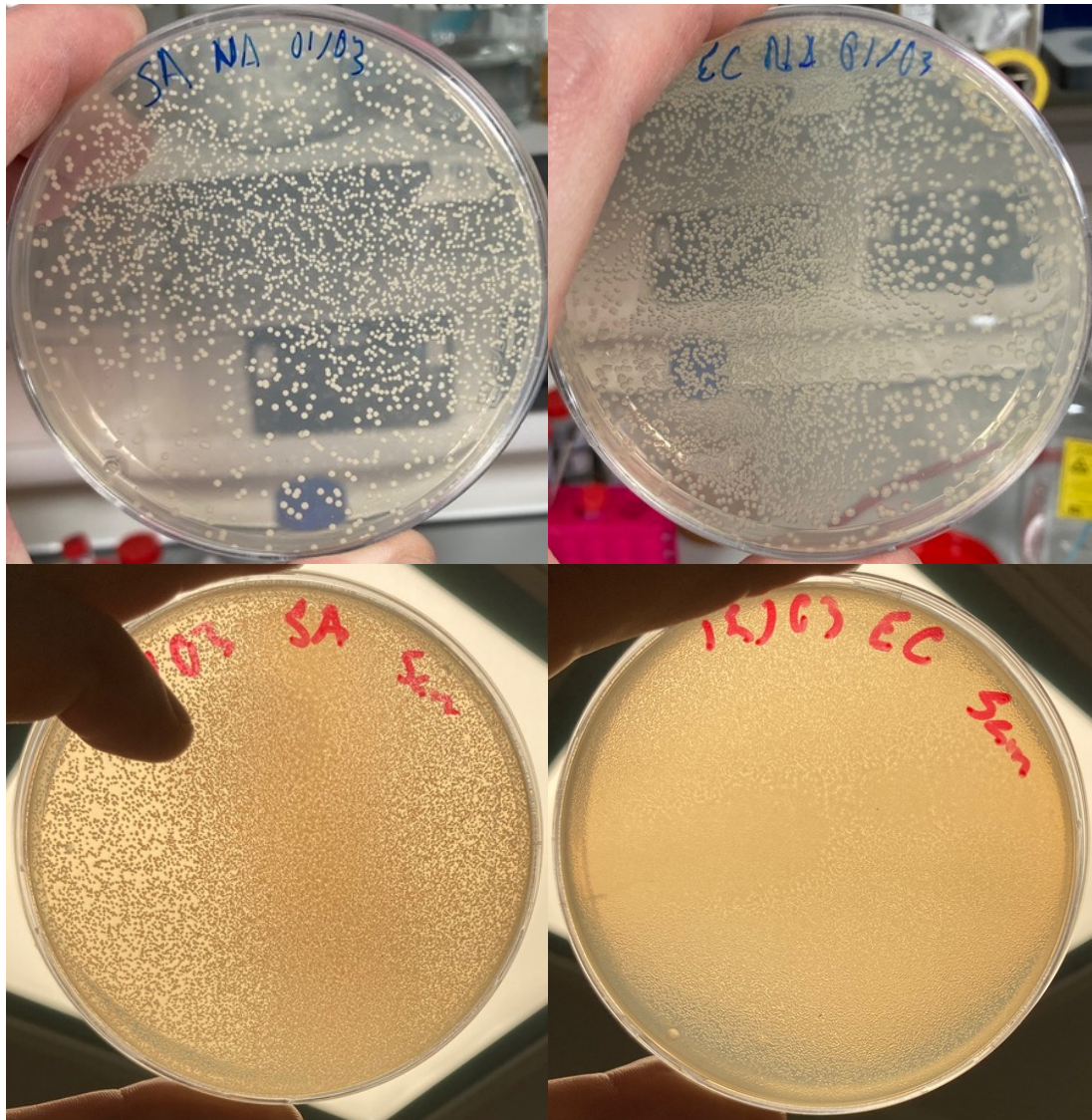


Figure 5-8 Nutrient agar plates sprayed with different concentrations of bacterial inocula. Top left: *S. aureus* 10^5 CFU. Top right: *E. coli* 10^5 CFU. Bottom left: *S. aureus* 10^7 CFU. Bottom right: *E. coli* 10^7 CFU.

The next stage of the experiment was to spray samples. To begin with, two samples each of both an Altro Seal and a functionalised superhydrophobic ZnO Altro Seal coating were sprayed with an inoculum. The samples were then left for 24 h to propagate, before one sample of each was left as was, while the other one of each was rinsed with sterilised deionised water. The logic behind this was that the unrinsed sample could be inspected for biofilm formation, where the rinsed samples could be checked for bacterial adhesion.

Prior to SEM analysis, samples needed to be prepared in order to stop the bacterial cells bursting or flying off the surface under high vacuum pressure.

To do this samples are first fixed with 3% glutaraldehyde in 0.1 M cacodylate buffer for at least 12 h. Next, the samples undergo dehydration using a series of ethanol dilutions. Samples spend 10 min in each solution, starting with a 20% ethanol solution, before progressing to 50%, 70%, 90%, and 100%. Finally, samples undergo critical-point drying by immersing the sample in hexamethyldisilazane for 2 mins. Once dry, samples can undergo SEM analysis.

Unfortunately, due to the nature of the polyurethane coatings, the coatings swelled when interacting with the solvents used in the fixing process. While this meant they came away from the glass substrate, it was hoped that the resultant films could still be analysed. However, when inspected by SEM, there were no visible bacteria present on the films. After considering the results, it was realised that 10^5 CFU was most likely too low a concentration to be spraying the samples, regardless of the other issues.

As such a repeat experiment was tried with 10^7 CFU inocula. The dehydration process was also reduced with the hope that reducing the time the coatings were in ethanol, the less of an impact the swelling would have on the surfaces. Even with the reduced dehydration process, the coatings still separated from the substrate. Despite this, the films were still analysed using SEM. However, even with a 10^7 CFU spray, there were no visible cells on the surface. This would suggest that the swelling process maybe dislodging the bacterial cells from the surface.

Despite these initial issues, the methodology behind this testing is sound. With this in mind, efforts should be made to test better suited materials using this method. It may also be possible to test these materials using a different means of fixing the bacteria to the coatings, including the use of freeze-drying for the dehydration step. If carried out successfully this method would give an excellent insight into both that bacterial adhesion, and biofilm formation properties of the coatings.

6 Conclusion

The outline of this project was to investigate antimicrobial and superhydrophobic surfaces. The goal was to manufacture surfaces that would be economically viable across multiple industries, using manufacturing techniques that would be scalable for large scale production. This required the avoidance of expensive materials and techniques known to produce good antimicrobial or superhydrophobic properties, such as gold or ion etching.^{1,2}

Chapter 2 began the project by attempting to produce antimicrobial surfaces using a ZnO incorporated PVC nanocomposite. A nanocomposite was produced by mixing ZnO with a PVC blend, before forming samples with a compression mould. The antimicrobial properties of the sample surfaces were then tested and found to have qualitative antimicrobial properties against both *S. aureus* and *E. coli*. However, quantitatively, the sample's antimicrobial properties against *S. aureus* fell short of the 99.9% hope for.

Shortly after it was ascertained that, not only was it a reactive oxygen species predominantly responsible for the surfaces kill, but that it was specifically singlet oxygen. When considering *S. aureus*, it was hypothesised that the carotenoids were responsible for giving the *S. aureus* cells their colour, could also be responsible for the cell's resistance to the nanocomposite's antimicrobial properties. However, this did not prove to be the case.

Chapter 3 shifted towards the project's superhydrophobic aspect. This aspect of the project aimed to develop fluorine free superhydrophobic surfaces. This began with ZnO particles being functionalised with a fatty acid and achieving an \bar{x} WCA of 174.2°. The functionalisation of SiO₂ particles was also attempted, but failed, possibly due to their non-polar nature.

Next, the particles were used in combination with a latex to make superhydrophobic paints. Once optimised, the resulting paints were capable of achieving an \bar{x} WCA of 170.3°. These paints also displayed self-cleaning and stain resistant properties, which are both advantageous properties for a

superhydrophobic paint. However, the paints lacked the durability required for touch surfaces.

In an effort to create a coating more suitable for touch surfaces, Chapter 4 began investigating the use of more durable polymers. Both epoxy and polyurethane were investigated, but the polyurethane performing far better as a durable superhydrophobic coating, with the optimised coating having an \bar{x} WCA of 170.3° . This chapter also explored the antimicrobial properties of both the paints and the polyurethane coatings. Again, while both of them showed qualitative antimicrobial properties against *S. aureus*, and *E. coli*, the antimicrobial properties were quantitatively very poor, with ion leaching most likely the main mechanism of kill.

Chapter 5 outlined the concepts currently being considered to improve both the nanocomposite and the coatings. This includes using new methods to better characterise and measure the surfaces' properties, including the SFE, surface roughness, and antibiofouling properties. It also included possible fabrication methods to be explored for producing a bulk polymer, as well as including ideas on how to increase the surfaces' antimicrobial properties.

Overall, this project has produced a qualitatively antimicrobial nanocomposite PVC, which has promise, but still requires improved quantitative antimicrobial properties. A self-cleaning, stain resistant paint has also been produced, which may require some final optimisation to its durability in order to achieve commercial viability. Finally, a superhydrophobic durable polyurethane coating has been produced, which is currently having its commercial viability assessed by the project's industrial partners.

7 Bibliography

- 1 D. Ebert and B. Bhushan, *J Colloid Interface Sci*, 2016, **481**, 82–90.
- 2 K. Zheng, M. I. Setyawati, D. T. Leong and J. Xie, *ACS Nano*, 2017, **11**, 6904–6910.
- 3 I. Loudon, *J R Soc Med*, 2013, **106**, 461–463.
- 4 K. A. Smith, *Front Immunol*, , DOI:10.3389/fimmu.2012.00068.
- 5 S. M. Blevins and M. S. Bronze, *International Journal of Infectious Diseases*, 2010, **14**, 744–751.
- 6 J. Wong, *Prim Care Update Ob Gyns*, 2003, **10**, 124–126.
- 7 S. B. Levy and M. Bonnie, *Nat Med*, 2004, **10**, 122–129.
- 8 WHO, *Antimicrobial Resistance* , .
- 9 WHO, *Health Care-associated Infections Fact Sheet*, Geneva, 2016.
- 10 H. W. Cho and C. Chu, *Osong Public Health Res Perspect*, 2011, **2**, 149–150.
- 11 WHO, *Managing epidemics*, 2018.
- 12 WHO, WHO Coronavirus (COVID-19) Dashboard, <https://covid19.who.int/>, (accessed 4 August 2022).
- 13 A. O'Neill, Global gross domestic product (GDP) at current prices from 1985 to 2027, <https://www.statista.com/statistics/268750/global-gross-domestic-product-gdp/>, (accessed 4 August 2022).
- 14 Office for National Statistics, *Consumer price inflation, UK: June 2022*, 2022.
- 15 WHO, *Public health advice for gatherings during the current monkeypox outbreak*, 2022.
- 16 C. J. Duncan and S. Scott, *Postgrad Med J*, 2005, **81**, 315–320.
- 17 J. K. Taubenberger and D. M. Morens, *Emerg Infect Dis*, 2006, **12**, 15–22.
- 18 J. Mossong, N. Hens, M. Jit, P. Beutels, K. Auranen, R. Mikolajczyk, M. Massari, S. Salmaso, G. S. Tomba, J. Wallinga, J. Heijne, M. Sadkowska-Todys, M. Rosinska and W. J. Edmunds, *PLoS Med*, 2008, **5**, e74.
- 19 L. L. Nwido, B. Oveh, T. Okoriye and N. A. Vaikosen, *Afr J Biotechnol*, 2008, **7**, 2993–2997.

- 20 K. Abu-Elteen, A. Elkarmi and M. Hamad, *Assessment of airborne pathogens in healthcare settings*, 2009.
- 21 A. Offner and J. Vanneste, *Physics of Fluids*, 2022, **34**, 053320.
- 22 S. S. Cassidy, D. J. Sanders, J. Wade, I. P. Parkin, C. J. Carmalt, A. M. Smith and E. Allan, *PLoS Pathog*, 2020, **16**, 1–10.
- 23 Civil Aviation Authority, *Terminal and Transit Passengers 2018*, 2019.
- 24 Mayor of London, *TfL Annual Report and Statement of Accounts 2018/19*, London, 2019.
- 25 W. A. Rutala and D. J. Weber, *Bennett & Brachman's Hospital Infections: Sixth Edition*.
- 26 P. C. Carling, M. F. Parry, L. A. Bruno-Murtha and B. Dick, *Crit Care Med*, 2010, **38**, 1054–1059.
- 27 J. Lenard, in *Encyclopedia of Virology*, Elsevier, 1999, pp. 1920–1925.
- 28 T. Theoharides and P. Conti, *J Biol Regul Homeost Agents*, 2021, 833–838.
- 29 T. Thanh Le, Z. Andreadakis, A. Kumar, R. Gómez Román, S. Tollefsen, M. Saville and S. Mayhew, *Nat Rev Drug Discov*, 2020, **19**, 305–306.
- 30 L. Leclercq and V. Nardello-Rataj, *European Journal of Pharmaceutical Sciences*, 2020, **155**, 105559.
- 31 G. Kampf, *Journal of Hospital Infection*, 2018, **98**, 331–338.
- 32 G. McDonnell and A. D. Russell, *Clin Microbiol Rev*, 1999, **12**, 147–179.
- 33 Q. Lin, J. Y. C. Lim, K. Xue, P. Y. M. Yew, C. Owh, P. L. Chee and X. J. Loh, *View*, , DOI:10.1002/viw2.16.
- 34 M. Schieber and N. S. Chandel, *Current Biology*, 2014, **24**, R453–R462.
- 35 I. Wessels, B. Rolles and L. Rink, *Front Immunol*, 2020, **11**, 1712.
- 36 Y.-J. Zhang, S. Li, R.-Y. Gan, T. Zhou, D.-P. Xu and H.-B. Li, *Int J Mol Sci*, 2015, **16**, 7493–7519.
- 37 M. S. M. Jetten, M. Schmid, I. Schmidt, M. Wubben, U. van Dongen, W. Abma, O. Sliemers, N. P. Revsbech, H. J. E. Beaumont, L. Ottosen, E. Volcke, H. J. Laanbroek, J. L. Campos-Gomez, J. Cole, M. van Loosdrecht, J. W. Mulder, J. Fuerst, D. Richardson, K. van de Pas, R. Mendez-Pampin, K. Third, I. Cirpus, R. van Spanning, A. Bollmann, L. P. Nielsen, H. O. den Camp, C. Schultz, J. Gundersen, P. Vanrolleghem,

- M. Strous, M. Wagner and J. G. Kuenen, *Rev Environ Sci Biotechnol*, 2002, **1**, 51–63.
- 38 L. P. Villarreal and G. Witzany, *J Theor Biol*, 2010, **262**, 698–710.
- 39 M. R. Brown, P. J. Collier and P. Gilbert, *Antimicrob Agents Chemother*, 1990, **34**, 1623–1628.
- 40 T. Beveridge, *Biotechnic & Histochemistry*, 2001, **76**, 111–118.
- 41 C. Jiménez-Jiménez, V. M. Moreno and M. Vallet-Regí, *Nanomaterials*, 2022, **12**, 288.
- 42 S. Berezin, Y. Aviv, H. Aviv, E. Goldberg and Y. R. Tischler, *Sci Rep*, 2017, **7**, 3810.
- 43 T. J. Silhavy, D. Kahne and S. Walker, *Cold Spring Harb Perspect Biol*, 2010, **2**, a000414–a000414.
- 44 W. T. Doerrler, *Mol Microbiol*, 2006, **60**, 542–552.
- 45 U. Choi and C.-R. Lee, *Front Microbiol*, , DOI:10.3389/fmicb.2019.00953.
- 46 R. Nahra and R. P. Dellinger, *Curr Opin Anaesthesiol*, 2008, **21**, 98–104.
- 47 J. Tamarit, E. Cabisco and J. Ros, *Journal of Biological Chemistry*, 1998, **273**, 3027–3032.
- 48 T. Chautrand, D. Souak, S. Chevalier and C. Duclairoir-Poc, *Microorganisms*, 2022, **10**, 924.
- 49 S. L. Begg, *Biochem Soc Trans*, 2019, **47**, 77–87.
- 50 S. Silver and L. T. Phung, *J Ind Microbiol Biotechnol*, 2005, **32**, 587–605.
- 51 A. H. Delcour, *Biochimica et Biophysica Acta (BBA) - Proteins and Proteomics*, 2009, **1794**, 808–816.
- 52 J. G. Swoboda, J. Campbell, T. C. Meredith and S. Walker, *ChemBioChem*, 2009, **11**, 35–45.
- 53 S. I. Miller and N. R. Salama, *PLoS Biol*, 2018, **16**, e2004935.
- 54 R. Nazir, S. Rehman, M. Nisa and U. ali Baba, in *Freshwater Microbiology*, Elsevier, 2019, pp. 263–306.
- 55 T. Hemnani and M. S. Parihar, *Indian J Physiol Pharmacol*, 1998, **42**, 440–52.

- 56 A. Hartwig, M. Asmuss, I. Ehleben, U. Herzer, D. Kostelac, A. Pelzer, T. Schwerdtle and A. Bürkle, *Environ Health Perspect*, 2002, **110**, 797–799.
- 57 H. Koo, R. N. Allan, R. P. Howlin, P. Stoodley and L. Hall-Stoodley, *Nat Rev Microbiol*, 2017, **15**, 740–755.
- 58 V. B. Damodaran and S. N. Murthy, *Biomater Res*, 2016, **20**, 1–11.
- 59 Z. Huang and H. Ghasemi, *Adv Colloid Interface Sci*, 2020, **284**, 102264.
- 60 J. Jenkins, J. Mantell, C. Neal, A. Gholinia, P. Verkade, A. H. Nobbs and B. Su, *Nat Commun*, 2020, **11**, 1626.
- 61 S. Pogodin, J. Hasan, V. A. Baulin, H. K. Webb, V. K. Truong, T. H. Phong Nguyen, V. Boshkovikj, C. J. Fluke, G. S. Watson, J. A. Watson, R. J. Crawford and E. P. Ivanova, *Biophys J*, 2013, **104**, 835–840.
- 62 E. P. Ivanova, J. Hasan, H. K. Webb, V. K. Truong, G. S. Watson, J. A. Watson, V. A. Baulin, S. Pogodin, J. Y. Wang, M. J. Tobin, C. Löbbe and R. J. Crawford, *Small*, 2012, **8**, 2489–2494.
- 63 L. R. Braga, E. T. Rangel, P. A. Z. Suarez and F. Machado, *Food Packag Shelf Life*, 2018, **15**, 122–129.
- 64 T. Walker, M. Canales, S. Noimark, K. Page, I. Parkin, J. Faull, M. Bhatti and L. Ciric, *Sci Rep*, 2017, **7**, 1–10.
- 65 T. C. Dakal, A. Kumar, R. S. Majumdar and V. Yadav, *Front Microbiol*, 2016, **7**, 1–17.
- 66 J. A. Lemire, J. J. Harrison and R. J. Turner, *Nat Rev Microbiol*, 2013, **11**, 371–384.
- 67 T. Dai, B. B. Fuchs, J. J. Coleman, R. A. Prates, C. Astrakas, T. G. Denis, M. S. Ribeiro, E. Mylonakis, M. R. Hamblin and G. P. Tegos, *Front Microbiol*, , DOI:10.3389/fmicb.2012.00120.
- 68 M. S. Baptista, J. Cadet, P. di Mascio, A. A. Ghogare, A. Greer, M. R. Hamblin, C. Lorente, S. C. Nunez, M. S. Ribeiro, A. H. Thomas, M. Vignoni and T. M. Yoshimura, *Photochem Photobiol*, 2017, **93**, 912–919.
- 69 S. J. Dixon and B. R. Stockwell, *Nat Chem Biol*, 2014, **10**, 9–17.
- 70 G. Valduga, G. Bertoloni, E. Reddi and G. Jori, *J Photochem Photobiol B*, 1993, **21**, 81–86.
- 71 J. F. Siqueira and H. P. Lopes, *Int Endod J*, 1999, **32**, 361–369.

- 72 S. Kang, M. Yang, Z. Hong, L. Zhang, Z. Huang, X. Chen, S. He, Z. Zhou, Z. Zhou, Q. Chen, Y. Yan, C. Zhang, H. Shan and S. Chen, *Acta Pharm Sin B*, 2020, **10**, 1228–1238.
- 73 K. Page, M. Wilson and I. P. Parkin, *J Mater Chem*, 2009, **19**, 3819.
- 74 H. Sies, *Klin Wochenschr*, 1991, **69**, 965–968.
- 75 M. Moustakas, *Materials*, 2021, **14**, 549.
- 76 H. Einsele, M. R. Clemens, U. Wegner and H.-D. Waller, *Free Radic Res Commun*, 1987, **3**, 257–263.
- 77 C. R. Crick and I. P. Parkin, *Chemistry - A European Journal*, 2010, **16**, 3568–3588.
- 78 R. H. Dettre and R. E. Johnson, *Contact Angle Hysteresis*, 1964.
- 79 K. Liu and L. Jiang, *Nano Today*, 2011, **6**, 155–175.
- 80 W. Li, Y. Zhan and S. Yu, *Prog Org Coat*, 2021, **152**, 106117.
- 81 S. P. Dalawai, M. A. Saad Aly, S. S. Latthe, R. Xing, R. S. Sutar, S. Nagappan, C.-S. Ha, K. Kumar Sadasivuni and S. Liu, *Prog Org Coat*, 2020, **138**, 105381.
- 82 P. Nguyen-Tri, H. N. Tran, C. O. Plamondon, L. Tuduri, D.-V. N. Vo, S. Nanda, A. Mishra, H.-P. Chao and A. K. Bajpai, *Prog Org Coat*, 2019, **132**, 235–256.
- 83 G. He, C. Zhou and Z. Li, *Procedia Eng*, 2011, **16**, 640–645.
- 84 O. Parent and A. Ilinca, *Cold Reg Sci Technol*, 2011, **65**, 88–96.
- 85 N. B. Vargaftik, B. N. Volkov and L. D. Voljak, *J Phys Chem Ref Data*, 1983, **12**, 817–820.
- 86 A. Docoslis, R. F. Giese and C. J. van Oss, *Colloids Surf B Biointerfaces*, 2000, **19**, 147–162.
- 87 M. Jin, F. Thomsen, T. Skrivaneck and T. Willers, in *Advances in Contact Angle, Wettability and Adhesion*, John Wiley & Sons, Inc., Hoboken, NJ, USA, 2015, pp. 419–438.
- 88 T. Young, *Philos Trans R Soc Lond*, 1805, **95**, 65–87.
- 89 J. T. Simpson, S. R. Hunter and T. Aytug, *Reports on Progress in Physics*, , DOI:10.1088/0034-4885/78/8/086501.
- 90 S. S. Chhatre, J. O. Guardado, B. M. Moore, T. S. Haddad, J. M. Mabry, G. H. McKinley and R. E. Cohen, *ACS Appl Mater Interfaces*, 2010, **2**, 3544–3554.

- 91 M. Żenkiewicz, *Journal of achievements in materials and manufacturing engineering*, 2007, **24**, 137–145.
- 92 R. N. Wenzel, *Ind Eng Chem*, 1936, **28**, 988–994.
- 93 A. B. D. Cassie and S. Baxter, *Transactions of the Faraday Society*, 1944, **40**, 546.
- 94 I. P. Parkin and R. G. Palgrave, *J Mater Chem*, 2005, **15**, 1689.
- 95 E. Lee and D. H. Kim, *Colloids Surf A Physicochem Eng Asp*, 2021, **625**, 126927.
- 96 Z. He, Y. Zhuo, Z. Zhang and J. He, *Coatings*, 2021, **11**, 1343.
- 97 J. Kloubek, *J Colloid Interface Sci*, 1974, **46**, 185–190.
- 98 A. Azimi Yancheshme, G. Momen and R. Jafari Aminabadi, *Adv Colloid Interface Sci*, 2020, **279**, 102155.
- 99 A. Alizadeh, M. Yamada, R. Li, W. Shang, S. Otta, S. Zhong, L. Ge, A. Dhinojwala, K. R. Conway, V. Bahadur, A. J. Vinciguerra, B. Stephens and M. L. Blohm, *Langmuir*, 2012, **28**, 3180–3186.
- 100 X. Y. Liu, *J Chem Phys*, 2000, **112**, 9949–9955.
- 101 S. Özcan, G. Açıkbash and N. Çalış Açıkbash, *Appl Surf Sci*, 2018, **438**, 136–146.
- 102 S. Li, Y. Liu, Z. Zheng, X. Liu, H. Huang, Z. Han and L. Ren, *Chemical Engineering Journal*, 2019, **372**, 852–861.
- 103 S. M. Kelleher, O. Habimana, J. Lawler, B. O’reilly, S. Daniels, E. Casey and A. Cowley, *ACS Appl Mater Interfaces*, 2016, **8**, 14966–14974.
- 104 H. Xie, H. X. Huang and Y. J. Peng, *Nanoscale*, 2017, **9**, 11951–11958.
- 105 C. D. Bandara, S. Singh, I. O. Afara, A. Wolff, T. Tesfamichael, K. Ostrikov and A. Oloyede, *ACS Appl Mater Interfaces*, 2017, **9**, 6746–6760.
- 106 E. P. Ivanova, S. H. Nguyen, H. K. Webb, J. Hasan, V. K. Truong, R. N. Lamb, X. Duan, M. J. Tobin, P. J. Mahon and R. J. Crawford, *PLoS One*, 2013, **8**, 1–8.
- 107 T. Sun, G. Qing, B. Su and L. Jiang, *Chem Soc Rev*, 2011, **40**, 2909.
- 108 E. P. Ivanova, J. Hasan, H. K. Webb, G. Gervinskis, S. Juodkazis, V. K. Truong, A. H. F. Wu, R. N. Lamb, V. A. Baulin, G. S. Watson, J. A. Watson, D. E. Mainwaring and R. J. Crawford, *Nat Commun*, 2013, **4**, 2838.

- 109 S. Liu, J. Zheng, L. Hao, Y. Yegin, M. Bae, B. Ulugun, T. M. Taylor, E. A. Scholar, L. Cisneros-Zevallos, J. K. Oh and M. Akbulut, *ACS Appl Mater Interfaces*, 2020, **12**, 21311–21321.
- 110 Y. Huang, D. K. Sarkar and X.-G. Chen, *Mater Lett*, 2010, **64**, 2722–2724.
- 111 I. Manners, *Angewandte Chemie International Edition in English*, 1996, **35**, 1602–1621.
- 112 R. O. Ebewele, *Polymer Science and Technology*, CRC Press, 2000.
- 113 C. F. Jasso-Gastinel, J. F. A. Soltero-Martínez and E. Mendizábal, in *Modification of Polymer Properties*, Elsevier, 2017, pp. 1–21.
- 114 M. Morton, *Journal of Macromolecular Science: Part A - Chemistry*, 1981, **15**, 1289–1302.
- 115 E. Neil and G. Marsh, *Chem Biol*, 2000, **7**, R153–R157.
- 116 T.-L. Liu, J. Wu and Y. Zhao, *Chem Sci*, 2017, **8**, 3885–3890.
- 117 J. G. Riess, *Artificial Cells, Blood Substitutes, and Biotechnology*, 2005, **33**, 47–63.
- 118 C. J. Drummond, G. Georgaklis and D. Y. C. Chan, *Langmuir*, 1996, **12**, 2617–2621.
- 119 W.-T. Tsai, H.-P. Chen and W.-Y. Hsien, *J Loss Prev Process Ind*, 2002, **15**, 65–75.
- 120 K. R. Miner, H. Clifford, T. Taruscio, M. Potocki, G. Solomon, M. Ritari, I. E. Napper, A. P. Gajurel and P. A. Mayewski, *Science of The Total Environment*, 2021, **759**, 144421.
- 121 C. Beans, *Proceedings of the National Academy of Sciences*, , DOI:10.1073/pnas.2105018118.
- 122 P. C. Calder, *Journal of Parenteral and Enteral Nutrition*, 2015, **39**, 18S-32S.
- 123 S. T. Oh and A. D. Martin, *Process Biochemistry*, 2010, **45**, 335–345.
- 124 L. D. A. Chumpitaz, L. F. Coutinho and A. J. A. Meirelles, *J Am Oil Chem Soc*, 1999, **76**, 379–382.
- 125 F. Garnier, *Angewandte Chemie*, 1989, **101**, 529–533.
- 126 M.-A. de Paoli, R. J. Waltman, A. F. Diaz and J. Bargon, *J Chem Soc Chem Commun*, 1984, 1015.

- 127 J. Vartiainen, E. Skytta, J. Enqvist and R. Ahvenainen, *Packaging Technology and Science*, 2003, **16**, 223–229.
- 128 H. Y. Erbil, A. L. Demirel, Y. Avci and O. Mert, *Science (1979)*, 2003, **299**, 1377–1380.
- 129 R. Geyer, in *Plastic Waste and Recycling*, Elsevier, 2020, pp. 13–32.
- 130 W. v. Titow, *PVC Technology*, Springer Netherlands, Dordrecht, 1984.
- 131 D. Friedrich and A. Luible, *Journal of Building Engineering*, 2016, **8**, 152–161.
- 132 B. Lundgren, B. Jonsson and B. Ek-Olausson, *Indoor Air*, 1999, **9**, 202–208.
- 133 S. S. Hill, B. R. Shaw and A. H. B. Wu, *Clinica Chimica Acta*, 2001, **304**, 1–8.
- 134 F.-L. Jin, X. Li and S.-J. Park, *Journal of Industrial and Engineering Chemistry*, 2015, **29**, 1–11.
- 135 A. Das and P. Mahanwar, *Advanced Industrial and Engineering Polymer Research*, 2020, **3**, 93–101.
- 136 M. S. Soh and A. U. J. Yap, *J Dent*, 2004, **32**, 321–326.
- 137 G.-N. Chen and K.-N. Chen, *J Appl Polym Sci*, 1997, **63**, 1609–1623.
- 138 J. W. Taylor and M. A. Winnik, *J Coat Technol Res*, 2004, **1**, 163–190.
- 139 A. N. M. B. El-hoshoudy, in *Recent Research in Polymerization*, InTech, 2018.
- 140 A. M. van Herk and R. G. Gilbert, in *Chemistry and Technology of Emulsion Polymerisation*, John Wiley & Sons Ltd, Oxford, UK, 2013, pp. 43–73.
- 141 P. A. Tran and T. J. Webster, *Nanotechnology*, 2013, **24**, 155101.
- 142 K. Aalto-Korte, K. Alanko, M.-L. Henriks-Eckerman and R. Jolanki, *Arch Dermatol*, DOI:10.1001/archderm.142.10.1326.
- 143 M. Balouiri, M. Sadiki and S. K. Ibensouda, *J Pharm Anal*, 2016, **6**, 71–79.
- 144 J. H. Jorgensen and M. J. Ferraro, *Clinical Infectious Diseases*, 2009, **49**, 1749–1755.
- 145 S. D. Brugger, C. Baumberger, M. Jost, W. Jenni, U. Brugger and K. Mühlemann, *PLoS One*, 2012, **7**, e33695.

- 146 A. F. Widmer, S. Kuster, M. Dangel, S. Jäger and R. Frei, *Antimicrob Resist Infect Control*, 2021, **10**, 120.
- 147 S. T. Gaballah, A. M. Khalil and S. T. Rabie, *Journal of Vinyl and Additive Technology*, 2019, **25**, E137–E146.
- 148 J. Zhao, X. M. Cai, H. Q. Tang, T. Liu, H. Q. Gu and R. Z. Cui, *J Mater Sci Mater Med*, 2009, **20**, 101–105.
- 149 S. Maharubin, C. Nayak, O. Phatak, A. Kurhade, M. Singh, Y. Zhou and G. Tan, *Mater Lett*, 2019, **249**, 108–111.
- 150 M. Vincent, P. Hartemann and M. Engels-Deutsch, *Int J Hyg Environ Health*, 2016, **219**, 585–591.
- 151 M. Birkett, L. Dover, C. Cherian Lukose, A. Wasy Zia, M. M. Tambuwala and Á. Serrano-Aroca, *Int J Mol Sci*, 2022, **23**.
- 152 U. Bogdanović, V. Lazić, V. Vodnik, M. Budimir, Z. Marković and S. Dimitrijević, *Mater Lett*, 2014, **128**, 75–78.
- 153 I. A. Hassan, I. P. Parkin, S. P. Nair and C. J. Carmalt, *J. Mater. Chem. B*, 2014, **2**, 2855–2860.
- 154 B. Abebe, E. A. Zereffa, A. Tadesse and H. C. A. Murthy, *Nanoscale Res Lett*, 2020, **15**, 190.
- 155 M. Visnapuu, M. Rosenberg, E. Truska, E. Nömmiste, A. Šutka, A. Kahru, M. Rähn, H. Vija, K. Orupöld, V. Kisand and A. Ivask, *Colloids Surf B Biointerfaces*, 2018, **169**, 222–232.
- 156 P. Kanmani and J.-W. Rhim, *Carbohydr Polym*, 2014, **106**, 190–199.
- 157 S. Noimark, J. Weiner, N. Noor, E. Allan, C. K. Williams, M. S. P. Shaffer and I. P. Parkin, *Adv Funct Mater*, 2015, **25**, 1367–1373.
- 158 S. K. Sehmi, S. Noimark, J. C. Bear, W. J. Peveler, M. Bovis, E. Allan, A. J. MacRobert and I. P. Parkin, *J Mater Chem B*, 2015, **3**, 6490–6500.
- 159 S. Herbert, A. K. Ziebandt, K. Ohlsen, T. Schäfer, M. Hecker, D. Albrecht, R. Novick and F. Götz, *Infect Immun*, 2010, **78**, 2877–2889.
- 160 G. B. Hwang, H. Huang, G. Wu, J. Shin, A. Kafizas, K. Karu, H. du Toit, A. M. Alotaibi, L. Mohammad-Hadi, E. Allan, A. J. MacRobert, A. Gavriilidis and I. P. Parkin, *Nat Commun*, 2020, **11**, 4–13.
- 161 G. Y. Liu, A. Essex, J. T. Buchanan, V. Datta, H. M. Hoffman, J. F. Bastian, J. Fierer and V. Nizet, *Journal of Experimental Medicine*, 2005, **202**, 209–215.

- 162 J. L. Bose, P. D. Fey and K. W. Bayles, *Appl Environ Microbiol*, 2013, **79**, 2218–2224.
- 163 Cadillac Plastics, *Melinex 726 (polyester) Technical data sheet*, .
- 164 A. Nasser and U. Mingelgrin, *Appl Clay Sci*, 2012, **67–68**, 141–150.
- 165 M. Nafees, W. Liaqut, S. Ali and M. A. Shafique, *Appl Nanosci*, 2013, **3**, 49–55.
- 166 N. B. Khelladi and N. E. C. Sari, *Advances in Materials Sciences*, 2013, **13**, 799–800.
- 167 A. Adewuyi and W. J. Lau, in *Handbook of Nanotechnology Applications*, Elsevier, 2021, pp. 67–97.
- 168 M. Pudukudy and Z. Yaakob, *J Clust Sci*, 2015, **26**, 1187–1201.
- 169 K. R. Sreekumari, Y. Sato and Y. Kikuchi, *Mater Trans*, 2005, **46**, 1636–1645.
- 170 H. Lkigai, H. Kanematsu, K. Kuroda and A. Ohmori, *National Association for Surface Finishing Annual Technical Conference 2005, SUR/FIN 2005*, 2005, 497–503.
- 171 M. Yasuyuki, K. Kunihiro, S. Kurissery, N. Kanavillil, Y. Sato and Y. Kikuchi, *Biofouling*, 2010, **26**, 851–858.
- 172 S. Noimark, E. Allan and I. P. Parkin, *Chem Sci*, 2014, **5**, 2216–2223.
- 173 N. Bukorović, *Lighting guide 2: hospitals and health care buildings*, Society of Light and Lighting, Chartered Institution of Building Services Engineers, London, 2008.
- 174 S. Aryal, Differences between Gram Positive and Gram Negative Bacteria, <https://microbiologyinfo.com/differences-between-gram-positive-and-gram-negative-bacteria/>, (accessed 20 August 2019).
- 175 M.-Y. Lin and C.-L. Yen, *J Agric Food Chem*, 1999, **47**, 1460–1466.
- 176 J. Glaeser, A. M. Nuss, B. A. Berghoff and G. Klug, in *Advances in Microbial Physiology*, Elsevier Ltd., 1st edn., 2011, vol. 58, pp. 141–173.
- 177 H. Tatsuzawa, T. Maruyama, N. Misawa, K. Fujimori and M. Nakano, *FEBS Lett*, 2000, **484**, 280–284.
- 178 P. F. Conn, W. Schalch and T. G. Truscott, *J Photochem Photobiol B*, 1991, **11**, 41–47.
- 179 K. Manoharan and S. Bhattacharya, *Journal of Micromanufacturing*, 2019, **2**, 59–78.

- 180 S. Parvate, P. Dixit and S. Chattopadhyay, *J Phys Chem B*, 2020, **124**, 1323–1360.
- 181 Gh. Barati Darband, M. Aliofkhazraei, S. Khorsand, S. Sokhanvar and A. Kaboli, *Arabian Journal of Chemistry*, 2020, **13**, 1763–1802.
- 182 Y. Wang, B. Li and C. Xu, *Superlattices Microstruct*, 2012, **51**, 128–134.
- 183 Q. Wang, B. Zhang, M. Qu, J. Zhang and D. He, *Appl Surf Sci*, 2008, **254**, 2009–2012.
- 184 M. E. Mohamed and B. A. Abd-El-Nabey, *ECS Journal of Solid State Science and Technology*, 2020, **9**, 061006.
- 185 J. Li, R. Gao, Y. Wang, T. C. Zhang and S. Yuan, *Colloids Surf A Physicochem Eng Asp*, 2022, **637**, 128249.
- 186 N. Agrawal, S. Munjal, M. Z. Ansari and N. Khare, *Ceram Int*, 2017, **43**, 14271–14276.
- 187 W. Zhu, Y. Wu and Y. Zhang, *Mater Res Express*, 2019, **6**, 1150d1.
- 188 F. L. Heale, UCL, 2020.
- 189 R. Jafari and M. Farzaneh, *J Compos Mater*, 2013, **47**, 3125–3129.
- 190 C. Ma, Y. Li, J. Zhang, F. Ning, M. Kang, H. Li and Z. Qiu, *J Coat Technol Res*, 2021, **18**, 415–433.
- 191 T. Simovich, A. H. Wu and R. N. Lamb, *Thin Solid Films*, 2015, **589**, 472–478.
- 192 B. Sutter, D. Bémer, J.-C. Appert-Collin, D. Thomas and N. Midoux, *Aerosol Science and Technology*, 2010, **44**, 395–404.
- 193 F. L. Heale, K. Page, J. S. Wixey, P. Taylor, I. P. Parkin and C. J. Carmalt, *RSC Adv*, 2018, **8**, 27064–27072.
- 194 F. L. Heale, M. Einhorn, K. Page, I. P. Parkin and C. J. Carmalt, *RSC Adv*, 2019, **9**, 20332–20340.
- 195 Zn oxide - FTIR - Spectrum - SpectraBase, <https://spectrabase.com/spectrum/B5DJSAc6BYj>, (accessed 13 July 2022).
- 196 K. Handore, S. Bhavsar, A. Horne, P. Chhattise, K. Mohite, J. Ambekar, N. Pande and V. Chabukswar, *Journal of Macromolecular Science, Part A: Pure and Applied Chemistry*, 2014, **51**, 941–947.

- 197 IR Spectrum Table, <https://www.sigmaaldrich.com/GB/en/technical-documents/technical-article/analytical-chemistry/photometry-and-reflectometry/ir-spectrum-table>, (accessed 13 July 2022).
- 198 Infrared Spectroscopy Absorption Table - Chemistry LibreTexts, https://chem.libretexts.org/Ancillary_Materials/Reference/Reference_Tables/Spectroscopic_Reference_Tables/Infrared_Spectroscopy_Absorption_Table, (accessed 16 July 2022).
- 199 B. Smith, *Infrared Spectral Interpretation*, CRC Press, 2018.
- 200 Basic Quantification of XPS Spectra, www.casaxps.com, (accessed 14 July 2022).
- 201 Dow, OROTAN™ CA-2500 Dispersant Hydrophobic Copolymer Pigment Dispersant for Tinted Waterborne Coatings Regional Product Availability • Asia-Pacific, www.dow.com, (accessed 15 July 2022).
- 202 The Coalescing Aid for Latex Paints, <https://5.imimg.com/data5/SELLER/Doc/2021/8/FG/BJ/WG/22787275/texanol-ester-alcohol.pdf>, (accessed 18 July 2022).
- 203 Beauchamp Spectroscopy Tables, https://www.cpp.edu/~psbeauchamp/pdf/spec_ir_nmr_spectra_tables.pdf, (accessed 18 July 2022).
- 204 poly(acrylic ester-co-styrene) - FTIR - Spectrum - SpectraBase, <https://spectrabase.com/spectrum/KLIhkqPviOv>, (accessed 16 July 2022).
- 205 E. San Andrés, A. del Prado, F. L. Martínez, I. Mártel, D. Bravo and F. J. López, *J Appl Phys*, 2000, **87**, 1187–1192.
- 206 A. Aparna, A. S. Sethulekshmi, A. Saritha and K. Joseph, *Prog Org Coat*, 2022, **166**, 106819.
- 207 C. Qi, H. Chen, L. Shen, X. Li, Q. Fu, Y. Zhang, Y. Sun and Y. Liu, *ACS Appl Nano Mater*, 2020, **3**, 2047–2057.
- 208 H. Liu, H. Zhang, J. Pang, Y.-J. Ning, F. Jia, W.-F. Yuan, B. Gu and Q.-P. Zhang, *Mater Lett*, 2019, **247**, 204–207.
- 209 M. O. Penna, A. A. Silva, F. F. do Rosário, S. de Souza Camargo and B. G. Soares, *Mater Chem Phys*, 2020, **255**, 123543.
- 210 H. Zhao, W.-C. Gao, Q. Li, M. R. Khan, G.-H. Hu, Y. Liu, W. Wu, C.-X. Huang and R. K. Y. Li, *Adv Colloid Interface Sci*, 2022, **303**, 102644.

- 211 I. Hejazi, G. Mir Mohamad Sadeghi, J. Seyfi, S.-H. Jafari and H. A. Khonakdar, *Appl Surf Sci*, 2016, **368**, 216–223.
- 212 C. Jiang, Y. Zhang, Q. Wang and T. Wang, *J Appl Polym Sci*, 2013, **129**, 2959–2965.
- 213 Z. Wu, H. Wang, M. Xue, X. Tian, X. Ye, H. Zhou and Z. Cui, *Compos Sci Technol*, 2014, **94**, 111–116.
- 214 D. P. Linklater and E. P. Ivanova, *Nano Today*, 2022, **43**, 101404.
- 215 Y. Zhan, S. Yu, A. Amirfazli, A. Rahim Siddiqui and W. Li, *Adv Eng Mater*, 2022, **24**, 2101053.
- 216 M. Seth and S. Jana, *NanoWorld J*, , DOI:10.17756/nwj.2020-077.
- 217 Y. Lai, Y. Guo, L. Xu, X. Chang, X. Zhang, G. Xu and J. Shi, *Coatings*, 2020, **11**, 15.
- 218 M. Shaban, F. Mohamed and S. Abdallah, *Sci Rep*, 2018, **8**, 3925.
- 219 T. Huhtamäki, X. Tian, J. T. Korhonen and R. H. A. Ras, *Nat Protoc*, 2018, **13**, 1521–1538.
- 220 S. Caddeo, F. Baino, A. M. Ferreira, S. Sartori, G. Novajra, G. Ciardelli and C. Vitale-Brovarone, *Key Eng Mater*, 2014, **631**, 184–189.
- 221 D. Wang, Q. Sun, M. J. Hokkanen, C. Zhang, F.-Y. Lin, Q. Liu, S.-P. Zhu, T. Zhou, Q. Chang, B. He, Q. Zhou, L. Chen, Z. Wang, R. H. A. Ras and X. Deng, *Nature*, 2020, **582**, 55–59.
- 222 H. B. Eral, D. J. C. M. 'T Mannelje and J. M. Oh, *Colloid Polym Sci*, 2013, **291**, 247–260.
- 223 A. T. Tyowua and S. G. Yiase, in *Progress in Adhesion and Adhesives*, Wiley, 2021, pp. 47–67.
- 224 L. Gao and T. J. McCarthy, *Langmuir*, 2006, **22**, 6234–6237.
- 225 W. Chen, A. Y. Fadeev, M. C. Hsieh, D. Öner, J. Youngblood and T. J. McCarthy, *Langmuir*, 1999, **15**, 3395–3399.
- 226 G. Grass, C. Rensing and M. Solioz, *Appl Environ Microbiol*, 2011, **77**, 1541–1547.
- 227 G. Yi, X. Li, Y. Yuan and Y. Zhang, *Environ Sci Nano*, 2019, **6**, 68–74.
- 228 *BS ISO 21702:2019: Measurement of antiviral activity on plastics and other non-porous surfaces*, British Standards Institute, 2019.

